BIS(IMINO)PYRIDINE IRON AND COBALT COMPLEXES: PREPARATION, ELECTRONIC STRUCTURE DETERMINATION AND REACTIVITY OF METAL-LIGAND MULTIPLE BONDS

A Dissertation

Presented to the Faculty of the Graduate School

of Cornell University

In Partial Fulfillment of the Requirements for the Degree of

Doctor of Philosophy

by

Amanda Catherine Bowman

February 2010

BIS(IMINO)PYRIDINE IRON AND COBALT COMPLEXES: PREPARATION, ELECTRONIC STRUCTURE DETERMINATION AND REACTIVITY OF METAL-LIGAND MULTIPLE BONDS

Amanda Catherine Bowman, Ph. D.

Cornell University 2010

The synthesis, reactivity and electronic structures of a series of bis(imino)pyridine iron and cobalt complexes was investigated. A series of monomeric bis(imino)pyridine cobalt dinitrogen complexes was investigated using a combination of ^{1}H NMR and infrared spectroscopies, X-ray crystallography, EPR spectroscopy, solution and solid state magnetic measurements and density functional theory. The neutral bis(imino)pyridine cobalt dinitrogen complexes have doublet ground states and are best described as low-spin cobalt(I) centers with an unpaired electron on the singly reduced chelate, while the anionic bis(imino)pyridine cobalt dinitrogen complexes are also best described as low-spin cobalt(I) centers with dianionic chelates. These investigations established that reduction of monochloride precursors occurs at the metal center, in contrast to the related bis(imino)pyridine iron bis(dinitrogen) complex, (^{iPr}PDI)Fe(N_2)$_2$, where reduction of the chelate is observed. A series of bis(imino)pyridine iron imide complexes was also investigated. A combination of X-ray crystallography, variable temperature SQUID magnetization data and Mössbauer spectroscopy was used to elucidate the electronic structures of these complexes. In contrast to the previously reported *N*-aryl substituted bis(imino)pyridine iron imide complexes, where an iron(III) metal center and a singly reduced chelate was observed, an iron(IV) metal center and a triplet diradical chelate was observed for *N*-alkyl substituted bis(imino)pyridine iron imide complexes. For (^{iPr}PDI)FeN(^{2}Ad) (^{iPr}PDI =

2,6-(2,6-$^{i}Pr_2$-C_6H_3-N=CMe)$_2C_5H_3N$), thermal spin crossover from $S = 0$ to $S = 1$ was observed when warming from 15 K to 200 K. (^{Ar}PDI)FeNR compounds with an $S = 0$ ground state promoted C-H bond activation of both imine methyl groups of the bis(imino)pyridine ligand. The C-H bond activation with (^{iPr}PDI)FeN(^{Cy}Oct) was first-order in iron with a rate constant of $k = 3.4(2)\times10^{-5}$ s^{-1} at 25 °C and a primary kinetic isotope effect of 3.3(2), consistent with a rate-determining step of intramolecular C-H bond activation. In contrast, no C-H bond activation of the ligand was observed for the iron imide complexes that are $S = 1$ at 23 °C. The reactivity of bis(imino)pyridine iron imide compounds with hydrogen, silanes, terminal alkynes and organic azides, and the electronic structures of the resulting iron complexes, was also investigated.

BIOGRAPHICAL SKETCH

Amanda Catherine Bowman was born in San Francisco, CA, the day after her mother finished writing her dissertation at the University of California, San Francisco. She was raised in Madison, Wisconsin, where she grew to love cheese, and graduated with honors from Madison West High School in 2001. After deciding to stay in her home state to attend the University of Wisconsin, Madison, she began studying chemistry by accident and subsequently discovered a passion for it. Amanda was fortunate to have the opportunity to do undergraduate research under the supervision of Prof. Clark Landis (and graduate student Ryan Nelson), where she characterized a series of rhodium and iridium 3,4-diazaphospholane complexes. In the Landis group, she received a good foundation in air-sensitive synthetic chemistry, including drybox work and Schlenk techniques. After graduating from UW-Madison with honors in 2005, Amanda moved to Ithaca to begin graduate studies at Cornell University under the supervision of Prof. Paul J. Chirik. While at Cornell, she investigated the reactivity and electronic structure of bis(imino)pyridine iron imide complexes and learned a great deal about organometallic chemistry. In addition, her time at Cornell taught her invaluable research skills and prepared her for a postdoctoral position at the Max Planck Institute for Bioinorganic Chemistry in Mülheim an der Ruhr, where she plans to continue electronic structure investigations of transition metal ions there under the supervision of Prof. Dr. Karl Wieghardt.

My parents

&

Robert and Leona Bowers

ACKNOWLEDGMENTS

This dissertation, and all of my research at Cornell, would not have been possible without the time and support of quite a few people. Foremost, I would like to thank my advisor, Prof. Paul Chirik, for giving me the opportunity to work on such remarkable chemistry and for always taking an interest in my research. His knowledge and motivation helped me to become the scientist that I am today, and I learned many valuable skills during my time in the group that have prepared me for the future. I would also like to thank Paul for giving me the opportunity to travel to Germany and share my work with collaborators there. I would like to thank Prof. Dr. Karl Wieghardt and Dr. Eckhard Bill not only for hosting me during my graduate career, but also for giving me the opportunity to continue learning with them for my postdoc. Dr. Carsten Milsmann also deserves a huge thank you for running endless calculations on my wacky molecules, and for still finding them interesting even after all that work!

In addition to Paul, I would like to thank the other members of my committee, Prof. Pete Wolczanski, Prof. Peng Chen and (recently) Prof. Serena DeBeer George. Between classes and lit lunches, Pete in particular has been a valuable source of knowledge and has helped resolve several questions about the complicated molecules discussed herein. In addition, Serena's interest in our molecules, as well as her input (and willingness to run K-edge samples!), has been greatly appreciated.

I would also like to thank several former Chirik group members who helped me along in the beginning when I most needed it. Suzanne Bart started the iron imide project that became my baby, and she was always patient and helpful with my endless questions throughout the years (even after she left!). Her dedication to chemistry is inspiring, and her willingness to take me around Erlangen to find the best pretzels was also appreciated. And I would definitely not be as prepared for my adventures in Germany without her advice about toothpaste and the "five magic tickets." Wes

Bernskoetter also deserves a ton of thanks for training me in the lab and answering my questions, and for generously offering to set me up with the construction workers who were renovating our hallways. Without Wes, I don't think my lab skills would be half as good as they are today, and I like to think he would be proud of how clean I managed to keep the drybox after he left. Ryan Trovitch also deserves thanks for being a great resource and a fearless safety officer, as well as a good friend. Graduate school would not have been the same without Reggae Explosions and his motivation to "go hard or go home!"

The current members of the Chirik group deserve thanks for being supportive, most especially Doris Pun! Doris has been both a good friend and coworker, and I will miss being able to giggle with her. I will also probably lose weight immediately after I leave Cornell, because she has fed me so many M&Ms® over the years. It was comforting to have Doris around as we went through all the trials of graduate school together (although I always seemed to go first!), and I am infinitely glad that I have gotten to know her over the past four years. I would also like to thank Aaron Tondreau for being my SQUID buddy and keeping me company all the times when we had to change samples and fix bent sample rods at four in the morning during a blizzard. And good luck to Crisita, who has taken on my old project. It's good to know that the job of Drybox Czar is in safe hands.

Numerous other people around Cornell deserves thanks, namely Emil Lobkovsky. His amazing expertise contributed to a large part of this dissertation, and his patience with my (lack of) crystal-growing abilities was always appreciated. I would also like to thank Dave Wise for repairing J. Young tubes and putting together awesome vacuum and Schlenk lines for our shiny new labs. Ivan Keresztes (and his enthusiasm) was always helpful with NMR experiments. In addition, Sharon Calhoun, Pat Hine, Dave Neish and Larry were all extremely helpful, cheerful, and made

everything run more smoothly!

Finally, I would like to thank my family and friends for all of their support over the years. Big love to my “husband” Brittany, you were a fantastic roommate and friend and I don’t think I would have made it through without your brightness (your glitter, one might say) and your willingness to listen to all of my drama over the years! I would also like to thank Kevin for being so supportive during the finale of this work, and for bringing levity to my life when I most needed it. Lastly and most importantly, I would to thank my parents (all of them), for being incredibly supportive over the years and for always believing in me. I would like to thank my mom especially for always being excited about the work I was doing, even though she only looked at the pictures.

TABLE OF CONTENTS

LIST OF FIGURES

LIST OF TABLES

CHAPTER 1

SYNTHESIS AND ELECTRONIC STRUCTURE INVESTIGATION OF REDUCED BIS(IMINO)PYRIDINE COBALT COMPLEXES

1.1 Abstract

A series of reduced aryl-substituted bis(imino)pyridine cobalt complexes was prepared and studied using a combination of ^{1}H NMR and infrared spectroscopies, X-ray crystallography, solution and solid state magnetic measurements and density functional theory. Monomeric bis(imino)pyridine cobalt dinitrogen complexes, (^{Ar}PDI)Co(N_2) (^{Ar}PDI = 2,6-(*Ar*N=CMe)$_2C_5H_3N$; *Ar* = 2,6-$^{i}Pr_2$-C_6H_3 (^{iPr}PDI), 2,6-Et_2-C_6H_3 (^{Et}PDI), 2,6-Me_2-C_6H_3 (^{Me}PDI)), were prepared from the corresponding cobalt dichloride complex by sodium amalgam reduction or treatment with two equivalents of sodium triethylborohydride under a dinitrogen atmosphere. The anionic cobalt dinitrogen complexes, [Na(solv)$_3$][(^{iPr}PDI)Co(N_2)] and [Na(solv)$_3$][(^{iPr}APDI)Co(N_2)] (solv = Et_2O, THF), were prepared by treatment of the corresponding dichloride complex with three equivalents of sodium naphthalenide under a dinitrogen atmosphere. In contrast, reduction of (^{R}APDI)$CoCl_2$ (^{R}APDI = 2,6-(RN=CMe)$_2C_5H_3N$; R = ^{Cy}Hex (^{Cy}APDI), ^{i}Pr (^{iPr}APDI)) with sodium amalgam furnished the bis(chelate) complex, (^{R}APDI)$_2$Co. In addition to aryl-substituted bis(imino)pyridine cobalt dinitrogen complexes, cobalt complexes with mono-X type ligands were investigated. A series of cobalt monochloride complexes (^{Ar}PDI)CoCl (^{Ar}PDI = ^{Et}PDI, ^{Me}PDI) and (^{R}APDI)CoCl (^{R}APDI = ^{Cy}APDI, ^{iPr}APDI) was prepared by reduction of the corresponding dichloride with zinc metal. Similarly, a series of cobalt monomethyl complexes (^{Ar}PDI)CoMe (^{Ar}PDI = ^{Et}PDI, ^{Me}PDI) and (^{R}APDI)CoMe (^{R}APDI = ^{Cy}APDI, ^{iPr}APDI) was prepared by alkylation of the appropriate monochloride species with methyllithium. The electronic structure of the

reduced cobalt complexes was investigated using X-ray crystallography, SQUID magnetometry and density functional theory. The neutral aryl-substituted bis(imino)pyridine cobalt dinitrogen complexes have doublet ground states and are best described as low-spin cobalt(I) centers with an unpaired electron on the singly reduced chelate. The anionic bis(imino)pyridine cobalt dinitrogen complexes are also best described as low-spin cobalt(I) centers, but with dianionic chelates. The aryl-substituted bis(imino)pyridine cobalt complexes with mono-X type ligands, (^{Ar}PDI)CoCl and (^{Ar}PDI)CoMe, as well as the alkyl-substituted cobalt monomethyl complexes, (^{R}APDI)CoMe, were found to have singlet ground states with a monoanionic bis(imino)pyridine chelate antiferromagnetically coupled to the cobalt(II) metal center. Alkyl-substituted cobalt monochloride complexes, (^{R}APDI)CoCl, exhibited spin-crossover from $S = 0$ at low temperatures to $S = 1$ at higher temperatures, as judged by SQUID magnetometry.

1.2 Introduction

Bis(imino)pyridine cobalt complexes were initially investigated by Sacconi and coworkers in the 1960s, including classical coordination compounds with halide, nitrate and thiocyanate ligands.[1] Great interest has been shown in this class of compounds since work both by Gibson and coworkers[2,3] and Brookhart and coworkers[4] demonstrated that the dihalide derivatives, (^{Ar}PDI)CoX$_2$ (X = Cl, Br; ^{Ar}PDI = 2,6-(*Ar*N=CMe)$_2$C$_5$H$_3$N), are highly active for olefin polymerization upon activation with methylaluminoxane (MAO). Much synthetic work has been undertaken with the goal of elucidating the mechanism of polymerization[5] and identifying the active species during chain propagation.[6,7,8] Gal and coworkers established that bis(imino)pyridine cobalt monoalkyl complexes (^{iPr}PDI)CoR (R = Me, CH$_2$Ph, CH$_2$SiMe$_3$) are competent for ethylene polymerization following activation with

MAO, suggesting that the active species for polymerization may be a cationic cobalt monoalkyl derivative.[6]

In addition, Gibson and coworkers isolated several cationic bis(imino)pyridine cobalt complexes likely to result from MAO activation of (^{iPr}PDI)$CoCl_2$ (^{iPr}PDI = 2,6-(^{i}PrN=CMe)$_2C_5H_3N$; **1-Cl$_2$**) (Figure 1.1). Treatment of the neutral bis(imino)pyridine cobalt monomethyl complex, (^{iPr}PDI)CoMe (**1-Me**), with the Lewis acid $B(C_6F_5)_3$ under dinitrogen furnished the cationic dinitrogen complex, [(^{iPr}PDI)Co(N_2)][$MeB(C_6F_5)_3$], by methide abstraction.[7] Subsequent addition of ethylene afforded the cationic ethylene adduct, [(^{iPr}PDI)Co(η-C_2H_4)][$MeB(C_6F_5)_3$].[7] Based on these observations, a cationic cobalt complex is proposed as the active species during polymerization, although the oxidation state of the metal and the mechanism of propagation is still under debate. Similar reactivity was observed by Erker and coworkers for phenylated bis(imino)pyridine cobalt complexes.[8]

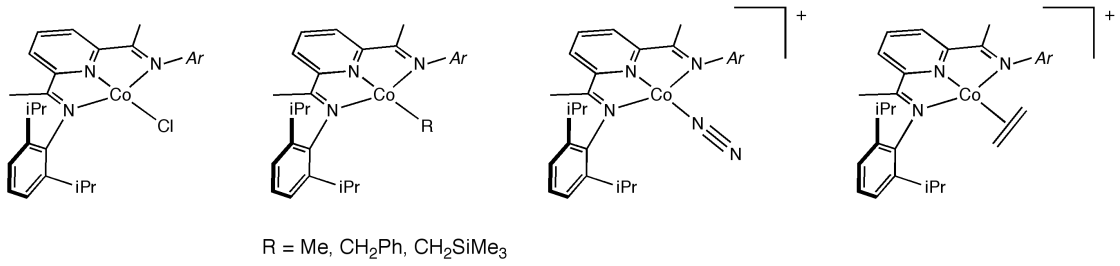

R = Me, CH_2Ph, CH_2SiMe_3

Figure 1.1 Bis(imino)pyridine cobalt complexes related to ethylene polymerization.

Understanding the electronic structures of reduced bis(imino)pyridine cobalt complexes may have significant importance to understanding the mechanism and active species of olefin polymerization. Computational studies by Budzelaar and coworkers predict that one electron reduction of bis(imino)pyridine cobalt complexes should occur at the ligand to afford a low-spin cobalt(II) center and a monoanionic chelate.[9] Investigation of cationic bis(chelate) metal complexes by Wieghardt and

coworkers establishes that reduction of one or both ligands to afford a metal center in the 2+ or 3+ oxidation state is often observed, although the metal center is formally +1.[10,11] The electronic structure of analogous iron compounds was subsequently investigated both experimentally and computationally.[12] One important question that arises is whether one- and two-electron reduction of cobalt dihalide complexes occurs at the ligand in all cases, as is observed with bis(imino)pyridine iron complexes.[12,13]

Bis(imino)pyridine cobalt dinitrogen complexes may also have applications in catalytic reactions other than olefin polymerization. The analogous bis(imino)pyridine iron dinitrogen complex, (^{iPr}PDI)Fe(N_2)$_2$, is competent for a variety of catalytic transformations such as olefin hydrogenation,[14,15] aldehyde and ketone hydrosilylation,[16] [2π + 2π] cyclization of olefins[17] and reductive cyclization of enynes and diynes.[18] Although catalytic olefin hydrogenation by (^{iPr}PDI)Fe(N_2)$_2$ has been observed in the presence of functional groups such as ketones and amines,[19] C-O bond cleavage of ester groups leads to catalyst deactivation.[20] Development and study of bis(imino)pyridine cobalt complexes may lead to catalysts with better functional group tolerance.

1.3 Neutral and Anionic Cobalt Dinitrogen Complexes

Stirring a toluene slurry of (^{iPr}PDI)$CoCl_2$ (**1-Cl$_2$**) with excess 0.5 % sodium amalgam furnished the cobalt dinitrogen complex, (^{iPr}PDI)Co(N_2) (**1-N$_2$**) in good yield (65 %). The analogous *p*-^{t}Bu substituted cobalt dinitrogen complex, (^{iPr}*p*-^{t}BuPDI)Co(N_2) (**^{tBu}1-N$_2$**), was also prepared by sodium amalgam reduction of the corresponding dichloride complex, (^{iPr}*p*-^{t}BuPDI)$CoCl_2$ (**^{tBu}1-Cl$_2$**). Similarly, reduction of (^{Et}PDI)$CoCl_2$ (**2-Cl$_2$**) and (^{Me}PDI)$CoCl_2$ (**3-Cl$_2$**) with sodium amalgam furnished the corresponding cobalt dinitrogen compounds, (^{Et}PDI)Co(N_2) (**2-N$_2$**) and (^{Me}PDI)Co(N_2) (**3-N$_2$**), in moderate yields of 44 % and 53 %, respectively. This is notable because

reduction of bis(imino)pyridine iron dihalide complexes with relatively less sterically hindered aryl rings, such as 2,6-Et_2-C_6H_3 and *p*-OMe-C_6H_4, and alkyl substituents resulted in formation of the iron bis(chelate) complex instead of the desired iron bis(dinitrogen) complex.[21] In addition, the cobalt dinitrogen compounds were also prepared by sequential addition of two equivalents of $NaEt_3BH$ to the appropriate cobalt dichloride complex in toluene (Figure 1.2), or by direct reduction of the isolated monochloride complexes, (^{Ar}PDI)CoCl (^{Ar}PDI = ^{iPr}PDI, ^{Et}PDI, ^{Me}PDI).[6]

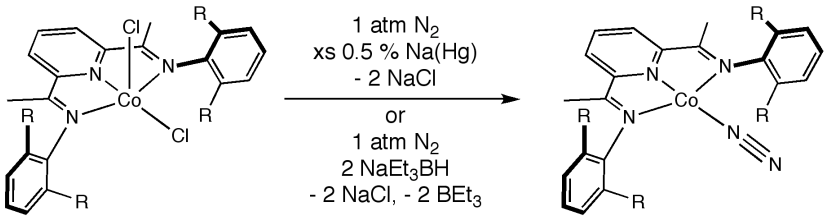

1-Cl_2 (R = ^{i}Pr)
2-Cl_2 (R = Et)
3-Cl_2 (R = Me)

1-N_2 (R = ^{i}Pr)
2-N_2 (R = Et)
3-N_2 (R = Me)

Figure 1.2 Preparation of neutral bis(imino)pyridine cobalt dinitrogen complexes by two electron reduction of dichloride precursors.

The benzene-d_6 ^{1}H NMR spectra of the dinitrogen complexes at 20 °C exhibit only three paramagnetically broadened resonances, preventing individual peak assignments. Solution magnetic moments, measured in benzene-d_6 at 20 °C, of 1.6(2) μ_B for **1-N_2**, 1.8(2) μ_B for **2-N_2** and 1.7(2) μ_B for **3-N_2** were determined. These values are consistent with one unpaired electron and a doublet ground state for each cobalt dinitrogen complex. Variable temperature magnetic data was also collected for the bis(imino)pyridine cobalt dinitrogen complexes (*vide infra*). The infrared spectra (toluene solution) display a single, intense N≡N stretch at ~ 2093 cm^{-1} for each cobalt dinitrogen complex (Table 1.2). These values indicate that the cobalt metal center is less reducing than the related iron metal center of (^{iPr}PDI)Fe(N_2), which exhibits a

stretch of 2036 cm^{-1} in toluene solution.[14] The single stretch observed in the infrared spectrum indicates coordination of only one dinitrogen molecule in solution. Toepler pump experiments also support this formulation, with 76 % of the expected dinitrogen collected for **1-N_2**. For **2-N_2** and **3-N_2**, 84 % and 83 % of the expected dinitrogen was collected, respectively.

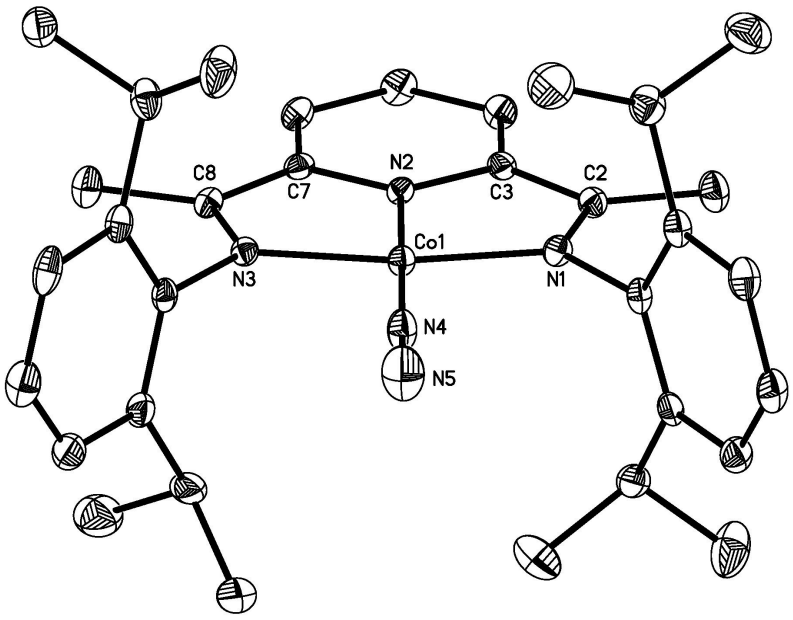

Figure 1.3 Molecular structure of **1-N_2** at 30 % probability ellipsoids. Hydrogen atoms omitted for clarity.

Table 1.1 Selected bond distances (Å) and angles (°) for **1-N_2**.

Co(1)-N(4)	1.7884(16)	N(1)-C(2)	1.341(2)
N(4)-N(5)	1.104(2)	N(3)-C(8)	1.331(2)
Co(1)-N(1)	1.8719(15)	C(2)-C(3)	1.418(2)
Co(1)-N(2)	1.8084(14)	C(7)-C(8)	1.429(2)
Co(1)-N(3)	1.8773(14)	N(2)-Co(1)-N(4)	179.80(8)

Characterization of **1-N_2** by X-ray crystallography indicates that only one molecule of dinitrogen is bound in the solid state, consistent with solution data (Figure 1.3). A summary of the metrical parameters for **1-N_2** is presented in Table 1.1. The solid state structure establishes idealized square planar geometry, with the sum of the angles around cobalt equal to 360.01(13)° and an N_{pyr}-Co-N_2 angle of 179.80(8)°. In addition, the N-N bond length of the dinitrogen ligand, 1.104(2) Å, demonstrates virtually no reduction compared to free dinitrogen (d_{NN} = 1.0975 Å). The metrical parameters of **1-N_2** show distortions to the chelate that are consistent with one-electron reduction,[22] with the C_{imine}-N_{imine} bonds elongated to 1.341(2) Å and 1.331(2) Å, and the C_{imine}-C_{ipso} bonds contracted to 1.418(2) Å and 1.429(2) Å. Some asymmetry in the extent of ligand reduction between the two sides of the bis(imino)pyridine chelate is apparent. The observed C_{imine}-C_{ipso} bond length of 1.429(2) Å is consistent with a singly reduced bis(imino)pyridine chelate, while the C_{imine}-C_{ipso} bond length of 1.418(2) Å is generally more consistent with a doubly reduced chelate.[22] However, the overall distortions are consistent with a singly reduced bis(imino)pyridine ligand, and the shorter C_{imine}-C_{ipso} bond length can be explained by π-backbonding between the chelate and the cobalt(I) metal center (*vide infra*).[22]

For bis(imino)pyridine iron compounds, the spin state of the metal center can sometimes be determined by inspection of the Fe-N_{imine} and Fe-N_{pyr} distances.[13] Comparison of the Co-N_{imine} and Co-N_{pyr} bond distances between the high-spin cobalt(II) complex **1-Cl_2**[3] and the low-spin cobalt(II) complex (^{iPr}PDI)CoCl (**1-Cl**)[6] indicates that the metal-ligand bond distances may also be used to probe the spin-state of the metal center for cobalt. For example, the Co-N_{imine} distances contract from 2.211(3) Å and 2.211(3) Å in **1-Cl_2** to 1.916(3) Å and 1.912(3) Å in **1-Cl**. The Co-N_{pyr} bond distance also contracts from 2.051(3) Å in **1-Cl_2** to 1.797(3) Å in **1-Cl**. By comparison, the Co-N_{pyr} distance of 1.8084(14) Å and the Co-N_{imine} distances of

1.8719(15) Å and 1.8773(14) Å for **1-N_2** indicate a low-spin cobalt(I) center, where the d_{x2-y2} orbital is empty.

Preparation of a cobalt dinitrogen complex with a genuine monoanionic bis(imino)pyridine ligand was also explored. Previous work[23,24,25] has demonstrated that the imine methyl groups of the bis(imino)pyridine chelate are susceptible to deprotonation to afford either the mono- or dianionic forms of the chelate. Treatment of (^{iPr}PDI)CoCl with sodium *t*-butoxide in tetrahydrofuran at 23 °C furnished the monomeric dinitrogen complex, (^{iPr}PIEA)Co(N_2) (^{iPr}PIEA = 2-(2,6-$^{i}Pr_2$-$C_6H_3N(C{=}CH_2)$)-6-(2,6-$^{i}Pr_2$-$C_6H_3N{=}CMe)C_5H_3N$), where one side of the bis(imino)pyridine chelate has been deprotonated (Figure 1.4). A similar dimeric cobalt dinitrogen complex, [(2,6-$^{i}Pr_2$-$C_6H_3N(C{=}CH_2)$](C_5H_3N)[2-6-$^{i}Pr_2$-$C_6H_3N{=}C(CH_2)]_2$[Co(N_2)]$_2$, was prepared by Gambarotta and coworkers by treatment of [(^{iPr}PDEA)Li(THF)][Li(THF)$_4$] (^{iPr}PDEA = 2,6-(2,6-$^{i}Pr_2$-$C_6H_3N(C{=}CH_2)_2C_5H_3N$)) with $CoCl_2(THF)_{1.5}$ under a dinitrogen atmosphere.[26] The monomeric iron analog, (^{iPr}PIEA)Fe(N_2), was also prepared by Gambarotta and coworkers by treatment of **1-Cl_2** with excess sodium hydride in tetrahydrofuran.[25c]

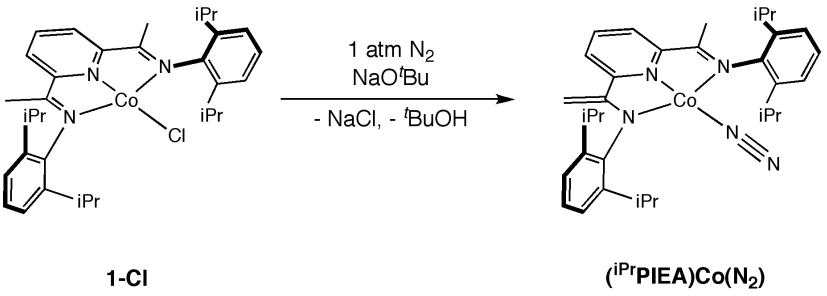

Figure 1.4 Preparation of (^{iPr}PIEA)Co(N_2) by deprotonation of the bis(imino)pyridine chelate.

As expected for a formally cobalt(I) species, (^{iPr}PIEA)Co(N_2) is diamagnetic. The benzene-d_6 ^{1}H NMR spectrum of (^{iPr}PIEA)Co(N_2) at 23 ºC is consistent with a C_1

symmetric molecule, and exhibits distinct resonances for the methyl backbone protons, at -0.71 ppm, and the methylene backbone protons, at 4.05 and 4.73 ppm. Infrared spectroscopy (KBr) also confirms formation of the methylene backbone, with observation of a C=C stretch at 1583 cm^{-1}. In addition, the intense N≡N stretches observed by infrared spectroscopy in both KBr (2148 cm^{-1}) and toluene solution (2145 cm^{-1}) establish a less reducing metal center than the neutral (^{Ar}PDI)Co(N_2) complexes (Table 1.2). A similar N≡N stretch of 2153 cm^{-1} (Nujol) is observed for the dimeric cobalt dinitrogen complex, [(2,6-$^{i}Pr_2$-$C_6H_3N(C=CH_2)$](C_5H_3N)[2-6-$^{i}Pr_2$-$C_6H_3N=C(CH_2)$]$_2$[Co(N_2)]$_2$, while for the monomeric iron complex, (^{iPr}PIEA)Fe(N_2), an N≡N stretch of 2159 cm^{-1} (Nujol) is observed. The N≡N stretching frequencies for (^{iPr}PIEA)Co(N_2) and (^{iPr}PIEA)Fe(N_2) are likely higher energy than those observed for the ^{iPr}PDI iron and cobalt dinitrogen complexes because the anionic ^{iPr}PIEA chelate removes electron density from the metal center.

Table 1.2 N≡N stretches of dinitrogen complexes by infrared spectroscopy.

Complex	ν_{NN} (cm^{-1})
[1-N_2][MeB(C_6F_5)$_3$][7]	2184 (toluene)
1-N_2	2093 (toluene)
^{tBu}1-N_2	2090 (toluene)
2-N_2	2095 (toluene)
3-N_2	2093 (toluene)
(^{iPr}PIEA)Co(N_2)	2145 (toluene)
[Na(Et_2O)$_3$][1-N_2]	2046 (KBr)
[Na(Et_2O)$_3$][5-N_2]	2037 (KBr)
[Na(THF)$_3$][1-N_2]	1981 (KBr)
[Na(THF)$_3$][5-N_2]	1991 (KBr)

Inspired by the isolation of several aryl-substituted cobalt dinitrogen complexes, the preparation of alkyl-substituted bis(imino)pyridine derivatives was investigated. However, treatment of (^{Cy}APDI)$CoCl_2$ (^{Cy}APDI = 2,6-(^{Cy}HexN=CMe)$_2C_5H_3N$, **4-Cl$_2$**) or (^{iPr}APDI)$CoCl_2$ (^{iPr}APDI = 2,6-(^{i}PrN=CMe)$_2C_5H_3N$, **5-Cl$_2$**) with two equivalents of reductant under a variety of conditions did not yield the desired cobalt dinitrogen complex. The product in each case was identified as the bis(chelate) complex, (^{R}APDI)$_2$Co (R = ^{Cy}Hex, ^{i}Pr), although the isolated yields were poor (< 40 %). The cobalt bis(chelate) complexes were subsequently prepared by sodium amalgam reduction of the appropriate cobalt dichloride complex under vacuum at 23 °C. An additional equivalent of bis(imino)pyridine ligand was added to increase the isolated yield of the reaction to 63 % for (^{Cy}APDI)$_2$Co and 70 % for (^{iPr}APDI)$_2$Co (Figure 1.5).

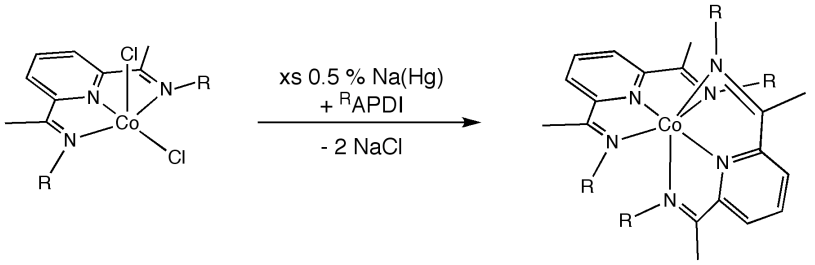

Figure 1.5 Preparation of cobalt bis(chelate) complexes by sodium amalgam reduction.

The ^{1}H NMR spectra of (^{Cy}APDI)$_2$Co and (^{iPr}APDI)$_2$Co in benzene-*d*$_6$ at 20 °C establish that the two bis(imino)pyridine chelates are equivalent on the NMR timescale, with paramagnetically broadened resonances. Solid state magnetic data for the cobalt bis(chelate) complexes established an effective magnetic moment of 3.0(2) μ_B and 3.6(2) μ_B for (^{Cy}APDI)$_2$Co and (^{iPr}APDI)$_2$Co, respectively. Significantly lower

effective magnetic moments of 2.6(2) μ_B and 3.0(2) μ_B were measured in solution for (^{Cy}APDI)$_2$Co and (^{iPr}APDI)$_2$Co, respectively. For each complex, the observed magnetic moment (both solution and solid state) was reproducibly obtained from 2-3 separate measurements. For (^{iPr}APDI)$_2$Co, the effective magnetic moment is consistent with three unpaired electrons, although the value is somewhat low. The observed value of 3.0(2) μ_B for (^{Cy}APDI)$_2$Co, consistent with two unpaired electrons, is unexpected because either a d^7 or d^9 metal center is anticipated, which should result in either a $S = 1/2$ or $S = 3/2$ molecule. The anomalous effective magnetic moment observed for (^{Cy}APDI)$_2$Co is likely due to a mixture of $S = 1/2$ and $S = 3/2$ species which increases in solution.

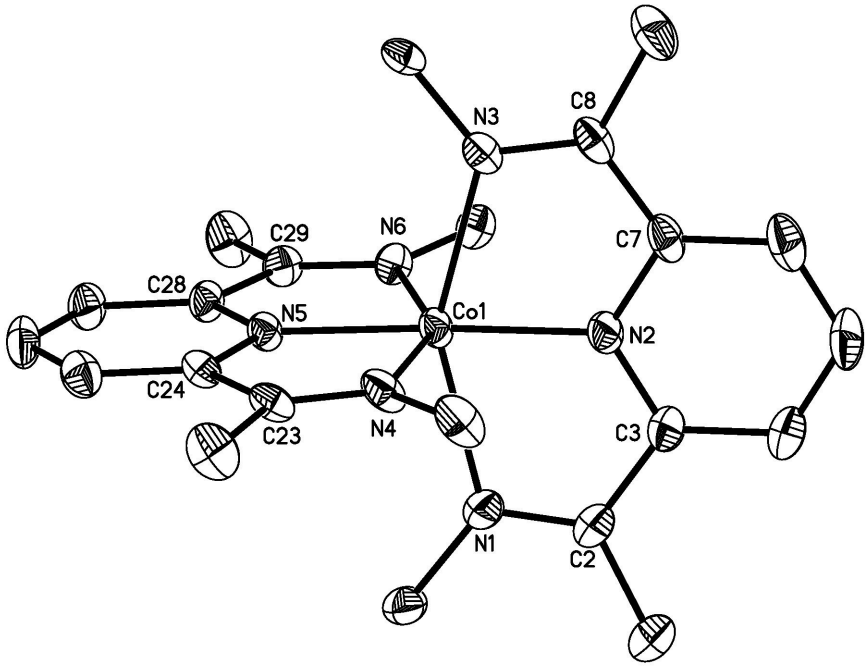

Figure 1.6 Molecular structure of **(^{Cy}APDI)$_2$Co** at 30 % probability ellipsoids. Hydrogen atoms and cyclohexyl groups omitted for clarity.

Table 1.3 Selected bond distances (Å) and angles (°) for **(^{Cy}APDI)$_2$Co**.

Co(1)-N(1)	2.286(2)	N(6)-C(29)	1.303(3)
Co(1)-N(2)	1.9520(19)	C(2)-C(3)	1.458(4)
Co(1)-N(3)	2.2197(19)	C(7)-C(8)	1.451(4)
Co(1)-N(4)	2.2442(19)	C(23)-C(24)	1.451(3)
Co(1)-N(5)	1.9704(18)	C(28)-C(29)	1.450(3)
Co(1)-N(6)	2.2320(18)	N(2)-Co(1)-N(5)	177.13(8)
N(1)-C(2)	1.285(3)	N(1)-Co(1)-N(3)	152.21(7)
N(3)-C(8)	1.299(3)	N(4)-Co(1)-N(6)	151.74(7)
N(4)-C(23)	1.297(3)		

The molecular structure of (^{Cy}APDI)$_2$Co was determined by X-ray diffraction (Figure 1.6) and establishes two orthogonal bis(imino)pyridine ligands and an idealized D_{2d} symmetric compound, with N_{imine}-Co-N_{imine} angles of 152.21(7)° and 151.74(7)° and a N_{pyr}-Co-N_{pyr} angle of 177.13(8)°. The deviation of these angles from the ideal 180° is likely caused by the constraints of the bis(imino)pyridine chelate. Examination of the metrical parameters of (^{Cy}APDI)$_2$Co, presented in Table 1.2, establishes C_{imine}-C_{ipso} bonds lengths that are contracted to ~ 1.45 Å compared to the average distance of ~ 1.49 Å observed for the neutral ligand bis(chelate) cobalt dication, [(^{Cy}APDI)$_2$Co](BF$_4$)$_2$.[27] However, the C_{imine}-N_{imine} bond lengths are not significantly elongated compared to [(^{Cy}APDI)$_2$Co](BF$_4$)$_2$, as would also be expected with ligand reduction.[22] The iron analog, (^{Cy}APDI)$_2$Fe, is best described as high-spin iron(II) with two mono-reduced bis(imino)pyridine chelates (Figure 1.7).[21] Comparison of the metrical parameters of (^{Cy}APDI)$_2$Co and (^{Cy}APDI)$_2$Fe establishes

less pronounced distortions for both chelates of the cobalt species. However, it is likely that each bis(imino)pyridine chelate is singly reduced for (^{Cy}APDI)$_2$Co, resulting in a cobalt(II) metal center and a 19-electron complex.

For (^{Cy}APDI)$_2$Co, a quartet ground state would result from antiferromagnetic coupling between the high-spin cobalt(II) center and one ligand-centered radical (Figure 1.7). With (^{Cy}APDI)$_2$Fe, each ligand-centered radical is antiferromagnetically coupled to the metal center, one through the d_{xy} orbital and the other through the d_{xz} orbital (Figure 1.7).[21] For (^{Cy}APDI)$_2$Co, one bis(imino)pyridine chelate radical can antiferromagnetically couple to the unpaired electron in the cobalt d_{xy} orbital. However, the second chelate radical likely does not couple to the metal center because the remaining unpaired electrons reside in idealized "e_g" ($d_{\sigma*}$) parentage orbitals (d_{z2}/d_{x2-y2}), and do not have the appropriate symmetry for coupling with the bis(imino)pyridine π* orbital (Figure 1.7). From this electronic structure description, an overall $S = 3/2$ molecule is expected. The low values observed experimentally may be explained by a mixture of $S = 1/2$ and $S = 3/2$ species.

A similar six-coordinate, $S = 3/2$ cobalt tris(chelate) complex, Co(3,6-DBSQ)$_3$ (DBSQ = 3,6-di-*tert*-butylsemiquinonato), was prepared by Pierpont and coworkers.[28] The molecular structure of Co(3,6-DBSQ)$_3$ establishes an idealized octahedral complex with D_3 symmetry. The DBSQ semiquinone ligand is redox active, and Co(3,6-DBSQ)$_3$ was found to have a low-spin cobalt(III) metal center and three unpaired electrons, with one electron centered on each DBSQ ligand. The EPR spectrum of Co(3,6-DBSQ)$_3$ in toluene glass at 77 K exhibits a slightly anisotropic signal with a g value of 1.998, characteristic of a ligand-centered radical.[28] The effective magnetic moment of Co(3,6-DBSQ)$_3$ at 350 K is 3.04 μ_B, also somewhat lower than expected for a $S = 3/2$ complex. This is purportedly due to the non-interacting nature of the three unpaired electrons.[28]

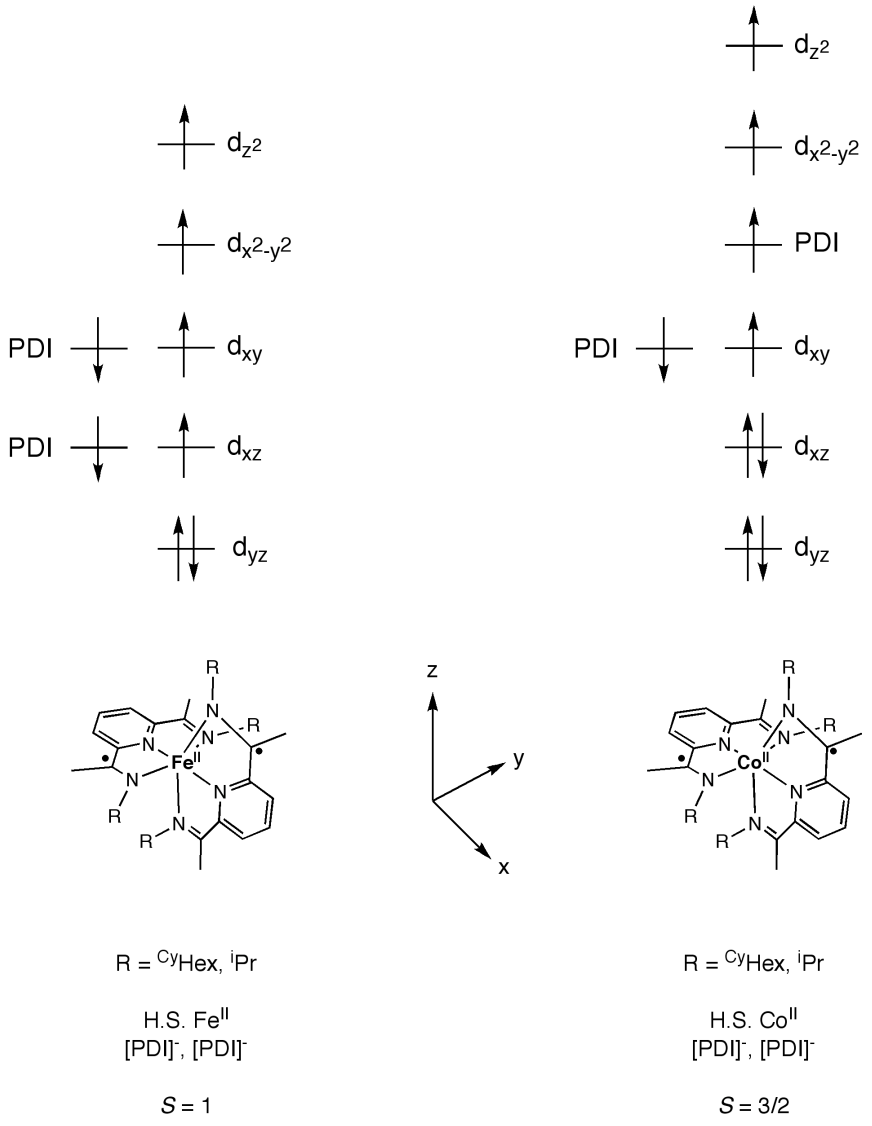

Figure 1.7 Comparison of electronic structure descriptions for iron and cobalt bis(chelate) complexes, (**^{R}APDI)$_2$Co**.

In addition to the series of neutral dinitrogen complexes, the preparation of anionic cobalt dinitrogen complexes by three electron reduction of the cobalt dichloride precursors was explored. Treatment of **1-Cl$_2$** with three equivalents of sodium naphthalenide in tetrahydrofuran at 23 °C furnished the cobalt dinitrogen anion, [Na(THF)$_3$][(^{iPr}PDI)Co(N$_2$)] (**[Na(THF)$_3$][1-N$_2$]**) (Figure 1.8). Recrystallization from diethyl ether afforded a mixture of **[Na(THF)$_3$][1-N$_2$]** and the diethyl etherate

complex, $[Na(Et_2O)_3][(^{iPr}PDI)Co(N_2)]$ (**$[Na(Et_2O)_3][1\text{-}N_2]$**). Notably, while two electron reduction of $(^{R}APDI)CoCl_2$ resulted in formation of the bis(chelate) complex, treatment of **$5\text{-}Cl_2$** with three equivalents of sodium naphthalenide in tetrahydrofuran at 23 °C furnished the alkyl bis(imino)pyridine dinitrogen anion, $[Na(THF)_3]$-$[(^{iPr}APDI)Co(N_2)]$ (**$[Na(THF)_3][5\text{-}N_2]$**). Recrystallization from diethyl ether cleanly afforded $[Na(Et_2O)_3][(^{iPr}APDI)Co(N_2)]$ (**$[Na(Et_2O)_3][5\text{-}N_2]$**) (Figure 1.8).

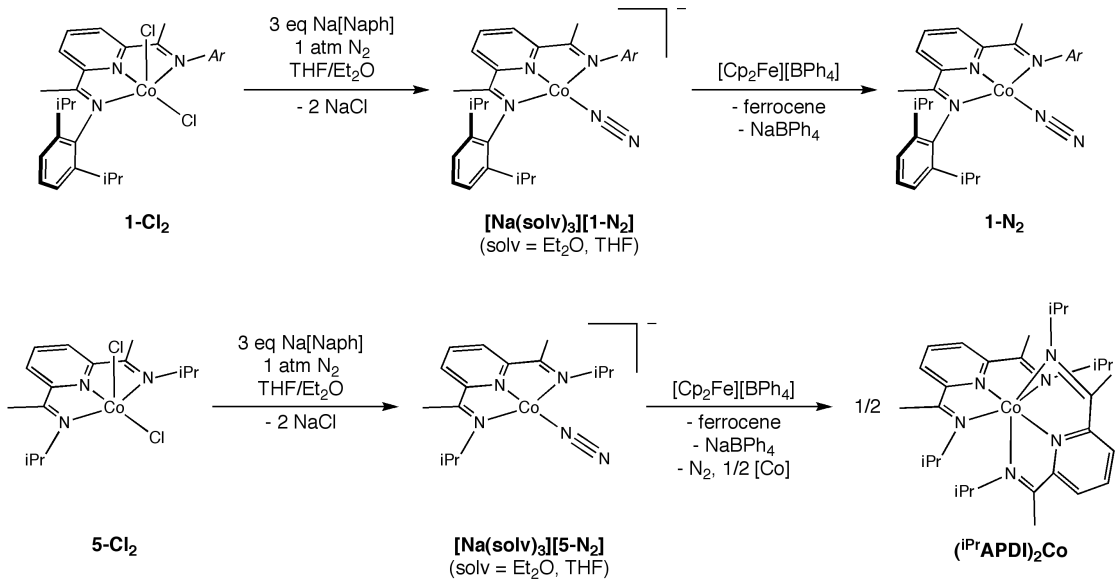

Figure 1.8 Preparation and oxidation of anionic bis(imino)pyridine cobalt dinitrogen complexes.

$[Na(Et_2O)_3][1\text{-}N_2]$ and **$[Na(Et_2O)_3][5\text{-}N_2]$** (solv = Et_2O, THF) exhibit strong N≡N stretches at 2046 cm^{-1} and 2037 cm^{-1}, respectively, in the solid state (KBr) infrared spectrum. The observed bands appear at lower frequency than the N≡N stretches of the neutral dinitrogen complexes (Table 1.2), indicative of the more reducing metal center. For both **$[Na(Et_2O)_3][1\text{-}N_2]$** and **$[Na(Et_2O)_3][5\text{-}N_2]$**, a significantly more reduced N≡N stretch is observed where solv = THF, likely due to better solvation of the sodium cation by the tetrahydrofuran molecules (Table 1.2). This would prevent the cation from interacting with the metal center and increase

electron density on cobalt, leading to a more reducing metal center. This has also been observed for anionic ^{iPr}PIEA iron dinitrogen complexes, where the tetrahydrofuran complex, $[Na(THF)_3][(^{iPr}PIEA)Fe(N_2)]$ has a more reduced N≡N stretch (1912 cm^{-1}) than the corresponding etherate complex, $[Na(Et_2O)_3][(^{iPr}PIEA)Fe(N_2)]$ (ν_{NN} = 1965 cm^{-1}).[25c] As with the neutral cobalt dinitrogen complexes, the presence of a single N≡N stretch for each anion indicates that only one dinitrogen molecule is bound to the metal center.

The ^{1}H NMR spectra of **[Na(THF)$_3$][1-N$_2$]** and **[Na(THF)$_3$][5-N$_2$]** in a 1:1 THF-d_8/benzene-d_6 mixture at 20 °C establish pure diamagnetic ground states for the molecules. Formally cobalt(I) bis(imino)pyridine complexes, such as (^{iPr}PDI)CoCl and (^{iPr}PDI)CoMe, are also diamagnetic but triplet excited states that are only slightly higher in energy (within a few kcal/mol) lead to unusual ^{1}H NMR shifts for the in-plane chelate hydrogens.[7,9] For **[Na(THF)$_3$][1-N$_2$]**, the chemical shifts of the methyl backbone and the *p*-pyridine resonances, 1.85 ppm and 7.07 ppm, respectively, are close to the chemical shifts of the free ligand. The methyl backbone and *p*-pyridine resonances for **[Na(THF)$_3$][5-N$_2$]**, 2.24 ppm and 6.68 ppm, are also close to the chemical shift values for the free ligand.

Oxidation of **[Na(THF)$_3$][1-N$_2$]** with $[Cp_2Fe][BPh_4]$ cleanly furnished **1-N$_2$**, along with ferrocene and $NaBPh_4$ (Figure 1.8). Inspired by this result, oxidation of **[Na(solv)$_3$][5-N$_2$]** with $[Cp_2Fe][BPh_4]$ was also investigated. Because direct two electron reduction of **5-Cl$_2$** generated the bis(chelate) complex, (^{iPr}APDI)$_2$Co, oxidation of **[Na(solv)$_3$][5-N$_2$]** was explored as an alternate route for preparation of a neutral alkyl-substituted bis(imino)pyridine cobalt dinitrogen complex. Unfortunately, treatment of **[Na(solv)$_3$][5-N$_2$]** with $[Cp_2Fe][BPh_4]$ furnished (^{iPr}APDI)$_2$Co and ferrocene with no evidence for formation of other cobalt species (Figure 1.8).

1.4 Electronic Structure of Cobalt Dinitrogen Complexes

With a family of aryl-substituted bis(imino)pyridine cobalt dinitrogen complexes in hand, determination of their electronic structures was undertaken. Based on previous work with bis(imino)pyridine iron complexes,[12] a question that arises from investigation of the cobalt analogs is whether reduction occurs at the ligand or the metal center. The solid state structure of **1-Cl** establishes one electron reduction of the chelate and indicates that the metal center is best described as cobalt(II).[7] Computational studies by Budzelaar and coworkers present **1-Cl** as a low-spin, d^7 cobalt(II) complex with the unpaired metal-based electron antiferromagnetically coupled to a ligand-centered radical.[9] The results of this study were confirmed by Milsmann and Wieghardt, where more modern computational methods successfully reproduced the calculations obtained by Budzelaar and coworkers.[29] In contrast to the series of bis(imino)pyridine iron complexes,[12] the metrical parameters of **1-N_2** suggest that reduction of **1-Cl** occurs at the metal center, furnishing a neutral dinitrogen complex that is best described as cobalt(I) with a singly reduced bis(imino)pyridine chelate. More detailed spectroscopic measurements were carried out to more accurately determine the electronic structure of **1-N_2**.

Variable temperature SQUID magnetometry was used to study the magnetic behavior of **1-N_2** between 4 and 300 K. A nearly temperature-independent effective magnetic moment of 1.77-1.65 μ_B is observed between 300 K and 50 K, consistent with a doublet ground state. Below 50 K, the effective magnetic moment of **1-N_2** undergoes a sharp decrease to 1.37 μ_B at 4 K (Figure 1.9). These measurements are consistent with the solution magnetic moment at 20 °C. The observation of an effective magnetic moment close to the spin-only value for one unpaired electron indicates a radical in a ligand-based orbital. This is also supported by the g value of 1.99 obtained by modeling the variable temperature magnetic data.[30] For a complex

with a square planar ligand field, a larger effective magnetic moment would be expected due to orbital contributions if the electron were located in a principally metal-based orbital.[31]

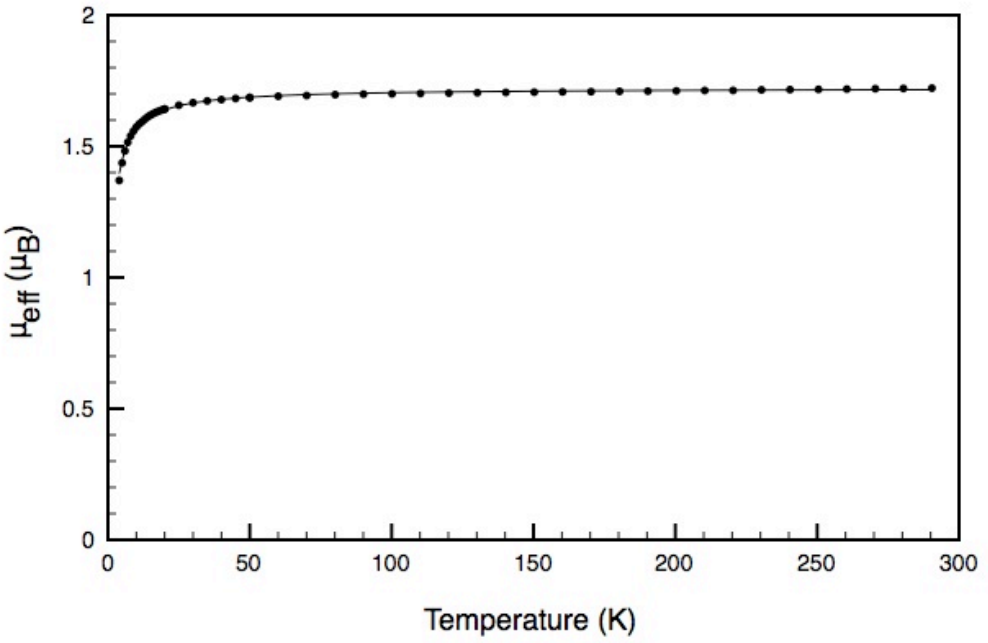

Figure 1.9 Experimental and simulated variable temperature SQUID magnetization data (at 1 T) for **1-N_2**; g = 1.99. Data are corrected for underlying diamagnetism.

The *S* = 1/2 ground state of **1-N_2** is conducive to X-band EPR measurements, which were conducted at 296 K in toluene solution (microwave frequency 9.43 GHz, power 1.26 mW, modulation 1mT/100 kHz). An isotropic g value of 2.003 is observed (Figure 1.10), consistent with an organic radical.[32] The solid state magnetic data for **1-N_2** demonstrates that there is one unpaired electron in the molecule, and the EPR spectrum indicates that the electron resides in a primarily ligand-based orbital. For an unpaired electron in a metal-based orbital, a g value that deviates significantly from the ideal 2.002 is expected.[32] The sigmoidal shape of the spectrum derives from eight overlapping hyperfine lines, arising from hyperfine coupling to the ^{59}Co nucleus (I = 7/2).

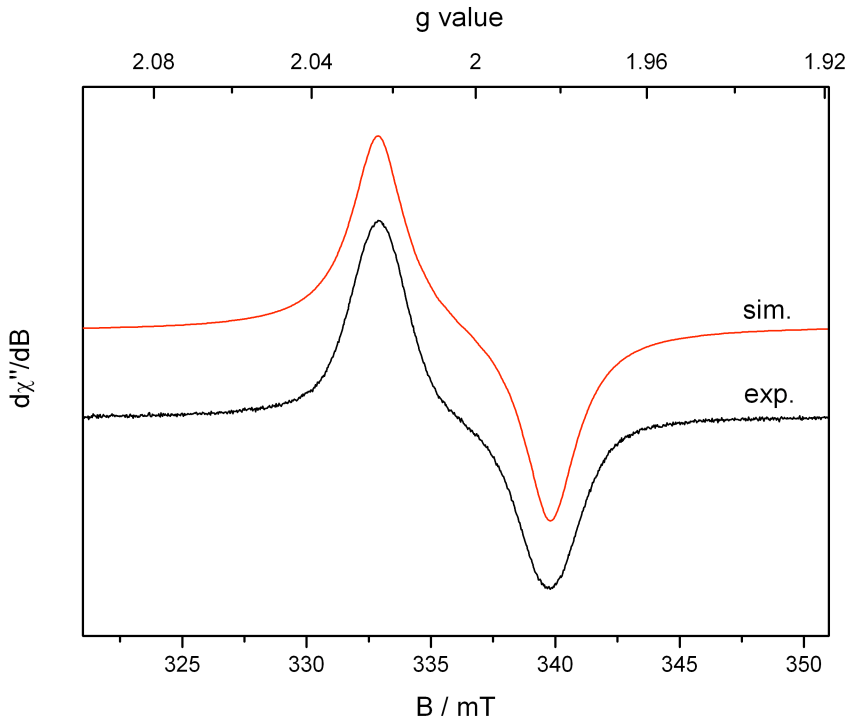

Figure 1.10 Experimental (296 K in toluene solution) and simulated EPR spectra for **1-N$_2$**; g = 2.003, A^{Co} = 8 x 10^{-4} cm^{-1}, line broadening = 32 G.

The spectrum was modeled using an isotropic g value of 2.003, a hyperfine coupling constant (A) of 8 x 10^{-4} cm^{-1} to the ^{59}Co nucleus and a linewidth of 32 G (Figure 1.10).[33] No hyperfine coupling to hydrogen or nitrogen is observed due to the large line width caused by fast relaxation of the cobalt nucleus. The EPR spectrum of a related bis(imino)pyridine aluminum compound, (^{iPr}PDI)AlMe$_2$, exhibits a ligand-centered radical with observable hyperfine coupling to ^{15}N and ^{1}H nuclei. The magnitude of the hyperfine couplings between the ligand-centered radical and the ^{15}N and ^{1}H nuclei is 1-5 x 10^{-4} cm^{-1} in this case.[34] These couplings are smaller than the line broadening for **1-N$_2$**, therefore it is unlikely that hyperfine interactions to ^{15}N and ^{1}H would be observed for **1-N$_2$**.

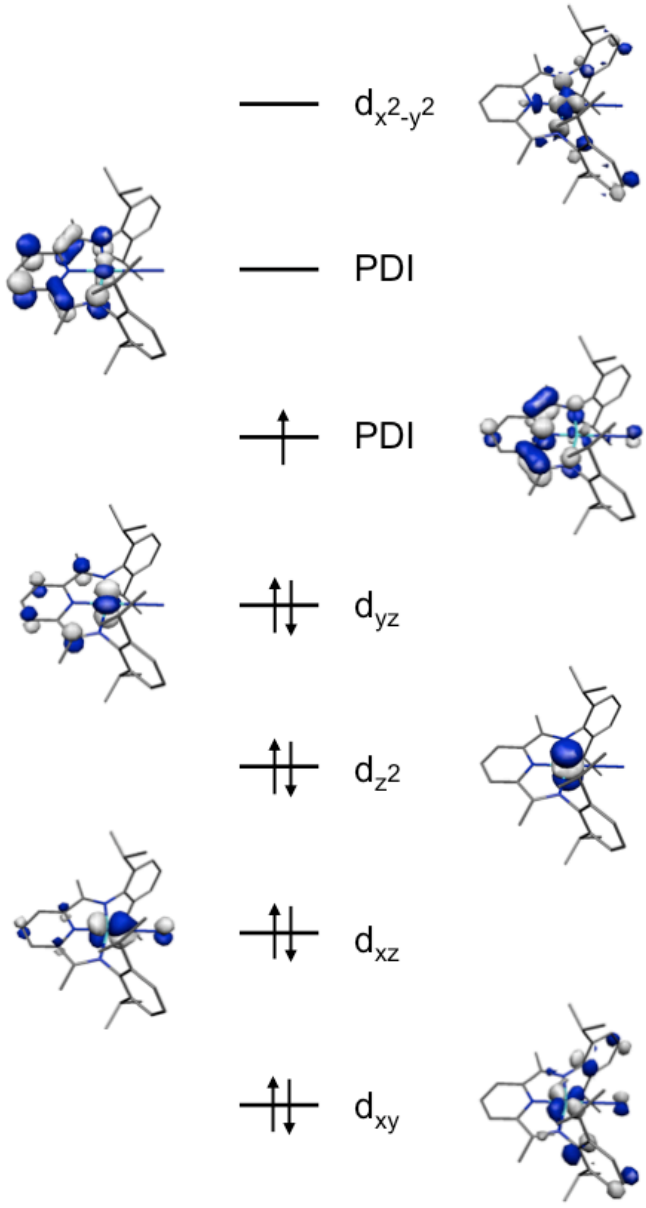

Figure 1.11 DFT computed (B3LYP) qualitative molecular orbital diagram for **1-N_2**.

DFT calculations for **1-N_2** as a spin-unrestricted doublet (B3LYP functional) predict a low-spin cobalt(I) center with an unpaired electron in an essentially ligand-based orbital (Figure 1.11).[35] The LUMO for **1-N_2** is a second PDI π* orbital, while the LUMO+1 is the $d_{x^2-y^2}$ metal orbital. The Mulliken spin density plot also

demonstrates that the unpaired spin resides mainly on the bis(imino)pyridine chelate, with only a small amount of electron density on the metal center (Figure 1.12).

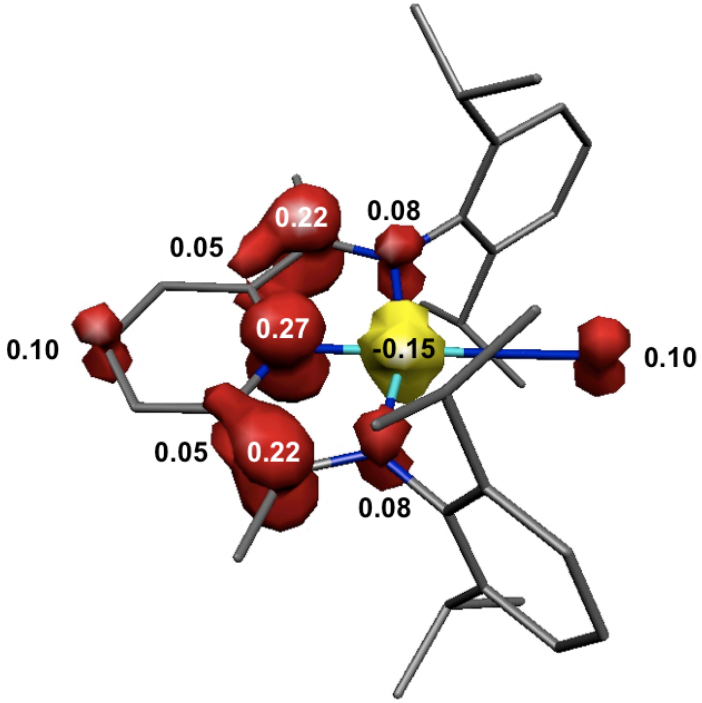

Figure 1.12 Spin density plot for **1-N_2** obtained from a Mulliken population analysis.

The low-spin cobalt(I) description is consistent with the spectroscopic data, which establish a single unpaired electron in a PDI π* orbital and an $S = 1/2$ molecule. The calculated bond lengths for **1-N_2** (Appendix A) are consistent with a monoanionic chelate,[22] and are overall in good agreement with the crystallographic data. The experimental C_{imine}-C_{ipso} bond lengths are somewhat shorter than the distances obtained from DFT calculations, so the possibility of a cobalt(II) center coupled to a doubly reduced bis(imino)pyridine chelate was also examined. However, BS(1,2) and BS(3,2) calculations both converged back to the cobalt(I) solution, suggesting that low-spin cobalt(I) with a ligand-centered radical is the best electronic structure description for **1-N_2**.

As mentioned above, one the C_{imine}-C_{ipso} bonds observed in the X-ray structure of **1-N_2** is shorter than expected for a monoanionic chelate.[22] However, a cobalt(I) d^8 metal center is expected to participate in significant back-bonding with the π* orbitals of the chelate, which could also contribute to the observed contraction in bond length. Thus, the X-ray structure, in combination with the other spectroscopic data and DFT calculations, supports a cobalt(I) center and a singly reduced bis(imino)pyridine ligand. This establishes that while one electron reduction of the bis(imino)pyridine iron monochloride complex occurs at the ligand to afford an iron dinitrogen complex with a doubly reduced chelate, reduction of the cobalt(II) monochloride complex occurs at the metal center to afford a low-spin cobalt(I) species with a singly reduced chelate (Figure 1.13).

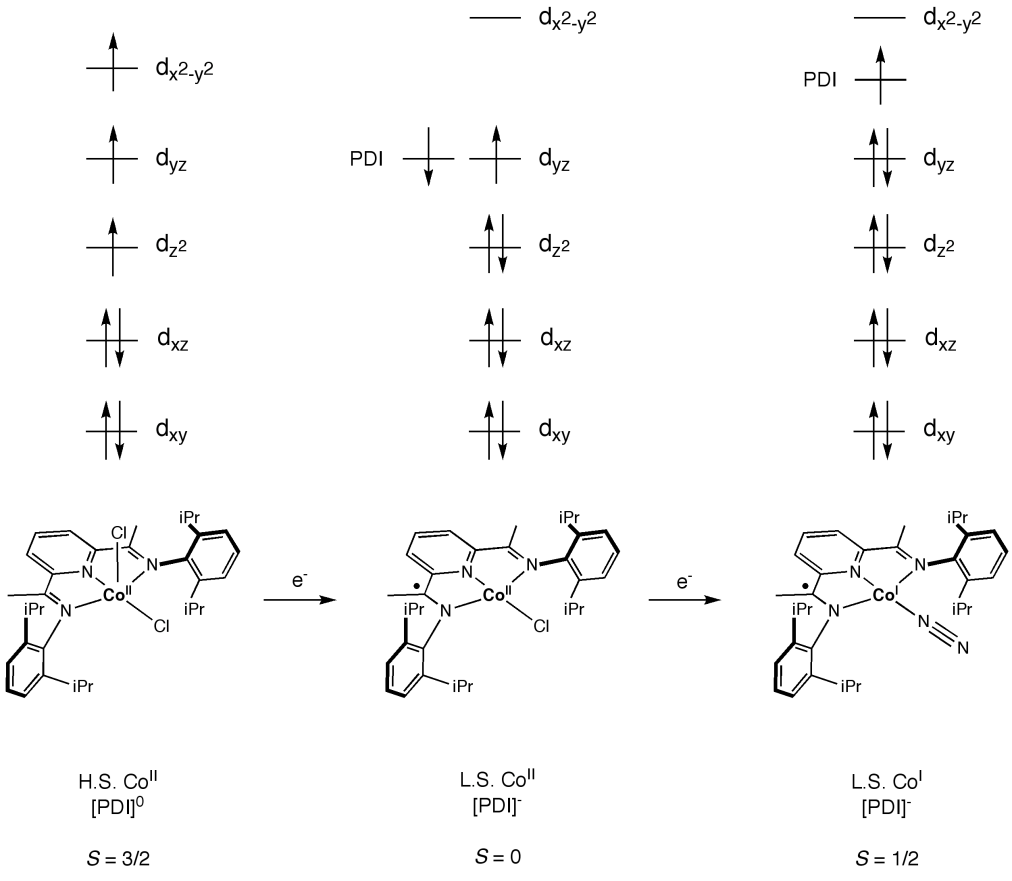

Figure 1.13 Electronic structures of bis(imino)pyridine cobalt complexes.

To describe the electronic structure of the cobalt dinitrogen anions, **[Na(solv)$_3$][1-N$_2$]** and **[Na(solv)$_3$][5-N$_2$]**, a cobalt(I) metal center with a dianionic bis(imino)pyridine chelate is likely, to give an overall $S = 0$ molecule. The observation of a pure $S = 0$ ground state by ^{1}H NMR spectroscopy, with no anomalous in-plane chelate hydrogen resonances, is more consistent with a closed shell dianion description of the chelate than a singlet diradical. DFT calculations for the anionic bis(imino)pyridine cobalt dinitrogen complex (**[1-N$_2$]$^-$**) as a spin-restricted singlet suggest are also consistent with this electronic structure description (Appendix A).[35] As with **1-N$_2$**, a low-spin cobalt(I) metal center is predicted, although with a doubly reduced chelate instead of a singly reduced chelate. The calculated bond distances for **[1-N$_2$]$^-$** are also in agreement with a doubly reduced bis(imino)pyridine ligand (Appendix A).[22] This electronic structure description indicates that reduction of the neutral cobalt dinitrogen complexes occurs at the ligand, rather than the metal center, to furnish the corresponding anionic cobalt(I) dinitrogen complex (Figure 1.14).

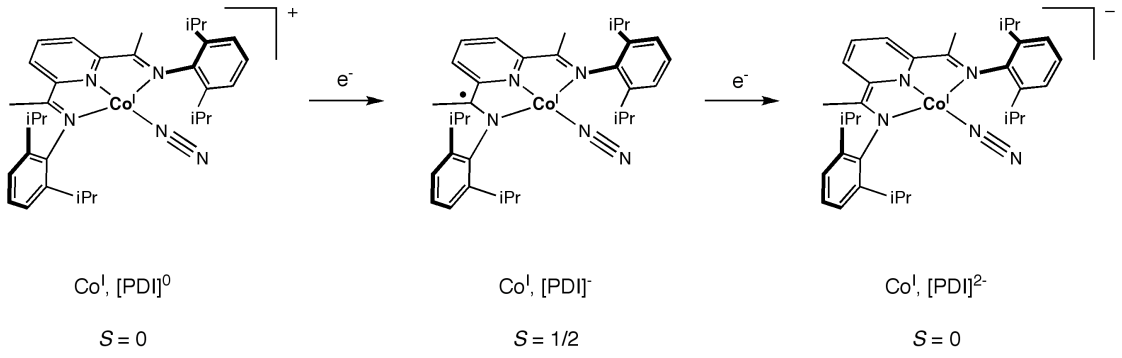

Figure 1.14 Ligand-centered reduction of bis(imino)pyridine cobalt dinitrogen complexes.

The electronic structure of the cationic bis(imino)pyridine cobalt dinitrogen complex, **[1-N$_2$]$^+$**, was also investigated using DFT calculations (B3LYP). Calculation

of **[1-N_2]**$^+$, without the corresponding cation, as a spin-restricted singlet predicts a low-spin cobalt(I) metal center with a neutral bis(imino)pyridine chelate (Table 1.4). The cobalt d_{x2-y2} orbital is empty, while the remaining d-orbitals each contain a pair of electrons, establishing an $S = 0$ metal center. A neutral chelate is indicated by two empty ligand-based orbitals, which comprise the LUMO and LUMO+1 for **[1-N_2]**$^+$. In addition, the calculated C_{imine}-C_{ipso} and C_{imine}-N_{imine} bond lengths of 1.479 Å and 1.302 Å, respectively, are in good agreement with the experimental values (Appendix A) and are consistent with a neutral bis(imino)pyridine chelate.[22]

Table 1.4 Summary of electronic structure descriptions for bis(imino)pyridine cobalt complexes.

Complex	^{iPr}PDI ox. state[a]	Co ox. state	Spin state	ν_{NN} (cm^{-1}) exp.	ν_{NN} (cm^{-1}) calc.
1-Cl_2	0	+2 (H.S.)	$S = 2$	-	-
1-Cl	-1	+2 (L.S.)	$S = 0$	-	-
[1-N_2]$^+$	0	+1 (L.S.)	$S = 0$	2184	2190
[1-N_2]	-1	+1 (L.S.)	$S = 1/2$	2093	2116
[1-N_2]$^-$	-2	+1 (L.S.)	$S = 0$	2046	2041

[a]Assigned based on DFT and X-ray data.

The electronic structure descriptions of the bis(imino)pyridine cobalt dinitrogen complexes, as well as the cobalt dichloride and monochloride complexes, are summarized in Table 1.4. The calculated N≡N stretches for the cobalt dinitrogen complexes are in good agreement with experimental values (Table 1.4), supporting the proposed electronic structures. Elucidation of the electronic structures of the bis(imino)pyridine cobalt dinitrogen complexes highlights the redox activity of the bis(imino)pyridine chelates. Sequential one electron reduction of the cationic and neutral cobalt dinitrogen complexes occurs at the ligand, conserving the cobalt(I)

metal center throughout the series of dinitrogen complexes. Although one electron reduction of the bis(imino)pyridine cobalt dichloride complex occurs at the ligand and maintains the 2+ oxidation state at cobalt,[9] one electron reduction of the bis(imino)pyridine cobalt monochloride complex occurs at the metal center to afford the neutral cobalt(I) dinitrogen complex.

1.5 Preparation of Monochloride and Monomethyl Complexes

Previous investigations into the active species for polymerization by bis(imino)pyridine cobalt have mostly focused on complexes with the ^{iPr}PDI ligand in particular. In addition, little work has been done on the preparation of reduced alkyl-substituted bis(imino)pyridine cobalt complexes. A notable exception is Budzelaar and coworkers recent work with several (^{R}APDI)CoX complexes (^{R}APDI = 2,6-(RN=CMe)$_2$C$_5$H$_3$N; R = *n*-C$_6$H$_{13}$, C$_{18}$H$_{37}$; X = H, Me, Cl).[9] With this in mind, preparation of a series of aryl- and alkyl-substituted cobalt monohalide and monoalkyl complexes was explored. Treatment of **2-Cl$_2$** and **3-Cl$_2$** with one equivalent of sodium triethylborohydride in toluene at -78 °C furnished the corresponding monochloride species, (^{Et}PDI)CoCl (**2-Cl**) and (^{Me}PDI)CoCl (**3-Cl**) (Figure 1.15). Although **2-Cl** and **3-Cl** are diamagnetic, the benzene-d_6 ^{1}H NMR spectra of these compounds at 20 °C exhibit unusual chemical shifts for the in-plane chelate hydrogens. The methyl backbone resonances are shifted upfield to -0.02 ppm (**2-Cl**) and -0.05 ppm (**3-Cl**) while the *p*-pyridine resonances appear downfield at 9.55 ppm (**2-Cl**) and 9.52 ppm (**3-Cl**).

The desired bis(imino)pyridine cobalt monomethyl complexes were prepared by treatment of the appropriate cobalt monochloride with a slight excess of methyllithium in toluene at -95 °C (Figure 1.15). Like the corresponding cobalt monochloride complexes, the benzene-d_6 ^{1}H NMR spectra of (^{Et}PDI)CoMe (**2-Me**)

and (^{Me}PDI)CoMe (**3-Me**) at 20 °C exhibit significantly shifted in-plane chelate resonances. The methyl backbone resonances are shifted upfield to -1.19 ppm for **2-Me** and -1.27 ppm for **3-Me**, while the *p*-pyridine resonances are shifted downfield to 10.17 ppm and 10.10 ppm for **2-Me** and **3-Me**, respectively. The Co-Me resonances appear at 0.58 ppm and 0.53 ppm for **2-Me** and **3-Me**, respectively.

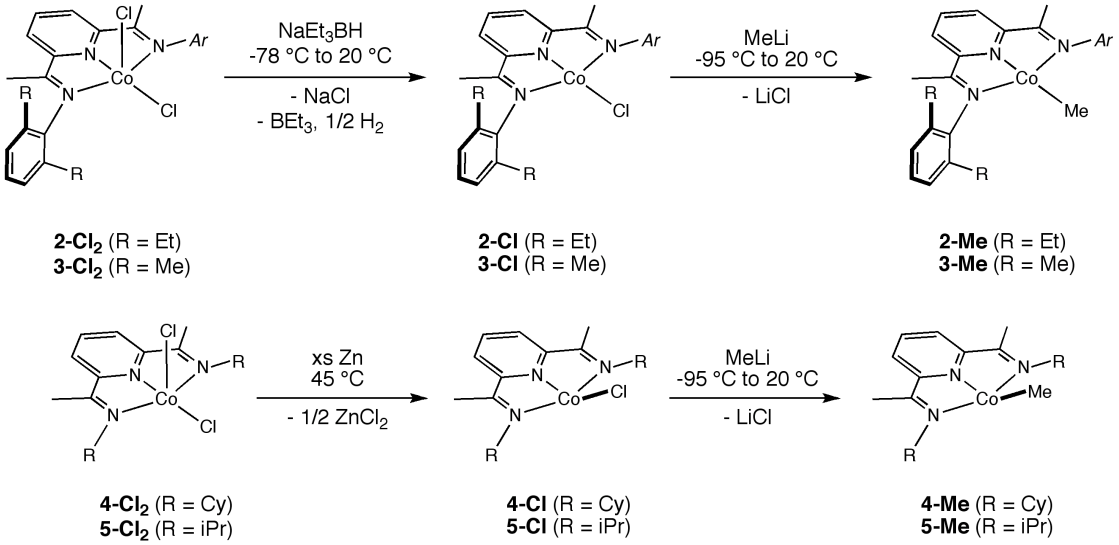

Figure 1.15 Preparation of bis(imino)pyridine cobalt monochloride and monomethyl complexes.

The one electron reduction products of the related alkyl-substituted bis(imino)pyridine cobalt dichloride complexes are strikingly different. Treatment of **4-Cl$_2$** and **5-Cl$_2$** with excess zinc metal in toluene at 45 °C furnished the desired monochloride species, (^{Cy}APDI)CoCl (**4-Cl**) and (^{iPr}APDI)CoCl (**5-Cl**), respectively (Figure 1.15). However, in contrast to the aryl bis(imino)pyridine complexes, the benzene-d_6 ^{1}H NMR spectra of **4-Cl** and **5-Cl** at 20 °C exhibit large chemical shift ranges (> 60 ppm) and paramagnetically broadened resonances. The solution magnetic moments at 23 °C for **4-Cl** and **5-Cl** of 2.5(2) μ_B and 1.0(2) μ_B, respectively, further

establish the paramagnetism of these complexes. A more detailed analysis of the magnetic properties of **4-Cl** and **5-Cl** is presented below.

The molecular structure of **5-Cl** was determined by single crystal X-ray diffraction and establishes a distorted square planar molecule (Figure 1.16). The chlorine atom is lifted significantly out of the idealized plane of the molecule, with an N_{pyr}-Co-Cl angle of 150.73(5)°. In contrast, **1-Cl** has idealized square planar geometry, with the sum of the angles around cobalt equal to 359.99(24)° and a N_{pyr}-Co-Cl angle of 179.15(10)°.[7] The Co-Cl bond length in **5-Cl** is 2.2188(6) Å, similar to the distance of 2.1807(10) Å observed for **1-Cl**.[7] Examination of the metrical parameters of **5-Cl** establishes distortions to the bis(imino)pyridine chelate that are diagnostic of one electron reduction. The C_{imine}-N_{imine} bond lengths, 1.321(3) Å and 1.314(3) Å, are elongated from neutral ligand reference values,[22] while the C_{imine}-C_{ipso} distances are contracted to 1.435(3) Å and 1.438(3) Å.

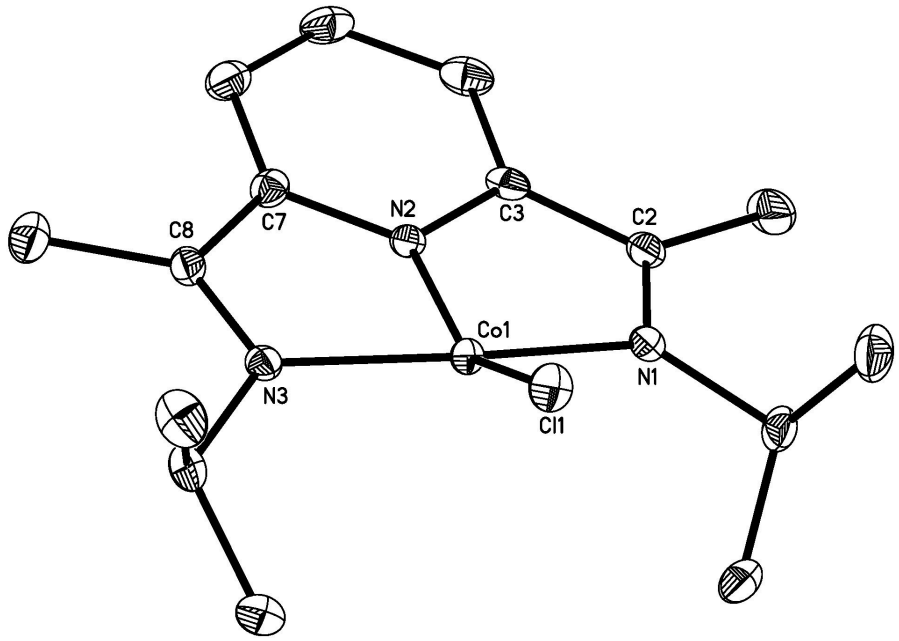

Figure 1.16 Molecular structure of **5-Cl** at 30 % probability ellipsoids. Hydrogen atoms omitted for clarity.

Table 1.5 Selected bond distances (Å) and angles (°) for **5-Cl**.

Co(1)-Cl(1)	2.2188(6)	N(3)-C(8)	1.314(3)
Co(1)-N(1)	1.9334(15)	C(2)-C(3)	1.435(3)
Co(1)-N(2)	1.7870(16)	C(7)-C(8)	1.438(3)
Co(1)-N(3)	1.9203(16)	N(2)-Co(1)-Cl(1)	150.73(5)
N(1)-C(2)	1.321(3)		

Because the alkyl bis(imino)pyridine cobalt monochloride complexes proved to be different from their aryl counterparts both electronically and geometrically, preparation of the corresponding monomethyl compounds was also explored. Treatment of **4-Cl** and **5-Cl** with a slight excess of methyllithium in toluene at -95 °C followed by warming to ambient temperature furnished (^{Cy}APDI)CoMe (**4-Me**) and (^{iPr}APDI)CoMe (**5-Me**), respectively, upon warming to room temperature (Figure 1.15). The benzene-d_6 ^{1}H NMR spectra of **4-Me** and **5-Me** at 20 °C establish diamagnetic ground states, unlike the corresponding monochloride complexes. Similar to the (^{Ar}PDI)CoMe complexes, upfield-shifted methyl backbone resonances at 0.13 ppm (**4-Me**) and 0.14 ppm (**5-Me**) are observed, while the *p*-pyridine resonances are shifted downfield to 9.15 ppm (**4-Me**) and 9.41 ppm (**5-Me**).

The molecular structure of **5-Me** exhibits a distorted square planar geometry almost identical to **5-Cl**, with a N_{pyr}-Co-C_{Me} angle of 147.11(8)° (Figure 1.17). In contrast, **1-Me** exhibits idealized square planar geometry, with the sum of the angles around cobalt equal to 359.98(24)°.[36] A Co-C_{Me} bond length of 1.967(2) Å is observed, similar to the Co-C_{Me} distance of 1.960(4) Å for **1-Me**.[36] Compared to neutral ligand reference values,[22] elongated C_{imine}-N_{imine} bonds, 1.326(2) Å and

1.326(2) Å, and contracted C_{imine}-C_{ipso} bonds, 1.440(3) Å and 1.434(3) Å, are observed (Table 1.5). These distortions are consistent with one electron reduction of the chelate,[22] similar to **5-Cl**.

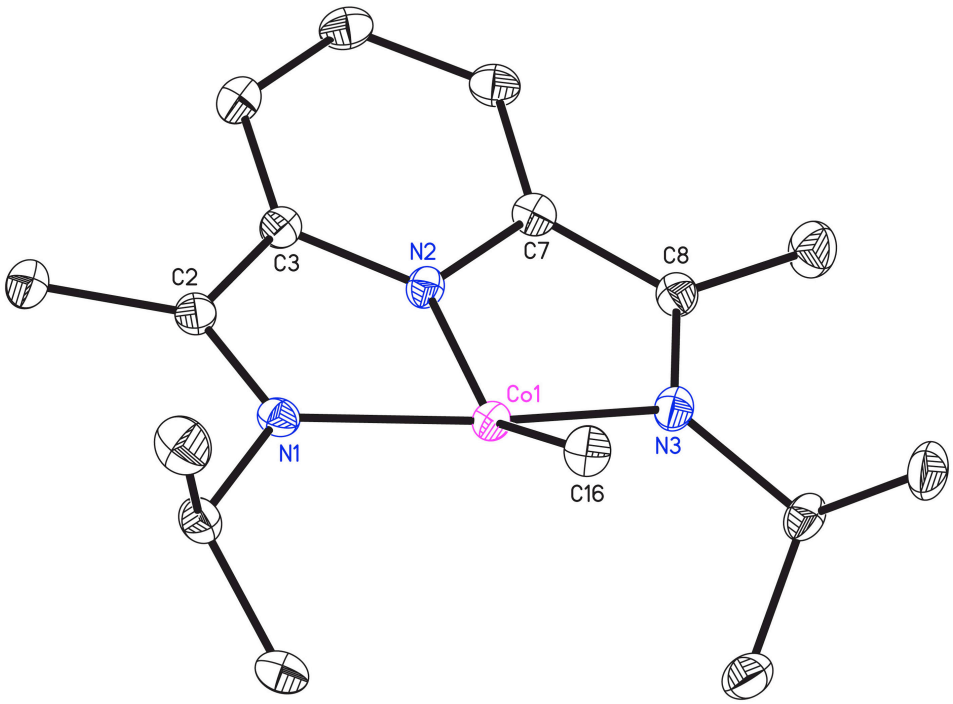

Figure 1.17 Molecular structure of **5-Me** at 30 % probability ellipsoids. Hydrogen atoms omitted for clarity.

Table 1.6 Selected bond distances (Å) and angles (°) for **5-Me**.

Co(1)-C(16)	1.967(2)	N(3)-C(8)	1.326(2)
Co(1)-N(1)	1.9228(16)	C(2)-C(3)	1.440(3)
Co(1)-N(2)	1.8072(16)	C(7)-C(8)	1.434(3)
Co(1)-N(3)	1.9103(16)	N(2)-Co(1)-C(16)	147.11(8)
N(1)-C(2)	1.326(2)		

1.6 Comparison of Monochloride and Monomethyl Complexes

Previous studies of **1-Cl** and **1-Me**[7,10,36] indicate that both complexes have idealized square planar geometry, with a low-spin cobalt(II) center antiferromagnetically coupled to a ligand centered-radical to give an overall diamagnetic complex. The additional aryl-substituted bis(imino)pyridine cobalt monochloride and monomethyl complexes discussed herein appear to have similar geometric and electronic structures as **1-Cl** and **1-Me** (Table 1.7). However, the unexpected paramagnetism of **4-Cl** and **5-Cl** and the non-planar geometries of **5-Cl** and **5-Me** prompted further investigation. The spectroscopic and magnetic properties of the bis(imino)pyridine cobalt monochloride and monomethyl complexes are summarized in Table 1.7.

Table 1.7 Summary of spectroscopic and magnetic properties for bis(imino)pyridine cobalt monochloride and monomethyl complexes at 20 °C.

Complex	N_{pyr}-Co-X (°)[a]	Spin state	N=C(CH_3) (ppm)	*p-pyr* (ppm)
1-Cl[6]	179.15(10)	$S = 0$	0.05	9.53
2-Cl	-	$S = 0$	-0.02	9.55
3-Cl	-	$S = 0$	-0.05	9.52
4-Cl	-	$S = 1$	-22.79	66.27
5-Cl	150.73(5)	$S = 1$	-12.62	41.60
1-Me[6]	178.94(17)	$S = 0$	-1.15	10.19
2-Me	-	$S = 0$	-1.19	10.17
3-Me	-	$S = 0$	-1.27	10.10
4-Me	-	$S = 0$	0.13	9.41
5-Me	147.11(8)	$S = 0$	0.14	9.15

[a]X-ray data collected at 173 K.

Variable temperature SQUID magnetic measurements were collected between 4 K and 300 K for both **4-Cl** and **5-Cl**. For **4-Cl**, a steep decrease in effective magnetic moment from 2.67 μ_B to 0.23 μ_B is observed with decreasing temperature, characteristic of spin-crossover behavior (Figure 1.18). The variable temperature magnetic data establish a singlet state below ~ 50 K, and a triplet state at ambient temperature. This is supported by the solution magnetic moment of 2.5(2) μ_B and the paramagnetic features of the ^{1}H NMR spectrum at 23 °C. The observation of a non-zero effective magnetic moment even at 4 K indicates the presence of temperature independent paramagnetism for **4-Cl**.

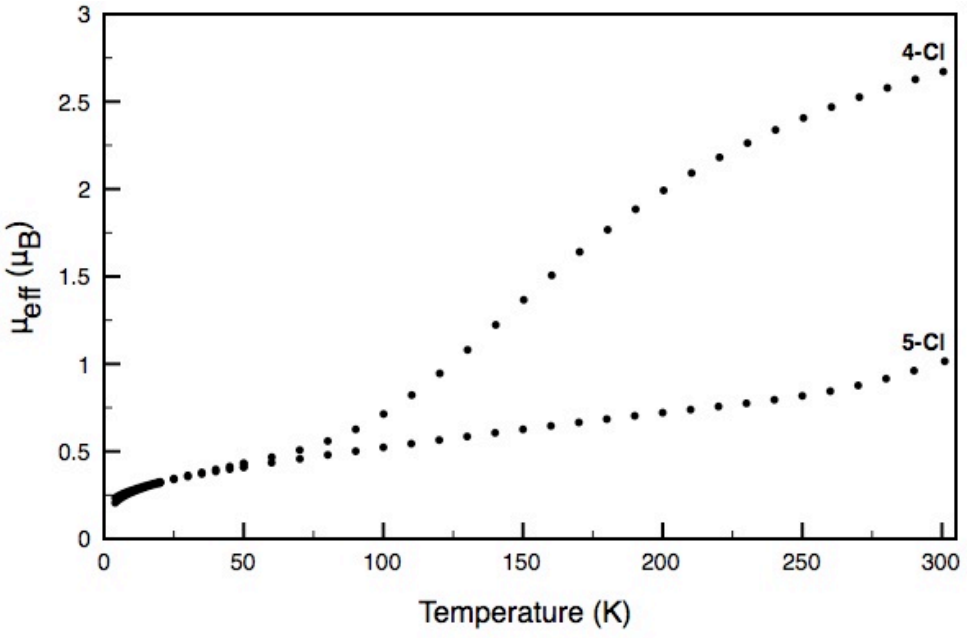

Figure 1.18 Variable temperature SQUID magnetization data (at 1 T) for **4-Cl** and **5-Cl**. Data are corrected for underlying diamagnetism.

Variable temperature magnetic data suggest that **5-Cl** also exhibits spin-crossover behavior, albeit less pronounced than **4-Cl**. A steady decrease in effective magnetic moment from 1.01 μ_B to 0.21 μ_B is observed upon cooling from 300 K to 4

K (Figure 1.18). An $S = 0$ ground state is observed at very low temperatures, however full conversion to the $S = 1$ state is not achieved upon warming to 300 K. The solution magnetic moment of 1.0(2) μ_B at 23 °C also indicates incomplete spin-crossover. As with **4-Cl**, the observation of a non-zero effective magnetic moment at 4 K indicates the presence of temperature independent paramagnetism for **5-Cl**.

Variable temperature ^{1}H NMR spectroscopy in benzene-d_6 demonstrates that upon warming to 65 °C, the chemical shifts of the methyl backbone and the *p*-pyridine resonances for **5-Cl** approach the values observed for **4-Cl** at 23 °C (Figure 1.19). Additionally, upon cooling a toluene-d_8 solution of **4-Cl** to -60 °C, a large decrease in the chemical shift range is observed, although the resonances are still outside the normal diamagnetic range at this temperature (Figure 1.19).

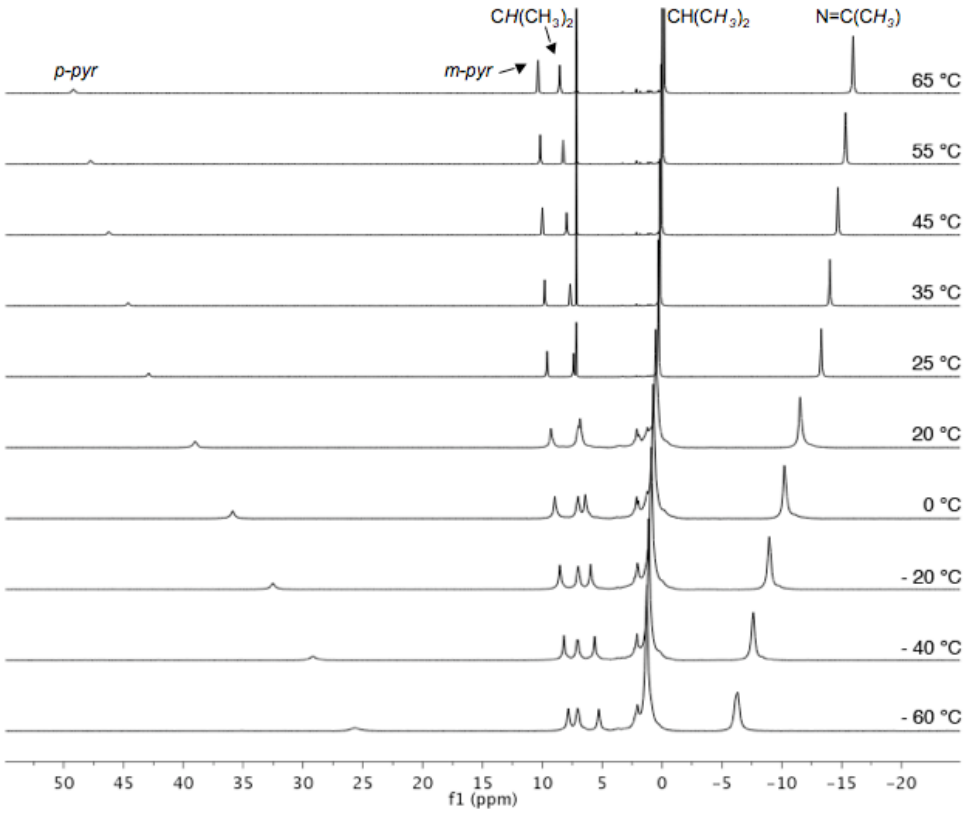

Figure 1.19 Variable temperature ^{1}H NMR spectra of **5-Cl** in benzene-d_6 (25 °C to 65 °C) and toluene-d_8 (-60 °C to 20 °C).

To explore whether the alkyl bis(imino)pyridine cobalt monomethyl complexes exhibit spin-crossover behavior similar to the monochloride complexes at higher temperatures, variable temperature ^{1}H NMR spectra of **5-Me** were obtained between 25 °C to 65 °C (Figure 1.20). No substantial increase in the chemical shift range was observed, although the *p*-pyridine resonance shifts slightly downfield. Notably, the Co-Me resonance broadens and shifts significantly downfield from 2.05 ppm to 5.00 ppm upon heating. Significant broadening was not observed for any other resonances in the spectra, including the methyl backbone and the *p*-pyridine.

Similar behavior has been observed for cobalt(III) porphyrin[37] and macrocyclic[38] alkyl complexes, where the ^{1}H NMR resonances for the alkyl group directly bound to the metal center shift downfield with increasing temperature. For the six-coordinate macrocyclic cobalt(III) complex, [Co($C_{10}H_{14}N_8$)(MeNHNH$_2$)(Me)], the Co-Me resonance shifted by 0.57 ppm when warming from -50 °C to 50 °C,[37] while for the five-coordinate cobalt(III) porphyrin complex, [Co($C_{36}H_{44}N_4$)(Me)], the Co-Me resonance shifted 0.19 ppm downfield and broadened when warming from -55 °C to 55 °C.[38] In both cases, the other ligand ^{1}H NMR resonances did not shift significantly over the same temperature ranges. Similar broadening of the ^{1}H NMR hydride resonance was observed for cobalt cluster compounds, HM$Co_3(CO)_{12}$ (M = Fe, Ru), upon warming from -50 °C to 27 °C.[39] For both the cobalt porphyrin and cluster compounds, the broadening is attributed to the quadrupolar effect of the ^{59}Co nucleus (I = 7/2).

Thus, it is likely that the observed change in ^{1}H NMR chemical shift for the Co-Me resonance of **5-Me** is due to thermal population of a low-lying triplet state. Because no significant changes are observed for the bis(imino)pyridine ligand ^{1}H NMR resonances, the population of the triplet state for **5-Me** must be small compared

to **5-Cl**. The increased linewidth of the Co-Me resonance may result from population of the triplet state, however it is also possible that the observed broadening arises from the quadrupolar effect of the ^{59}Co nucleus (I = 7/2) to which it is directly bound.

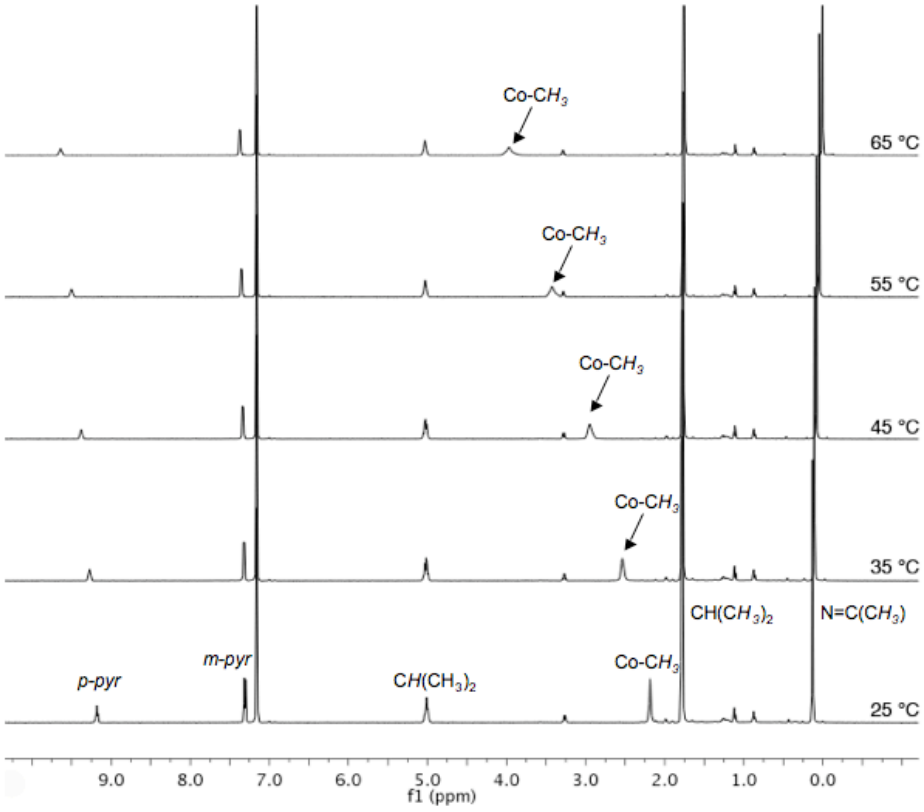

Figure 1.20 Variable temperature ^{1}H NMR spectra of **5-Me** in benzene-d_6.

Computational studies by Budzelaar and coworkers on a series of (^{Ar}PDI)CoX and (^{R}APDI)CoX compounds (X = H, Me, Cl) predicted consistently smaller singlet-triplet gaps for cobalt monomethyl complexes than cobalt monochloride complexes, although the difference is less than 3.0 kcal/mol.[10] Alkyl-substituted bis(imino)pyridine cobalt complexes were also predicted to have smaller singlet-triplet gaps than the corresponding aryl-substituted bis(imino)pyridine cobalt complexes,[10] which has been experimentally verified when X = Cl. However, contrary to

computational predictions, spin-crossover is observed for (^{R}APDI)CoX when X = Cl with no evidence of similar behavior when X = Me. This may be due to the weaker field strength of the chloride ligand. When X = Me, the better sigma donating ability of the ligand raises the energy of the $d_{x^2-y^2}$ orbital, preventing thermal access to the triplet state over the temperature range studied.

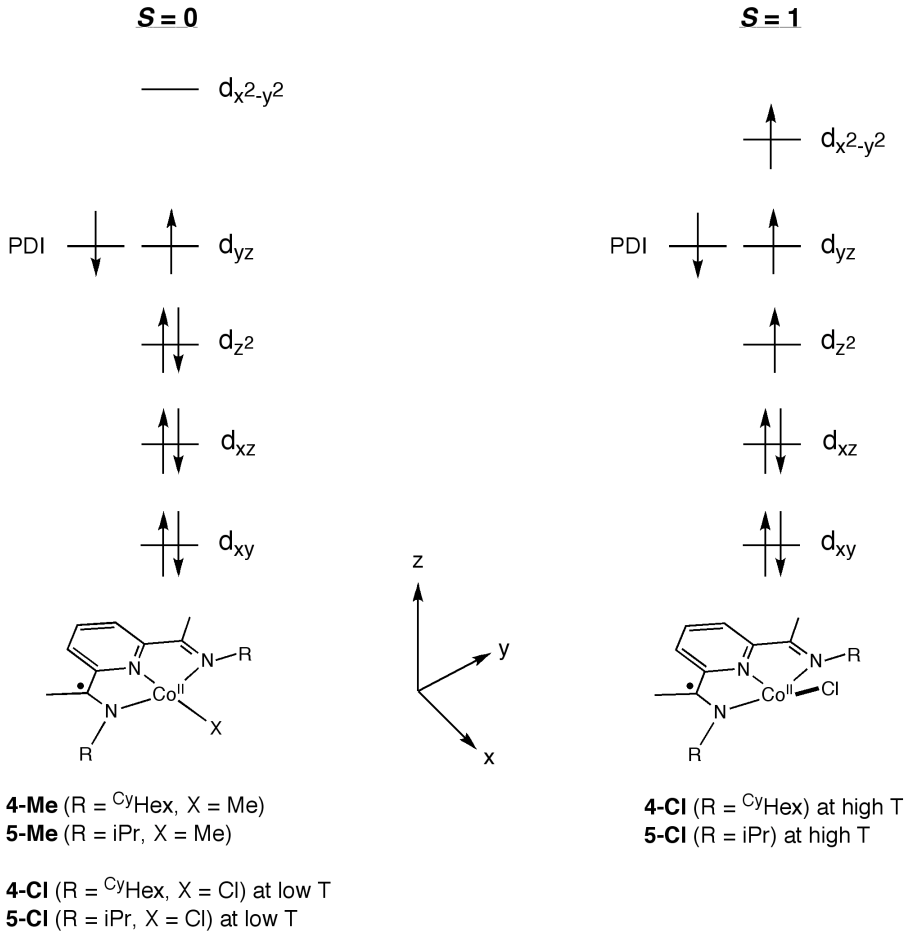

Figure 1.21 Electronic structure descriptions for singlet and triplet states of alkyl bis(imino)pyridine cobalt complexes.

Bis(imino)pyridine cobalt monohydride and monomethyl complexes are predicted to have non-planar geometries when optimized using restricted DFT, with the substituent lifted approximately 20° out of the plane.[9] This is observed

experimentally for alkyl-substituted bis(imino)pyridine cobalt complexes with methyl and chloride substituents. However, optimization at the unrestricted DFT level predicts square-planar geometries for all complexes, as is observed experimentally for aryl-substituted bis(imino)pyridine cobalt complexes.[5,6] This may be related to the greater population of the triplet state for the alkyl-substituted cobalt complexes. For four-coordinate, low-spin cobalt(II) complexes, a square-planar geometry is predicted to have the greatest crystal field stabilization energy.[40] However, for four-coordinate, high-spin cobalt(II) complexes a tetrahedral geometry would be more stable.[40] Because the bis(imino)pyridine chelate prevents a tetrahedral geometry, a distorted square-planar geometry is observed instead.

Based on previous study of **1-Cl** and **1-Me**,[10] the aryl-substituted bis(imino)pyridine cobalt monochloride and monomethyl complexes are best described as having a low-spin cobalt(II) center (S_{Co} = 1/2) antiferromagnetically coupled to a ligand-centered radical (S_{PDI} = 1/2) to give an overall diamagnetic complex. The molecular structure of **5-Me** and diamagnetic ground states of **4-Me** and **5-Me** establish that this electronic structure description also likely applies to alkyl-substituted bis(imino)pyridine cobalt monomethyl complexes (Figure 1.21). Because ligand reduction is also observed for **4-Cl** and **5-Cl**, the triplet state is best described as high-spin cobalt(II) (S_{Co} = 3/2) antiferromagnetically coupled to a mono-reduced chelate (S_{PDI} = 1/2). The difference between a high-spin and a low-spin cobalt(II) center should be evident from examination of the Co-N_{imine} and Co-N_{pyr} bond lengths.[3,7] However, the solid state structure of **5-Cl** was obtained at 173 K, where a majority of the molecules are in the singlet state, and thus the metal-ligand bond lengths cannot be used to differentiate the possible electronic structures for the triplet state.

1.7 Reactivity of Reduced Bis(imino)pyridine Cobalt Complexes

Inspired by the isolation of a series of reduced bis(imino)pyridine cobalt complexes, further reactivity was explored. Exposure of a toluene solution of **1-N_2** to excess carbon monoxide at -196 °C furnished the desired carbonyl complex, (^{iPr}PDI)Co(CO) (**1-CO**), upon warming to ambient temperature (Figure 1.22). The benzene-d_6 ^{1}H NMR spectrum of **1-CO** at 23 °C exhibits four paramagnetically broadened resonances, similar to (^{Ar}PDI)Co(N_2). The infrared spectrum of **1-CO** in toluene establishes binding of one carbon monoxide ligand, with a single, intense C≡O stretch at 1975 cm^{-1}. The frequency of the C≡O stretch for **1-CO** is similar to one stretch observed for the analogous iron carbonyl complex, (^{iPr}PDI)Fe($CO)_2$ (ν_{CO} = 1974, 1914 cm^{-1}).[14]

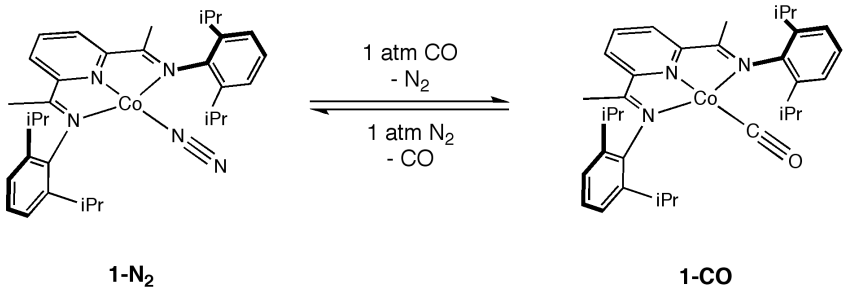

Figure 1.22 Preparation of a bis(imino)pyridine cobalt carbonyl complex.

The relative binding affinities of the N_2 and CO ligands towards the reduced cobalt center were explored using variable temperature *in situ* infrared spectroscopy (Figure 1.23). A toluene solution of **1-N_2** was exposed to vacuum at -78 °C, with no apparent loss of the dinitrogen ligand. Introduction of one atmosphere of carbon monoxide -78 °C rapidly generated the carbonyl complex, **1-CO**, with complete disappearance of **1-N_2**. Removal of the carbon monoxide atmosphere did not result in any loss of the CO ligand. The carbonyl complex persisted upon re-exposure to a

dinitrogen atmosphere at -78 °C. However, ^{1}H NMR spectroscopy indicates that complete removal of volatiles from a solution of **1-CO**, followed by re-dissolution in benzene-d_6 at 23 °C leads to regeneration of **1-N$_2$**.

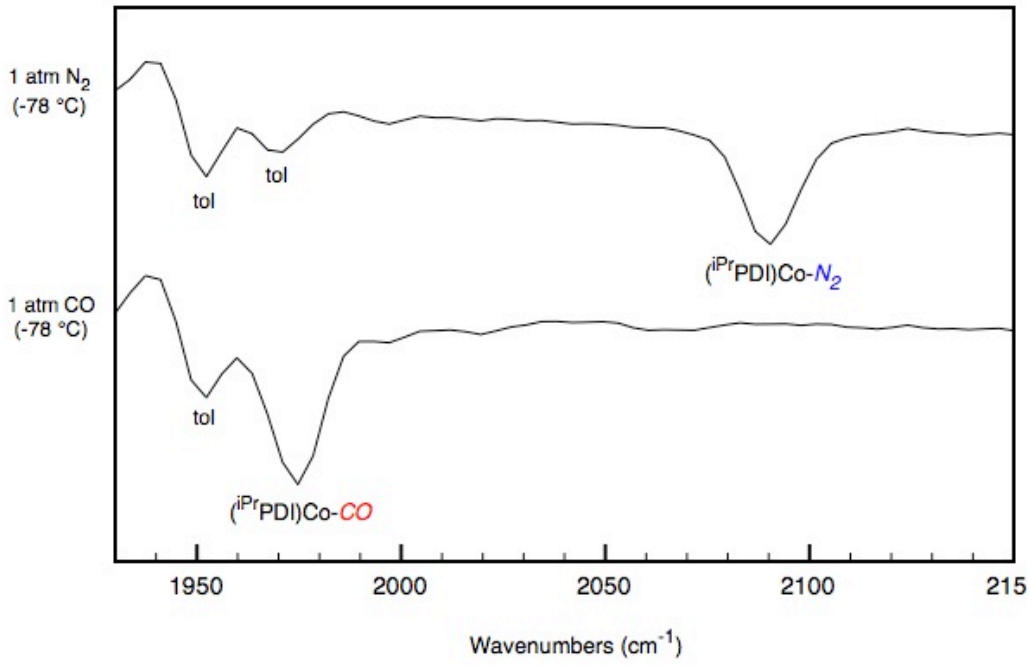

Figure 1.23 *In situ* infrared spectroscopy for toluene solutions of **1-N$_2$** and **1-CO** at -78 °C.

With the goal of preparing a bis(imino)pyridine cobalt nitride complex in mind, the analogous cobalt azide and nitrosyl complexes were investigated. Treatment of a tetrahydrofuran solution of **1-Cl** with five equivalents of sodium azide at 23 °C resulted in quantitative conversion to the bis(imino)pyridine cobalt azide complex, (^{iPr}PDI)CoN$_3$ (**1-N$_3$**), after three days (Figure 1.24). Like **1-Cl**, the benzene-d_6 ^{1}H NMR spectrum of **1-N$_3$** at 20 °C establishes that **1-N$_3$** is diamagnetic, and exhibits the number of resonances expected for a C_{2v} symmetric compound. The in-plane chelate resonances are shifted significantly from diamagnetic reference values, as is observed with many other bis(imino)pyridine cobalt complexes with mono-X type ligands.[6,7]

The methyl backbone resonance is shifted upfield to 0.17 ppm, while the *p*-pyridine is shifted downfield to 9.16 ppm. The infrared spectrum (toluene) of **1-N$_3$** exhibits an intense stretch at 2055 cm^{-1}.

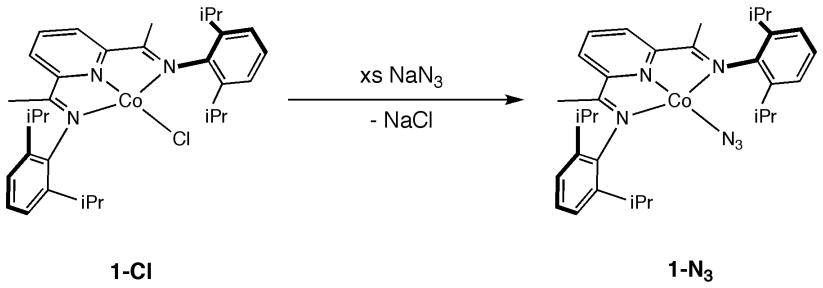

Figure 1.24 Preparation of a bis(imino)pyridine cobalt azide complex.

Attempts were made, using both thermal and photochemical techniques, to induce dinitrogen loss to generate the corresponding bis(imino)pyridine cobalt nitride complex, (^{iPr}PDI)CoN. Heating a benzene-d_6 solution of **1-N$_3$** under vacuum to 65 °C for 48 hours produced no change in the reaction mixture. Similarly, heating **1-N$_3$** in the solid state under vacuum to 65 °C for 48 hours produced no change. Irradiating a toluene solution of **1-N$_3$** in a quartz reaction vessel with 365 nm or 254 nm light for one hour also produced no change.

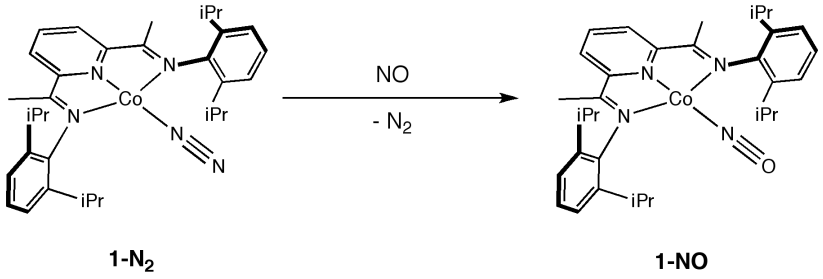

Figure 1.25 Preparation of a bis(imino)pyridine cobalt nitrosyl complex.

The bis(imino)pyridine cobalt nitrosyl complex, (^{iPr}PDI)Co(NO) (**1-NO**) was prepared by treatment of a diethyl ether solution of the cobalt dinitrogen complex, **1-**

N₂, with one equivalent of NO gas at 23 °C (Figure 1.25). The benzene-d_6 ^{1}H NMR spectrum of **1-NO** at 20 °C establishes a diamagnetic, C_{2v} symmetric molecule. Unlike **1-N₃**, no anomalous in-plane chelate hydrogen resonances are observed for **1-NO**. Both the methyl backbone and p-pyridine resonances are close to the values for the free ligand at 2.05 ppm and 6.98 ppm, respectively. The strong field nitrosyl ligand likely results in a larger singlet-triplet gap than is generally observed for (^{iPr}PDI)CoX complexes (X = H, Me, Cl),[9] with little to no population of the triplet state at 20 °C. Infrared spectroscopy (toluene solution) indicates an intense NO stretch at 1711 cm^{-1}. Attempts to obtain the corresponding nitride, (^{iPr}PDI)CoN, through deoxygenation by treating a benzene-d_6 solution of **1-NO** with (silox)$_3$Ta[41] at 23 °C were unsuccessful.

1.8 Conclusions

A series of reduced bis(imino)pyridine cobalt complexes has been prepared and their electronic structures explored. Investigation of several neutral bis(imino)pyridine cobalt dinitrogen complexes, (^{Ar}PDI)Co(N$_2$) (^{Ar}PDI = ^{iPr}PDI, ^{Et}PDI, ^{Me}PDI), established that reduction of monochloride precursors occurs at the metal center, in contrast to the related bis(imino)pyridine iron bis(dinitrogen) complex, (^{iPr}PDI)Fe(N$_2$)$_2$, where reduction of the chelate is observed. Infrared spectroscopy demonstrates that the cobalt metal center is less reducing than iron for this series of compounds. The doublet ground state of the cobalt dinitrogen complexes derives from a singly reduced chelate (S_{PDI} = 1/2) that is coupled to the low-spin d^8 metal center (S_{Co} = 0). X-band EPR spectroscopy and variable temperature magnetic data verify that the unpaired electron is located in an essentially ligand-based orbital. Further reduction furnished the diamagnetic anionic cobalt dinitrogen complexes [(^{iPr}PDI)Co(N$_2$)][Na(solv)$_3$] and [(^{iPr}APDI)Co(N$_2$)][Na(solv)$_3$]. DFT calculations on the cationic, neutral and anionic dinitrogen complexes indicate that each complex has

a low-spin cobalt(I) metal center, and reduction occurs at the chelate throughout the series of cobalt dinitrogen complexes. Examination of a series of (^{Ar}PDI)CoX (X = Cl, Me; ^{Ar}PDI = ^{Et}PDI, ^{Me}PDI) compounds established a similar electronic structure to (^{iPr}PDI)CoX (X = Cl, Me), where a low-spin cobalt(II) center is antiferromagnetically coupled to a monoanionic bis(imino)pyridine chelate. Furthermore, (^{R}APDI)CoMe complexes (^{R}APDI = ^{Cy}APDI, ^{iPr}APDI) were also consistent with this electronic structure description. Spin-crossover behavior was observed for the related (^{R}APDI)CoCl complexes (^{R}APDI = ^{Cy}APDI, ^{iPr}APDI), with a transition from $S = 0$ to $S = 1$ upon warming from 4 K to 300 K for (^{Cy}APDI)CoCl. For (^{iPr}APDI)CoCl the spin transition was incomplete at 300 K, although a substantial increase in the effective magnetic moment from 4 K was observed. The singlet state of the monochloride complexes is best described as low-spin cobalt(II) with antiferromagnetic coupling to a ligand-centered radical. The triplet state can be described as a high-spin cobalt(II) antiferromagnetically coupled to a monoreduced chelate.

1.9 Experimental Procedures

General Considerations. All air- and moisture-sensitive manipulations were carried out using standard vacuum line, Schlenk, and cannula techniques or in an MBraun inert atmosphere dry box containing an atmosphere of purified nitrogen. Solvents for air- and moisture-sensitive manipulations were initially dried and deoxygenated using literature procedures.[42] Benzene-d_6 was purchased from Cambridge Isotope Laboratories and dried over 4 Å molecular sieves. ^{iPr}p-^{t}BuPDI was prepared according to the literature procedure.[43] The complexes **1-Cl$_2$**,[4] **2-Cl$_2$**,[44] **3-Cl$_2$**[44] and $[Cp_2Fe][BPh_4]$[45] were prepared according to literature procedures. ^{tBu}**1-Cl$_2$** was prepared according to the literature procedure for **1-Cl$_2$**[4] using ^{iPr}p-^{tBu}PDI and $CoCl_2$.

^{1}H NMR spectra were recorded on Varian Mercury 300, Inova 400, 500, and 600 spectrometers operating at 299.76, 399.78, 500.62, and 599.78 MHz, respectively. ^{13}C NMR spectra were recorded on an Inova 500 spectrometer operating at 125.893 MHz. All ^{1}H and ^{13}C NMR chemical shifts are reported relative to $SiMe_4$ using the ^{1}H (residual) and ^{13}C chemical shifts of the solvent as a secondary standard. For diamagnetic complexes, many assignments were made based on COSY and HSQC NMR experiments. Solution magnetic moments were determined by Evans method[46] using a ferrocene standard and are the average value of at least two independent measurements. Gouy balance measurements were performed with a Johnson Matthey instrument that was calibrated with $HgCo(SCN)_4$. Peak widths at half heights are reported for paramagnetically broadened and shifted resonances. Infrared spectra were collected on a Thermo Nicolet spectrometer. Elemental analyses were performed at Robertson Microlit Laboratories, Inc., in Madison, NJ.

Single crystals suitable for X-ray diffraction were coated with polyisobutylene oil in a drybox, transferred to a nylon loop and then quickly transferred to the goniometer head of a Bruker X8 APEX2 diffractometer equipped with a molybdenum X-ray tube (λ = 0.71073 Å). Preliminary data revealed the crystal system. A hemisphere routine was used for data collection and determination of lattice constants. The space group was identified and the data were processed using the Bruker SAINT+ program and corrected for absorption using SADABS. The structures were solved using direct methods (SHELXS) completed by subsequent Fourier synthesis and refined by full-matrix least-squares procedures.

SQUID magnetization data of crystalline powdered samples were recorded with a SQUID magnetometer (Quantum Design) at 10 kOe between 5 and 300 K for all samples. Values of the magnetic susceptibility were corrected for the underlying diamagnetic increment by using tabulated Pascal constants and the effect of the blank

sample holders (gelatin capsule/straw). Samples used for magnetization measurement were recrystallized multiple times and checked for chemical composition by ^{1}H NMR spectroscopy. The program julX written by E. Bill was used for (elements of) the simulation and analysis of magnetic susceptibility data.[47]

X-band EPR data were collected on a Bruker ELEXSYS E500 spectrometer equipped with the Bruker standard cavity (ER4102ST) and a helium flow cryostat (Oxford Instruments ESR 910). Microwave frequencies were calibrated with a Hewlett-Packard frequency counter (HP5352B), and the field control was calibrated with a Bruker NMR field probe (ER035M). The spectra were simulated with the program GFIT (by Eckhard Bill) for the calculation of powder spectra with effective g values and anisotropic line widths (Lorentzian line shapes were used). In each case, a 2 mM solution of the complex was prepared in toluene. Data was recorded at 296 K with a frequency of 9.43 GHz, a modulation amplitude of 10 G and a microwave power of 1.26 mW. Simulations were conducted using the W95EPR software package.

Preparation of (^{iPr}PDI)Co(N_2) (1-N_2). A 250 mL round bottom flask was charged with 21.6 g (107.7 mmol) of Hg, approximately 100 mL of toluene and a stir bar. To the flask was added 0.108 g (4.68 mmol) of Na in small pieces with vigorous stirring. The amalgam was stirred 20 minutes then 0.477 g (0.780 mmol) of (^{iPr}PDI)$CoCl_2$ was added to the flask. A color change to purple over 30 minutes was initially observed followed by gradual color change to dark teal. The reaction was stirred for 6 hours then filtered through Celite and concentrated. Cooling the solution to -35 °C afforded 0.301 g (65 %) of dark teal crystals identified as (^{iPr}PDI)Co(N_2). Analysis for $C_{33}H_{43}N_5Co$: Calc. C, 69.70; H, 7.62; N, 12.32. Found C, 69.48; H, 7.81; N, 12.07. ^{1}H NMR (benzene-d_6): δ = 2.90 (124.5 Hz), 4.27 (242.9 Hz), 6.01 (54.5 Hz). IR (toluene): ν_{NN} = 2093 cm^{-1}.

Alternative preparation of (^{iPr}PDI)Co(N_2). A 250 mL round-bottom flask was charged with 0.502 g (0.821 mmol) of (^{iPr}PDI)$CoCl_2$, approximately 100 mL of toluene and a stir bar. The reaction was cooled in a liquid nitrogen chilled cold well and $NaEt_3BH$ (820 μL of a 1.0 M solution, 0.821 mmol) was added dropwise with stirring. The reaction was warmed to room temperature accompanied by a color change to dark purple. The solution was again chilled in the cold well and $NaEt_3BH$ (820 μL of a 1.0 M solution, 0.821 mmol) was added dropwise. The reaction was warmed to room temperature resulting in a color change to dark teal. The solution was filtered through Celite and concentrated, cooled to -35 °C and yielded 0.294 (63 %) of dark teal crystals of (^{iPr}PDI)Co(N_2).

Preparation of (^{iPr}*p*-^{t}BuPDI)Co(N_2) (^{tBu}1-N_2). This compound was prepared in a similar manner to **(^{iPr}PDI)Co(N_2)** with 0.111 g (4.83 mmol) Na, 22.1 g (110.1 mmol) Hg and 0.536 g (0.803 mmol) **(^{iPr}*p*-^{t}BuPDI)$CoCl_2$**. Recrystallization from pentane/toluene (5:1) yielded 0.306 g (61 %) of teal crystals identified as **(^{iPr}*p*-^{t}BuPDI)Co(N_2)**. Analysis for $C_{37}H_{51}N_5Co$: Calc. C, 71.13; H, 8.23; N, 11.21. Found C, 70.91; H, 8.41; N, 11.47. ^{1}H NMR (benzene-d_6): δ = 1.23 (89.7 Hz), 3.02 (180.3 Hz), 4.21 (223.8 Hz), 6.05 (48.5 Hz). IR (toluene): ν_{NN} = 2090 cm^{-1}.

Preparation of (^{Et}PDI)Co(N_2) (2-N_2). This compound was prepared in a similar manner to **(^{iPr}PDI)Co(N_2)** with 0.125 g (5.44 mmol) Na, 25.0 g (124.6 mmol) Hg and 0.503 g (0.906 mmol) (^{Et}PDI)$CoCl_2$. Recrystallization from pentane/toluene (5:1) yielded 0.204 g (44 %) of teal crystals identified as **(^{Et}PDI)Co(N_2)**. Analysis for $C_{29}H_{35}N_5Co$: Calc. C, 67.96; H, 6.88; N, 13.66. Found C, 68.10; H, 6.86; N, 13.41.

Magnetic susceptibility (benzene-d_6, 293 K): μ_{eff} = 1.8(2) μ_B. ^{1}H NMR (benzene-d_6): δ = 2.99 (216.0 Hz), 4.42 (236.5 Hz), 6.19 (59.12 Hz). IR (toluene): ν_{NN} = 2095 cm^{-1}.

Preparation of (^{Me}PDI)Co(N_2) (3-N_2). This compound was prepared in an analogous manner to **(^{iPr}PDI)Co(N_2)** with 0.050 g (2.17 mmol) Na, 9.92 g (49.5 mmol) Hg and 0.205 g (0.431 mmol) **(^{Me}PDI)CoCl_2**. Recrystallization from pentane/toluene (5:1) yielded 0.187 g (56 %) of teal crystals identified as **(^{Me}PDI)Co(N_2)**. Analysis for $C_{25}H_{27}N_5Co$: Calc. C, 65.78; H, 5.96; N, 15.34. Found C, 66.03; H, 5.78; N, 14.92. Magnetic susceptibility (benzene-d_6, 293 K): μ_{eff} = 1.7(2) μ_B. ^{1}H NMR (benzene-d_6): δ = 3.38 (271.7 Hz), 6.38 (478.0 Hz). IR (toluene): ν_{NN} = 2093 cm^{-1}.

Toepler Pump Experiments for (^{Ar}PDI)Co(N_2). A 100 mL round-bottom flask was charged with 0.017 g (0.030 mmol) of **(^{iPr}PDI)Co(N_2)**, 0.042 g (0.151 mmol) $PbCl_2$ and a stir bar. Diethyl ether was vacuum-transferred into the flask at -78 °C and the solution was warmed to ambient temperature and stirred for 12 hours. A color change of the solution to purple was observed. The free dinitrogen was collected with a Toepler pump into a volume of 44.2 mL. After 2 hours, 26 Torr (76 %) of dinitrogen was collected. Similar procedures were used for **(^{Et}PDI)Co(N_2)** and **(^{Me}PDI)Co(N_2)**, where 84 % and 83 % of the expected dinitrogen was collected, respectively.

Preparation of (^{iPr}PIEA)Co(N_2). A 100 mL round-bottom flask was charged with 0.207 g (0.359 mmol) of (^{iPr}PDI)CoCl, approximately 50 mL of tetrahydrofuran and a stir bar. NaO*t*Bu (0.035 g, 0.364 mmol) was added by spatula, and the reaction was let stir three days, during which time there was a gradual color change to purple-brown. The volatiles were removed, and the dark brown solid was extracted into diethyl ether and toluene (75:25) and filtered through Celite. The solution was concentrated and

cooled to -35 °C, yielding 0.130 g (63 %) of dark brown powder identified as (^{iPr}PIEA)Co(N_2). Analysis for $C_{33}H_{42}N_5Co$: Calc. C, 69.82; H, 7.46; N, 12.34. Found C, 69.84; H, 7.59; N, 11.98. ^{1}H NMR (benzene-d_6): δ = -0.71 (s, 3H, C(C*H*$_3$)), 0.89 (d, 6.9 Hz, 6H, CH(C*H*$_3$)$_2$), 1.22 (d, 6.6 Hz, 6H, CH(C*H*$_3$)$_2$), 1.23 (d, 6.6 Hz, 6H, CH(C*H*$_3$)$_2$), 1.39 (d, 6.9 Hz, 6H, CH(C*H*$_3$)$_2$), 2.70 (septet, 6.9 Hz, 2H, C*H*(CH$_3$)$_2$), 3.25 (septet, 6.6 Hz, 2H, C*H*(CH$_3$)$_2$), 4.05 (s, 1H, C=C*H*$_2$), 4.73 (s, 1H, C=C*H*$_2$), 7.08-7.22 (m, 6H, *m-aryl* and *p-aryl*), 7.24 (t, 7.7 Hz, 1H, *p-pyridine*), 7.38 (d, 7.7 Hz, 1H, *m-pyridine*), 8.30 (d, 7.7 Hz, 1H, *m-pyridine*). ^{13}C {^{1}H} NMR (benzene-d_6): δ = 19.84 (C(*C*H$_3$)), 24.03 (CH(*C*H$_3$)$_2$), 24.69 (CH(*C*H$_3$)$_2$), 24.72 (CH(*C*H$_3$)$_2$), 25.89 (CH(*C*H$_3$)$_2$), 28.16 (*C*H(CH$_3$)$_2$), 29.03 (*C*H(CH$_3$)$_2$), 90.33 (C=*C*H$_2$), 111.30 (*m-pyridine*), 117.94 (*m-pyridine*), 123.74 (*m-* or *p-aryl*), 123.87 (*m-* or *p-aryl*), 123.99 (*m-* or *p-aryl*), 126.00 (*m-* or *p-aryl*), 132.81 (*p-pyridine*), 139.91, 141.42, 142.06, 145.57, 151.43, 159.54, 161.43, 164.67. IR (toluene): ν_{NN} = 2145 cm^{-1}. IR (KBr): ν_{NN} = 2148 cm^{-1}, ν_{CC} = 1583 cm^{-1}.

Preparation of (^{Cy}APDI)CoCl$_2$ (4-Cl$_2$). This compound was synthesized by a modification of the literature procedure.[1] A 100-mL round bottom flask was charged with 0.507 g (1.56 mmol) of ^{Cy}APDI and 0.184 g (1.42 mmol) of $CoCl_2$. Approximately 50 mL of tetrahydrofuran was added to the flask and the reaction was stirred for 12 hours during which time a pale green precipitate formed. The solid was collected by filtration and washed with pentane to yield 0.627 g (94 %) of a pale green powder identified as (**^{Cy}APDI)CoCl$_2$**. ^{1}H NMR (CD_2Cl_2): δ = -59.37 (170.8 Hz, 4H, Cy C*H*$_2$), -35.44 (237.9 Hz, 4H, Cy C*H*$_2$), -21.44 (133.6 Hz, 6H, C(C*H*$_3$)), -18.79 (149.8 Hz, 4H, Cy C*H*$_2$), -9.64 (123.3 Hz, 4H, Cy C*H*$_2$), -7.64 (121.3 Hz, 2H, Cy C*H*$_2$), -4.93 (17.7 Hz, 1H, *p-pyridine*), -3.38 (150.7 Hz, 2H, Cy C*H*$_2$), 77.92 (162.2 Hz, 2H, *m-pyridine* or Cy C*H*), 84.91 (151.1 Hz, 2H, *m-pyridine* or Cy C*H*).

Preparation of (^{Cy}APDI)$_2$Co. This compound was prepared in a similar manner to **(^{iPr}APDI)$_2$Co** with 25.0 g (124.6 mmol) Hg, 0.125 g (5.44 mmol) sodium metal, 0.355 g (1.09 mmol) ^{Cy}APDI and 0.496 g (1.09 mmol) of **(^{Cy}APDI)CoCl$_2$**. Recrystallization of the resulting red-brown solid from pentane at -35 °C yielded 0.485 g (63 %) of dark red-brown crystals identified as **(^{Cy}APDI)$_2$Co**. Analysis for $C_{42}H_{62}N_6Co$: Calc. C, 71.06; H, 8.80; N, 11.84. Found C, 70.71; H, 8.42; N, 11.45. Magnetic susceptibility (293 K): $\mu_{eff} = 3.0(2)\ \mu_B$. ^{1}H NMR (benzene-$d_6$): δ = -62.361 (938.1 Hz, 2H, *p-pyridine*), -21.11 (83.2 Hz, 8H, Cy CH_2), -8.67 (197.2 Hz, 8H, Cy CH_2), -3.53 (31.2 Hz, 8H, Cy CH_2), 0.26 (20.8 Hz, 4H, Cy CH_2), 2.34 (7.1 Hz, 4H, Cy CH_2), 6.51 (30.7 Hz, 8H, Cy CH_2), 47.91 (140.0 Hz, 4H, *m-pyridine* or Cy C*H*), 61.09 (30.9 Hz, 12H, C(CH_3)), 178.17 (9.1 Hz, 4H, *m-pyridine* or Cy C*H*).

Preparation of ^{iPr}APDI. This compound was synthesized by a modification of the literature procedure.[48] A 250 mL round-bottom flask was charged with 3.00 g (18.38 mmol) 2,6-diacetylpyridine, ~ 100 mL of isopropyl amine and a stir bar. *p*-Toluenesulfonic acid (0.340 g, 1.97 mmol) was added, and the reaction was heated to a gentle reflux for three days. The solution was cooled to ambient temperature, and excess isopropyl amine was removed in vacuo. The resulting tan solid was extracted into dichloromethane, washed with 2 x 100 mL water and 100 mL saturated sodium bicarbonate solution, and dried over $MgSO_4$. Volatiles were removed and the resulting solid was recrystallized from methanol at -35 °C to give 1.30 g (28 %) of off-white plates identified as **^{iPr}APDI**.

Preparation of (^{iPr}APDI)CoCl$_2$ (5-Cl$_2$). A 100 mL round-bottom flask was charged with 0.489 g (1.99 mmol) of ^{iPr}APDI and 0.246 g (1.89 mmol) $CoCl_2$. Approximately

50 mL of tetrahydrofuran was then added to the flask and the reaction was stirred for 12 hours over which time a gray-green precipitate formed. The precipitate was collected by filtration and washed with pentane to yield 0.717 g (96 %) of a gray-green solid identified as **(^{iPr}APDI)CoCl$_2$**. Analysis for $C_{15}H_{23}N_3CoCl_2$: Calc. C, 48.02; H, 6.18; N, 11.20. Found C, 47.94; H, 5.85; N, 10.94. Magnetic susceptibility (Gouy balance, 293 K): μ_{eff} = 4.2(2) μ_B. ^{1}H NMR (CD_2Cl_2): δ = -38.23 (111.0 Hz, 12H, CH(C*H*$_3$)$_2$), -20.26 (60.5 Hz, 6H, C(C*H*$_3$)), -2.30 (58.2 Hz, 1H, *p-pyridine*), 74.39 (4.6 Hz, 2H, *m-pyridine* or C*H*(CH$_3$)$_2$), 87.14 (4.6 Hz, 2H, *m-pyridine* or C*H*(CH$_3$)$_2$).

Preparation of (^{iPr}APDI)$_2$Co. A thick walled glass vessel was charged with 28.2 g of Hg (140.6 mmol) and approximately 100 mL of toluene. Sodium metal (0.141 g, 6.13 mmol) was added in small pieces and the amalgam was stirred 15 minutes. The flask was cooled in a liquid nitrogen chilled cold well, followed by addition of **(^{iPr}APDI)CoCl$_2$** (0.460 g, 1.23 mmol) and ^{iPr}APDI (0.301 g, 1.23 mmol). The flask was quickly removed from the drybox and submerged in liquid nitrogen. The solution was degassed four times on a high vacuum line and the reaction was warmed to room temperature and stirred for 16 hours, during which time there was a color change to red. The solution was filtered through Celite, volatiles were removed and the remaining red-brown solid was recrystallized from pentane at -35 °C to yield 0.108 g (70 %) of red crystals identified as **(^{iPr}APDI)$_2$Co**. Analysis for $C_{30}H_{46}N_6Co$: Calc. C, 65.55; H, 8.43; N, 15.29. Found C, 65.28; H, 8.46; N, 15.22. Magnetic susceptibility (293 K): μ_{eff} = 3.6(2) μ_B. ^{1}H NMR (benzene-*d*$_6$): δ = -64.35 (193.3 Hz, 2H, *p-pyridine*), -4.32 (77.4 Hz, 24H, CH(C*H*$_3$)$_2$), 46.24 (119.0 Hz, 4H, *m-pyridine* or C*H*(CH$_3$)$_2$), 64.49 (189.0 Hz, 12H, C(C*H*$_3$)), 185.13 (211.0 Hz, 4H, *m-pyridine* or C*H*(CH$_3$)$_2$).

Preparation of [Na(solv)$_3$][(^{iPr}PDI)Co(N$_2$)] ([Na(solv)$_3$][1-N$_2$]). Sodium naphthalenide was prepared in situ by addition of approximately 50 mL tetrahydrofuran to a 100 mL round bottom flask containing 0.026 g (1.13 mmol) of sodium metal and 0.147 g (1.14 mmol) of naphthalene. The reaction was stirred for three hours during which time the solution became green in color and the solids had dissolved. 0.200 g (0.327 mmol) of **(^{iPr}PDI)CoCl$_2$** was added to the flask and the reaction was stirred for one hour after which time the volatiles were removed. The residual solid was extracted into diethyl ether and stirred for one hour to give a bright green solution. The solution was filtered through Celite, concentrated and cooled to -35 °C to yield forest green crystals identified as a mixture of **[Na(Et$_2$O)$_3$][(^{iPr}PDI)Co(N$_2$)]** and **[Na(THF)$_3$][(^{iPr}PDI)Co(N$_2$)]**. Dissolution of the crystals in tetrahydrofuran followed by removal of volatiles gave quantitative conversion to **[(^{iPr}PDI)Co(N$_2$)][Na(THF)$_3$]** (0.277 g, 52 %). Analysis for $C_{45}H_{67}N_5O_3NaCo$: Calc. C, 66.89; H, 8.36; N, 8.67. Found C, 66.91; H, 8.60; N, 8.69. ^{1}H NMR (1:1 THF-d_8/benzene-d_6): δ = 1.19 (br s, 24H, CH(CH_3)$_2$), 1.85 (br s, 6H, C(CH_3)), 3.02 (br s, 4H, CH(CH$_3$)$_2$), 7.07 (br s, 1H, *p-pyridine*), 7.25 (br s, 4H, *m-aryl*), 7.36 (br s, 2H, *p-aryl*), 8.39 (br s, 2H, *m-pyridine*). IR (KBr): ν_{NN} = 2046 cm^{-1} (solv = Et$_2$O), 1981 cm^{-1} (solv = THF).

Preparation of [Na(solv)$_3$][(^{iPr}APDI)Co(N$_2$)] ([Na(solv)$_3$][5-N$_2$]). This compound was prepared in a similar manner to **[Na(solv)$_3$][(^{iPr}PDI)Co(N$_2$)]** using 0.072 g (3.13 mmol) sodium metal and 0.402 g (3.13 mmol) naphthalene to prepare the sodium naphthalenide and 0.335 g (0.893 mmol) of **(^{iPr}APDI)CoCl$_2$**. The resulting solid was recrystallized from diethyl ether at -35 °C to yield 0.366 g (71 %) of dark green crystals identified as **[Na(Et$_2$O)$_3$][(^{iPr}APDI)Co(N$_2$)]**. Dissolution of the dark green

crystals in tetrahydrofuran followed by removal of volatiles gave quantitative yield of a dark green powder identified as **[Na(Et$_2$O)$_3$][(^{iPr}APDI)Co(N$_2$)]**. ^{1}H NMR (1:1 THF-d_8/benzene-d_6): δ = 1.89 (s, 12H, CH(C*H*$_3$)$_2$), 2.24 (s, 6H, C(C*H*$_3$)), 4.70 (s, 2H, C*H*(CH$_3$)$_2$), 6.68 (s, 1H, *p-pyridine*), 8.04 (s, 2H, *m-pyridine*). IR (KBr): ν_{NN} = 2037 cm^{-1} (solv = Et$_2$O), 1991 cm^{-1} (solv = THF).

Oxidation of [Na(THF)$_3$][(^{iPr}PDI)Co(N$_2$)] with [Cp$_2$Fe][BPh$_4$]. A 20 mL scintillation vial was charged with 0.025 g (0.031 mmol) of **[Na(THF)$_3$][(^{iPr}PDI)Co(N$_2$)]**, approximately 5 mL of diethyl ether and a stir bar yielding a bright green solution. [Cp$_2$Fe][BPh$_4$] (0.016 g, 0.032 mmol) was added to the vial by spatula and the reaction was stirred for several hours during which time a slight color change to teal was observed. The solution was filtered through Celite and volatiles were removed to give a dark teal solid. Quantitative conversion of the starting material to **(^{iPr}PDI)Co(N$_2$)** and Cp$_2$Fe was determined by ^{1}H NMR spectroscopy.

Oxidation of [Na(Et$_2$O)$_3$][(^{iPr}APDI)Co(N$_2$)] with [Cp$_2$Fe][BPh$_4$]. A 20 mL scintillation vial was charged with 0.036 g (0.062 mmol) of **[Na(Et$_2$O)$_3$][(^{iPr}APDI)Co(N$_2$)]**, approximately 5 mL diethyl ether and a stir bar, yielding a bright green solution. 0.031 g (0.061 mmol) Cp$_2$Fe was added by spatula and the reaction was stirred for one hour. A color change to brown was observed. The solution was filtered though Celite and volatiles were removed to give a dark brown solid. Formation of **(^{iPr}APDI)$_2$Co** and Cp$_2$Fe was observed by ^{1}H NMR spectroscopy.

Preparation of (^{Et}PDI)CoCl (2-Cl). A 100 mL round bottom flask was charged with 0.144 g (0.259 mmol) of **(^{Et}PDI)CoCl$_2$**, approximately 50 mL of toluene and a stir

bar. The toluene slurry was cooled in a liquid nitrogen chilled cold well, $NaEt_3BH$ (259 μL of a 1.0 M solution in toluene, 0.259 mmol) was added dropwise with stirring. The reaction was warmed to ambient temperature with stirring. Upon warming gradual color change to bright purple occurred and the resulting purple solution was filtered through Celite and concentrated. The solution was cooled to -35 °C and yielded 0.116 g (86 %) of purple crystals identified as **(^{Et}PDI)CoCl**. ^{1}H NMR (benzene-d_6): δ = -0.02 (s, 6H, C(CH_3)), 1.03 (t, 7.1 Hz, 12H, CH_2CH_3), 2.59 (m, 4H, CH_2CH_3), 2.72 (m, 4H, CH_2CH_3), 6.93 (d, 7.5 Hz, 2H, *m-pyridine*), 7.22 (d, 7.1 Hz, 4H, *m-aryl*), 7.37 (t, 7.1 Hz, 2H, *p-aryl*), 9.55 (t, 7.5 Hz, 1H, *p-pyridine*). ^{13}C {^{1}H} NMR (benzene-d_6): δ = 14.25 (CH_2CH_3), 21.21 (C(CH_3)), 25.69 (CH_2CH_3), 115.59 (*p-pyridine*), 125.99 (*m-pyridine*), 126.51 (*m-aryl*), 126.80 (*p-aryl*), 136.08 (*o-aryl*), 153.22 (*o-pyridine* or *i-aryl*), 153.35 (*o-pyridine* or *i-aryl*), 167.84 ($C(CH_3)$).

Preparation of (^{Me}PDI)CoCl (3-Cl). This compound was prepared in a similar manner to **(^{Et}PDI)CoCl** with 0.105 g (0.221 mmol) of **(^{Me}PDI)CoCl$_2$** and $NaEt_3BH$ (221 μL of a 1.0 M solution in toluene, 0.221 mmol) and yielded 0.090 g (93% yield) of a purple powder identified as **(^{Me}PDI)CoCl**. ^{1}H NMR (benzene-d_6): δ = -0.05 (s, 6H, C(CH_3)), 2.20 (s, 12H, CH_3), 6.93 (d, 7.3 Hz, 2H, *m-pyridine*), 7.19 (d, 6.5 Hz, 4H, *m-aryl*), 7.27 (t, 6.5 Hz, 2H, *p-aryl*), 9.52 (t, 7.3 Hz, 1H, *p-pyridine*). ^{13}C {^{1}H} NMR (benzene-d_6): δ = 19.80 (CH_3), 20.50 (C(CH_3)), 115.35 (*p-pyridine*), 125.61 (*m-pyridine*), 126.45 (*p-aryl*), 128.87 (*m-aryl*), 130.54 (*o-aryl*), 153.24 (*o-pyridine* or *i-aryl*), 154.68 (*o-pyridine* or *i-aryl*), 167.29 ($C(CH_3)$).

Preparation of (^{Cy}APDI)CoCl (4-Cl). This compound was prepared in a similar manner to **(^{Et}PDI)CoCl** with 0.171 g (0.376 mmol) of ^{Cy}APDICoCl$_2$ and $NaEt_3BH$ (376 μL of a 1.0 M solution in toluene, 0.376 mmol) and yielded 0.099 g (63 %) of a

dark red-brown solid identified as (**^{Cy}APDI)CoCl**. Analysis for $C_{21}H_{31}N_3Co$: Calc. C, 60.07; H, 7.44; N, 10.01. Found C, 59.87; H, 7.64; N, 9.80. Magnetic susceptibility (benzene-*d_6*, 296 K): μ_{eff} = 2.5(2) μ_B. ^{1}H NMR (benzene-*d_6*): δ = -22.79 (57.6 Hz, 6H, C(C*H_3*)), -4.38 (48.5 Hz, 4H, Cy C*H_2*), 0.55 (50.0 Hz, 4H, Cy C*H_2*), 0.65 (63.5 Hz, 4H, Cy C*H_2*), 1.50 (67.1 Hz, 6H, Cy C*H_2*), 2.47 (56.7 Hz, 2H, Cy C*H_2*), 8.72 (45.9 Hz, 2H, Cy C*H*), 12.07 (41.8 Hz, 2H, *m-pyridine*), 66.27 (76.5 Hz, 1H, *p-pyridine*).

Preparation of (iPrAPDI)CoCl (5-Cl). This compound was prepared in a similar manner to **(EtPDI)CoCl** using 0.544 g (1.45 mmol) **(iPrAPDI)CoCl$_2$** and $NaEt_3BH$ (1450 μL of a 1.0 M solution in toluene, 1.45 mmol). The resulting dark mauve solid was recrystallized from diethyl ether at -35 °C yielding 0.294 g (60 %) of dark mauve crystals of **(iPrAPDI)CoCl**. Analysis for $C_{15}H_{23}N_3CoCl$: Calc. C, 53.03; H, 6.82; N, 12.37. Found C, 53.17; H, 6.79; N, 12.24. Magnetic susceptibility (benzene-*d_6*, 296 K): μ_{eff} = 1.0(2) μ_B. ^{1}H NMR (benzene-*d_6*): δ = -12.62 (47.4 Hz, 6H, C(C*H_3*)), 0.42 (47.1 Hz, 12H, CH(C*H_3*)$_2$), 7.20 (51.8 Hz, 2H, C*H*(CH$_3$)$_2$), 9.52 (42.1 Hz, 2H, *m-pyridine*), 41.6 (71.6 Hz, 1H, *p-pyridine*).

Preparation of (EtPDI)CoMe (2-Me). A 20 mL scintillation vial was charged with a 0.070 g (0.135 mmol) (**EtPDI)CoCl**, approximately 15 mL of toluene and a stir bar. The solution was frozen in a liquid nitrogen chilled cold well and MeLi (118 μL of a 1.6 M solution in diethyl ether, 0.189 mmol) was added to the thawing solution. The reaction was warmed to ambient temperature with stirring then filtered through Celite. The volatiles were removed in vacuo and the resulting dark purple solid was recrystallized from diethyl ether at -35 °C to yield 0.049 g (73% yield) of purple crystals identified as (**EtPDI)CoMe**. ^{1}H NMR (benzene-*d_6*): δ = -1.19 (s, 6H, C(C*H_3*)), 0.58 (s, 3H, Co-C*H_3*), 0.78 (t, 7.5 Hz, 12H, CH$_2$C*H_3*), 2.43 (m, 8H, C*H_2*CH$_3$), 7.33 (d,

7.6 Hz, 4H, *m-aryl*), 7.44 (t, 7.6 Hz, 2H, *p-aryl*), 7.89 (d, 7.6 Hz, 2H, *m-pyridine*), 10.17 (t, 7.6 Hz, 1H, *p-pyridine*). ^{13}C {^{1}H} NMR (benzene-d_6): δ = -16.36 (Co-CH_3), 13.93 (CH_2CH_3), 25.08 (C(CH_3)), 25.32 (CH_2CH_3), 117.81 (*p-pyridine*), 122.85 (*m-pyridine*), 126.29 (*p-aryl*), 126.62 (*m-aryl*), 135.85 (*o-aryl*), 156.88 (*o-pyridine* or *i-aryl*), 157.47 (*o-pyridine* or *i-aryl*), 166.26 ($C(CH_3)$).

Preparation of (^{Me}PDI)CoMe (3-Me). This compound was prepared in a similar manner to **(^{Et}PDI)CoMe** using 0.103 g (0.234 mmol) **(^{Me}PDI)CoCl** and MeLi (205 μL of a 1.6 M solution in diethyl ether, 0.328 mmol). Recrystallization of the resulting purple solid from diethyl ether at -35 °C yielded 0.080 g (81 %) a purple powder identified as **(^{Me}PDI)CoMe**. ^{1}H NMR (benzene-d_6): δ = -1.27 (s, 6H, C(CH_3)), 0.53 (s, 3H, Co-CH_3), 1.96 (s, 12H, CH_3) 7.22 (d, 7.6 Hz, 4H, *m-aryl*), 7.30 (t, 7.6 Hz, 2H, *p-aryl*), 7.87 (d, 7.6 Hz, 2H, *m-pyridine*), 10.10 (t, 7.6 Hz, 1H, *p-pyridine*). ^{13}C {^{1}H} NMR (benzene-d_6): δ = -17.71 (Co-CH_3), 19.50 (CH_3), 24.45 (C(CH_3)), 117.80 (*p-pyridine*), 122.60 (*m-pyridine*), 125.85 (*m-aryl*), 128.91 (*p-aryl*), 130.27 (*o-aryl*), 157.37 (*o-pyridine* or *i-aryl*), 158.15 (*o-pyridine* or *i-aryl*), 165.72 ($C(CH_3)$).

Preparation of (^{Cy}APDI)CoMe (4-Me). This compound was prepared in a similar manner to **(^{Et}PDI)CoMe** using 0.204 g (0.486 mmol) of **(^{Cy}APDI)CoCl** and MeLi (425 μL of a 1.6 M solution in diethyl ether, 0.680 mmol) to yield 0.100 g (52 %) of a dark red-brown solid identified as **(^{Cy}APDI)CoMe**. Analysis for $C_{22}H_{34}N_3Co$: Calc. C, 66.15; H, 8.58; N, 10.52. Found C, 66.04; H, 8.24; N, 10.04. ^{1}H NMR (benzene-d_6): δ = 0.13 (s, 6H, C(CH_3)), 1.41 (m, 2H, Cy C^4H_2), 1.56 (m, 4H, Cy C^3H_2), 1.70 (m, 2H, Cy C^4H_2), 1.78 (m, 4H, Cy C^3H_2), 2.36 (m, 4H, Cy C^2H_2), 2.53 (m, 4H, Cy C^2H_2), 3.37 (s, 3H, Co-CH_3), 4.65 (m, 2H, Cy C^1H), 7.35 (d, 7.6 Hz, 2H, *m-pyridine*), 9.41 (t, 7.6 Hz, 1H, *p-pyridine*). ^{13}C {^{1}H} NMR (benzene-d_6): δ = 21.16 (C(CH_3)), 26.42 (Cy

C^3H_2), 26.70 (Cy C^4H_2), 32.11 (Cy C^2H_2), 70.77 (Cy C^1H), 111.09 (*p-pyridine*), 126.61 (*m-pyridine*), 146.63 (*o-pyridine*), 158.87 ($C(CH_3)$), one resonance not located.

Preparation of (^{iPr}APDI)CoMe (5-Me). This compound was prepared using a similar method to **(^{Et}PDI)CoMe** using 0.136 g (0.400 mmol) **(^{iPr}APDI)CoCl** and MeLi (350 μL of a 1.6 M solution in diethyl ether, 0.560 mmol). Recrystallization from diethyl ether at -35 °C yielded 0.104 g (81 %) of a dark red solid identified as **(^{iPr}APDI)CoMe**. Analysis for $C_{16}H_{26}N_3Co$: Calc. C, 60.18; H, 8.21; N, 13.16. Found C, 60.04; H, 8.18; N, 13.18. ^{1}H NMR (benzene-d_6): δ = 0.14 (s, 6H, C(CH_3)), 1.78 (d, 6.6 Hz, 12H, CH(CH_3)$_2$, 2.05 (s, 3H, Co-CH_3), 5.01 (septet, 6.6 Hz, 2H, CH(CH_3)$_2$), 7.30 (d, 7.6 Hz, 2H, *m-pyridine*), 9.15 (t, 7.6 Hz, 1H, *p-pyridine*). ^{13}C {^{1}H} NMR (benzene-d_6): δ = 20.49 (C(CH$_3$)), 22.06 (CH(CH$_3$)$_2$), 60.78 (CH(CH$_3$)$_2$), 112.49 (*p-pyridine*), 123.74 (*m-pyridine*), 147.68 (*o-pyridine*), 158.43 (C(CH$_3$)), one resonance not located.

Spectroscopic Characterization of (^{iPr}PDI)Co(CO). A J. Young NMR tube was charged with 0.009 g (0.016 mmol) of (^{iPr}PDI)Co(N_2) in benzene-d_6. The tube was degassed, and 20 equivalents (50 Torr in a 100.1 mL gas bulb) of carbon monoxide was added at -196 °C. Upon warming to room temperature there was a rapid color change to red-brown. ^{1}H NMR spectroscopy confirmed quantitative conversion to (^{iPr}PDI)Co(CO). The infrared spectrum of (^{iPr}PDI)Co(CO) was obtained by exposing a 7.0 mM solution of the compound to an atmosphere of carbon monoxide in a three-neck flask containing the infrared probe. ^{1}H NMR (benzene-d_6): δ = 2.63 (183.6 Hz), 3.21 (140.3 Hz), 6.03 (256.7 Hz), 10.62 (405.5 Hz). IR (toluene): ν_{NN} = 1975 cm^{-1}.

Preparation of (^{iPr}PDI)CoN$_3$ (1-N$_3$). A 20 mL scintillation vial was charged with 0.084 g (0.145 mmol) **(^{iPr}PDI)CoCl**, ~ 15 mL of tetrahydrofuran and a stir bar. Sodium azide (0.048 g, 0.738 mmol) was added to the vial and the fuschia solution was stirred for 24 hours, then volatiles were removed. The dark pink solid was extracted into diethyl ether and filtered through Celite. The solution was concentrated and cooled to -35 °C to give 0.066 g (78 %) of dark pink crystals identified as **(^{iPr}PDI)CoN$_3$**. Analysis for $C_{33}H_{43}N_6Co$: Calc. C, 68.02; H, 7.44; N, 14.42. Found C, 68.38; H, 7.64; N, 14.19.[1] H NMR (benzene-d_6): δ = 0.17 (s, 6H, C(C*H*$_3$)), 1.07 (d, 6.6 Hz, 12H, CH(C*H*$_3$)), 1.17 (d, 6.6 Hz, 12H, CH(C*H*$_3$)), 3.27 (septet, 6.6 Hz, 4H, C*H*(CH$_3$)), 6.99 (d, 7.7 Hz, 2H, *m-pyridine*), 7.31 (d, 7.6 Hz, 4H, *m-aryl*), 7.43 (t, 7.6 Hz, 2H, *p-aryl*), 9.16 (t, 7.7 Hz, 1H, *p-pyridine*). ^{13}C {^{1}H} NMR (benzene-d_6): δ = 20.48 (C(*C*H$_3$)), 23.53 (CH(*C*H$_3$)$_2$), 23.93 (CH(*C*H$_3$)$_2$), 29.15 (*C*H(CH$_3$)$_2$), 115.59 (*p-pyridine*), 124.39 (*m-aryl*), 127.53 (*m-pyridine* or *p-aryl*), 140.64 (*o-aryl*), 149.37 (*i-aryl*), 152.67 (*o-pyridine*), 165.63 (*C*(CH$_3$)), one resonance not located. IR (toluene): ν_{NNN} = 2055 cm^{-1}.

Preparation of (^{iPr}PDI)Co(NO) (1-NO). A short bomb was charged with 0.102 g (0.179 mmol) **(^{iPr}PDI)Co(N$_2$)**, ~ 50 mL of toluene and a stir bar to give a teal solution. NO was added by gas bulb, and upon warming the reaction to ambient temperature there was an immediate color change to fuschia. In a drybox, the solution was filtered through Celite and volatiles were removed. The resulting solid was recrystallized from pentane at -35 °C to give 0.086 g (84 %) of dark pink crystals identified as **(^{iPr}PDI)Co(NO)**. ^{1}H NMR (benzene-d_6): δ = 1.08 (d, 6.9 Hz, 12H, CH(C*H*$_3$)), 1.15 (d, 6.9 Hz, 12H, CH(C*H*$_3$)), 2.05 (s, 6H, C(C*H*$_3$)), 3.18 (septet, 6.9 Hz, 4H, C*H*(CH$_3$)), 6.98 (t, 7.5 Hz, 1H, *p-pyridine*), 7.16 (d, 6.8 Hz, 4H, *m-aryl*), 7.21 (t, 6.8 Hz, 2H, *p-aryl*), 7.45 (d, 7.5 Hz, 2H, *m-pyridine*). ^{13}C {^{1}H} NMR (benzene-d_6): δ = 17.24

(C(*C*H_3)), 24.13 (CH(*C*H_3)$_2$), 24.45 (CH(*C*H_3)$_2$), 28.59 (*C*H(CH$_3$)$_2$), 120.58 (*m-pyridine* or *p-aryl*), 121.68 (*p-pyridine*), 123.90 (*m-aryl*), 126.99 (*m-pyridine* or *p-aryl*), 141.11 (*i-aryl* or *o-aryl*), 141.72 (*i-aryl* or *o-aryl*), 149.73 (*o-pyridine*), 155.72 (*C*(CH$_3$)). IR (toluene): ν_{NO} = 1711 cm^{-1}.

REFERENCES

[1] Sacconi, L.; Morassi, R.; Midollini, S. *J. Chem. Soc. (A)* **1968**, 1510.

[2] Britovsek, G. J. P.; Gibson, V. C.; Kimberley, B. S.; Maddox, P. J.; McTavish, S. J.; Solan, G. A.; White, A. J. P.; Williams, D. J. *Chem. Commun.* **1998**, 849-850.

[3] Britovsek, G. J. P.; Bruce, M.; Gibson, V. C.; Kimberely, B. S.; Maddox, P. J.; Mastroianni, S.; McTavish, S. J.; Redshaw, C.; Solan, G. A.; Strömberg, S.; White, A. J. P.; Williams, D. J. *J. Am. Soc.* **1999**, *121*, 8728.

[4] Small, B. L.; Brookhart, M.; Bennett, A. M. A. *J. Am. Chem. Soc.* **1998**, *120*, 4049.

[5] (a) Gibson, V. C.; Tellmann, K. P.; Humphries, M. J.; Wass, D. F. *Chem. Commun.* **2002**, 2316. (b) Tellmann, K. P.; Humphries, M. J.; Rzepa, H. S.; Gibson, V. C. *Organometallics* **2004**, *23*, 5503-5513. (c) Humphries, M. J.; Tellmann, K. P.; Gibson, V. C.; White, A. J. P.; Williams, D. J. *Organometallics* **2005**, *24*, 2039-2050.

[6] Kooistra, T. M.; Knijnenburg, Q.; Smits, J. M. M.; Horton, A. D.; Budzelaar, P. H. M.; Gal, A. W. *Angew. Chem. Int. Ed.* **2001**, *40*, 4719-4722.

[7] Gibson, V. C.; Humphries, M. J.; Tellmann, K. P.; Wass, D. F.; White, A. J. P.; Williams, D. J. *Chem. Commun.* **2001**, 2252-2253.

[8] Steffen, W.; Blömker, T.; Kleigrewe, N.; Kehr, G.; Fröhlich, R.; Erker, G. *Chem. Commun.* **2004**, 1188-1189.

[9] Knijnenburg, Q.; Hetterscheid, D.; Kooistra, T. M.; Budzelaar, P. H. M. *Eur. J. Inorg. Chem.* **2004**, 1204-1211.

[10] Budzelaar, P. H. M.; de Bruin, B.; Gal, A. W. ; Wieghardt, K.; van Lenthe, J. H. *Inorg. Chem.* **2001**, *40*, 4649-4655.

[11] de Bruin, B.; Bill, E.; Bothe, E.; Weyhermüller, T.; Wieghardt, K. *Inorg. Chem.* **2000**, *39*, 2936-2947.

[12] Bart, S. C.; Chlopek, K.; Bill, E.; Bouwkamp, M. W.; Lobkovsky, E.; Neese, F.; Wieghardt, K.; Chirik, P. J. *J. Am. Chem. Soc.* **2006**, *128*, 13901-13912.

[13] Trovitch, R. J.; Ph.D. Thesis, Cornell University, 2009.

[14] Bart, S. C.; Lobkovsky, E.; Chirik, P. J. *J. Am. Chem. Soc.* **2004**, *126*, 13794-13807.

[15] Archer, A. M.; Bouwkamp, M. W.; Cortez, M. P.; Lobkovsky, E.; Chirik, P. J. *Organometallics* **2006**, *25*, 4269-4278.

[16] Tondreau, A. M.; Lobkovsky, E.; Chirik, P. J. *Org. Lett.* **2008**, 2789-2892.

[17] Bouwkamp, M. W.; Bowman, A. C.; Lobkovsky, E.; Chirik, P. J. *J. Am. Chem. Soc.* **2006**, *128*, 13340-13341.

[18] Sylvester, K. T.; Chirik, P. J. *J. Am. Chem. Soc.* **2009**, *131*, 8772-8774.

[19] Trovitch, R. J.; Lobkovsky, E.; Bill, E.; Chirik, P. J. *Organometallics* **2008**, *27*, 1470-1478.

[20] Trovitch, R. J.; Lobkovsky, E.; Bouwkamp, M. W.; Chirik, P. J. *Organometallics* **2008**, *37*, 6264-6278.

[21] Wile, B. M.; Trovitch, R. J.; Bart, S. C.; Tondreau, A. M.; Lobkovsky, E.; Milsmann, C.; Bill, E.; Wieghardt, K.; Chirik, P. J. *Inorg. Chem.* **2009**, *48*, 4190-4200.

[22] Knijnenburg, Q.; Gambarotta, S.; Budzelaar, P. H. M. *Dalton Trans.* **2006**, 5442-5448.

[23] Bouwkamp, M. W.; Lobkovsky, E.; Chirik, P. J. *Inorg. Chem.* **2006**, *45*, 2.

[24] Bowman, A. C.; Bart, S. C.; Heinemann, F. W.; Meyer, K.; Chirik, P. J. *Inorg. Chem.* **2009**, *48*, 5587.

[25] (a) Sugiyama, A. G.; Gambarotta, S.; Yap, G. P. A.; Budzelaar, P. H. M. *J. Am. Chem. Soc.* **2002**, *124*, 12268. (b) Khorobkov, I.; Gambarotta, S.; Yap, G. P. A. *Organometallics* **2002**, *21*, 3088. (c) Scott, J.; Vidyaratne, I.; Korobkov, I.; Gambarotta, S.; Budzelaar, P. H. M. *Inorg. Chem.* **2008**, *47*, 896-911.

[26] Scott, J.; Gambarotta, S.; Korobkov, I. *Can. J. Chem.* **2005**, *83*, 279.

[27] Davis, R. N.; Tanski, J. M.; Adrian Jr., J. C.; Tyler, L. A. *Inorg. Chim. Acta* **2007**, *360*, 3061-3068.

[28] Lange, C. W.; Conklin, B. J.; Pierpont, C. G. *Inorg. Chem.* **1994**, *33*, 1276-1283.

[29] Milsmann, C.; Wieghardt, K. Unpublished results.

[30] Variable temperature magnetic data modeled by Dr. Carsten Milsmann.

[31] Cotton, F. A.; Wilkinson, G. *Advance Inorganic Chemistry*, 4th ed.; Wiley: New York, 1980.

[32] Drago, R. S. *Physical Methods in Inorganic Chemistry*; Reinhold Publishing Co.: New York, 1965.

[33] EPR data modeled by Drs. Eckhard Bill and Carsten Milsmann.

[34] Scott, J.; Gambarorra, S.; Korobkov, I.; Knijnenburg, Q.; de Bruin, B.; Budzelaar, P. H. M. *J. Am. Chem. Soc.* **2005**, *127*, 17204-17206.

[35] DFT calculations performed by Dr. Carsten Milsmann.

[36] Humphries, M. J.; Tellmann, K. P.; Gibson, V. C.; White, A. J. P.; Williams, D. J. *Organometallics* **2005**, *24*, 2039-2050.

[37] Goedken, V. L.; Peng, S. *J. Chem. Soc., Chem. Commun.* **1975**, 258-260.

[38] Cao, Y.; Petersen, J. L.; Stolzenberg, A. M. *Inorg. Chim. Acta* **1997**, *263*, 139-148.

[39] Saito, T.; Sawada, S. *Bull. Chem. Soc. Jpn.* **1985**, *58*, 459-463.

[40] Wiberg, N.; Holleman, A. F.; Wiberg, E. *Inorganic Chemistry*, 1st ed.; Academic Press: San Diego, 2001.

[41] LaPointe, R. E.; Wolczanski, P. T.; Mitchell, J. F. *J. Am. Chem. Soc.* **1986**, *108*, 6382-6384.

[42] Pangborn, A. B.; Giardello, M. A.; Grubbs, R. H.; Rosen, R. K.; Timmers, F. J. *Organometallics* **1996**, *15*, 1518.

[43] Kooistra, T. M.; Hetterscheid, D. G. H.; Schwartz, E.; Knijnenburg, Q.; Budzelaar, P. H. M.; Gal, A. W. *Inorg. Chim. Acta* **2004**, *357*, 2945-2952.

[44] Kim, I.; Hwang, J.; Lee, J. K.; Ha, C. S.; Woo, S. I. *Macromol. Rapid Commun.* **2003**, *24*, 508.

[45] Aggarwal, R. P.; Connelly, N. G.; Crespo, M. C.; Dunne, B. J.; Hopkins, P. M.; Orpen, A. G. *J. Chem. Soc. Dalton Trans.* **1992**, 655.

[46] Sur, S. K. *J. Mag. Res.* **1989**, *82*, 169-173.

[47] http://ewww.mpi-muelheim.mpg.de/bac/logins/bill/julX_en.php

[48] Castro, P. M.; Lappalainen, K.; Ahlgrén, M.; Leskelä, M.; Repo, T. *J. Polym. Sci. Part A: Polym, Chem.* **2003**, *41*, 1380-1389.

CHAPTER 2

INVESTIGATION OF THE ELECTRONIC STRUCTURE AND C-H BOND ACTIVATION CHEMISTRY OF BIS(IMINO)PYRIDINE IRON IMIDES

2.1 Abstract

A series of bis(imino)pyridine iron alkyl imides (^{Ar}PDI)FeNR (^{Ar}PDI = 2,6-(2,6-^{i}Pr$_2$-C$_6$H$_3$-N=CMe)$_2$C$_5$H$_3$N (^{iPr}PDI), 2,6-(2,6-^{i}Pr$_2$-C$_6$H$_3$-N=CMe)$_2$-4-*t*Bu-C$_5$H$_3$N (^{iPr}*p*-^{t}BuPDI); R = 1-Ad, 2-Ad, ^{Cy}Octyl) was prepared by treatment of the iron bis(dinitrogen) compound (^{Ar}PDI)Fe(N$_2$)$_2$ (^{Ar}PDI = ^{iPr}PDI, ^{iPr}*p*-^{t}BuPDI) with the appropriate organic azide. A combination of X-ray crystallography, variable temperature SQUID magnetization data and Mössbauer spectroscopy was used to elucidate the electronic structure of each iron imide. When R = 1-Ad or ^{Cy}Octyl, (^{Ar}PDI)FeNR is best described as having an intermediate-spin iron(IV) center antiferromagnetically coupled to a triplet diradical bis(imino)pyridine chelate. When R = 2-Ad, thermal spin crossover from $S = 0$ to $S = 1$ was observed when warming from 15 K to 200 K. The $S = 0$ state is likely identical to the electronic structure of the other $S = 0$ bis(imino)pyridine iron imides, while the $S = 1$ state is best described as a high-spin iron(IV) center antiferromagnetically coupled to a triplet diradical bis(imino)pyridine chelate. In compounds where R = 1-Ad or ^{Cy}Octyl, (^{Ar}PDI)FeNR promoted C-H bond activation of both imine methyl groups of the bis(imino)pyridine ligand. The C-H bond activation with (^{iPr}PDI)FeN(^{Cy}Oct) was first-order in iron with a rate constant of $k = 3.4(2)\times10^{-5}$ s^{-1} at 25 °C and a primary kinetic isotope effect of 3.3(2), consistent with a rate-determining step of intramolecular C-H bond activation. In contrast, no C-H bond activation of the ligand was observed for the iron imide complexes that are $S = 1$ at 23 °C.

2.2 Introduction

Iron complexes containing Fe-N multiple bonds are attractive synthetic targets due to their relevance to nitrogen fixation and group transfer chemistry. A number of terminal iron imides have been characterized to date, although complexes of this sort are still not common.[1] The isolated iron imide species range in oxidation state from +2 to +5,[2] and utilize both *N*-alkyl and *N*-aryl imide substituents. Several of these iron imide species exhibit radical character on the nitrogen and participate in both intramolecular C-H bond activation of the ligand and intermolecular C-H bond activation of substrates such as 1,4-cyclohexadiene.[1e,3]

The first well-characterized terminal iron imide species were prepared by Lee and coworkers in 2000.[4] The imido-cubane complexes, $[Fe_4(\mu_3\text{-}N^tBu)_4Cl_4]$ and $[Fe_4(\mu_3\text{-}N^tBu)_4(N^tBu)Cl_3]$, feature three bridging imide groups, as well as a terminal iron imide in the case of $[Fe_4(\mu_3\text{-}N^tBu)_4(N^tBu)Cl_3]$.[4] For the terminal iron imide group, a short Fe-N_{imide} bond length of 1.635(4) Å was observed, with a near-linear Fe-N_{imide}-$C_{t\text{Bu}}$ angle of 178.6(3)°. Other examples of iron imide complexes with pseudotetrahedral metal centers have been prepared both by Peters and coworkers,[1b-d,2] and Smith and coworkers.[3d] The tris(phosphino)borate ligands employed by Peters and coworkers support a variety of iron imide complexes, including aryl- and alkyl-substituted imide groups. The aryl-substituted iron(III) imide complex, $[PhBP_3]$Fe(N-*p*-tolyl), exhibits an Fe-N_{imide} bond length of 1.6578(2) Å that is significantly longer than the bond length observed for Lee's imido-cubane complex, but is still consistent with a triple bond.[1b] $[PhBP_3]$Fe(N-*p*-tolyl) also exhibits interesting reactivity, demonstrating both hydrogenation of the Fe-N bond and group transfer to afford the corresponding isocyanate. The reactivity of iron imide complexes will be discussed in greater detail in Chapter 3.

The series of alkyl-substituted tris(phosphino)borate complexes prepared by Peters and coworkers demonstrates the ability to synthesize iron imide complexes with a range of metal oxidation states. Anionic iron(II), neutral iron(III) and cationic Fe(IV) complexes were all isolated and crystallographically characterized.[1c-d] The anionic iron(II) complex, $\{[PhBP_3]FeN(^1Ad)\}\{^nBu_4N\}$, has an Fe-$N_{imide}$ bond length of 1.651(3) Å, similar to the aryl-substituted iron imide complex,[1c] while the Fe-N_{imide} bond length for the neutral iron(III) complex, $[PhBP_3]FeN(^1Ad)$, is 1.641(2) Å. The Fe-N_{imide} bond length observed for the cationic iron(IV) complex, $\{[PhBP^{t\mathrm{Bu}}{}_2(pz)]FeN(^1Ad)\}\{(B(Ar_F)_4)\}$ (pz = pyrazolyl), was 1.634(4) Å.[1d] Similarly, Smith and coworkers isolated both a neutral iron(III) imide, $L^{Mes}FeN(Ad)$ (L^{Mes} = phenyltris(1-mesitylimidazol-2-ylidene)borate), and the corresponding cationic iron(IV) complex, $[L^{Mes}FeN(Ad)]OTf$.[3d] As with the complexes synthesized by Peters and coworkers, the Fe-N_{imide} bond length of 1.618(3) Å observed for the cation was contracted compared to the bond length of 1.624(5) Å for the neutral complex. Notably, the Fe-N_{imine} distances for these two complexes are the shortest that have been observed to date for both neutral and cationic iron imide complexes.

Apart from the opportunity for investigating interesting electronic structures, iron imide complexes often display remarkable reactivity. Activation of weak C-H bonds by iron and cobalt imide complexes has commonly been observed.[3] In several cases, C-H bond activation occurs even when the corresponding iron imide complex was not isolated. Borovik and coworkers observed formation of an iron amide complex, $[FeH_2\mathbf{2}(NHTol)]^-$, upon treatment of $[FeH_2\mathbf{2}]^-$ with *p*-tolyl azide.[3b] When the reaction was carried out in the presence of diphenylhydrazine, formation of azobenzene was observed, indicating that the C-H activation could be either inter- or intramolecular (Figure 2.1).

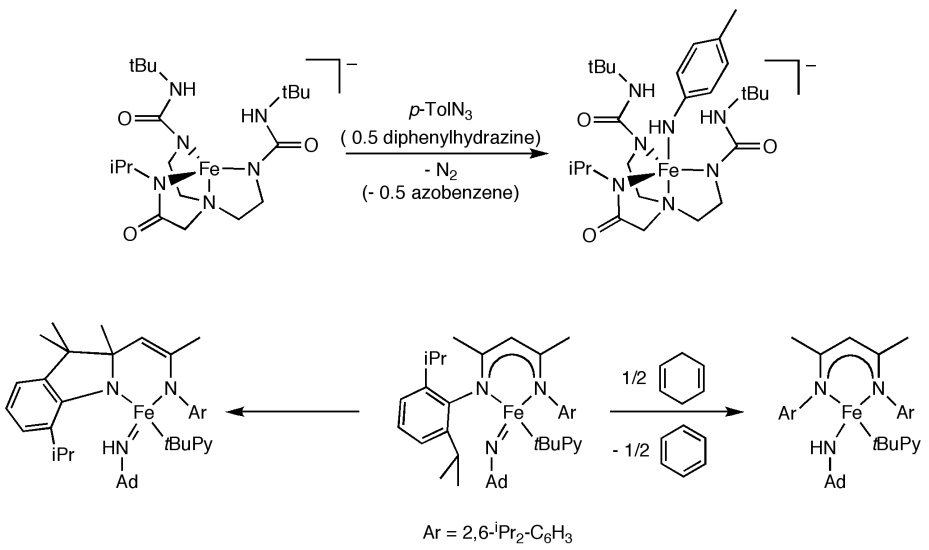

Figure 2.1 Examples of inter- and intramolecular C-H bond activation by iron imide complexes.

Similarly, both inter- and intramolecular C-H bond activation was observed by Holland and coworkers with the iron(III) imide species, LFe(N^1Ad)(tBuPy).[3e] Although LFe(N^1Ad)(tBuPy) has been spectroscopically characterized, the complex was not isolated and the C-H activation reaction occurs *in situ*. In the absence of an external H-atom source, modification of the β-diketiminate ligand is observed (Figure 2.1). Addition of 1,4-cyclohexadiene promotes intermolecular C-H bond activation to give the iron amide complex, LFe(NH^1Ad)(tBuPy), and benzene.[3e] Betley and coworkers also observed modification of the ligand as a result of intramolecular C-H activation by a putative iron imide species.[3c]

Terminal bis(imino)pyridine iron imides (^{iPr}PDI)FeN*Ar* (^{iPr}PDI = 2,6-(2,6-$^{i}Pr_2$-C_6H_3-N=CMe)$_2C_5H_3N$; *Ar* = 2,6-$^{i}Pr_2$-C_6H_3, 2,6-Et_2-C_6H_3, 2,5-$^{t}Bu_2$-C_6H_3, 2,4,6-Me_3-C_6H_3) previously prepared by our research group have served as the foundation for electronic structure investigation of additional bis(imino)pyridine iron imide complexes (Figure 2.2).[5] A combination of crystallographic data, variable temperature SQUID magnetization data and Mössbauer spectroscopy established that these

complexes have a triplet ground state and are best described as intermediate-spin iron(III) antiferromagnetically coupled to a monoreduced bis(imino)pyridine chelate.[5]

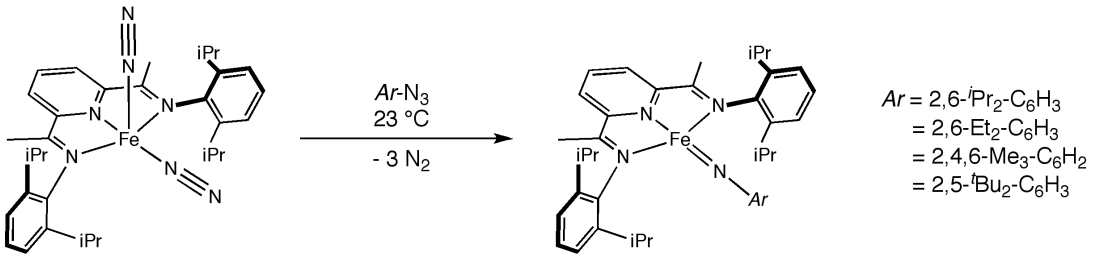

Figure 2.2 Preparation of aryl-substituted bis(imino)pyridine iron imide complexes.

A notable feature of these molecules is that the imide substituent is lifted significantly out of the plane of the bis(imino)pyridine chelate. For (^{iPr}PDI)FeN(^{iPr2}Ph) (**1-N(^{iPr2}Ph)**) the observed N_{pyr}-Fe-N_{imide} angle was 138.79(7)°, while for (^{iPr}PDI)FeN(^{Me3}Ph) (**1-N(^{Me3}Ph)**) a less distorted angle of 154.75(7)° was observed.[5] This geometric distortion is likely to avoid steric interactions between the ortho substituents on the imide group and the isopropyl groups of the bis(imino)pyridine chelate. In addition, repulsion between the electron pairs in the iron d_{xy} and imide nitrogen p_x orbitals may contribute to the deviation from planarity.[5]

For (^{iPr}PDI)FeN*Ar* complexes, complete hydrogenation of the Fe-N_{imide} bond upon exposure to dihydrogen was observed, furnishing the corresponding aniline and the bis(imino)pyridine iron dihydrogen complex, (^{iPr}PDI)Fe(H_2). Catalytic hydrogen of azide by (^{iPr}PDI)Fe(N_2)$_2$ (**1-(N_2)$_2$**) was achieved where *Ar* = 2,6-^{i}Pr$_2$-C_6H_3, 2,6-Et$_2$-C_6H_3 and 2,5-^{t}Bu$_2$-C_6H_3.[5] In addition, stoichiometric N*Ar* group transfer to carbon monoxide to furnish the corresponding isocyanate was observed for all (^{iPr}PDI)FeN*Ar* complexes.[5] The promising reactivity of these compounds prompted exploration into synthesis of the *N*-alkyl analogs.

2.3 Preparation of Alkyl Iron Imides

Slow addition of either 1-adamantyl azide or cyclooctyl azide to a pentane solution of **1-$(N_2)_2$** furnished the corresponding iron imide species, (^{iPr}PDI)FeNR (R = 1-Ad (**1-N(^{1}Ad)**, R = ^{Cy}Oct, **1-N(^{Cy}Oct)**), respectively (Figure 2.3). In contrast to the previously prepared deep blue or indigo aryl iron imides, **1-N(^{1}Ad)** and **1-N(^{Cy}Oct)** are bright purple. Also in striking contrast to the aryl imides, the benzene-d_6 ^{1}H NMR spectra of **1-N(^{1}Ad)** and **1-N(^{Cy}Oct)** at 23 °C are indicative of diamagnetic, C_{2v} symmetric compounds. Although the chemical shift range is wider than that of a "typical" diamagnetic compound and spans approximately 45 ppm, the expected proton-proton coupling is observed for nearly all resonances, as opposed to the broad and featureless peaks typically observed with paramagnetic compounds. In addition, ^{13}C NMR spectra were obtained for **1-N(^{1}Ad)** and **1-N(^{Cy}Oct)**, something that is generally not feasible for paramagnetic compounds.

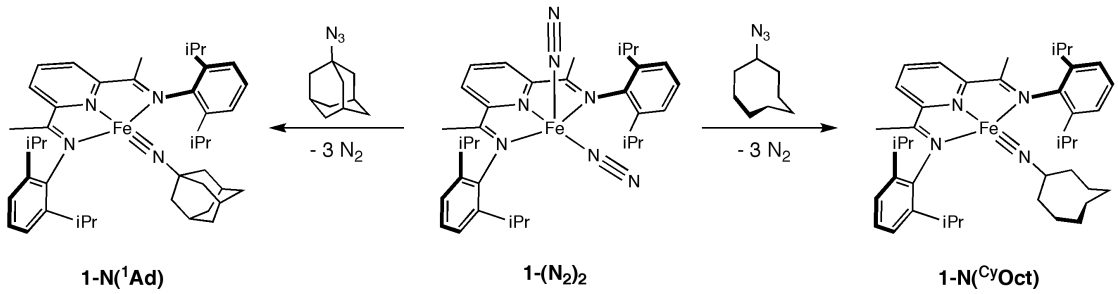

Figure 2.3 Preparation of (^{iPr}PDI) alkyl iron imides.

X-ray quality crystals of **1-N(^{1}Ad)** and **1-N(^{Cy}Oct)** were obtained by cooling a pentane solution of each compound to -35 °C. The solid state structure of **1-N(^{1}Ad)** establishes distorted square planar geometry (Figure 2.4). Selected bond angles and distances are presented in Table 2.1. Consistent with the C_{2v} symmetry observed by ^{1}H NMR spectroscopy, a mirror-plane bisects the pyridine ring and equivalences the two halves of the molecule. While **1-N(^{1}Ad)** is not as distorted as the crystallographically

characterized bis(imino)pyridine aryl iron imides,[5] the imide nitrogen is still lifted appreciably out of the idealized plane of the bis(imino)pyridine chelate, with an N_{py}-Fe-N_{imide} angle of 168.10(8)° (Figure 2.5). The imide substituent itself is slightly bent with an Fe-N_{imide}-C_{imide} angle of 159.87(15)°. The majority of crystallographically characterized iron and cobalt imides have M-N_{imide}-C_{imide} angles that are within several degrees of linear,[6] however the β-diketiminate cobalt imide, [Me_2NN]CoN(Ad) (Me_2NN = 3,5-bis(2,6-dimethylphenylimido)pent-4-yl) prepared by Warren and coworkers has a slightly more bent Co-N_{imide}-C_{imide} angle of 161.5(3)°.[6a] Similarly, for **1-N(^iPr2Ph)** and **1-N(^Me3Ph)** Fe-N_{imide}-C_{imide} angles of 165.68(15)° and 159.00(13)°, respectively, are observed.

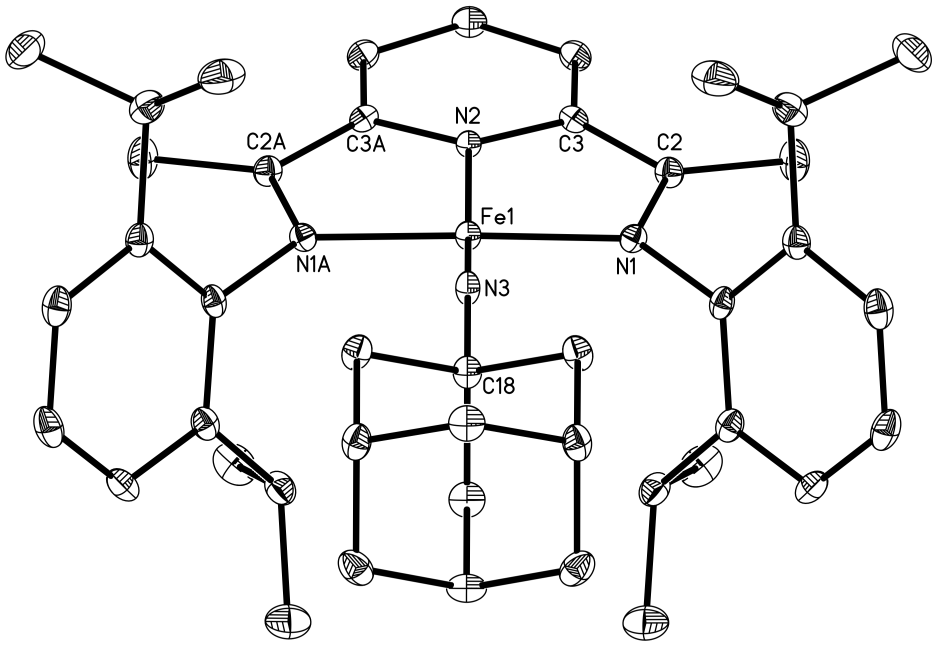

Figure 2.4 Molecular structure of **1-N(^1Ad)** at 30 % probability ellipsoids. Hydrogen atoms omitted for clarity.

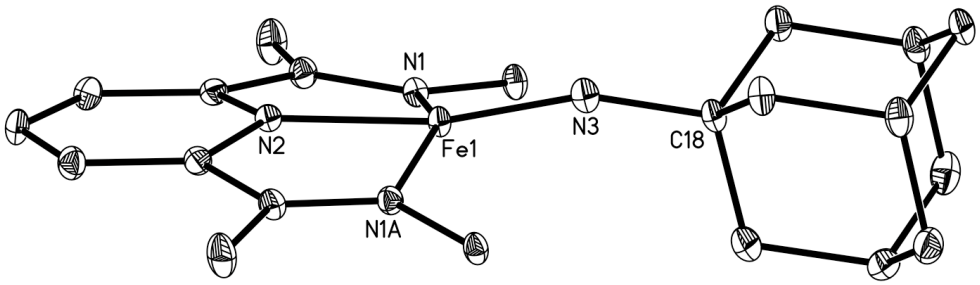

Figure 2.5 Molecular structure of **1-N(1Ad)** at 30 % probability ellipsoids. Hydrogen atoms and aryl groups omitted for clarity.

Table 2.1 Selected bond distances (Å) and angles (°) for **1-N(1Ad)**.

Fe(1)-N(3)	1.6481(15)	C(2)-C(3)	1.4178(19)
Fe(1)-N(1)	1.9325(11)	N(2)-Fe(1)-N(3)	168.10(8)
Fe(1)-N(2)	1.8950(15)	Fe(1)-N(3)-C(18)	159.87(15)
N(1)-C(2)	1.3395(16)		

The Fe-N_{imide} bond distance of 1.6481(15) Å is consistent with other crystallographically characterized neutral, monomeric iron imide species, which range in value from 1.625(4) Å to 1.6578(2) Å.[1,3d] The Fe-N_{imide} bond length observed for **1-N(1Ad)** is significantly shorter than the Fe-N_{imide} bond lengths of 1.7048(16) Å and 1.7165(15) Å observed for **1-N(iPr2Ph)** and **1-N(Me3Ph)**, respectively, indicating a higher Fe-N bond order for **1-N(1Ad)**.[5] The metrical parameters of the bis(imino)pyridine chelate in **1-N(1Ad)** establish distortions that are consistent with two-electron reduction.[7] The C_{imine}-N_{imine} distance of 1.3395(16) Å (both sides of the molecule are identical due to symmetry) is elongated while the C_{imine}-C_{ipso} distance of

1.4178(19) Å, also related by symmetry, are noticeably contracted compared to reference values for the neutral chelate.[7]

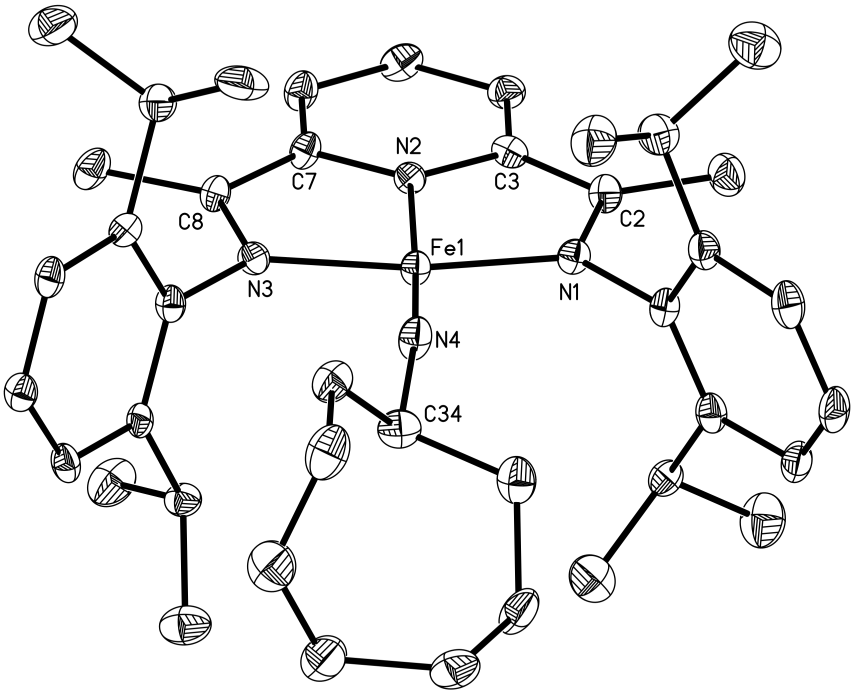

Figure 2.6 Molecular structure of **1-N(^{Cy}Oct)** at 30 % probability ellipsoids. Hydrogen atoms omitted for clarity.

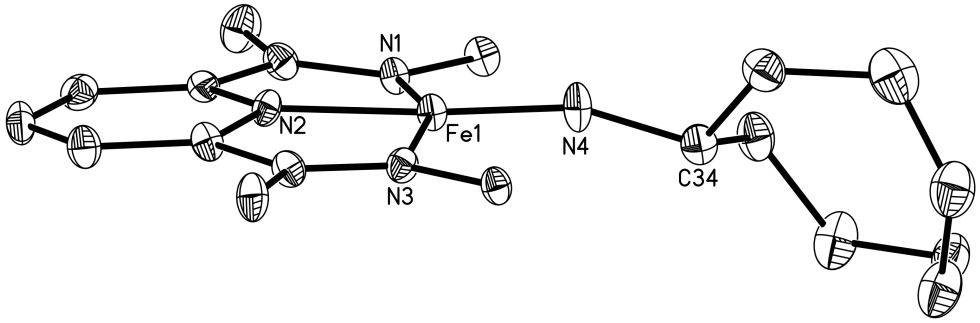

Figure 2.7 Molecular structure of **1-N(^{Cy}Oct)** at 30 % probability ellipsoids. Hydrogen atoms and aryl groups omitted for clarity.

Table 2.2 Selected bond distances (Å) and angles (°) for **1-N(^{Cy}Oct)**.

Fe(1)-N(4)	1.648(3)	N(3)-C(8)	1.355(5)
Fe(1)-N(1)	1.901(3)	C(2)-C(3)	1.405(5)
Fe(1)-N(2)	1.870(3)	C(7)-C(8)	1.406(5)
Fe(1)-N(3)	1.908(3)	N(2)-Fe(1)-N(4)	175.14(16)
N(1)-C(2)	1.345(5)	Fe(1)-N(4)-C(34)	160.9(3)

The molecular structure of **1-N(^{Cy}Oct)** (Figure 2.6) is similar to that of **1-N(^{1}Ad)**, although the geometry of **1-N(^{Cy}Oct)** is closer to idealized square planar, with the sum of the angles around iron equal to 360.42(27)°. The N_{py}-Fe-N_{imide} angle is 175.14(16)°, demonstrating that the imide substituent is not lifted significantly out of idealized plane of the chelate (Table 2.2). As with **1-N(^{iPr2}Ph)** and **1-N(^{Me3}Ph)**,[5] a bend is observed at the imide nitrogen, resulting in an Fe-N_{imide}-C_{imide} angle of 160.9(3)°. The Fe-N_{imide} bond length in **1-N(^{Cy}Oct)**, 1.648(3) Å, is almost identical to **1-N(^{1}Ad)** and thus is also consistent with a higher Fe-N bond order than the *N*-aryl substituted iron imide complexes. Distortions of the chelate compared to the neutral bis(imino)pyridine ligand are observed, with the C_{imine}-N_{imine} bonds elongated to 1.345(5) Å and 1.355(5) Å and the C_{imine}-C_{ipso} bonds contracted to 1.405(5) Å and 1.406(5) Å (Table 2.2). These changes in bond length are consistent a doubly-reduced chelate.[7]

Encouraged by the isolation of two new iron imide complexes, the syntheses of similar compounds with variations of the bis(imino)pyridine ligand were attempted (Figure 2.8). Slow addition of 1-adamantyl azide to a pentane solution of (^{iPr}*p*-^{t}BuPDI)Fe(N_2)$_2$ (**^{tBu}1-N_2**) (^{iPr}*p*-^{t}BuPDI = 2,6-(2,6-$^{i}Pr_2$-C_6H_3N=CMe)$_2$-4-^{t}Bu-C_5H_3N)[8] resulted in formation of the corresponding iron imide, (^{iPr}*p*-^{t}BuPDI)FeN(^{1}Ad) (**^{tBu}1-**

N(1Ad)). Likewise, treatment of **tBu1-N2** with cyclooctyl azide in pentane furnished (^{iPr}p-^{t}BuPDI)FeN(^{Cy}Oct) (**tBu1-N(CyOct)**). Unfortunately, **tBu1-N(CyOct)** could not be isolated cleanly due to the similar solubilities of the compound and the impurity. Both iron imide complexes exhibit benzene-d_6 ^{1}H NMR spectra similar to **1-N(1Ad)** and **1-N(CyOct)** at 23 °C, with widened chemical shift ranges but observable splitting for the majority of resonances.

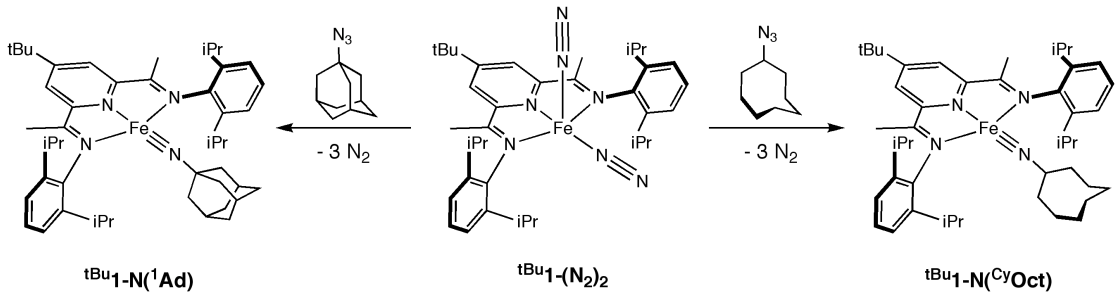

Figure 2.8 Preparation of (^{iPr}p-^{t}BuPDI) alkyl iron imides.

The series of alkyl iron imides was further investigated using zero-field ^{57}Fe Mössbauer spectroscopy, with the exception of **tBu1-N(CyOct)**. A representative spectrum of **tBu1-N(1Ad)** is presented in Figure 2.9. For **1-N(CyOct)**, a small amount of an impurity (3 %) was present in the Mössbauer sample. This impurity was identified as (^{iPr}PDI)Fe[(N^{Cy}Oct)NN(N^{Cy}Oct)], the product from cycloaddition of cyclooctyl azide to **1-N(CyOct)**.[9] For **1-N(1Ad)**, **1-N(CyOct)** and **tBu1-N(1Ad)** the Mössbauer parameters are almost identical. A comparison of Mössbauer parameters for all bis(imino)pyridine iron imides is presented in Table 2.5 (*vide infra*). For **1-N(1Ad)** an isomer shift of 0.04 mm·s^{-1} and a quadrupole splitting of -2.38 mm·s^{-1} were observed, while for **tBu1-N(1Ad)** an isomer shift of 0.00 mm·s^{-1} and a quadrupole splitting of $|2.38|$ mm·s^{-1} were observed. The sign of the quadrupole splitting for **1-N(1Ad**) was determined by applied-field (70 kG) Mössbauer spectroscopy at 4.2 K (Figure 2.10). The applied-field Mössbauer spectrum also established that **1-N(1Ad**) is diamagnetic

at 4.2 K. The similarity of the parameters for **1-N(**^{1}**Ad)** and **^{tBu}1-N(**^{1}**Ad)** indicates there is little electronic difference between the ^{iPr}PDI and ^{iPr}*p*-^{t}BuPDI ligands. For **1-N(**^{Cy}**Oct)**, a isomer shift of -0.02 mm·s^{-1} and a quadrupole splitting of $|2.61|$ mm·s^{-1} were observed.

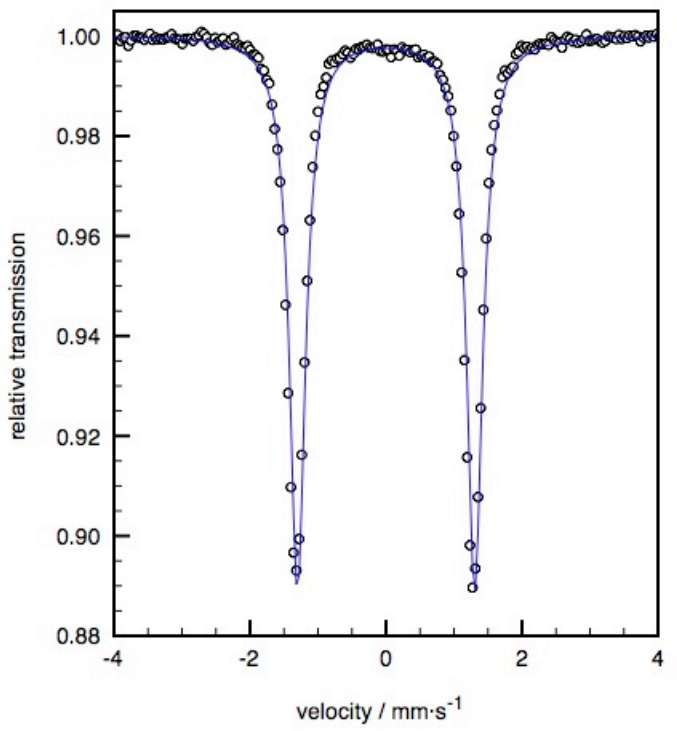

Figure 2.9 Zero-field Mössbauer spectrum of **^{tBu}1-N(**^{1}**Ad)** at 80 K; δ = 0.00 mm·s^{-1}, ΔE_Q = 2.61 mm·s^{-1}.

For all three alkyl iron imides, the Mössbauer isomer shifts establish covalent molecules and are significantly lower than the δ value of 0.30 mm·s^{-1} observed for **1-N(**^{iPr2}**Ph)**.[5] Because the metal center in **1-N(**^{iPr2}**Ph)** is best described as intermediate-spin iron(III), the data for the *N*-alkyl iron imides are more consistent iron(IV). No bis(imino)pyridine compounds with iron(IV) centers have previously been synthesized, so an unambiguous assignment is not feasible based on the zero-field Mössbauer parameters alone. However, the zero-field Mössbauer spectrum of the

bis(imino)pyridine iron nitrosyl complex, (^{iPr}PDI)Fe(NO), which is likely best described as low-spin iron(III), exhibits an isomer shift of 0.10 mm·s^{-1},[10] suggesting that the iron(IV) description for the *N*-alkyl bis(imino)pyridine iron imide complexes is correct.

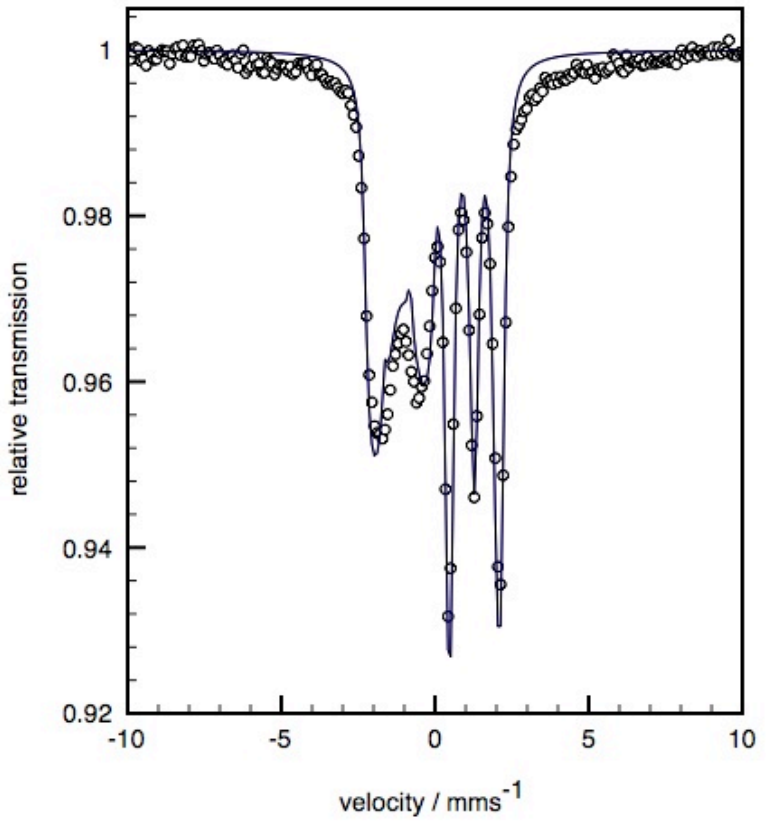

Figure 2.10 Applied-field Mössbauer spectrum of **1-N(^{1}Ad)** (70 kG) at 4.2 K; δ = 0.04 mm·s^{-1}, ΔE_Q = 2.38 mm·s^{-1}.

2.4 Preparation of A Spin-Crossover Alkyl Iron Imide

Inspired by the preparation of the aforementioned iron imides, the 2-adamantyl isomer of **1-N(^{1}Ad)** was also explored. Slow addition of 2-adamantyl azide to a pentane solution of **1-(N_2)$_2$** at 23 °C furnished (^{iPr}PDI)FeN(^{2}Ad) (**1-N(^{2}Ad)**) (Figure 2.11). Although **1-N(^{2}Ad)** is an isomer of **1-N(^{1}Ad)**, the spectroscopic properties of

the compounds are remarkably different at ambient temperature. While **1-N(1Ad)** and the other alkyl iron imides are bright purple, **1-N(2Ad)** is extremely dark in color and appears black both in solution and the solid state. Moreover, the benzene-d_6 ^{1}H NMR spectrum of **1-N(2Ad)** at 23 °C displays the number of resonances expected for a C_{2v} symmetric compound. The resonances are paramagnetically broadened and cover more than 200 ppm, in contrast to range of 45 ppm observed for **1-N(1Ad)**. Solution magnetic measurements for **1-N(2Ad)** establish an effective magnetic moment of 3.0(2) μ_B at 23 °C, consistent with two unpaired electrons.

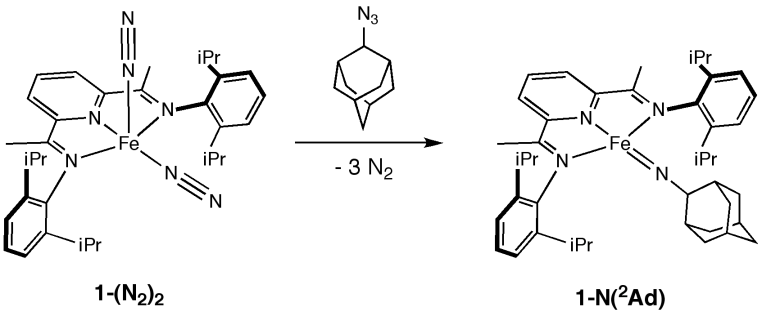

Figure 2.11 Treatment of **1-(N$_2$)$_2$** with 2-adamantyl azide.

X-ray quality crystals of **1-(N2Ad)** were obtained by cooling a concentrated pentane solution of the compound to -35 °C. The data were collected at 220 K in order to observe only the high-spin isomer of **1-(N2Ad)**. Previous attempts to collect X-ray data at 173 K were unsuccessful, likely because cooling the crystals caused spin-crossover and disruption of the ordering within the crystal. Positional disorder was observed in the atoms of the 2-adamantyl substituent, particularly the 2-adamantyl substituent. Selected bond distances and angles are presented in Table 2.3. The solid state structure establishes a C_{2v} symmetric molecule with idealized square planar geometry (Figure 2.12), with the sum of the angles around iron equal to 360.13(22)°. The N_{pyr}-Fe-N_{imide} angle of 175.64(13)° is nearly identical to that observed for **1-**

N(^Cy^Oct), indicating that the imide substituent is not significantly lifted out of the idealized plane of the chelate (Table 2.3).

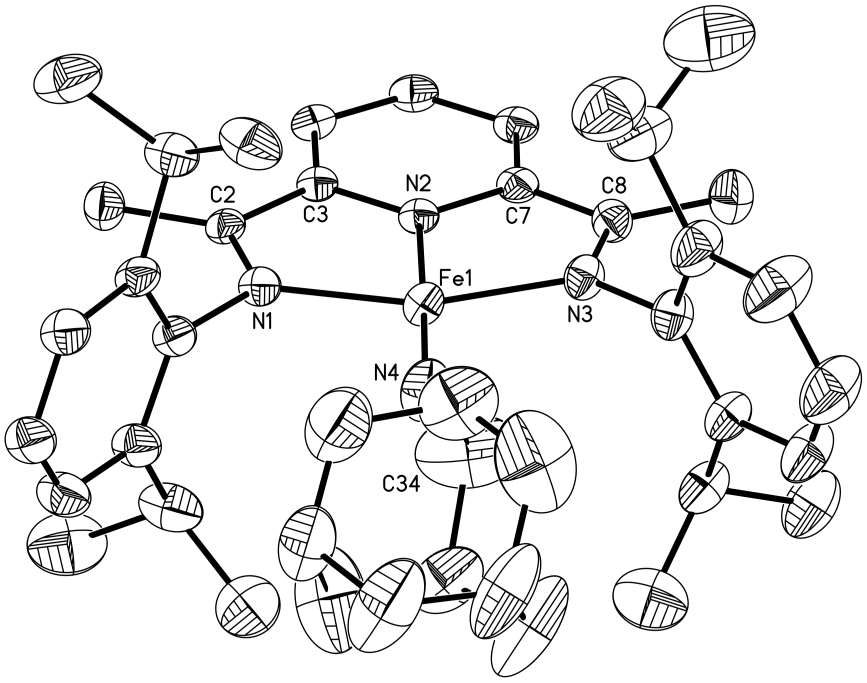

Figure 2.12 Molecular structure of **1-N(^2^Ad)** at 30 % probability ellipsoids. Hydrogen atoms omitted for clarity.

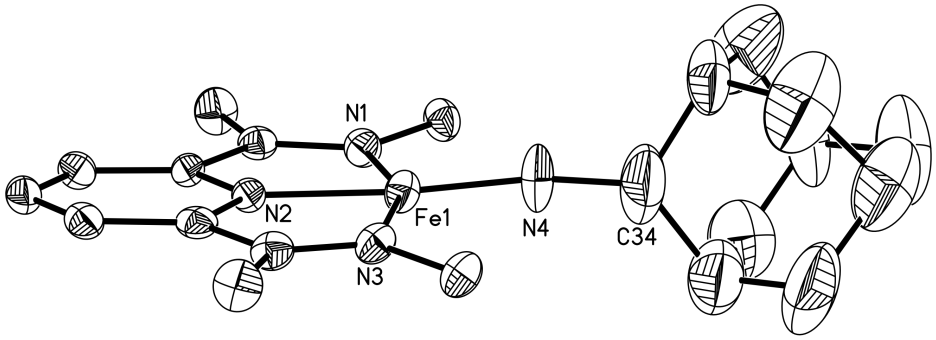

Figure 2.13 Molecular structure of **1-N(^2^Ad)** at 30 % probability ellipsoids. Hydrogen atoms and aryl groups omitted for clarity.

Table 2.3 Selected bond distances (Å) and angles (°) for **1-N(^{2}Ad)**.

Fe(1)-N(4)	1.675(3)	N(3)-C(8)	1.339(4)
Fe(1)-N(1)	1.978(2)	C(2)-C(3)	1.434(4)
Fe(1)-N(2)	1.898(2)	C(7)-C(8)	1.414(4)
Fe(1)-N(3)	1.960(2)	N(2)-Fe(1)-N(4)	175.64(13)
N(1)-C(2)	1.337(4)	Fe(1)-N(4)-C(34)	158.7(4)

The Fe-N_{imide} bond observed for **1-N(^{2}Ad)**, 1.675(3) Å, is notably longer than the Fe-N_{imide} distances for **1-N(^{1}Ad)** and **1-N(^{Cy}Oct)**. The Fe-N_{imide} distance for **1-N(^{2}Ad)** is also shorter than the Fe-N_{imide} distances for **1-N(^{iPr2}Ph)** and **1-N(^{Me3}Ph)**.[5] As with all other structurally characterized bis(imino)pyridine iron imide complexes, a modest bend is observed at the imide nitrogen. In this case the molecular structure exhibits a Fe-N_{imide}-C angle of 158.7(4)°. Examination of the metrical parameters of the bis(imino)pyridine chelate establish elongation of the C_{imine}-N_{imine} bonds and contraction of the C_{imine}-C_{ipso} bonds that are consistent with two electron reduction.[7] The C_{imine}-N_{imine} bond lengths are elongated to 1.337(4) Å and 1.339(4) Å, while the C_{imine}-C_{ipso} distances are contracted to 1.434(4) Å and 1.414(4) Å. These distortions are similar to the amount of ligand reduction established by the molecular structure of **1-N(^{1}Ad)**, and clearly indicate that the bis(imino)pyridine chelate is most consistent with a dianion. The Fe-N_{pyr} distance of 1.898(2) Å and the Fe-N_{imine} distances of 1.978(2) Å and 1.960(2) Å are significantly longer than the iron-ligand distances exhibited by the molecular structures of **1-N(^{1}Ad)** and **1-N(^{Cy}Oct)**. This is likely due to the greater steric bulk of the adamantyl substituent. Moving the chelate arms farther away from the metal center increase the size of the pocket at the metal center and relieves steric congestion.

Table 2.4 Selected bond distances (Å) and angles (°) for bis(imino)pyridine iron imide complexes.

	1-N(^{1}Ad)	**1-N(^{Cy}Oct)**	**1-N(^{2}Ad)**	**1-N(^{iPr2}Ph)**	**1-N(^{Me3}Ph)**
$Fe\text{-}N_{imide}$	1.6481(15)	1.648(3)	1.675(3)	1.7048(16)	1.7165(15)
$Fe\text{-}N_{imine}$	1.9325(11)	1.901(3) 1.908(3)	1.978(2) 1.960(2)	2.0343(16) 1.9870(17)	2.0105(14) 1.9786(14)
$Fe\text{-}N_{pyr}$	1.8950(15)	1.870(3)	1.898(2)	1.8403(15)	1.8718(14)
$N_{imine}\text{-}C_{imine}$	1.3395(16)	1.345(5) 1.355(5)	1.337(4) 1.339(4)	1.320(2) 1.331(2)	1.321(2) 1.334(2)
$C_{imine}\text{-}C_{ipso}$	1.4178(19)	1.405(5) 1.406(5)	1.434(4) 1.414(4)	1.437(3) 1.431(3)	1.436(2) 1.426(2)
$N_{pyr}\text{-}Fe\text{-}N_{imide}$	168.10(8)	175.14(16)	175.64(13)	138.79(7)	154.75(7)
$Fe\text{-}N_{imide}\text{-}C$	159.87(15)	160.9(3)	158.7(4)	165.68(15)	159.00(13)

A summary of the metrical parameters for all of the crystallographically characterized bis(imino)pyridine iron imides is presented in Table 2.4. As demonstrated by the overlay of the molecular structures of **1-N(^{1}Ad)** and **1-N(^{2}Ad)**, the imide nitrogen and *N*-adamantyl substituent of **1-N(^{1}Ad)** are lifted out of the plane of the chelate at an angle of 168.10(8)°, which is significantly larger than the angle of 175.14(16)° observed for **1-N(^{2}Ad)** (Figure 2.14). However, the adamantyl groups overlay quite well for both complexes. In addition, the shorter $Fe\text{-}N_{imide}$ bond length of 1.6481(15) Å is apparent **1-N(^{1}Ad)**.

Notably, both the bis(imino)pyridine chelates and the imide nitrogen in the molecular structures of **1-N(^{Cy}Oct)** and **1-N(^{2}Ad)** overlay almost perfectly (Figure 2.15). This is supported, in part, by the nearly identical $N_{pyr}\text{-}Fe\text{-}N_{imide}$ angles of 175.14(16)° and 175.64(13)° observed for **1-N(^{Cy}Oct)** and **1-N(^{2}Ad)**, respectively. Although **1-N(^{Cy}Oct)** has a singlet ground state and **1-N(^{2}Ad)** has a triplet ground state, the metrical parameters of the molecular structures, including extent of chelate reduction, are very similar. In contrast, the $N_{pyr}\text{-}Fe\text{-}N_{imide}$ angles of 165.68(15)° and

159.00(13)° observed for **1-N(^iPr2Ph)** and **1-N(^Me3Ph)**, respectively indicate that although these complexes possess a triplet ground state like **1-N(^2Ad)**, the electronic structure of the aryl bis(imino)pyridine iron imides is different than that of **1-N(^2Ad)**.

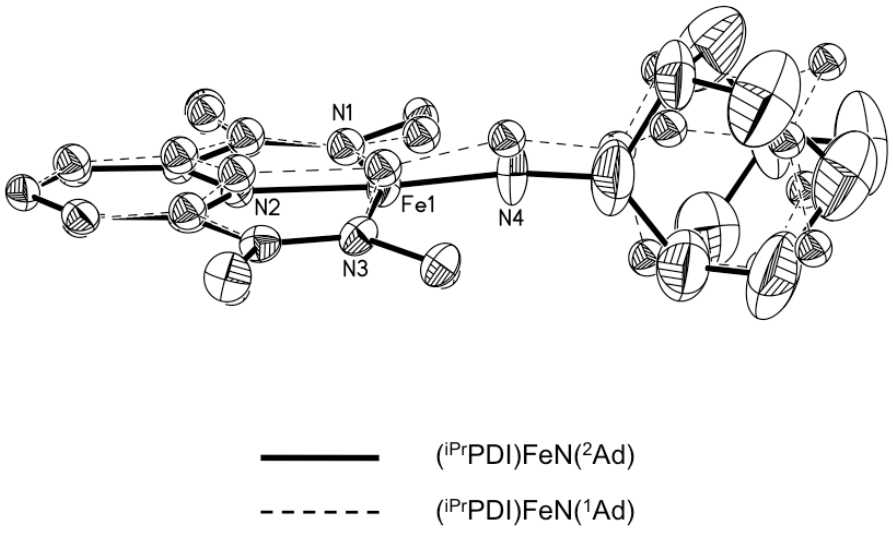

Figure 2.14 Overlay of molecular structures of **1-N(^1Ad)** and **1-N(^2Ad)** at 30 % probability ellipsoids. Hydrogen atoms omitted for clarity.

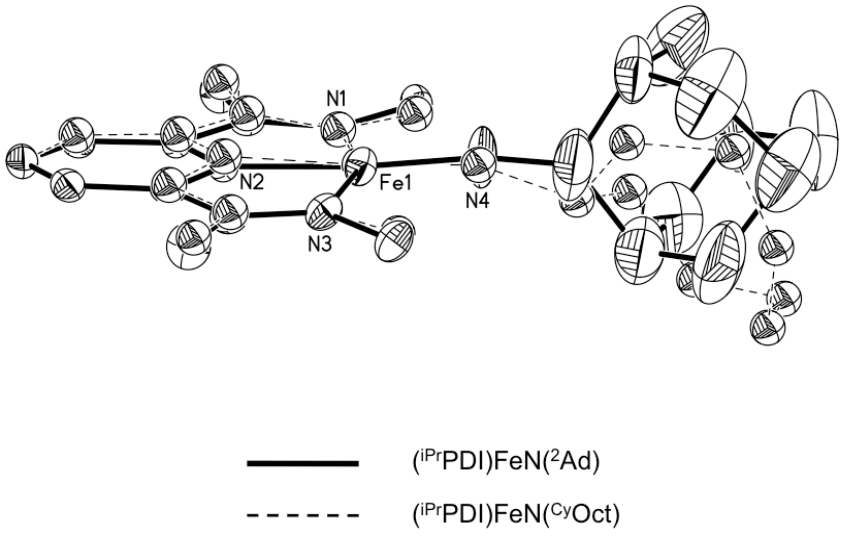

Figure 2.15 Overlay of molecular structures of **1-N(^CyOct)** and **1-N(^2Ad)** at 30 % probability ellipsoids. Hydrogen atoms omitted for clarity.

The solid state magnetic properties of **1-N(^{2}Ad)** were investigated using variable temperature SQUID magnetometry. The effective magnetic moment of 3.2 μ_B at 300 K is consistent with the value of 3.0(2) μ_B obtained by solution magnetic measurements. However, while a decrease in effective magnetic moment from 3.20 μ_B to 1.30 μ_B is seen with decreasing temperature, a plateau is observed around 50 K that indicates spin-crossover behavior (Figure 2.16). The data collected exhibit a gradual, rather than abrupt, spin transition between two different states. The variable temperature magnetic data were reproducibly measured five separate times with independently prepared crystalline sample material, suggesting that free iron metal is not responsible for the unusual magnetic behavior observed. Although variable temperature SQUID magnetization data for **1-N(^{iPr2}Ph)** establish a similar effective magnetic moment of 2.8(2) μ_B at 296 K, the change with decreasing temperature is consistent with a simple paramagnet and no spin transition is observed down to 5 K.[5]

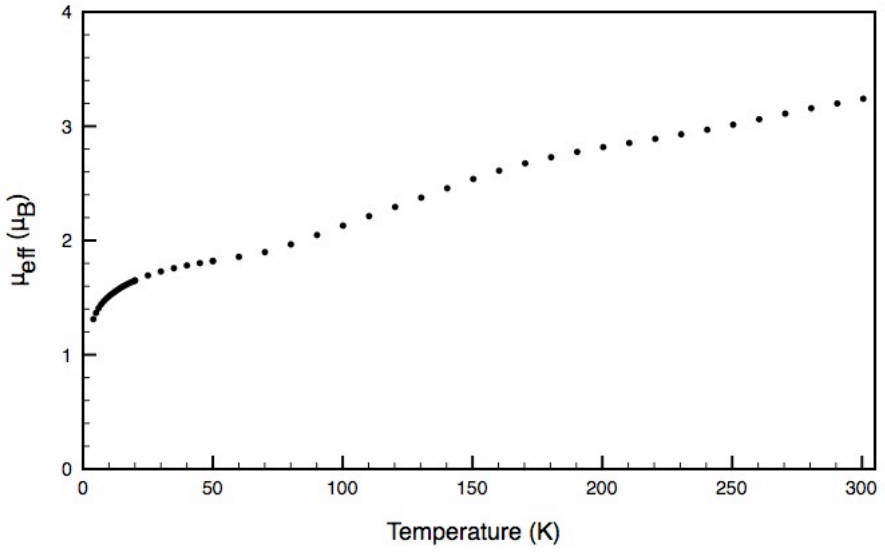

Figure 2.16 Variable temperature SQUID magnetization data (at 1 T) for **1-N(^{2}Ad)**. Data are corrected for underlying diamagnetism.

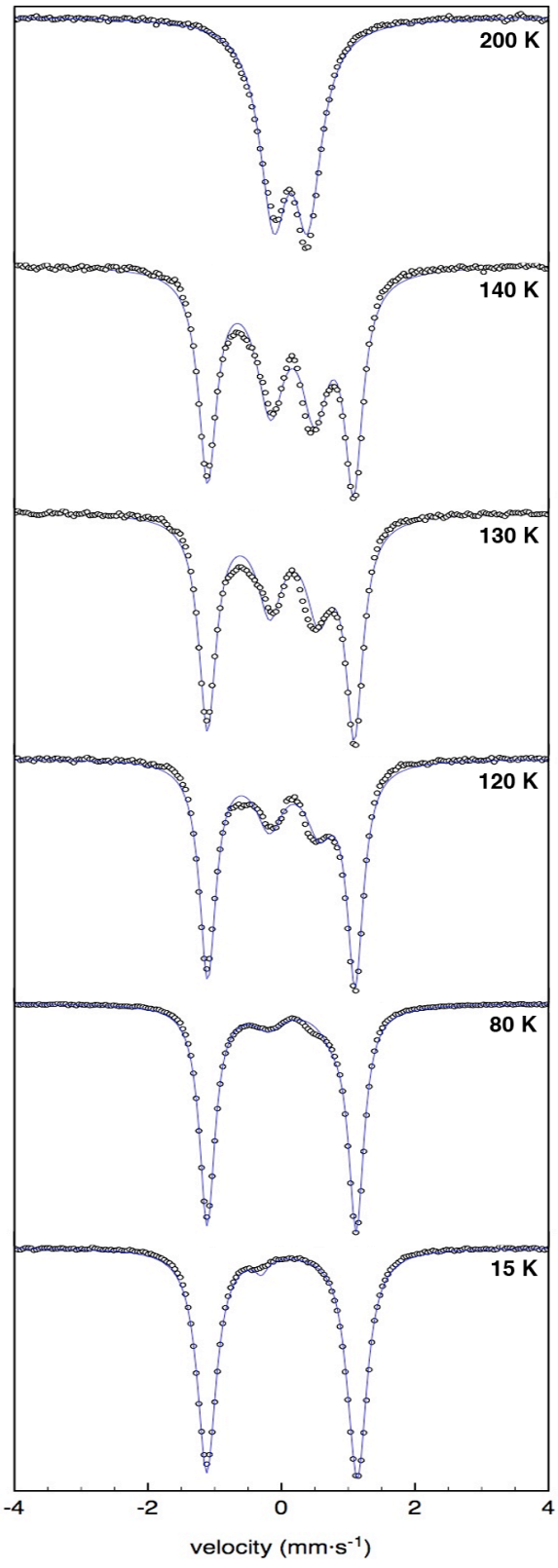

Figure 2.17 Variable temperature zero-field Mössbauer spectra of **1-N(^{2}Ad)**.

In order to better understand the spin crossover behavior of **1-N(²Ad)**, zero-field Mössbauer spectra were collected over a range of temperatures (Figure 2.17). The spectrum obtained at 15 K exhibits a doublet with an isomer shift of 0.01 $mm \cdot s^{-1}$ and a quadrupole splitting of 2.26 $mm \cdot s^{-1}$, parameters that are similar to the other alkyl iron imides (Table 2.5). However, upon warming the sample to 80 K, a second quadrupole doublet is observed that increases in intensity with further warming. The intensity of the doublet observed at 15 K decreases until it is no longer observed at 200 K (Figure 2.17). The parameters of the second quadrupole doublet, $\delta = 0.19$ $mm \cdot s^{-1}$ and $\Delta E_Q = 0.75$ $mm \cdot s^{-1}$, are significantly different than the parameters of the doublet observed at 15 K. Cooling the sample again to 15 K regenerates the initial spectrum observed at that temperature, indicating the spin-crossover behavior is reversible.

The presence of two temperature-dependent species in the zero-field Mössbauer spectrum is consistent with spin-crossover behavior, and the relative amounts of the two iron species at a given temperature are roughly consistent with the variable temperature magnetic data (Figure 2.16). Moreover, upon cooling a benzene-d_6 solution of **1-N(²Ad)** to 77 K there is a color change to bright purple, evidence of thermochromism due to spin crossover behavior.[11] Spin crossover behavior is commonly observed for iron(II) and iron(III) compounds, especially for complexes where strong field ligands such as 1,10-phenanthroline or bipyridine are combined with ligands of intermediate field strength, like thiocyanate (NCS^-).[12] Spin crossover behavior is also well-documented for iron complexes with terdentate ligands, such as the terpyridine derivatives 2,4-bis-(2-pyridyl)thiazole and 2-(2-pyridylamino)-4-(2-pyridyl)thiazole.[13] Notably, no spin crossover behavior was observed for **1-N(¹Ad)**. The zero-field Mössbauer spectrum of **1-N(¹Ad)** at 296 K exhibited a quadrupole doublet with parameters nearly identical to those observed at 80 K.

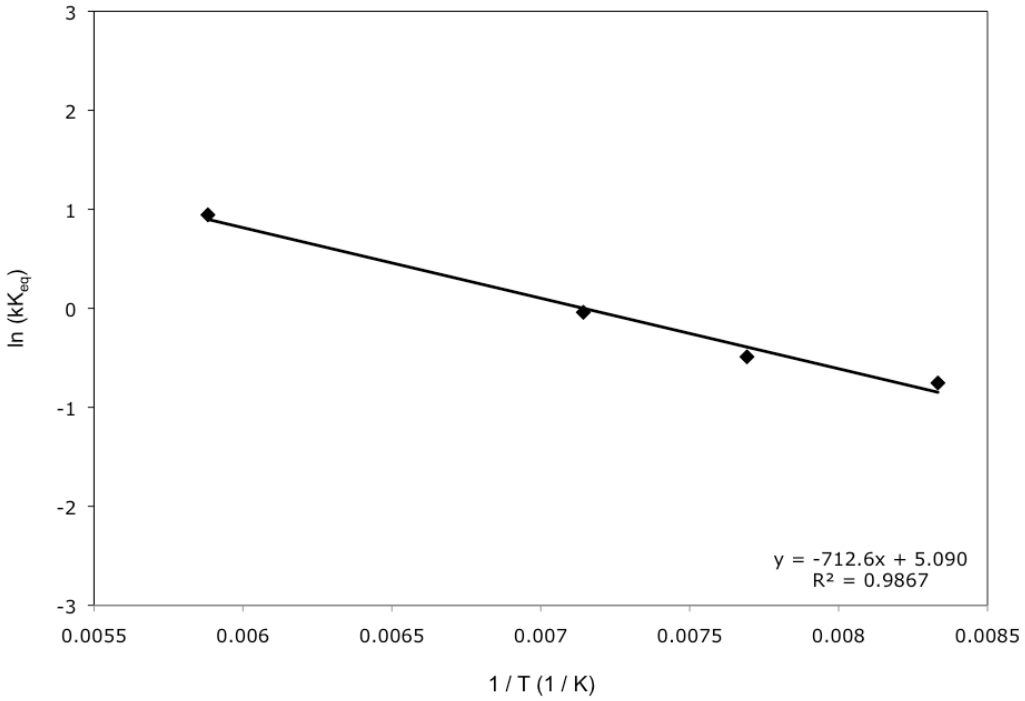

Figure 2.18 Van't Hoff plot of **1-N(^{2}Ad)** for spin-crossover from $S = 0 \leftrightarrow S = 1$.

The thermodynamic changes for spin-crossover from $S = 0$ to $S = 1$ were determined using a Van't Hoff plot of $\ln(K_{eq})$ versus 1/T (where T is the temperature at which the Mössbauer spectrum was obtained). K_{eq} was determined using the relative amounts of each spin-state, established from fitting the Mössbauer spectrum at each temperature. The slope obtained from this plot is equal to - $\Delta H°/R$ and the y-intercept is equal to $\Delta S°/R$. Based on these data, $\Delta H° = 5.9(5)$ kJ·mol^{-1} (1.4 kcal·mol^{-1}) and $\Delta S° = 42.3(4)$ J·K^{-1}·mol^{-1} (10.1 kcal·mol^{-1}) for the transition from $S = 0$ to $S = 1$ for **1-N(^{2}Ad)**. These parameters are similar to the thermodynamic changes measured for the spin crossover of $Fe(phen)_2(NCS)_2$, where $\Delta H° = 8.6(1)$ kJ·mol^{-1} and $\Delta S° = 48.8(7)$ J·K^{-1}·mol^{-1}.[14] Moreover, the positive value observed for $\Delta S°$ is consistent with conversion to the triplet state of **1-N(^{2}Ad)**, which likely has longer bonds are hence greater disorder than the singlet state.

2.5 Electronic Structure Comparison of Iron Imides

With a series of bis(imino)pyridine iron imide complexes in hand, the electronic structure of each was further investigated. The Mössbauer parameters, summarized in Table 2.5, establish that the electronic structure of **1-N(²Ad)** is similar to the $S = 0$ alkyl iron imides at low temperatures, while at higher temperatures spin-crossover to an $S = 1$ state was observed. Iron K-edge X-ray absorption spectroscopy was used to probe the relative oxidation states of the metal centers. The K-edge spectrum of **1-N(iPr2Ph)** (Appendix B) exhibits a pre-edge peak (7112.5 eV) that is approximately 1 eV higher in energy than (iPrPDI)Fe(dmap), consistent with an iron(III) metal center.[15] Preliminary data indicates that **1-N(¹Ad)** and **1-N(²Ad)** also have higher pre-edge energies than (iPrPDI)Fe(dmap) (Appendix B).

Table 2.5 Mössbauer parameters ($mm \cdot s^{-1}$) for representative bis(imino)pyridine iron imide complexes at 80 K.

Complex	δ	ΔE_Q	%
1-N(iPr2Ph)[5]	0.30	| 1.08 |	100
1-N(Me3Ph)	0.30	| 1.34 |	100
1-N(²Ad) (200K)	0.19	| 0.75 |	100
1-N(²Ad) (15 K)	0.01	| 2.26 |	> 99
1-N(¹Ad)	0.04	-2.38	100
1-N(CyOct)	-0.02	| 2.38 |	97
tBu1-N(¹Ad)	0.00	| 2.61 |	100

DFT calculations were carried out for **1-N(iPr2Ph)** as a spin-unrestricted triplet (B3LYP functional) and support an iron(III) metal center with a singly reduced chelate.[16] BS(3,1) calculations carried out for **1-N(iPr2Ph)** also predict this electronic structure description. Both the calculated bond distances and Mössbauer parameters

are in good agreement with the experimental values (Appendix A). The calculated isomer shift of 0.22 $mm \cdot s^{-1}$ is within the accepted error range of 0.10 $mm \cdot s^{-1}$ to the experimentally observed value of 0.30 $mm \cdot s^{-1}$. Moreover, the calculated quadrupole splitting of 0.77 $mm \cdot s^{-1}$ is close to the experimentally observed value of 1.08 $mm \cdot s^{-1}$. The Mulliken spin density plot indicates one unpaired electron delocalized on the bis(imino)pyridine chelate, while three unpaired electrons of the same sign reside on the metal center and the imide nitrogen (Figure 2.19). Because the Fe-N_{imide} bond is highly covalent, the sharing of electron density between the metal center and the imide nitrogen is still consistent with an intermediate-spin iron(III) center with three unpaired electrons.

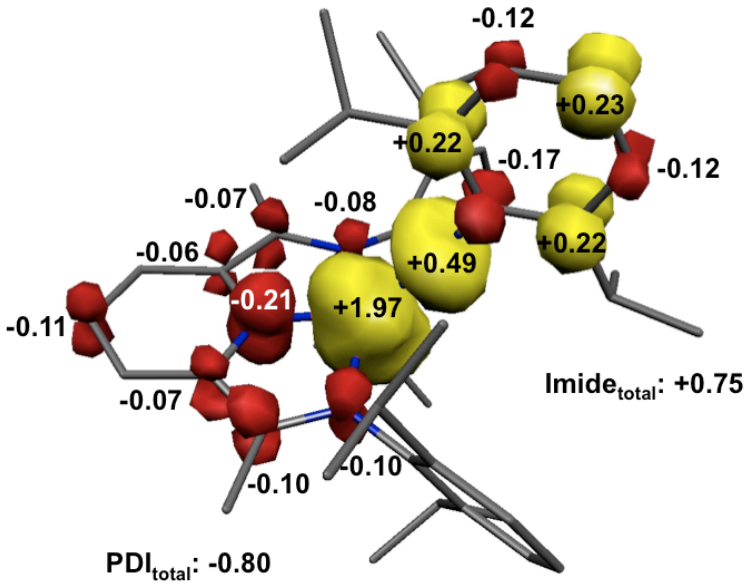

Figure 2.19 Spin density plot for **1-N(^{iPr2}Ph)** obtained from a Mulliken population analysis.

The spectroscopic data indicate that three different electronic configuration are necessary to describe the various classes of bis(imino)pyridine iron imides. As previously reported and consistent with the abovementioned iron K-edge and

computational data,[5] (^{iPr}PDI)FeN*Ar* is best described as an intermediate-spin iron(III) center antiferromagnetically coupled to a mono-reduced chelate to give an overall S = 1 molecule. In contrast, a doubly reduced bis(imino)pyridine chelate and singlet ground state are observed for (^{iPr}PDI)FeNR and (^{iPr}*p*-^{t}BuPDI)FeNR when R = 1-Ad or ^{Cy}Octyl. This indicates an intermediate-spin iron(IV) metal center antiferromagnetically coupled to a triplet diradical chelate. A ground state with a singlet diradical chelate is unlikely because previous investigation of bis(imino)pyridine iron imide complexes indicates that the triplet diradical chelate is generally lower in energy than the singlet diradical, although the separation between the states is small.[17]

Table 2.6 In-plane chelate hydrogen resonances of bis(imino)pyridine iron imide complexes by ^{1}H NMR spectroscopy in benzene-d_6 at 20 °C.

Complex	N=C(CH_3) (ppm)	*m-pyr* (ppm)	*p-pyr* (ppm)
1-N(^{1}Ad)	-15.25	16.41	22.30
$^{t\text{Bu}}$1-N(^{1}Ad)	-17.04	17.63	-
1-N(^{Cy}Oct)	-16.36	18.02	20.64
$^{t\text{Bu}}$1-N(^{Cy}Oct)	-16.75	18.38	-
1-N(^{2}Ad)	-121.05	72.80	94.01
1-N(^{Me3}Ph)[5]	-102.8	140.67	271.2

The anomalous in-plane chelate hydrogen resonances observed for the S = 0 bis(imino)pyridine iron imide complexes (Table 2.6) indicates that the triplet state is close in energy to the singlet ground state. However, the contribution is likely to be small, as these resonances are much closer to diamagnetic reference values than the in-plane chelate hydrogen resonances for the pure S = 1 bis(imino)pyridine iron imide complexes (Table 2.6). For examples, the imine methyl backbone of **1-N(^{1}Ad)** is

observed at -15.25 ppm at 20 °C while the corresponding resonance of **1-N(**^{Me3}**Ph)** is observed at -102.8 ppm. Variable temperature ^{1}H NMR spectra for **1-N(**^{1}**Ad)** indicates that the anomalous ^{1}H NMR resonances are due to thermal population of the triplet state. Upon cooling a toluene-d_8 solution of **1-N(**^{1}**Ad)**, a decrease in the chemical shift range is observed (Figure 2.20). The imine methyl resonance shifts from -15.25 ppm to -0.06 ppm, while the *p*-pyridine resonances moves upfield from 22.30 ppm to 9.27 ppm.

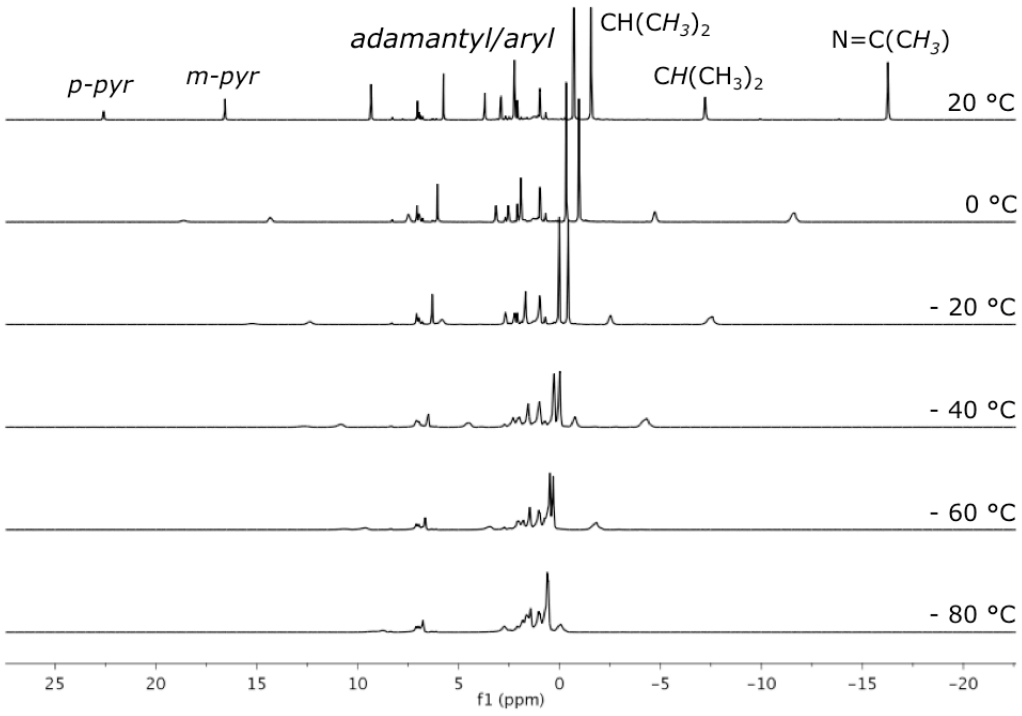

Figure 2.20 Variable temperature ^{1}H NMR spectra of **1-N(**^{1}**Ad)** in toluene-d_8 (-80 °C to 20 °C).

For **1-N(**^{2}**Ad)**, two distinct electronic configurations are observed, and the relative population of each depends on temperature. Below 80 K, **1-N(**^{2}**Ad)** has a similar electronic structure to the other alkyl iron imides, and is best described as intermediate-spin iron(IV) with antiferromagnetic coupling to a doubly reduced, triplet

diradical bis(imino)pyridine chelate. Above 200 K, a triplet ground state is observed. The molecular structure, determined at 220 K, establishes two electron reduction of the chelate and an elongated Fe-N bond compared to the other alkyl iron imides. Thus, the electronic structure of **1-N(^{2}Ad)** above 200 K can be described as a high-spin iron(IV) center with antiferromagnetic coupling to a doubly reduced, triplet diradical bis(imino)pyridine chelate.

Preliminary computational data indicates that the singlet and triplet states for the alkyl iron imides are within 7 kcal/mol in energy (Appendix A). The triplet state likely arises from a transition from intermediate-spin to high-spin at the metal center while maintaining antiferromagnetic coupling to the imide radical. This is also consistent with the observed increase in isomer shift between 15 K and 200 K. However, it is also possible that both spin isomers have intermediate-spin iron(IV) centers, and the $S = 1$ state arises from a singlet diradical chelate with no antiferromagnetic coupling to the metal center. Although this possibility cannot be ruled out based on the experimental data, it is disfavored due to reasons presented below.

It is likely that the bis(imino)pyridine ligand orbitals do not change significantly in energy between the iron imide complexes. However, lowering the imide substituent into the idealized plane of the chelate for the alkyl-subsituted bis(imino)pyridine iron imide complexes will cause the metal orbitals, in particular the d_{xy} orbital, to rise in energy (Figure 2.21). For **1-N(^{1}Ad)** and **1-N(^{Cy}Oct)**, the d_{xy} orbital is sufficiently energetic that it is empty, while both bis(imino)pyridine ligand orbitals are populated. For **1-N(^{1}Ad)**, the d_{xy} orbital is low enough in energy to be populated at higher temperatures but empty at lower temperatures, leading to the observed spin-crossover behavior (Figure 2.21). For the aryl-substituted bis(imino)pyridine iron imides, the metal orbitals are low enough in energy compared

to the ligand orbitals that d_{xy} is populated while only one ligand is populated as well. Based on these electronic structure descriptions, the overall bond order for the $S = 0$ bis(imino)pyridine iron imides, including **1-N(2Ad)** at low temperatures, is expected to be 2.5 while the bond order for the $S = 1$ bis(imino)pyridine iron imides is 2.

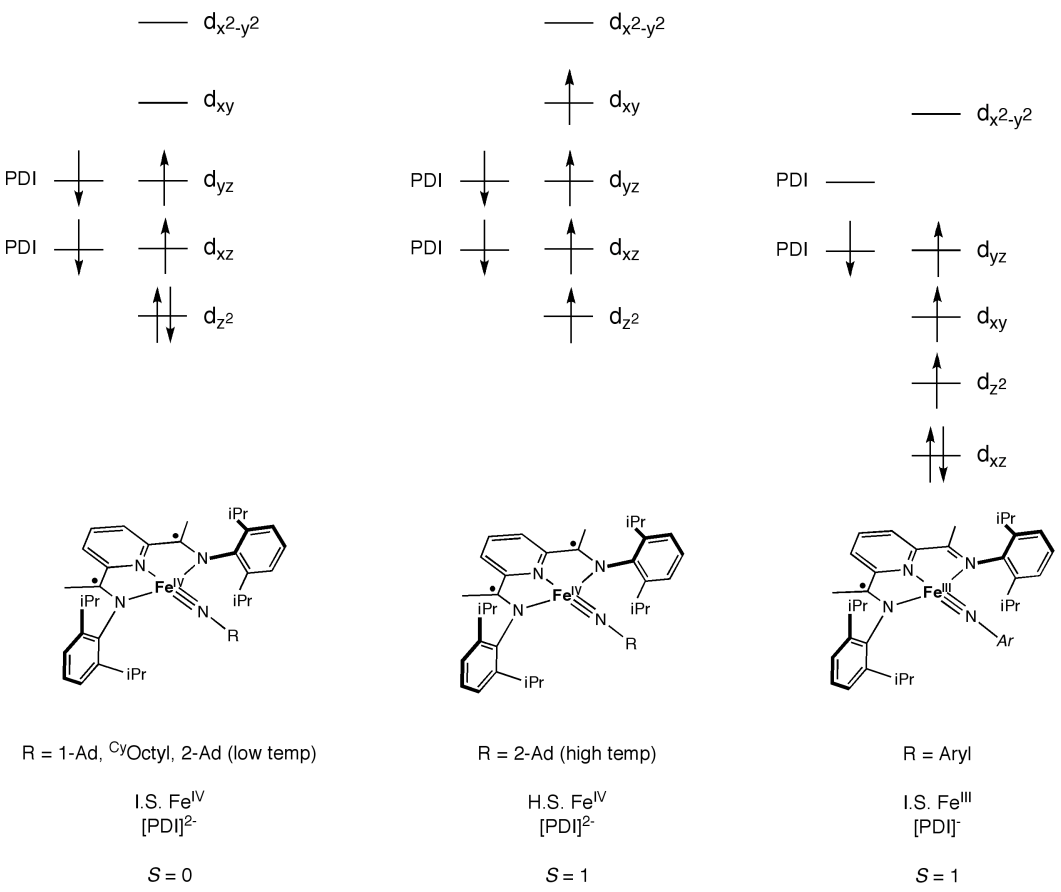

Figure 2.21 Proposed electronic structures of bis(imino)pyridine iron imide complexes, including qualitative d-splitting diagram.

In addition, a relationship between electronic structure and planarity of the imide is also evident (with the exception of **1-N(2Ad)**). When the iron imide is close to idealized square planar geometry, better π overlap between the metal and the lone pair on the imide nitrogen leads to a shorter Fe-N bond. The increased electron density at the metal center is also relieved by reduction of the ligand. For **1-N(iPr2Ph)** and **1-**

N(^{Me3}**Ph)**[5] the imide substituent is lifted substantially out of the idealized plane of the molecule, and for both complexes a longer iron-nitrogen bond and mono-reduced ligand is observed.

For **1-N(**^{1}**Ad)** and **1-N(**^{Cy}**Oct)**, the molecular structures establish essentially square planar molecules with shorter iron-nitrogen bonds and doubly-reduced chelates. It is likely that better overlap between the imide nitrogen and the metal center increases covalent bonding, leading to a more equal sharing of electrons and an imide substituent that behaves as a radical anion as opposed to a traditional dianion. **1-N(**^{2}**Ad)** is also observed to have a nearly square planar geometry and a doubly reduced bis(imino)pyridine chelate, along the iron-nitrogen bond is longer than those observed for **1-N(**^{1}**Ad)** and **1-N(**^{Cy}**Oct)**. Because the calculated singlet-triplet gap for alkyl iron imides is quite small, the triplet state for **1-N(**^{2}**Ad)** is likely lower in energy at 293 K, while for the other alkyl iron imides the singlet state is lower in energy.

2.6 C-H Activation by Diamagnetic Iron Imides

An important question that arises from investigation of the electronic structure of bis(imino)pyridine iron imides is whether the observed difference in electronic structure leads to a difference in reactivity. Allowing a benzene-d_6 solution of (^{Ar}PDI)FeNR (^{Ar}PDI = ^{iPr}PDI, ^{iPr}*p*-^{t}BuPDI; R = 1-Ad, ^{Cy}Octyl) to stand for 36-48 hours at 23 °C afforded the corresponding C-H bond activation product, (^{Ar}PDEA)Fe(NH_2R) (^{Ar}PDEA = 2,6-(2,6-$^{i}Pr_2$-$C_6H_3NC{=}CH_2)_2C_5H_3N$) (^{iPr}PDEA), 2,6-(2,6-$^{i}Pr_2$-$C_6H_3NC{=}CH_2)_2$-4-*t*Bu-C_5H_3N (^{iPr}*p*-^{t}BuPDEA); R = 1-Ad (**2-NH$_2$**^{1}**Ad**, ^{tBu}**2-NH$_2$**^{1}**Ad**), ^{Cy}Octyl (**2-NH$_2$**^{Cy}**Oct**, ^{tBu}**2-NH$_2$**^{Cy}**Oct**)), arising from formal deprotonation of the imine methyl groups (Figure 2.22). C-H bond activation, both intra- and intermolecular, has been documented for a number of iron[1f,3] and cobalt[18] imides complexes. In contrast, no C-H bond activation of the ligand was observed with **1-**

N(²Ad), **1-N(iPr2Ph)** or **1-N(Me3Ph)**, even upon heating a pentane solution of the iron imide complex to 65 °C for 24 hours. The iron C-H activation products were independently prepared by addition of the appropriate amine to (^{iPr}PDEA)Fe(THF)$_2$, including (^{iPr}PDEA)Fe(NH$_2$^{2}Ad). Thus, it is apparent that the lack of reactivity seen with **1-N(²Ad)** does not result from instability of the expected product.

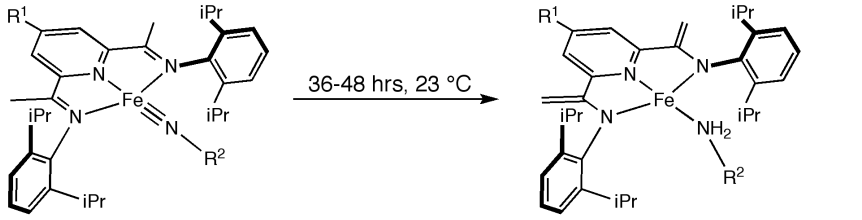

R^1 = H, R^2 = 1-Ad (**1-N(¹Ad)**)
R^1 = H, R^2 = ^{Cy}Octyl (**1-N(CyOct)**)
R^1 = ^{t}Bu, R^2 = 1-Ad (**tBu1-N(¹Ad)**)
R^1 = ^{t}Bu, R^2 = ^{Cy}Octyl (**tBu1-N(CyOct)**)

R^1 = H, R^2 = 1-Ad (**2-NH$_2$¹Ad**)
R^1 = H, R^2 = ^{Cy}Octyl (**2-NH$_2$CyOct**)
R^1 = ^{t}Bu, R^2 = 1-Ad (**tBu2-NH$_2$¹Ad**)
R^1 = ^{t}Bu, R^2 = ^{Cy}Octyl (**tBu2-NH$_2$CyOct**)

Figure 2.22 C-H activation of the bis(imino)pyridine ligand by $S = 0$ iron imides.

The benzene-d_6 ^{1}H NMR spectra of the (^{Ar}PDEA)Fe(NH$_2$R) complexes at 23 °C exhibit paramagnetically broadened resonances consistent with a C_{2v} symmetric molecule. Bis(eneamide)pyridine iron complexes typically exhibit two upfield-shifted methylene backbone resonances by ^{1}H NMR, which are summarized in Table 2.7. These characteristic resonances were observed at -49.91 and -49.31 ppm for **2-NH$_2$¹Ad**, and -47.40 and -45.04 ppm for $^{t\text{Bu}}$**2-NH$_2$¹Ad**. Similarly, the ^{1}H NMR spectra of **2-NH$_2$CyOct** and $^{t\text{Bu}}$**2-NH$_2$CyOct** exhibit methylene backbone resonances at -66.74 and -54.22 ppm, and -67.11 and -53.93 ppm, respectively. Effective magnetic moments of 3.7(1) μ_B and 4.3(2) μ_B were measured in benzene-d_6 at 20 °C for **2-NH$_2$¹Ad** and $^{t\text{Bu}}$**2-NH$_2$¹Ad**. Similar effective magnetic moments of 3.8(2) μ_B and 4.3(2) μ_B were measured for **2-NH$_2$CyOct** and $^{t\text{Bu}}$**2-NH$_2$CyOct**. The observed magnetic moments indicate an overall $S = 2$ molecule and a high-spin iron(II) center (*vide*

infra), although the values are somewhat lower than expected for four unpaired electrons. This may be a result of a mixture of intermediate-spin and high-spin metal centers at 20 °C.

The N*H*$_2$ hydrogens were not located by ^{1}H NMR spectroscopy, but were readily observed in the infrared spectrum (KBr) of each bis(eneamide)pyridine iron amine complex. Diagnostic infrared stretches are presented in Table 2.7. Two separate N-H stretches were observed for **2-NH$_2$^{1}Ad** at 3228 cm^{-1} and 3305 cm^{-1}, as well as an intense C=C stretch at 1571 cm^{-1}, indicating formation of two methylene backbones. Similarly, the infrared spectrum (KBr) of **$^{t\text{Bu}}$2-NH$_2$^{1}Ad** exhibits two N-H stretches at 3232 cm^{-1} and 3305 cm^{-1}, and a C=C stretch at 1582 cm^{-1}. The N-H stretches for **2-NH$_2$$^{\text{Cy}}$Oct** and **$^{t\text{Bu}}$2-NH$_2$$^{\text{Cy}}$Oct** are slightly higher in energy, at 3246 cm^{-1} and 3321 cm^{-1}, and 3246 cm^{-1} and 3317 cm^{-1}, respectively. The C=C stretches for **2-NH$_2$$^{\text{Cy}}$Oct** and **$^{t\text{Bu}}$2-NH$_2$$^{\text{Cy}}$Oct** are nearly identical to those observed for the 1-adamantyl amine complexes, at 1581 cm^{-1} and 1582 cm^{-1}, respectively.

Table 2.7 Summary of spectroscopic and magnetic properties for bis(eneamide)pyridine iron amine complexes.

Complex	$\nu_{NH(D)}$ (cm^{-1}) (KBr)	ν_{CC} (cm^{-1}) (KBr)	N=C(C*H*$_3$) (ppm)	μ_{eff} (μ_B)
2-NH$_2$^{1}Ad	3228, 3305 (2267, 2281)	1571	-49.91 -49.31	3.7(1)
$^{t\text{Bu}}$2-NH$_2$^{1}Ad	3232, 3305	1582	-47.40 -45.04	4.3(2)
($^{\text{Et}}$PDEA)Fe(NH$_2$^{1}Ad)	3244, 3291	1579	-47.84 -44.35	4.7(2)
2-NH$_2$$^{\text{Cy}}$Oct	3246, 3321 (2269, 2279)	1581	-66.74 -54.22	3.8(2)
$^{t\text{Bu}}$2-NH$_2$$^{\text{Cy}}$Oct	3246, 3317	1582	-67.11 -53.93	4.3(2)
2-NH$_2$^{2}Ad	3254, 3304	1581	-59.75 -50.42	3.8(2)

Notably, a bis(eneamide)pyridine iron complex was also prepared where the corresponding iron imide could not be isolated. Slow addition of 1-adamantyl azide to a pentane solution of $[(^{Et}PDI)Fe(N_2)]_2(\mu\text{-}N_2)$[19] ($^{Et}PDI$ = 2,6-(2,6-Et_2-C_6H_3-N=CMe)$_2C_5H_3N$) at 23 °C afforded ($^{Et}PDEA$)Fe($NH_2{}^1Ad$) ($^{Et}PDEA$ = 2,6-(2,6-Et_2-$C_6H_3NC{=}CH_2$)$_2C_5H_3N$)), with no evidence for the corresponding iron imide complex by ^1H NMR spectroscopy. Observation of a rapid color change of the reaction mixture to bright purple, immediately followed by a color change to amber suggests that the iron imide complex was initially formed but the rate of C-H activation of the imine methyl groups was too rapid to allow isolation or observation of the imide species (Figure 2.23). ($^{Et}PDEA$)Fe($NH_2{}^1Ad$) was independently prepared by addition of 1-adamantyl amine to a diethyl ether solution of ($^{Et}PDEA$)Fe(THF)$_2$ at 23 °C.

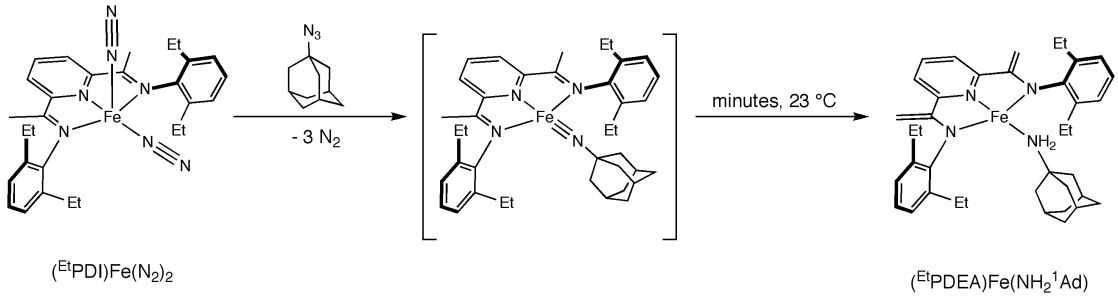

Figure 2.23 Preparation of ($^{Et}PDEA$)Fe($NH_2{}^1Ad$) by C-H activation.

As with $^{iPr}PDEA$ iron amine complexes, the benzene-d_6 ^1H NMR spectrum of ($^{Et}PDEA$)Fe($NH_2{}^1Ad$) at 23 °C exhibits the number of resonances expected for a C_{2v} symmetric compound. The resonances are paramagnetically broadened, with two distinct upfield-shifted methylene backbone resonances at -47.84 and -44.35 ppm, similar to **2-$NH_2{}^1$Ad**. Formation of two methylene backbones was also confirmed by the intense C=C stretch at 1579 cm^{-1} observed in the infrared spectrum (KBr) of ($^{Et}PDEA$)Fe($NH_2{}^1Ad$). In addition, the infrared spectrum (KBr) of ($^{Et}PDEA$)Fe($NH_2{}^1Ad$) exhibits two N-H stretches at 3244 cm^{-1} and 3291 cm^{-1}. The

effective magnetic moment observed for a benzene-d_6 solution of (^{Et}PDEA)Fe($NH_2{}^1$Ad) at 23 °C was 4.7(2) μ_B, consistent with four unpaired electrons and an overall $S = 2$ molecule.

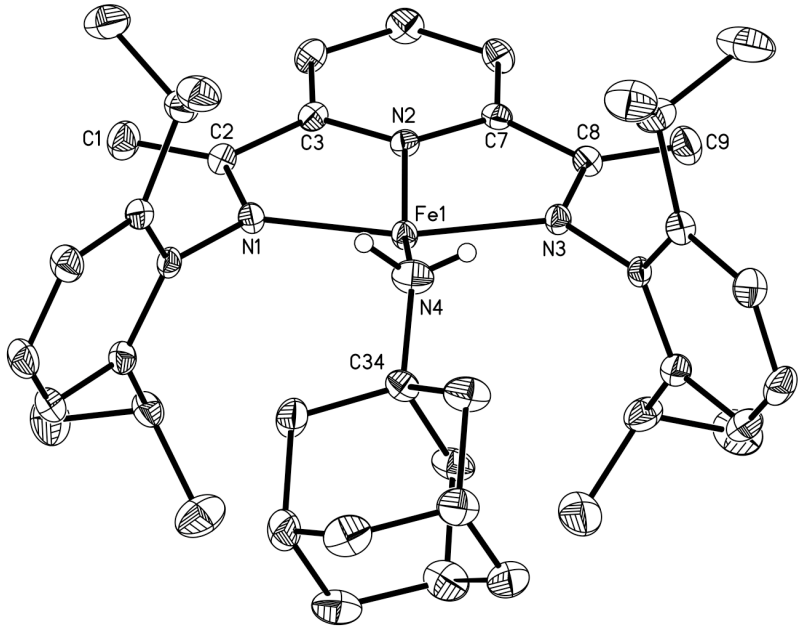

Figure 2.24 Molecular structure of **2-$NH_2{}^1$Ad** at 30 % probability ellipsoids. Hydrogen atoms, except those on the adamantyl amine substituent, omitted for clarity.

Table 2.8 Selected bond distances (Å) and angles (°) for **2-$NH_2{}^1$Ad**.

Fe(1)-N(4)	2.1606(19)	N(1)-C(2)	1.378(3)
Fe(1)-N(1)	2.0117(17)	N(3)-C(8)	1.378(2)
Fe(1)-N(2)	2.0776(16)	C(2)-C(3)	1.487(3)
Fe(1)-N(3)	2.0177(16)	C(7)-C(8)	1.482(3)
C(1)-C(2)	1.347(3)	N(2)-Fe(1)-N(4)	159.80(7)
C(8)-C(9)	1.350(3)	Fe(1)-N(4)-C(34)	126.17(14)

X-ray quality crystals of **2-NH$_2$[1]Ad** were obtained by cooling a dilute pentane solution to -35 °C (Figure 2.24). The solid state structure establishes a C_{2v} symmetric molecule with distorted square planar geometry and an N_{pyr}-Fe-N_{amine} angle of 159.80(7)°. The Fe-N_{amine} bond has lengthened considerably from the distance of 1.6481(15) Å observed in the molecular structure of **1-N([1]Ad)** to 2.1606(19) Å, consistent with coordination of an amine ligand. By comparison, the Fe-N_{amine} bond lengths for (^{iPr}PDEA)Fe(NHMe$_2$)[20] and (^{iPr}PDI)Fe(NH$_3$)[21] are 2.040(3) Å and 2.008(2) Å, respectively. The longer Fe-N_{amine} distance observed for **2-NH$_2$[1]Ad** is likely due to the greater steric bulk of the amine ligand. The C_{amide}-N_{amide} bond lengths of 1.378(3) Å and 1.378(2) Å are consistent with single bonds, as expected for the now anionic chelate arms. The C_{amide}-C_{ipso} distances of 1.487(3) Å and 1.482(3) Å are also consistent with single bonds, while the C_{CH2}-C_{amide} distances of 1.347(3) Å and 1.350(3) Å are considerably shorter, consistent with formation of two methylene backbones.

The electronic structure of the bis(eneamide)pyridine iron amine complexes was further investigated by Mössbauer spectroscopy. The zero-field Mössbauer spectrum of (^{Et}PDEA)Fe(NH$_2$[1]Ad) at 80 K exhibited a quadrupole doublet with an isomer shift of 0.75 mm·s^{-1} and a quadrupole splitting of 0.28 mm·s^{-1} (Figure 2.25). The observed isomer shift is consistent with a high-spin iron(II) metal center,[12] and is identical to the isomer shift observed for the high-spin iron(II) complex, (^{iPr}PDI)Fe(dbabh).[22] The isomer shift of (^{Et}PDEA)Fe(NH$_2$[1]Ad), in combination with the effective magnetic moment of 4.7(2) μ_B, indicates that the bis(eneamide)pyridine iron amine complexes are best described as high-spin iron(II) with traditional dianionic chelates.

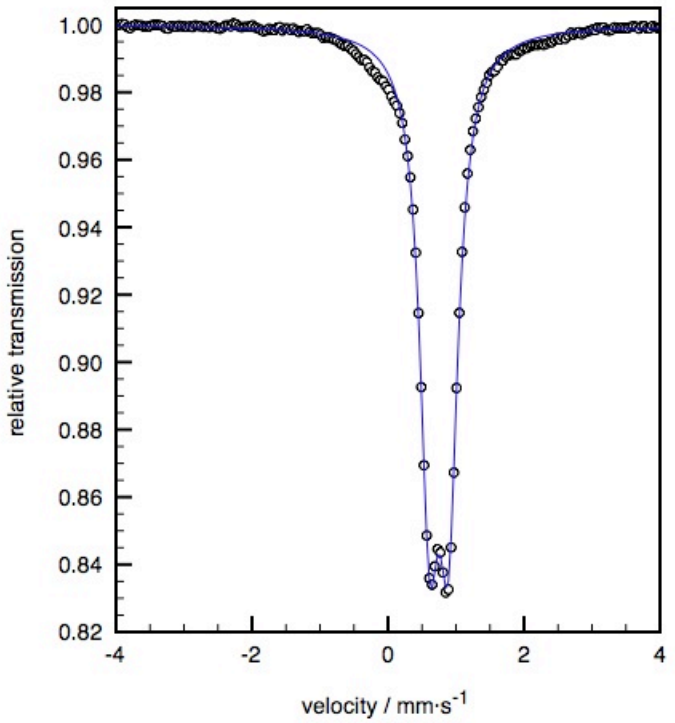

Figure 2.25 Zero-field Mössbauer spectrum of (^{Et}PDEA)Fe($NH_2{}^1$Ad) at 80 K; δ = 0.75 mm·s^{-1}, ΔE_Q = 0.28 mm·s^{-1}.

Isotopic labeling studies established that the hydrogens on the amine ligand derive only from the methyl backbone hydrogens in the starting material. Allowing a toluene solution of ****1-N(^{1}Ad)** or ****1-N(^{Cy}Oct)** (where ** denotes deuteration of the imine methyl position) to stand for 60 hours at 23 °C furnished ****1-N$D_2{}^1$Ad** and ****1-N$D_2{}^{Cy}$Oct** (Figure 2.26). Complete deuterium incorporation into the amine position was confirmed by infrared spectroscopy. Upon isotopic labeling, the two N-H(D) stretches shifted appropriately to 2267 cm^{-1} and 2281 cm^{-1} for ****1-N$D_2{}^1$Ad**, and 2269 cm^{-1} and 2279 cm^{-1} for ****1-N$D_2{}^{Cy}$Oct**. A small amount of deuterium incorporation (10 % of incorporation into amine position) into the isopropyl methyl groups of the ligand was observed as well, indicating a second site of C-H bond activation.

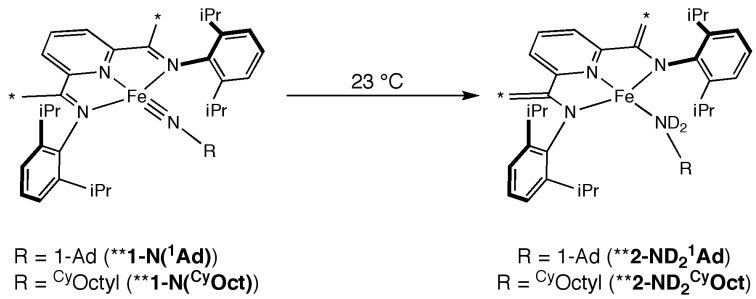

Figure 2.26 Deuterium labeling experiments for C-H activation of imine methyl groups.

The $S = 0$ iron imides were not observed to participate in intermolecular C-H activation chemistry with 1,4-cyclohexadiene, 1,3-cyclohexadiene or dihydroanthracene, consistent with an intramolecular C-H activation process. This is also supported by kinetic experiments that indicate the C-H bond activation of the bis(imino)pyridine ligand is first-order in **1-(N^{Cy}Oct)**. For an intermolecular C-H activation a second-order rate law would be expected. The disappearance of starting material in a benzene-d_6 solution of **1-(N^{Cy}Oct)** was measured as a function of time, at varying concentrations of **1-(N^{Cy}Oct)**.

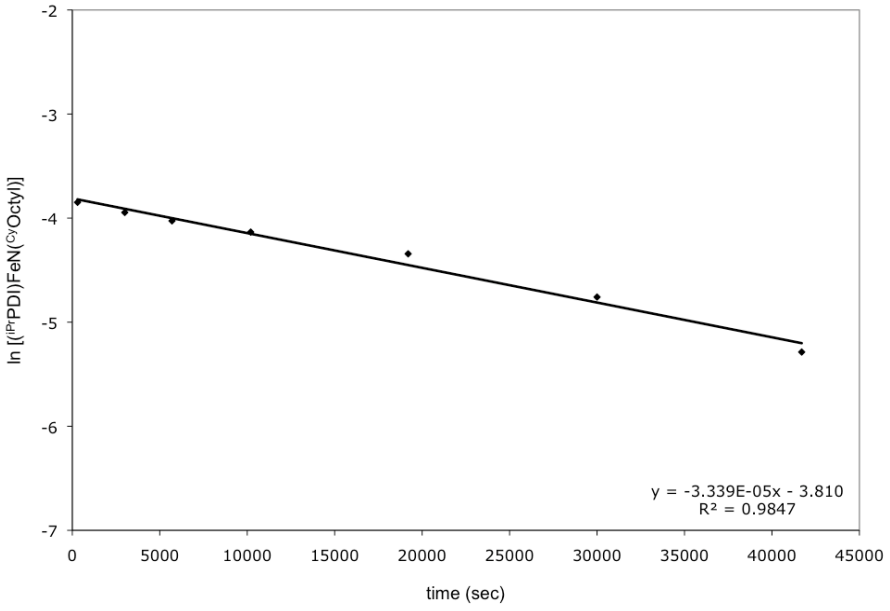

Figure 2.27 First-order plot for C-H activation of **1-N(CyOct)** at 25 °C.

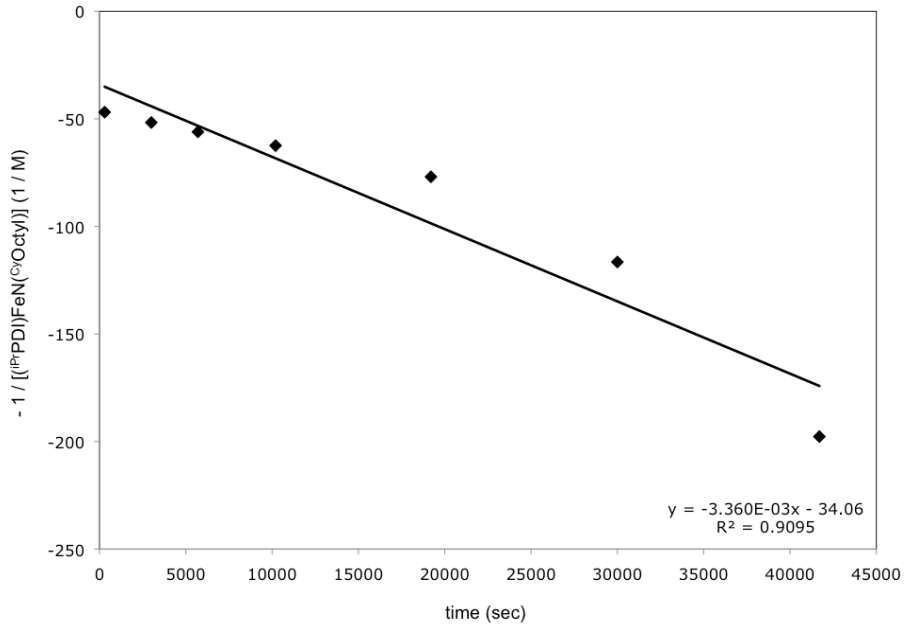

Figure 2.28 Second-order plot for C-H activation of **1-N(^{Cy}Oct)** at 25 °C.

Comparison of the first- and second-order plots of the C-H activation reaction establishes that the reaction is first-order in **1-(N^{Cy}Oct)**, with a rate constant of 3.4(2)x10^{-5} s^{-1} at 25 °C (Figures 2.27 and 2.28). Side by side measurements (Appendix D) of the rate of imine methyl group C-H activation by **1-(N^{Cy}Oct)** and ****1-(N^{Cy}Oct)** established a primary kinetic isotope effect of 3.3(2), consistent with C-H(D) bond activation as the rate determining step. The activation parameters for the C-H bond activation of bis(imino)pyridine iron imides were calculated from measurements of the rate constant at various temperatures. Based on the following Eyring plot, $\Delta H^{\ddagger}$ = 13.5(3) kcal·mol^{-1} and $\Delta S^{\ddagger}$ = -34.0(3) e.u. for the C-H bond activation of **1-N(^{Cy}Oct)** (Figure 2.29). The small enthalpy of activation ($\Delta H^{\ddagger}$) is consistent with the observation that C-H bond activation occurs at ambient temperature. The negative entropy of activation is consistent with an ordered transition state, for example where

the chelate arm must come together with the Fe-N_{imide} bond before C-H activation can occur (*vide infra*).

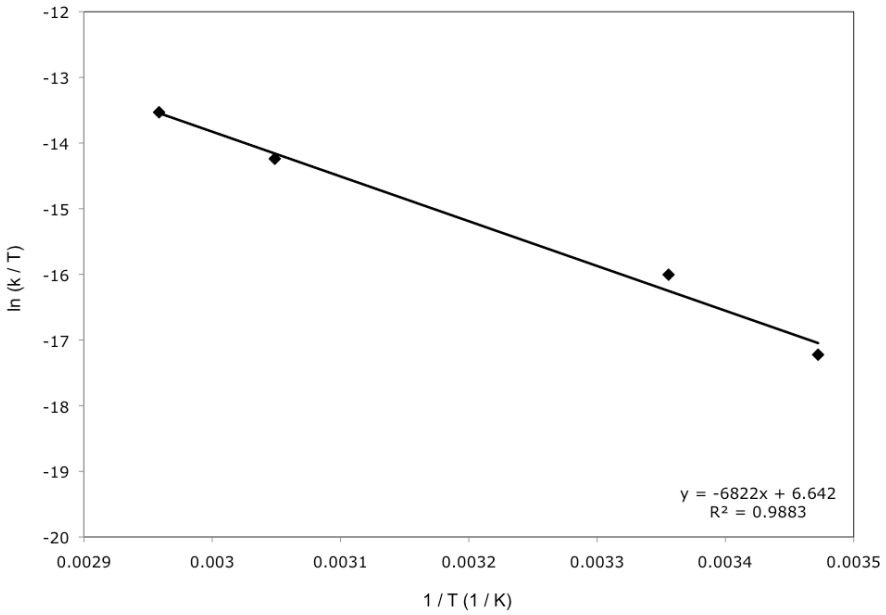

Figure 2.29 Eyring plot for C-H activation of **1-N(^{Cy}Oct)**.

To furnish the ^{iPr}PDEA product, two C-H bond activation steps are required. It is likely that the first C-H activation is the rate-determining step of the reaction, consistent with the observed kinetic isotope effect. A possible mechanism involves dissociation of one arm of the bis(imino)pyridine chelate, placing the imine methyl groups in proximity to the Fe-N_{imide} bond for intramolecular C-H activation (Figure 2.30). Bis(imino)pyridine iron complexes have been observed to undergo imine dissociation, as demonstrated by the formation of η^6-aryl and -phenyl complexes from the phenyl-substituted bis(imino)pyridine iron dinitrogen complex, (^{iPr}BPDI)Fe$(N_2)_2$ (^{iPr}BPDI = 2,6-(2,6-$^{i}Pr_2$-C_6H_3-N=CPh)$_2C_5H_3N$).[23] After re-coordination of the modified chelate arm, a second C-H activation would then follow by the same mechanism. No intermediates were observed by ^{1}H NMR spectroscopy during the reaction, however a delay between erosion of starting material and appearance of

product indicates the presence of intermediates. Initial dissociation of the chelate arm is supported by the dramatically increased rate of C-H activation observed for ^{Et}PDI. The decreased steric bulk of the chelate arms for ^{Et}PDI compared to ^{iPr}PDI would allow less hindered rotation around the C_{imine}-C_{ipso} bond after chelate arm dissociation, leading to a faster rate of C-H activation.

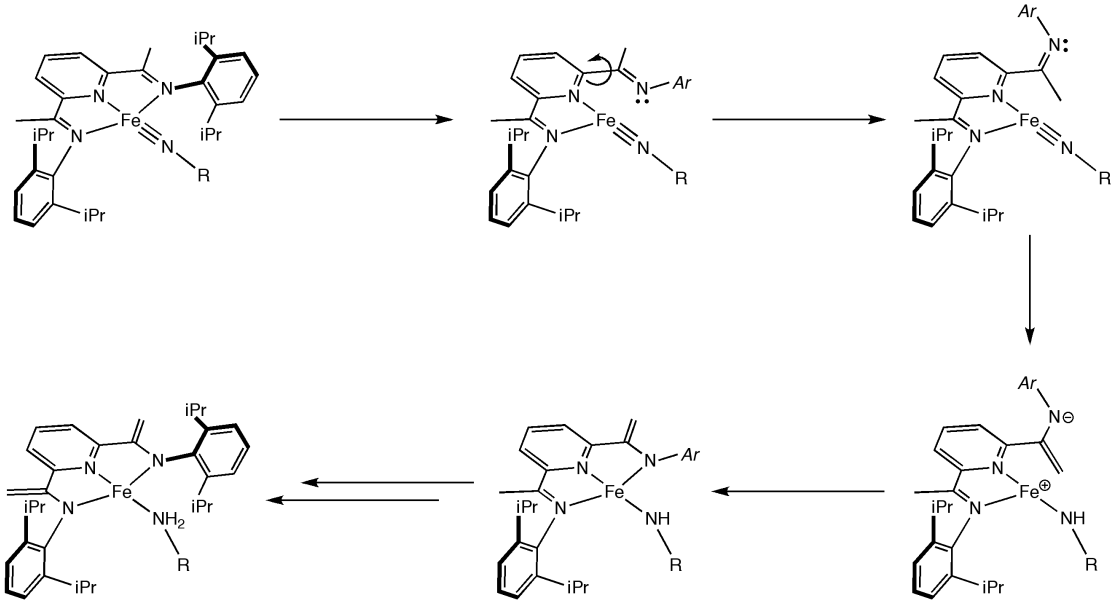

Figure 2.30 Proposed mechanism of intramolecular C-H activation by bis(imino)pyridine iron imides.

One question that remains is how the difference in electronic structure correlates to the observed difference in C-H bond activation chemistry. Why do the *S* = 0 bis(imino)pyridine iron imides activate C-H bonds while the *S* = 1 iron imide complexes do not? The bis(imino)pyridine iron imide complexes with singlet ground states participate in C-H activation of the chelate imine methyl groups, while those with triplet ground states do not. However, spectroscopic data suggest that although both (^{iPr}PDI)FeN*Ar* complexes and **1-N(**^{2}**Ad)** have *S* = 1 ground states, they have different electronic structures. Thus, the basis for the observed reactivity difference

must be common to the electronic structures of both (^{iPr}PDI)FeN*Ar* complexes and **1-N(^{2}Ad)**. While the *S* = 1 bis(imino)pyridine iron imide complexes, of both electronic structure descriptions, have d_{xy} metal orbitals occupied by an unpaired electron, the *S* = 0 bis(imino)pyridine iron imides have empty d_{xy} orbitals. The presence of an empty d_{xy} metal orbital for the *S* = 0 bis(imino)pyridine iron imide complexes, and the corresponding increase in electrophilicity of the Fe-N_{imide} bond, is likely responsible for the difference in reactivity. Similar C-H activation chemistry has been observed with electrophilic iron oxo complexes.[24]

2.7 Conclusions

The electronic structure of a series of alkyl iron imides was investigated using a combination of X-ray crystallography, variable temperature SQUID magnetization and Mössbauer spectroscopy. Based on these experimental techniques in combination with DFT calculations, the previously studied (^{iPr}PDI)FeN*Ar* complexes[5] are best described as an intermediate-spin iron(III) center antiferromagnetically coupled to a chelate radical For R = 1-Ad and ^{Cy}Octyl, (^{Ar}PDI)FeNR is best described as an intermediate-spin iron(IV) center antiferromagnetically coupled to a triplet diradical bis(imino)pyridine chelate. Thermal spin-crossover behavior is observed when R = 2-Ad, resulting in a transition form *S* = 0 at 15 K to *S* = 1 at 200 K. The *S* = 0 state is spectroscopically similar to other *S* = 0 bis(imino)pyridine iron imides, while the *S* = 1 state is best described as a high-spin iron(IV) center with antiferromagnetic coupling to a triplet diradical bis(imino)pyridine chelate.

C-H activation of the methyl backbone and isopropyl methyl groups of the bis(imino)pyridine ligand was observed when R = 1-Ad or ^{Cy}Octyl. The C-H activation of (^{iPr}PDI)FeN(^{Cy}Oct) was found to be first-order in iron. Notably, the electronic structure of the bis(imino)pyridine iron imides seemed to dictate whether a

given imide would participate in C-H activation chemistry. Although 1-adamantyl and 2-adamantyl substituents are not expected to be different electronically, dissimilar electronic configurations were observed for **1-N(**^{1}**Ad)** and **1-N(**^{2}**Ad)** at room temperature, and **1-N(**^{1}**Ad)** participated in C-H activation chemistry while **1-N(**^{2}**Ad)** did not. Moreover, no C-H activation of the chelate was observed for the $S = 1$ aryl iron imides. The presence of an empty d_{xy} metal orbital for the $S = 0$ bis(imino)pyridine iron imide complexes, and the corresponding increase in electrophilicity of the Fe-N_{imide} bond, is likely responsible for the difference in reactivity.

2.8 Experimental Procedures

General Considerations. All air- and moisture-sensitive manipulations were carried out using standard vacuum line, Schlenk, and cannula techniques or in an MBraun inert atmosphere dry box containing an atmosphere of purified nitrogen. Solvents for air- and moisture-sensitive manipulations were initially dried and deoxygenated using literature procedures. Benzene-d_6 was purchased from Cambridge Isotope Laboratories and dried over 4 Å molecular sieves. 1-adamantyl amine and 1-adamantyl azide were purchased from Acros and dried on the vacuum line before use. Cyclooctyl amine was purchased from Acros and distilled from calcium hydride before use. 2-adamantyl azide,[25] 2-adamantyl amine[26] and cyclooctyl azide[27] were prepared according to the literature procedures. The complexes **1-N(**^{Me3}**Ph)**[5] and **1-$(N_2)_2$**[15] were prepared according to literature procedures. The ligand ^{iPr}p-^{t}BuPDI was prepared according to the literature procedure.[28] The deuterated bis(imino)pyridine ligand, 2,6-(2,6-$^{i}Pr_2$-C_6H_3N=CMe)$_2C_5H_3N$-d_6 (^{iPr}PDI-d_6) was prepared according to the literature method.[29] The dinitrogen complexes **1**-$(N_2)_2$** and ^{tBu}**1-$(N_2)_2$** were prepared following the procedure for **1-$(N_2)_2$**.[15]

^{1}H NMR spectra were recorded on Varian Mercury 300, Inova 400, and 500 spectrometers operating at 299.76, 399.78, and 500.62 MHz, respectively. All ^{1}H chemical shifts are reported relative to $SiMe_4$ using the ^{1}H (residual) shift of the solvent as a secondary standard. Solution magnetic moments were determined by Evans method[30] using a ferrocene standard and are the average value of at least two independent measurements. Gouy balance measurements were performed with a Johnson Matthey instrument that was calibrated with $HgCo(SCN)_4$. Peak width at half height is given for paramagnetically broadened resonances. Infrared spectra were collected on a Thermo Nicolet spectrometer. Elemental analyses were performed at Robertson Microlit Laboratories, Inc., in Madison, NJ.

Single crystals suitable for X-ray diffraction were coated with polyisobutylene oil in a drybox, transferred to a nylon loop and then quickly transferred to the goniometer head of a Bruker X8 APEX2 diffractometer equipped with a molybdenum X-ray tube (λ = 0.71073 Å). Preliminary data revealed the crystal system. A hemisphere routine was used for data collection and determination of lattice constants. The space group was identified and the data were processed using the Bruker SAINT+ program and corrected for absorption using SADABS. The structures were solved using direct methods (SHELXS) completed by subsequent Fourier synthesis and refined by full-matrix least-squares procedures.

SQUID magnetization data of crystalline powdered samples were recorded with a SQUID magnetometer (Quantum Design) at 10 kOe between 5 and 300 K for all samples. Values of the magnetic susceptibility were corrected for the underlying diamagnetic increment by using tabulated Pascal constants and the effect of the blank sample holders (gelatin capsule/straw). Samples used for magnetization measurement were recrystallized multiple times and checked for chemical composition by ^{1}H NMR spectroscopy.

^{57}Fe Mössbauer spectra were recorded on a SEE Co. Mössbauer spectrometer (MS4) at 80 K in constant acceleration mode. ^{57}Co/Rh was used as the radiation source. WMOSS software was used for the quantitative evaluation of the spectral parameters (leastsquares fitting to Lorentzian peaks). The minimum experimental line widths were 0.23 mm s^{-1}. The temperature of the samples was controlled by a Janis Research Co. CCS-850 He/N_2 cryostat within an accuracy of ±0.3 K. Isomer shifts were determined relative to α-iron at 298 K.

Preparation of (^{iPr}PDI)FeN(^{1}Ad) (1-N(^{1}Ad)). A 20-mL scintillation vial was charged with 0.094 g (0.174 mmol) of **(^{iPr}PDI)Fe(N_2)$_2$** and approximately 15 mL of pentane, resulting in a dark green solution. A solution of 0.028 g (0.174 mmol) 1-adamantyl azide in 3 mL pentane was added dropwise to the vial, resulting in a slow color change of the solution to purple. The solution was stirred for 15 minutes, then filtered through a glass frit. The purple solution was cooled to -35 °C to give 0.065 g (60 %) of purple diamond-shaped crystals identified as **(^{iPr}PDI)FeN(^{1}Ad)**. Analysis for $C_{43}H_{58}N_4Fe$: Calc. C, 75.20; H, 8.51; N, 8.16. Found C, 74.82; H, 8.49; N, 7.80. ^{1}H NMR (benzene-d_6, 20 °C): δ = -15.25 (s, 6H, C(C*H*$_3$)), -6.72 (br s, 4H, C*H*(CH$_3$)$_2$), -1.23 (br s, 12H, CH(C*H*$_3$)$_2$), -0.48 (br s, 12H, CH(C*H*$_3$)$_2$), 2.54 (br s, 6H, adamantyl C*H*$_2$), 3.05 (d, 12 Hz, 3H, adamantyl C*H*$_2$), 3.88 (d, 12 Hz, 3H, adamantyl C*H*$_2$), 6.03 (d, 8 Hz, 4H, *m-aryl*), 7.27 (t, 8 Hz, 2H, *p-aryl*), 9.27 (br s, 3H, adamantyl C*H*$_2$), 16.41 (br s, 2H, *m-pyridine*), 22.30 (br s, 1H, *p-pyridine*). ^{1}H NMR (toluene-d_8, - 80 °C): -0.06 (s, 6H, C(C*H*$_3$)), 0.56 (br s, 12H, CH(C*H*$_3$)$_2$), 0.61 (br s, 12H, CH(C*H*$_3$)$_2$), 1.44 (br s, 6H, adamantyl C*H*$_2$), 1.65 (br s, 4H, C*H*(CH$_3$)$_2$), 1.82 (br s, 3H, adamantyl C*H*$_2$), 2.45 (br s, 3H, adamantyl C*H*$_2$), 2.75 (br s, 3H, adamantyl C*H*$_2$), 6.76 (br s, 4H, *m-aryl*), 7.10 (br s, 2H, *p-aryl*), 8.75 (br s, 2H, *m-pyridine*), 9.27 (br s, 1H, *p-pyridine*). ^{13}C {^{1}H}

NMR (benzene-d_6): δ = 20.61, 20.78, 29.93, 30.11, 33.39, 42.66, 42.93, 71.40, 95.52, 100.41, 117.73, 124.05, 124.23, 140.92, 178.98, 202.17.

Preparation of (^{iPr}PDI)FeN(^{Cy}Oct) (1-N(^{Cy}Oct)). A 100 mL round-bottom flask was charged with 0.244 g (0.411 mmol) (^{iPr}PDI)Fe(N_2)$_2$, approximately 50 mL of pentane and a stir bar. A solution of cyclooctyl azide (0.057 g , 0.372 mmol) in 4 mL of pentane was added dropwise to the stirring solution, resulting in a gradual color change to bright purple. The reaction was stirred 20 minutes, then volatiles were removed. The resulting dark purple solid was recrystallized from pentane at -35 °C to give 0.243 g (86 %) of dark purple crystals identified as (^{iPr}PDI)FeN(^{Cy}Oct). Analysis for $C_{41}H_{58}N_4Fe$: Calc. C, 74.30; H, 8.82; N, 8.45. Found C, 74.67; H, 8.80; N, 7.97. ^{1}H NMR (benzene-d_6): δ = -16.36 (s, 6H, C(CH_3)), -6.31 (br s, 4H, CH(CH_3)$_2$), -0.96 (br s, 12H, CH(CH_3)$_2$), -0.24 (br s, 12H, CH(CH_3)$_2$), 3.26 (m, 1H, cyclooctyl CH), 3.90 (m, 8H, cyclooctyl CH_2), 4.07 (m, 2H, cyclooctyl CH_2), 4.58 (m, 2H, cyclooctyl CH_2), 5.48 (m, 2H, cyclooctyl CH_2), 6.17 (d, 7.5 Hz, 4H, *m-aryl*), 7.40 (t, 7.5 Hz, 2H, *p-aryl*), 18.02 (br s, 2H, *m-pyridine*), 20.64 (br s, 1H, *p-pyridine*). ^{13}C {^{1}H} NMR (benzene-d_6): δ = 20.31, 31.84, 33.94, 34.37, 39.96, 72.71, 76.49, 106.04, 118.36, 124.22, 126.73, 136.45, 166.14, 189.59, 210.32.

Preparation of (^{iPr}*p*-^{t}BuPDI)FeN(^{1}Ad) (^{tBu}1-N(^{1}Ad)). This compound was prepared in a similar manner to (^{iPr}PDI)FeN(^{1}Ad) with 0.101 g (0.155 mmol) of (^{iPr}*p*-^{t}BuPDI)Fe(N_2)$_2$ and 0.028 g (0.155 mmol) of 1-adamantyl azide, and yielded 0.077 g (67 %) of dark purple crystals identified as (^{iPr}*p*-^{t}BuPDI)FeN(^{1}Ad). Analysis for $C_{47}H_{66}N_4Fe$: Calc. C, 77.87; H, 9.18; N, 7.73. Found C, 77.97; H, 9.19; N, 7.72. ^{1}H NMR (benzene-d_6): δ = -17.04 (s, 6H, C(CH_3)), -7.07 (br s, 4H, CH(CH_3)$_2$), -1.42 (br s, 12 H, CH(CH_3)$_2$), -0.52 (br s, 12 H, CH(CH_3)$_2$), 2.77 (s, 9H, ^{t}Bu CH_3), 2.91 (br s,

6H, adamantyl CH_2), 3.17 (d, 12 Hz, 3H, adamantyl CH_2), 4.01 (d, 12 Hz, 3H, adamantyl CH_2), 5.97 (d, 7.7 Hz, 4H, *m-aryl*), 7.25 (t, 7.7 Hz, 2H, *p-aryl*), 9.40 (br s, 3H, adamantyl CH_2), 17.63 (br s, 2H, *m-pyridine*). ^{13}C {^{1}H} NMR (benzene-d_6): δ = 10.90, 20.72, 29.26, 30.71, 33.58, 43.20, 63.77, 72.16, 93.12, 115.17, 123.63, 124.13, 129.24, 181.12, 207.99, 216.23, two resonances not located.

Preparation of (^{iPr}*p*-^{t}BuPDI)FeN(^{Cy}Oct) (^{tBu}1-N(^{Cy}Oct)). This compound was prepared in a similar manner to **(^{iPr}PDI)FeN(^{Cy}Oct)** with 0.209 g (0.322 mmol) of **(^{iPr}*p*-^{t}BuPDI)Fe(N_2)$_2$** and 0.047 g (0.307 mmol) of cyclooctyl azide, and yielded 0.123 g (53 %) of a dark purple powder identified as **(^{iPr}*p*-^{t}BuPDI)FeN(^{Cy}Oct)**. Analysis for $C_{45}H_{66}N_4Fe$: Calc. C, 75.19; H, 9.25; N, 7.79. Found C, 74.86; H, 9.29; N, 7.51. ^{1}H NMR (benzene-d_6): δ = -16.75 (s, 6H, C(CH_3)), -5.87 (br s, 4H, CH(CH_3)$_2$), -0.92 (br s, 12H, CH(CH_3)$_2$), -0.16 (br s, 12H, CH(CH_3)$_2$), 2.57 (s, 9H, ^{t}Bu CH_3), 3.19 (m, 1H, cyclooctyl CH), 3.84 (m, 8H, cyclooctyl CH_2), 4.02 (m, 2H, cyclooctyl CH_2), 4.50 (m, 2H, cyclooctyl CH_2), 5.46 (m, 2H, cyclooctyl CH_2), 6.21 (d, 7.4 Hz, 4H, *m-aryl*), 7.40 (t, 7.4 Hz, 2H, *p-aryl*), 18.38 (s, 2H, *m-pyridine*). ^{13}C {^{1}H} NMR (benzene-d_6): δ = 14.85, 20.56, 32.12, 33.80, 34.08, 39.31, 40.53, 58.61, 73.14, 117.99, 124.37, 126.35, 163.96, 189.84, 199.92, 210.86, three resonances not located.

Preparation of (^{iPr}PDI)FeN(^{2}Ad) (1-N(^{2}Ad)). A 20-mL scintillation vial was charged with 0.103 g (0.174 mmol) of **(^{iPr}PDI)Fe(N_2)$_2$** and approximately 15 mL of pentane, resulting in a dark green solution. A solution of 0.031 g (0.174 mmol) 2-adamantyl azide in 3 mL pentane was added dropwise to the vial, resulting in a gradual color change of the solution to black. The solution was stirred for 15 minutes, then filtered through a glass frit. The black solution was cooled to -35 °C to give 0.087 g (73 %) of black crystals identified as **(^{iPr}PDI)FeN(^{2}Ad)**. Analysis for $C_{43}H_{58}N_4Fe$: Calc. C,

75.20; H, 8.51; N, 8.16. Found C, 74.78; H, 7.75; N, 7.83. Magnetic susceptibility (benzene-d_6, 293 K): μ_{eff} = 2.8(1) μ_B. ^{1}H NMR (benzene-d_6): δ = -121.05 (152.0 Hz, 6H, C(CH_3)), -56.34 (273.0 Hz, 4H, CH(CH_3)$_2$), -12.11 (91.7 Hz, 12H, CH(CH_3)$_2$), -7.30 (44.6 Hz, 12H, CH(CH_3)$_2$), -0.03 (47.8 Hz, 4H), 7.87 (40.0 Hz, 2H), 12.07 (36.3 Hz, 2H), 14.07 (77.5 Hz, 4H), 21.68 (101.0 Hz, 4H), 21.95 (156.2 Hz, 2H), 60.74 (204.7 Hz, 2H), 72.80 (110.4 Hz, 2H, *m-pyridine*), 94.01 (104.3 Hz, 1H, adamantyl or *p-pyridine*), one resonance not located.

Preparation of (^{iPr}PDEA)Fe(NH_2^1Ad) (2-NH_2^1Ad). A 20-mL scintillation vial was charged with 0.087 g (0.127 mmol) of **(^{iPr}PDEA)Fe(THF)$_2$** and approximately 15 mL of diethyl ether, resulting in a dark orange-brown solution. A solution of 0.019 g (0.127 mmol) 1-adamantyl amine in 3 mL diethyl ether was added to the vial, resulting in a gradual darkening of the solution to brown. The solution was stirred for 30 minutes, followed by removal of the volatiles to give a dark orange-brown solid. The solid was redissolved in 10 mL of pentane and cooled to -35 °C to give 0.065 g (73 %) of a dark brown powder identified as **(^{iPr}PDEA)Fe(NH_2^1Ad)**. Analysis for $C_{43}H_{58}N_4Fe$: Calc. C, 75.20; H, 8.51; N, 8.16. Found C, 75.38; H, 8.24; N, 7.87. Magnetic susceptibility (benzene-d_6, 293 K): μ_{eff} = 3.7(1) μ_B. ^{1}H NMR (benzene-d_6): δ = -49.91 (173.3 Hz, 2H, C=CH_2), -49.31 (125.8 Hz, 2H, C=CH_2), -19.66 (175.7 Hz, 12H, CH(CH_3)$_2$), -13.55 (43.5 Hz, 1H, *p-pyridine*), -12.42 (45.7 Hz, 2H, *m-pyridine* or *p-aryl*), -9.35 (320.6 Hz, 6H, *adamantyl*), -5.00 (46.8 Hz, 3H, *adamantyl*), -3.06 (30.9 Hz, 3H, *adamantyl*), 14.27 (80.9 Hz, 12H, CH(CH_3)$_2$), 15.02 (566.3 Hz, 4H, CH(CH_3)$_2$), 47.36 (66.8 Hz, 4H, *m-aryl*), 128.17 (71.0 Hz, 2H, *m-pyridine* or *p-aryl*), NH_2 resonance and one additional resonance not located. IR (KBr): ν_{NH} = 3228, 3305 cm^{-1}; ν_{ND} = 2267, 2281 cm^{-1}; $\nu_{C=C}$ = 1571 cm^{-1}.

Preparation of (^{iPr}*p*-^{t}BuPDEA)Fe(NH$_2$^{1}Ad) (^{tBu}2-NH$_2$^{1}Ad). This compound was prepared in a similar manner to **(^{iPr}PDEA)Fe(NH$_2$^{1}Ad)** with 0.103 g (0.155 mmol) of **(^{iPr}*p*-^{t}BuPDEA)Fe(THF)$_2$** and 0.023 g (0.155 mmol) of 1-adamantyl amine, and yielded 0.093 g (81 %) of a dark brown solid identified as **(^{iPr}*p*-^{t}BuPDEA)-Fe(NH$_2$^{1}Ad)**. Analysis for $C_{47}H_{66}N_4Fe$: Calc. C, 75.99; H, 8.95; N, 7.54. Found C, 75.95; H, 8.96; N, 7.12. Magnetic susceptibility (benzene-d_6, 293 K): $\mu_{eff} = 4.3(1)\ \mu_B$. ^{1}H NMR (benzene-$d_6$): δ = -47.40 (187.9 Hz, 2H, C=CH_2), -45.04 (153.0 Hz, 2H, C=CH_2), -19.62 (202.3 Hz, 12H, CH(CH_3)$_2$), -12.82 (73.2 Hz, 2H, *m-pyridine* or *p-aryl*), -8.41 (324.4 Hz, 6H, *adamantyl*), -4.65 (75.0 Hz, 3H, *adamantyl*), -2.84 (60.2 Hz, 3H, *adamantyl*), -0.99 (36.6 Hz, ^{t}Bu CH_3), 13.86 (93.7 Hz, 12H, CH(CH_3)$_2$), 15.48 (1212.7 Hz, 4H, CH(CH$_3$)$_2$), 47.03 (92.9 Hz, 4H, *m-aryl*), 124.83 (101.2 Hz, *m-pyridine* or *p-aryl*), NH_2 resonance and one additional resonance not located. IR (KBr): $\nu_{NH} = 3232, 3305\ cm^{-1}$; $\nu_{C=C} = 1582\ cm^{-1}$.

Preparation of (^{iPr}PDEA)Fe(NH$_2$^{Cy}Oct) (2-NH$_2$^{Cy}Oct). This compound was prepared in a similar manner to **(^{iPr}PDEA)Fe(NH$_2$^{1}Ad)** with 0.092 g (0.135 mmol) of **(^{iPr}PDEA)Fe(THF)$_2$** and 19.0 μL (0.137 mmol) of cyclooctyl amine, and yielded 0.071 g (79 %) of dark brown crystals identified as **(^{iPr}PDEA)Fe(NH$_2$^{Cy}Oct)**. Analysis for $C_{41}H_{58}N_4Fe$: Calc. C, 74.30; H, 8.82; N, 8.45. Found C, 74.62; H, 8.47; N, 8.20. Magnetic susceptibility (benzene-d_6, 293 K): $\mu_{eff} = 3.8(2)\ \mu_B$. ^{1}H NMR (benzene-$d_6$): δ = -66.74 (125.5 Hz, 2H, C=CH_2), -54.22 (122.2 Hz, 2H, C=CH_2), -24.25 (148.1 Hz, 12H, CH(CH_3)$_2$), -19.82 (67.8 Hz, 1H, *p-pyridine*), -18.50 (402.4 Hz, 1H, cyclooctyl C*H*), -11.17 (373.0 Hz, 2H, cyclooctyl CH_2), -6.89 (58.1 Hz, 2H, *m-pyridine* or *p-aryl*), -4.77 (337.0 Hz, 2H, cyclooctyl CH_2), -2.79 (624.9 Hz, 8H, cyclooctyl CH_2), -0.68 (523.5 Hz, 2H, cyclooctyl CH_2), 14.38 (54.1 Hz, 12H, CH(CH_3)$_2$), 19.77 (626.3 Hz, 4H, CH(CH$_3$)$_2$), 43.98 (59.3 Hz, 4H, *m-aryl*), 108.25

(84.9 Hz, 2H, *m-pyridine* or *p-aryl*), NH_2 resonance not located. IR (KBr): ν_{NH} = 3246, 3321 cm^{-1}; ν_{ND} = 2269, 2279 cm^{-1}; $\nu_{C=C}$ = 1581 cm^{-1}.

Preparation of (^{iPr}*p*-^{t}BuPDEA)Fe(NH_2^{Cy}Oct) (^{tBu}2-NH_2^{Cy}Oct). This compound was prepared in a similar manner to **(^{iPr}PDEA)Fe(NH_2^{1}Ad)** with 0.084 g (0.114 mmol) of **(^{iPr}*p*-^{t}BuPDEA)Fe(THF)$_2$** and 17.0 μL (0.125 mmol) of cyclooctyl amine, and yielded 0.085 g (93 %) of dark brown crystals identified as **(^{iPr}*p*-^{t}BuPDEA)-Fe(NH_2^{Cy}Oct)**. Analysis for $C_{45}H_{66}N_4Fe$: Calc. C, 75.18; H, 9.25; N, 7.79. Found C, 75.07; H, 9.29; N, 7.33. Magnetic susceptibility (benzene-d_6, 293 K): μ_{eff} = 4.3(2) μ_B. ^{1}H NMR (benzene-d_6): δ = -67.11 (79.4 Hz, 2H, C=CH_2), -53.93 (79.1 Hz, 2H, C=CH_2), -23.49 (124.6 Hz, 12H, CH(CH_3)$_2$), -17.67 (426.3 Hz, 1H, cyclooctyl C*H*), -10.09 (349.8 Hz, 2H, cyclooctyl CH_2), -5.59 (27.7 Hz, 2H, *m-pyridine* or *p-aryl*), -4.08 (232.2 Hz, 2H, cyclooctyl CH_2), -2.38 (341.9 Hz, 8H, cyclooctyl CH_2), -1.29 (7.0 Hz, 9H, ^{t}Bu CH_3), -0.47 (100.5 Hz, 2H, cyclooctyl CH_2), 13.77 (43.7 Hz, 12H, CH(CH_3)$_2$), 18.52 (610.6 Hz, 4H, C*H*(CH$_3$)$_2$), 42.56 (34.2 Hz, 4H, *m-aryl*), 100.70 (37.9 Hz, 2H, *m-pyridine* or *p-aryl*), NH_2 resonance not located. IR (KBr): ν_{NH} = 3246, 3317 cm^{-1}; $\nu_{C=C}$ = 1582 cm^{-1}.

Preparation of (^{iPr}PDEA)Fe(NH_2^{2}Ad) (2-NH_2^{2}Ad). This compound was prepared in a similar manner to **(^{iPr}PDEA)Fe(NH_2^{1}Ad)** with 0.102 g (0.150 mmol) of **(^{iPr}PDEA)Fe(THF)$_2$** and 0.023 g (0.152 mmol) 2-adamantyl amine. Recrystallization from pentane at -35 °C yielded 0.085 g (82 %) of a dark brown powder identified as **(^{iPr}PDEA)Fe(NH_2^{2}Ad)**. Analysis for $C_{43}H_{58}N_4Fe$: Calc. C, 75.20; H, 8.51; N, 8.16. Found C, 74.95; H, 8.56; N, 8.14. Magnetic susceptibility (benzene-d_6, 293 K): μ_{eff} = 3.8(2) μ_B. ^{1}H NMR (benzene-d_6): δ = -59.75 (64.7 Hz, 2H, C=CH_2), -50.42 (81.2 Hz, 2H, C=CH_2), -26.69 (123.0 Hz, 12H, CH(CH_3)$_2$), -19.97 (29.3 Hz, 1H, *p-pyridine*), -

8.10 (30.2 Hz, 2H, *m-pyridine* or *p-aryl*), -5.74 (40.4 Hz, 3H, *adamantyl*), -3.26 (29.2 Hz, 4H, *adamantyl*), -2.36 (18.1 Hz, 4H, *adamantyl*), -1.97 (104.8 Hz, 2H, *adamantyl*), -0.93 (29.0 Hz, 2H, *adamantyl*), 14.06 Hz (39.4 Hz, 12H, $CH(C\mathit{H}_3)_2$), 22.53 (540.0 Hz, 4H, $C\mathit{H}(CH_3)_2$), 45.76 (35.5 Hz, 4H, *m-aryl*), 114.51 (34.7 Hz, 2H, *m-pyridine* or *p-aryl*), $N\mathit{H}_2$ resonance not located. IR (KBr): ν_{NH} = 3254, 3304 cm^{-1}; $\nu_{C=C}$ = 1581 cm^{-1}.

Preparation of (^{Et}PDEA)Fe($NH_2{}^1$Ad). A 100 mL round-bottom flask was charged with 0.103 g (0.098 mmol) of **[(^{Et}PDI)Fe(N_2)]$_2$(μ-N_2)**, approximately 50 mL of pentane and a stir bar. A solution of 0.035 g (0.197 mmol) of 1-adamantyl azide in 3 mL pentane was added dropwise with stirring, resulting in a rapid color change to bright purple, followed by a second rapid color change to amber. The solution was stirred for 15 minutes, then concentrated and cooled to -35 °C to give 0.076 g (76 %) of dark brown crystals identified as **(^{Et}PDEA)Fe($NH_2{}^1$Ad)**. Magnetic susceptibility (benzene-d_6, 293 K): μ_{eff} = 4.7(2) μ_B. ^{1}H NMR (benzene-d_6): δ = -47.84 (100.2 Hz, 2H, C=CH_2), -44.35 (128.3 Hz, 2H, C=CH_2), -15.20 (41.6 Hz, 1H, *p-pyridine*), -14.14 (836.0 Hz, 6H, *adamantyl*), -11.57 (41.2 Hz, 2H, *m-pyridine* or *p-aryl*), -6.01 (191.3 Hz, 3H, *adamantyl*), -3.70 (109.6 Hz, 3H, *adamantyl*), -2.05 (97.8 Hz 3H, *adamantyl*), -0.79 (89.1 Hz, 12H, $CH_2C\mathit{H}_3$), 16.83 (460.7 Hz, 4H, $C\mathit{H}_2CH_3$), 30.89 (541.5 Hz, 4H, $C\mathit{H}_2CH_3$), 47.68 (55.2 Hz, 4H, *m-aryl*), 125.20 (56.7 Hz, 2H, *m-pyridine* or *p-aryl*), $N\mathit{H}_2$ resonance not located. IR (KBr): ν_{NH} = 3244, 3291 cm^{-1}; $\nu_{C=C}$ = 1579 cm^{-1}.

REFERENCES

[1] (a) Ducan, J. S.; Zdilla, M. J.; Lee, S. C. *Inorg. Chem.* **2007**, *46*, 1071-1080. (b) Brown, S. D.; Betley, T. A.; Peters, J. C. *J. Am. Chem. Soc.* **2003**, *125*, 322-323. (c) Brown, S. D.; Peters, J. C. *J. Am. Chem. Soc.* **2005**, *127*, 1913-1923. (d) Thomas, C. M.; Mankad, N. P.; Peters, J. C. *J. Am. Chem. Soc.* **2006**, *128*, 4956-4957. (e) Eckert, N. A.; Vaddadi, S.; Stoian, S.; Lachicotte, R. J.; Cundari, T. R.; Holland, P. L. *Angew. Chem. Int. Ed.* **2006**, *45*, 6868-6871. (f) Ni, C. B.; Fettinger, J. C.; Long, G. J.; Brynda, M.; Power, P. P *Chem. Commun.* **2008**, 6045-6047.

[2] Mehn, M. P.; Peters, J. C. *J. Inorg. Biochem.* **2006**, *100*, 634-643.

[3] (a) Jensen, M. P.; Mehn, M. P.; Que, L. *Angew. Chem. Int. Ed.* **2003**, *42*, 4357-4360. (b) Lucas, R. L.; Powell, D. R.; Borovik, A. S. *J. Am. Chem. Soc.* **2005**, *127*, 11596-11597. (c) King, E. R.; Betley, T. A. *Inorg. Chem.* **2009**, *48*, 2361-2363. (d) Nieto, I.; Ding, F.; Bontchev, R. P.; Wang, H.; Smith, J. M. *J. Am. Chem. Soc.* **2008**, *130*, 2716-2717.

[4] Verna, A. K.; Nazif, T. N.; Achim, C.; Lee, S.; *J. Am. Chem. Soc.* **2000**, *122*, 11013-11014.

[5] Bart, S. C.; Lobkovsky, E.; Bill, E.; Chirik, P. J. *J. Am. Chem. Soc.* **2006**, *128*, 5302-5303.

[6] (a) Dai, X.; Kapoor, P.; Warren, T. H. *J. Am. Chem. Soc.* **2004**, *126*, 4798-4799. (b) Hu, X.; Meyer, K. *J. Am. Chem. Soc.* **2004**, *126*, 16322-16323. (c) Shay, D. T.; Yap, G. P. A.; Zakharov, L. N.; Rheingold, A. L.; Theopold, K. H. *Angew. Chem. Int. Ed.* **2005**, *44*, 1508-1510. (d) Cowley, R. E.; Bontchev, R. P.; Sorrell, J.; Sarracino, O.; Feng, Y.; Wang, H.; Smith, J. M. *J. Am. Chem. Soc.* **2007**, *129*, 2424-2425. (e) Lu, C. C.; DeBeer George, S.; Weyhermüller, T.; Bill, E.; Bothe, E.; Wieghardt, K. *Angew. Chem. Int. Ed.* **2008**, *47*, 6384-6387.

[7] Knijnenburg, Q.; Gambarotta, S.; Budzelaar, P. H. M. *Dalton Trans.* **2006**, 5442-5448.

[8] Darmon, J. M; Chirik, P. J. Unpublished results.

[9] See Chapter 4 of this work.

[10] Tondreau, A. M.; Chirik, P. J. Unpublished results.

[11] Gütlich, P.; Goodwin, H. A. Spin Crossover – An Overall Perspective. In *Spin Crossover in Transition Metal Compounds I;* Gütlich, P., Goodwin, H. A., Eds.; Springer-Verlag: Berlin, 2004; Vol. 233; p 1.

[12] Long, G. J. Mössbauer spectroscopy as a structural probe. In *Mössbauer Spectroscopy*; Dickson, D. P. E., Berry, F. J., Eds.; Cambridge University Press: Cambridge, 1986; p 70.

[13] Gütlich, P. Spin crossover in iron(II)-complexes. In *Metal Complexes*; Clarke, M. J., Hemmerich, P., Jørgensen, C. K., Reinen, D., Williams, R. J. P., Eds.; Springer-Verlag: Berlin, 1981; Vol. 44; p 83.

[14] Sorai, M.; Seki, S. *J. Phys. Chem. Solids* **1974**, *35*, 555-570.

[15] Bart, S. C.; Lobkovsky, E.; Chirik, P. J. *J. Am. Chem. Soc.* **2004**, *126*, 13794-13807.

[16] DFT calculations performed by Dr. Carsten Milsmann.

[17] Bart, S. C.; Chlopek, K.; Bill, E.; Bouwkamp, M. W.; Lobkovsky, E.; Neese, F.; Wieghardt, K.; Chirik, P. J. *J. Am. Chem. Soc.* **2006**, *128*, 13901-13912.

[18] (a) Thyagarajan, S.; Shay, D. T.; Incarvito, C. D.; Rheingold, A. L.; Theopold, K. H. *J. Am. Chem. Soc.* **2003**, *125*, 4440-4441. (b) Shay, D. T.; Yap, G. P. A.; Zakharov, L. N.; Rheingold, A. L.; Theopold, K. H. **2005**, *44*, 1508-1510. (c) Chomitz, W. A.; Arnold, J. *Chem. Commun.* **2008**, 3648-3650.

[19] Russell, S. K; Chirik. P. J. Unpublished results.

[20] Bouwkamp, M. W.; Lobkovsky, E.; Chirik, P. J. *Inorg. Chem.* **2006**, *45*, 2-4.

[21] Bart, S. C.; Bowman, A. C.; Lobkovsky, E.; Chirik, P. J. *J. Am. Chem. Soc.* **2007**, *129*, 7212-7213.

[22] Bowman, A. C.; Bart, S. C.; Heinemann, F. W.; Meyer, K.; Chirik, P. J. *Inorg. Chem.* **2009**, *48*, 5587-5589.

[23] Archer, A. M.; Bouwkamp, M. W.; Cortez, M.-P.; Lobkovsky, E.; Chirik, P. J. *Organometallics* **2006**, *25*, 4269-4278.

[24] (a) de Visser, S. P.; Shaik, S. *J. Am. Chem. Soc.* **2003**, *125*, 7413-7424. (b) Baerends, E. J.; Louwerse, M. J. *Phys. Chem. Chem. Phys.* **2007**, *9*, 156-166. (c) Hirao, H.; Que, L.; Nam, W.; Shaik, S. *Chem. Eur. J.* **2008**, *14*, 1740-1756. (d) Jeong, Y. J.; Kang, Y.; Han, A.; Lee, Y.; Kotani, H.; Fukuzumi, S.; Nam, W. *Angew. Chem. Int. Ed.* **2008**, *47*, 7321-7324.

[25] Prakash, G. K. S.; Stephenson, M. A.; Shih, J. G.; Olah, G. A. *J. Org. Chem.* **1986**, *51*, 3215-3217.

[26] Miriyala, B.; Bhattacharyya, S.; Williamson, J. S. *Tetrahedron* **2004**, *60*, 1463-1471.

[27] Alvarez, S. G.; Alvarez, M. T. *Synthesis* **1997**, 413-414.

[28] Kooistra, T. M.; Hetterscheid, D. G. H.; Schwartz, E.; Knijnenburg, Q.; Budzelaar, P. H. M.; Gal, A. W. *Inorg. Chim. Acta* **2004**, *357*, 2945-2952.

[29] Clentsmith, G. K. B.; Gibson, V. C.; Hitchcock, P. B.; Kimberley, B. S.; Rees, C. W. *Chem. Commun.* **2002**, *14*, 1498-1499.

[30] Sur, S. K. *J. Magn. Reson.* **1989**, *82*, 169-173.

CHAPTER 3

HYDROGENATION, SILANE ADDITION AND CYCLOADDITION CHEMISTRY OF BIS(IMINO)PYRIDINE IRON IMIDES

3.1 Abstract

The reactivity of bis(imino)pyridine iron imide compounds with hydrogen, silanes and terminal alkynes was investigated. Exposure of (^{Ar}PDI)FeN(R) (^{Ar}PDI = 2,6-(2,6-$^{i}Pr_2$-C_6H_3-N=CMe)$_2$$C_5H_3N$ (^{iPr}PDI), 2,6-(2,6-$^{i}Pr_2$-C_6H_3-N=CMe)$_2$-4-^{t}Bu-C_5H_3N (^{iPr}*p*-^{t}BuPDI); R = 1-Ad, 2-Ad, ^{Cy}Octyl) to one atmosphere of dihydrogen at 23 °C resulted in hydrogenation of the iron-nitrogen bond to furnish the corresponding bis(imino)pyridine iron amine complexes, (^{Ar}PDI)Fe(NH_2R) (^{Ar}PDI = ^{iPr}PDI, ^{iPr}*p*-^{t}BuPDI; R = 1-Ad, 2-Ad, ^{Cy}Octyl). One exception was for (^{iPr}PDI)FeN(^{1}Ad), where no hydrogenation reactivity was observed. The rate of hydrogenation of (^{iPr}PDI)FeN(^{2}Ad) was much faster than the other bis(imino)pyridine iron imides, with full conversion to the amine product, (^{iPr}PDI)Fe($NH_2{}^{2}$Ad), after 6 hours at 23 °C. Treatment of (^{iPr}PDI)FeN(^{1}Ad) and (^{iPr}PDI)FeN(^{2}Ad) with $PhSiH_3$ or Ph_2SiH_2 resulted in 1,2-addition of the silane across the iron-nitrogen bond, followed by reductive elimination of the free silylamine. Addition of phenylsilane to (^{iPr}PDI)FeN*Ar* (*Ar* = 2,6-$^{i}Pr_2$-C_6H_3, 2,4,6-Me_3-C_6H_2) resulted in modification of the bis(imino)pyridine ligand concomitant with loss of dihydrogen. The silane addition products (^{iPr}PDI)FeN*Ar*SiHPh are best described as high-spin iron(II), $S = 2$ complexes. The likely mechanism for formation of these products is 1,2 addition followed by nucleophilic attack at silicon and β-hydrogen elimination to lose dihydrogen. Treatment of (^{iPr}PDI)FeN(^{1}Ad) and (^{iPr}PDI)FeN(^{Me3}Ph) with trimethylsilylacetylene furnished the cycloaddition products, (^{iPr}PDI)FeN(^{1}Ad)CHC($SiMe_3$) and (^{iPr}PDI)FeN(^{Me3}Ph)CHC($SiMe_3$) respectively. Crystallographic studies and Mössbauer spectroscopy establish that the cycloaddition

products are consistent with a high-spin iron(II) center and a neutral bis(imino)pyridine chelate to account for the overall $S = 2$ molecule.

3.2 Introduction

Terminal iron imides have been observed to participate in useful bond-forming reactions such as hydrogenation, cycloaddition with heterocumulenes and alkynes, and group transfer to furnish isocyanates, carbodiimides and aziridines.[1] Such reactivity may also have interesting applications in the functionalization of azides and amines to furnish more complicated molecules. Previous work in our group has demonstrated that bis(imino)pyridine aryl iron imides are competent for catalytic hydrogenation of azides to anilines as well as stoichiometric N*Ar* group transfer to carbon monoxide to furnish the corresponding isocyanate (Figure 3.1).[2]

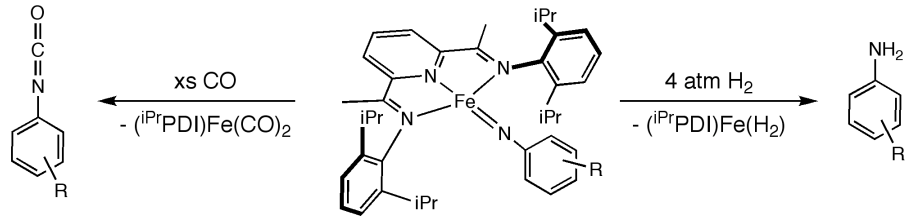

Figure 3.1 Hydrogenation and group transfer chemistry of bis(imino)pyridine aryl iron imide complexes.

Peters and coworkers have also prepared an example of an iron(III) imide, [$PhBP_3$]Fe(N-*p*-tolyl), that undergoes complete hydrogenation of the iron-nitrogen bond to afford *p*-tolylaniline.[3] In addition, [$PhBP_3$]Fe(N-*p*-tolyl) participates in group transfer to carbon monoxide to furnish *p*-tolyl-NCO and the corresponding iron dicarbonyl.[3] Similar group transfer chemistry from a β-diketiminate iron(III) imide was observed by Holland and coworkers, where treatment of L^{tBu}FeNAd (L^{tBu} = $HC[C(^tBu)N(2,6\text{-}^iPr_2C_6H_3)]_2$) with carbon monoxide afforded adamantyl isocyanate

and the corresponding iron carbonyl complex.[1c] Catalytic nitrene group transfer from L^{tBu}FeNAd to several isocyanides, CNR (R = ^{t}Bu, Cy), to furnish the corresponding carbodiimide, AdNCNR, was observed.[1c]

Hydrosilylation of metal-imide bonds, however, has rarely been observed. Therefore, hydrosilylation of a bis(imino)pyridine iron imide complex would be an interesting addition to the observed reactivity for terminal iron imides. There are some examples of hydrosilylation of early transition metal imide complexes, but reductive elimination to yield free silylamine is not observed in any of these cases.[4] Generally, only the initial 1,2-addition is observed to afford the metal amide species, with no subsequent reductive elimination. Fryzuk and coworkers observed that treatment of the tantalum dinitrogen complex, $([NPN]Ta)_2(\mu\text{-}H)_2(\mu\text{-}\eta^1\text{:}\eta^2\text{-}N_2)$ (NPN = $(PhNSiMe_2CH_2)_2PPh$), with two equivalents of $BuSiH_3$ resulted in silane addition across the Ta=N bond to furnish the bridging silanimine complex, although no subsequent reductive elimination of the silylamine was noted.[4c] In addition, silane addition across the Ta-N bond of the aryl-substituted tantalum imide complex, Cp*(*Ar*N=)Ta[(Si(SiMe$_3$)$_3$]H (*Ar* = 2,6-^{i}Pr$_2$-C$_6$H$_3$), with loss of dihydrogen was observed by Tilley and coworkers.[4a] The major organometallic reaction product was the ditantalum species $Cp^*_2Ta_2H_2(\mu\text{-}Ar NSiHPh)_2$, where the silanimine ligands bridge the two tantalum centers through pentacoordinate silicon atoms. However, no reductive elimination of the silylamines was observed.[4a]

In addition to hydrogenation and hydrosilylation, the cycloaddition chemistry of metal-ligand multiple bonds merits exploration. Cycloaddition reactions of heterocumulenes and other unsaturated substrates with zirconocene imide complexes have been well-documented by Bergman and coworkers.[5] The [2 + 2] cycloaddition of alkenes and alkynes to $Cp_2Zr{=}NR$ (R = 2,6-Me_2-C_6H_3; ^{t}Bu) furnished the corresponding azametallacyclobutane complex. These metallocycle compounds were

also proposed as intermediates in the catalytic hydroamination of alkynes by zirconocene bis(amide) complexes, $Cp_2Zr(NHAr)$ (*Ar* = 2,6-Me_2-C_6H_3).[5] In addition, Hillhouse and Waterman investigated the addition of ethylene to the nickel imide complex, (dtbpe)Ni=N*Ar* (dtbpe = 1,2-bis(di-*tert*-butylphosphino)ethane; *Ar* = 2,6-$^{i}Pr_2$-C_6H_3).[6] Following treatment of (dtbpe)Ni=N*Ar* with excess ethylene, nitrene group transfer to generate the corresponding aziridine was observed concomitant with formation of the nickel ethylene complex, (dtbpe)Ni(C_2H_4). The group transfer reaction likely proceeds through [2 + 2] cycloaddition of ethylene to the Ni-N bond to furnish the four-membered metallocycle, followed by reductive elimination of the aziridine.[6]

Based on the above-mentioned literature precedent, metal imide complexes are generally very reactive and display rich and varied chemistry. Previous work with aryl-substituted bis(imino)pyridine iron imides has demonstrated that these complexes also exhibit interesting 1,2-addition and group transfer chemistry, particularly with respect to complete cleavage of the iron-nitrogen bond.[2] The observation that electronic structure may influence the reactivity of bis(imino)pyridine iron imides[7] encourages exploration of the scope of possible reactions. Because aryl and alkyl iron imides differ greatly in their competency towards C-H bond activation reactions, it is possible that the hydrogenation chemistry of alkyl iron imides will be different than the aryl iron imides as well.

3.3 Hydrogenation and Hydrosilylation of Iron Imides

Inspired by the complete hydrogenation of the Fe-N bond in bis(imino)pyridine aryl iron imides to yield free anilines,[2] the hydrogenation of iron imides with *N*-alkyl imide substituents was investigated. Exposure of pentane solutions of (^{iPr}PDI)FeN(^{Cy}Oct) (**1-N(^{Cy}Oct)**) and (^{iPr}*p*-^{t}BuPDI)FeNR (R = 1-Ad (**^{tBu}1-**

N(1Ad)), CyOctyl (**tBu1-N(CyOct)**) to four atmospheres of dihydrogen at 23 °C yielded the corresponding amine compounds, (iPrPDI)Fe(NH_2CyOct) (**1-NH_2CyOct**) and (iPr*p*-tBuPDI)Fe(NH_2R) (R = 1-Ad (**tBu1-$NH_2$1Ad**)), CyOctyl (**tBu1-NH_2CyOct**), respectively, after 36 hours (Figure 3.2). While nearly quantitative conversion to the iron amine compound was observed in each case (~ 90% yield), some formation (< 10%) of the products of imine methyl group C-H activation, (iPrPDEA)Fe(NH_2CyOct) (**2-NH_2CyOct**) and (iPr*p*-tBuPDEA)Fe(NH_2R) (R = 1-Ad (**tBu2-$NH_2$1Ad**)), CyOctyl (**tBu2-NH_2CyOct**), was observed.[7] Performing the reaction under four atmospheres of dihydrogen minimized the formation of C-H activation products.

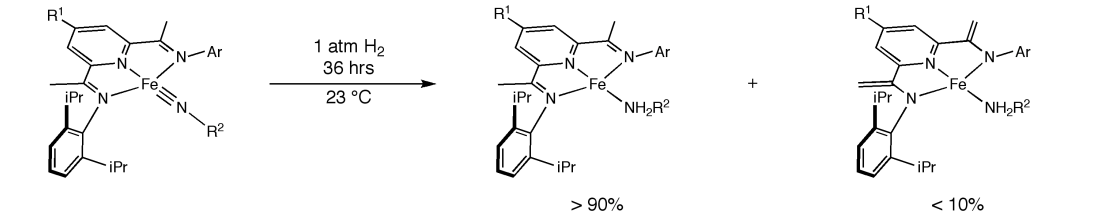

1-N(CyOct) (R^1 = H, R^2 = CyOct)
tBu1-N(1Ad) (R^1 = tBu, R^2 = 1-Ad)
tBu1-N(CyOct) (R^1 = tBu, R^2 = CyOct)

1-NH_2CyOct (R^1 = H, R^2 = CyOct)
tBu1-$NH_2$1Ad (R^1 = tBu, R^2 = 1-Ad)
tBu1-NH_2CyOct (R^1 = tBu, R^2 = CyOct)

2-NH_2CyOct (R^1 = H, R^2 = CyOct)
tBu2-$NH_2$1Ad (R^1 = tBu, R^2 = 1-Ad)
tBu2-NH_2CyOct (R^1 = tBu, R^2 = CyOct)

Figure 3.2 Hydrogenation of bis(imino)pyridine alkyl iron imides.

Notably, no hydrogenation of the Fe-N bond was observed for (iPrPDI)FeN(1Ad) (**1-N(1Ad)**). Heating a pentane solution of **1-N(1Ad)** to 45 °C for 24 hours under four atmospheres of dihydrogen resulted in quantitative formation of (iPrPDEA)Fe($NH_2$1Ad), with no evidence for hydrogenation of the Fe-N bond. A possible explanation is that the rate of hydrogenation of **1-N(1Ad)** is much slower than the rate of C-H activation, precluding formation of the iron amine compound. However, **1-N(1Ad)** and **tBu1-N(1Ad)** have similar steric and electronic environments,[7] thus it is surprising that **tBu1-N(1Ad)** readily hydrogenates while **1-N(1Ad)** did not.

The bis(imino)pyridine iron amine compounds, **1-NH_2CyOct**, **tBu1-$NH_2$1Ad** and **tBu1-NH_2CyOct**, were independently prepared by addition of the appropriate amine to

the iron bis(dinitrogen) compound, (^{iPr}PDI)Fe(N_2)$_2$ (**1-(N_2)$_2$**), at 23 °C. The benzene-d_6 ^{1}H NMR spectra of **1-NH_2^{Cy}Oct**, **^{tBu}1-NH_2^1Ad** and **^{tBu}1-NH_2^{Cy}Oct** at 20 °C exhibit the number of resonances expected for C_{2v} symmetric complexes. Similar to the benzene-d_6 ^{1}H NMR spectra observed for (^{iPr}PDI)Fe($NH_2{}^t$Bu)[8] and (^{iPr}PDI)FeNH_3,[9] the bis(imino)pyridine iron amine complexes exhibit in-plane chelate resonances shifted by temperature independent paramagnetism, consistent with mixing of an $S = 1$ excited state into an $S = 0$ ground state (Table 3.1).[8] For example, the methyl resonance for the imine backbone of **1-NH_2^{Cy}Oct** is shifted upfield to -6.21 ppm while the *m*-pyridine resonance is shifted downfield to 12.27 ppm. For each bis(imino)pyridine iron amine complex, the NH_2 resonance is observed in the vicinity of 5 ppm (Table 3.1).

Table 3.1 Summary of spectroscopic properties for bis(imino)pyridine iron amine complexes at 23 °C.

Complex	$\nu_{NH(D)}$ (cm^{-1}) (KBr)	NH_2 (ppm)	N=C(CH_3) (ppm)	*m-pyr* (ppm)
1-NH_2^1Ad	3268, 3303	5.35	-6.96	12.84
^{tBu}1-NH_2^1Ad	3244, 3300 (2270, 2299)	5.00	-7.60	13.06
1-NH_2^{Cy}Oct	3240, 3305 (2269, 2300)	4.81	-6.21	12.27
^{tBu}1-NH_2^{Cy}Oct	3232, 3299 (2260, 2302)	4.62	-6.74	12.47
1-NH_2^2Ad	3278, 3311 (2293, 2304)	5.21	-6.21	12.22

Exposure of a pentane solution of (^{iPr}PDI)FeN(^{2}Ad) (**1-N(^{2}Ad)**) to four atmospheres of dihydrogen at 23 °C also furnished the bis(imino)pyridine iron amine compound, (^{iPr}PDI)Fe($NH_2{}^2$Ad) (**1-NH_2^2Ad**) (Figure 3.3). There was no evidence, as judged by ^{1}H NMR spectroscopy, for formation of the C-H activation product, (^{iPr}PDEA)Fe($NH_2{}^2$Ad), during the course of the hydrogenation.[7] This is expected,

because **1-N(²Ad)** has not been observed to promote C-H activation of the bis(imino)pyridine ligand. Notably, the rate of hydrogenation was much faster for **1-N(²Ad)** than for the other alkyl iron imides, requiring only six hours for quantitative conversion to the iron amine compound, **1-NH$_2$²Ad**, at 23 °C. As with the bis(imino)pyridine iron amine compounds discussed above, **1-NH$_2$²Ad** was independently prepared by addition of 2-adamantyl amine to **1-(N$_2$)$_2$**. The benzene-d_6 ^{1}H NMR spectrum of **1-NH$_2$²Ad** at 20 °C establishes C_{2v} symmetry, and an $S = 0$ ground state with in-plane chelate resonances shifted by temperature independent paramagnetism (Table 3.1).

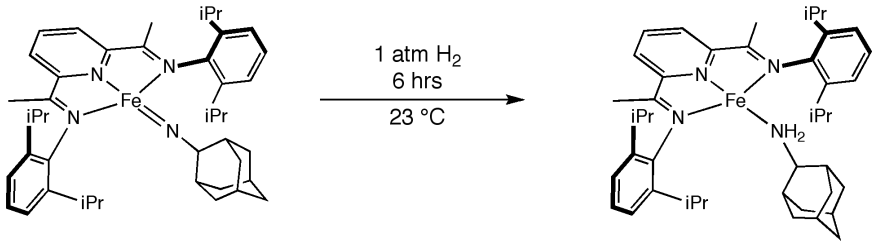

1-N(²Ad) **1-NH$_2$²Ad**

Figure 3.3 Hydrogenation of **1-N(²Ad)** at 23 °C.

Exposure of benzene-d_6 solutions of **1-N(CyOct)**, **tBu1-N(¹Ad)** and **tBu1-N(CyOct)** to four atmospheres of deuterium at 23 °C afforded **1-ND$_2$CyOct**, **tBu1-ND$_2$¹Ad** and **tBu1-ND$_2$CyOct**, respectively, as judged by ^{1}H NMR and infrared spectroscopies. Similarly, formation of **1-ND$_2$²Ad** following exposure of **1-N(²Ad)** to four atmospheres of deuterium in benzene-d_6 at 23 °C was confirmed by ^{1}H NMR and infrared spectroscopies. For each bis(imino)pyridine iron amine complex, the benzene-d_6 ^{1}H NMR spectrum established absence of the NH_2 peak, while the corresponding ND_2 peak was observed at the same chemical shift by ^{2}H NMR. The infrared spectrum (KBr) of each bis(imino)pyridine iron amine complex exhibits two distinct N-H

stretches. These stretches shift appropriately upon isotopic labeling with deuterium (Table 3.1).

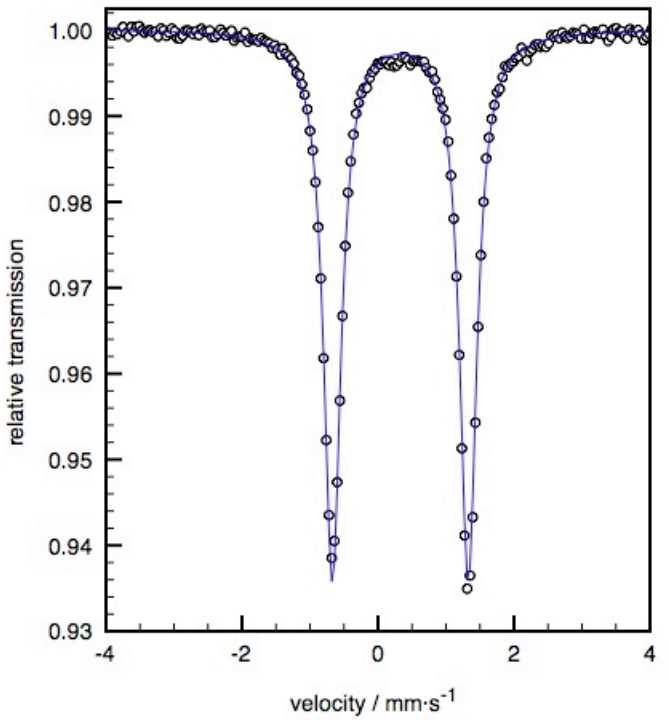

Figure 3.4 Zero-field Mössbauer spectrum of **1-NH_2^{Cy}Oct** at 80 K; δ = 0.33 mm·s^{-1}, ΔE_Q = 2.00 mm·s^{-1}.

To further elucidate the electronic structure of the bis(imino)pyridine iron amine compounds, the zero-field Mössbauer spectrum of (^{iPr}PDI)Fe(NH_2^{Cy}Oct) (**1-NH_2^{Cy}Oct**) was collected at 80 K. A doublet with an isomer shift of 0.33 mm·s^{-1} and a quadrupole splitting of 2.00 mm·s^{-1} (Figure 3.4) is observed in the zero-field Mössbauer spectrum of **1-NH_2^{Cy}Oct**. These parameters are similar to the observed values for (^{iPr}PDI)Fe($NH_2{}^t$Bu)[8] and (^{iPr}PDI)$FeNH_3$,[9] as well as other neutral ligand complexes of bis(imino)pyridine iron,[8] suggesting the iron amine compounds are best described as intermediate-spin iron(II) with antiferromagnetic coupling to a doubly reduced chelate.

One possible mechanism for hydrogenation of the Fe-N bond in bis(imino)pyridine iron imides is 1,2-addition of dihydrogen across the Fe-N bond followed by reductive coupling to form the amine. Hydrogenation of the related bis(imino)pyridine aryl iron imides, (^{iPr}PDI)FeN*Ar*, is also thought to involve 1,2-addition of hydrogen followed by reduction elimination of the aniline, *Ar*NH_2.[2] Reductive coupling is observed for amine ligands while reductive elimination occurs for aniline ligands, likely due to steric effects. Independent synthesis of the bis(imino)pyridine iron amine complexes establishes that one equivalent of each amine coordinates to the iron center. However, treatment of **1-$(N_2)_2$** with one equivalent of 2,6-disubstituted anilines in benzene-d_6 or pentane at 23 °C produced no reaction, demonstrating that the steric bulk of the anilines prohibits coordination to the metal center and leads to reductive elimination following iron imide hydrogenation. For (^{iPr}PDI)FeN*Ar*, the rate of catalytic hydrogenation dramatically decreases as the sterics of the imide substituent are decreased, suggesting that reductive elimination is the rate-limiting step.[2] Although a large difference in the rate of hydrogenation is observed between **1-N(^{2}Ad)** and the other alkyl iron imides, this may be due to a difference in electronic structure[7] as opposed to a steric influence. While hydrogenation of **1-N(^{2}Ad)** was complete in 6 hours at 23 °C, hydrogenation of the other bis(imino)pyridine alkyl iron imides required 36 hours at 23 °C. For all hydrogenation reactions, no intermediates were observed during the course of the reaction.

Inspired by the successful hydrogenation of bis(imino)pyridine alkyl iron imides, addition of organosilanes was also explored. Treatment of a pentane solution of **1-N(^{1}Ad)** with phenylsilane at 23 °C resulted in complete cleavage of the Fe-N bond to yield **1-$(N_2)_2$** and the corresponding silylamine, PhH_2Si-NH(^{1}Ad) (Figure 3.5). Similarly, formation of Ph_2HSi-NH(^{1}Ad) was observed following addition of

diphenylsilane to a pentane solution of **N(1Ad)** at 23 °C. With diphenylsilane, ^{1}H NMR spectroscopy established formation of both **1-(N$_2$)$_2$** and (^{iPr}PDI)Fe(Aryl) (**1-(Aryl)**), where **1-(Aryl)** is the product of η^6-coordination of the aryl ring on a dissociated bis(imino)pyridine ligand arm.[10] Performing the reaction under vacuum furnished **1-(Aryl)** as the sole iron species observed in the product mixture (Figure 3.5). Complete conversion of **1-N(1Ad)** was slow at ambient temperature, requiring 24 hours for completion with phenylsilane and 48 hours for completion with diphenylsilane. No intermediate iron species were observed by ^{1}H NMR spectroscopy over the course of the reaction. In contrast to hydrogenation of bis(imino)pyridine iron imides, coordination of the corresponding silylamine was not observed due to steric bulk. Thus, reductive elimination of the silylamine product was observed instead of reductive coupling.

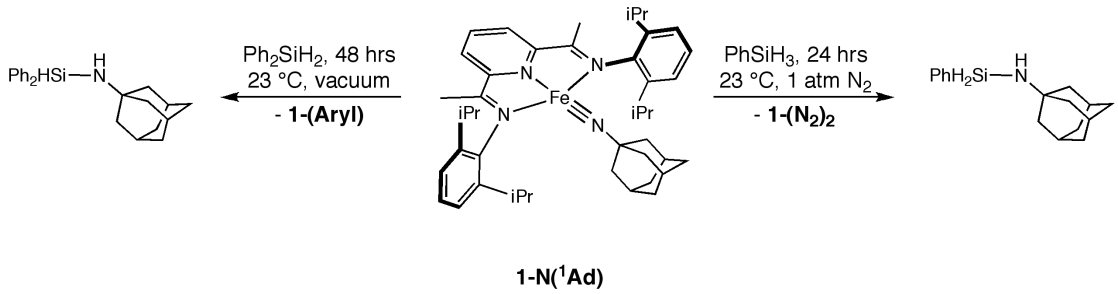

Figure 3.5 Hydrosilylation of **1-N(1Ad)** with $PhSiH_3$ and Ph_2SiH_2 to generate free silylamines.

Similar hydrosilylation chemistry was observed with **1-N(2Ad)**, however different reaction conditions were necessary to obtain the silylamine product when using phenylsilane. Treatment of a pentane solution of **1-N(2Ad)** with phenylsilane at ambient temperature resulted in a complex mixture of iron species, as well as **1-(N$_2$)$_2$** and PhH_2Si-NH(^{2}Ad). However, when addition of phenylsilane to **1-N(2Ad)** was carried out at -78 °C under vacuum with gradual warming to ambient temperature, the

only products of the reaction were **1-(Aryl)** and PhH_2Si-NH(^{2}Ad) (Figure 3.6). In contrast to the hydrosilylation of **1-N(^{1}Ad)**, quantitative conversion to **1-(Aryl)** and PhH_2Si-NH(^{2}Ad) was complete upon reaching ambient temperature. Treatment of a pentane solution of **1-N(^{2}Ad)** with diphenylsilane at 23 °C cleanly furnished **1-$(N_2)_2$** and Ph_2HSi-NH(^{2}Ad) after 48 hours (Figure 3.6). The slower reaction rate observed for addition of diphenylsilane was likely due to steric inhibition.

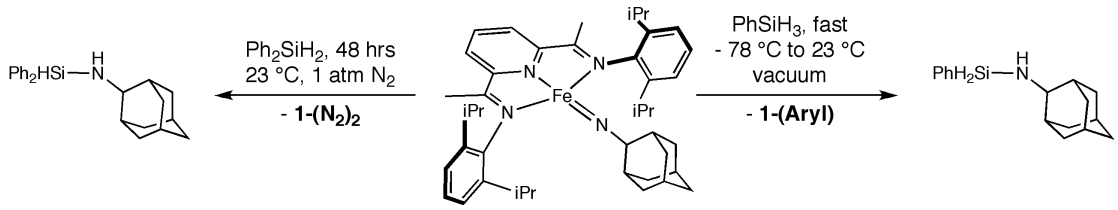

1-N(^{2}Ad)

Figure 3.6 Hydrosilylation of **1-N(^{2}Ad)** with $PhSiH_3$ and Ph_2SiH_2 to generate free silylamines.

The hydrosilylation chemistry of bis(imino)pyridine aryl iron imides was also investigated. In striking contrast to the hydrosilylation of **1-N(^{1}Ad)** and **1-N(^{2}Ad)**, treatment of a pentane solution of (^{iPr}PDI)FeN(2,6-^{i}Pr$_2$-C_6H_3) (**1-N(^{iPr2}Ph)**) with phenylsilane at 23 °C cleanly furnished a paramagnetic product identified as (^{iPr}PDI)FeN(^{iPr2}Ph)SiHPh (**1-N(^{iPr2}Ph)SiHPh**) (Figure 3.7). Loss of hydrogen was confirmed by Toepler pump experiment, where 88 % of the expected dihydrogen was collected. Treatment of a pentane solution of (^{iPr}PDI)FeN(2,4,6-Me_3-C_6H_3) (**1-N(^{Me3}Ph)**) at 23 °C afforded a similar product, (^{iPr}PDI)FeN(^{Me3}Ph)SiHPh (**1-N(^{Me3}Ph)SiHPh**) (Figure 3.7). No evidence for formation of the corresponding silylamine was observed in either case, even when the reaction was carried out at lower temperatures. Moreover, reaction of **1-N(^{iPr2}Ph)SiHPh** and **1-N(^{Me3}Ph)SiHPh** with phenylsilane occurred within minutes at ambient temperature, as judged by ^{1}H

NMR spectroscopy. Treatment of **1-N(^iPr2Ph)SiHPh** or **1-N(^Me3Ph)SiHPh** with one equivalent of Ph_2SiH_2 in pentane at 23 °C resulted in formation of an intractable mixture of iron products.

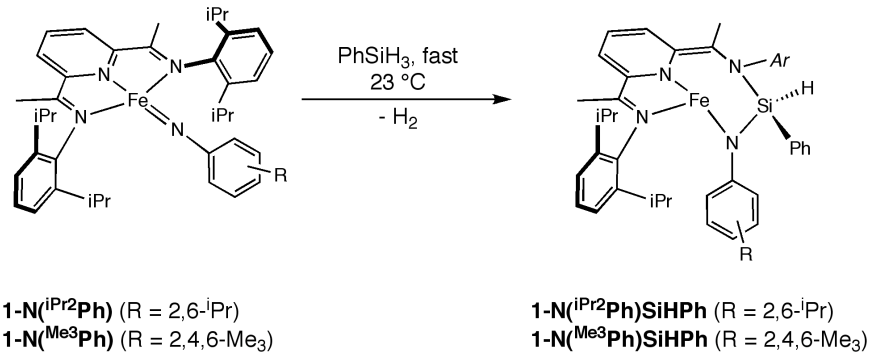

1-N(^iPr2Ph) (R = 2,6-^{i}Pr)
1-N(^Me3Ph) (R = 2,4,6-Me_3)

1-N(^iPr2Ph)SiHPh (R = 2,6-^{i}Pr)
1-N(^Me3Ph)SiHPh (R = 2,4,6-Me_3)

Figure 3.7 Hydrosilylation of bis(imino)pyridine aryl iron imides.

The benzene-d_6 ^{1}H NMR spectra of **1-N(^iPr2Ph)SiHPh** and **1-N(^Me3Ph)SiHPh** at 23 °C establish C_1 symmetry, with paramagnetically broadened resonances. The infrared spectrum (KBr) of **1-N(^iPr2Ph)SiHPh** exhibits a single Si-H stretch at 2168 cm^{-1}, while for **1-N(^Me3Ph)SiHPh** a single Si-H stretch was observed at 2107 cm^{-1}. The solution magnetic moments of **1-N(^iPr2Ph)SiHPh** and **1-N(^Me3Ph)SiHPh** in benzene-d_6 at 20 °C were 5.2(2) μ_B and 4.9(1) μ_B, respectively. These values are consistent with four unpaired electrons (S = 2), indicating a high-spin iron(II) metal center. Because the modified bis(imino)pyridine ligand in the hydrosilylation products is dianionic with two amido nitrogens, it is unlikely that the chelate exhibits redox activity.

The previously obtained solid state structure of **1-N(^iPr2Ph)SiHPh**[11] confirmed silane addition to the Fe-N imide bond and modification of the bis(imino)pyridine chelate. Although the molecular structure is not of high quality due to twinning (R-factor = 10.32 %), it is useful to establish the connectivity of the compound (Figure

3.8). The positions of the hydrogen atoms in the solid state structure of **1-N(^{iPr2}Ph)SiHPh** were calculated.

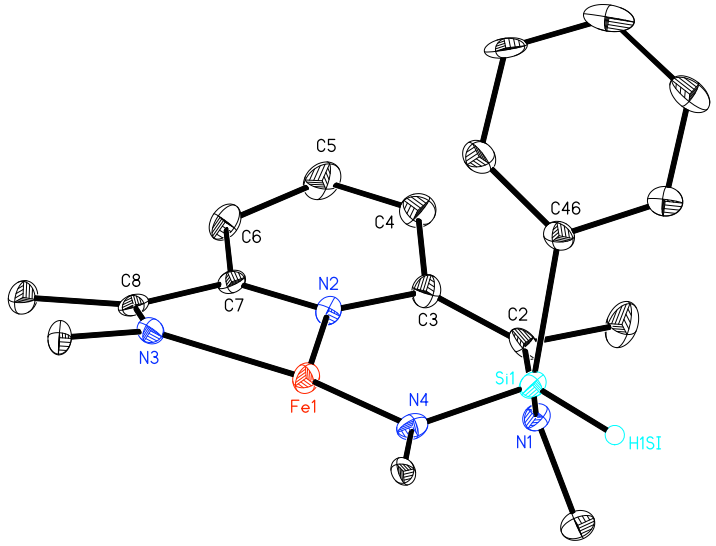

Figure 3.8 Molecular structure of **1-N(^{iPr2}Ph)SiHPh** at 30 % probability ellipsoids. Hydrogen atoms and aryl groups (except on silicon) omitted for clarity.[11]

Table 3.2 Selected bond distances (Å) and angles (°) for **1-N(^{iPr2}Ph)SiHPh**.[11]

Fe(1)-N(2)	1.969(4)	C(7)-C(8)	1.477(7)
Fe(1)-N(3)	2.038(4)	C(7)-N(2)	1.389(6)
Fe(1)-N(4)	1.901(4)	N(3)-Fe(1)-N(4)	148.09(17)
N(1)-C(2)	1.432(6)	C(1)-C(2)-C(3)	120.9(4)
C(2)-C(3)	1.397(7)	N(1)-C(2)-C(3)	122.3(4)
C(3)-N(2)	1.436(6)	N(1)-C(1)-C(2)	116.8(4)
N(3)-C(8)	1.297(7)		

Examination of the metrical parameters of the chelate, presented in Table 3.2, indicates that the former imide nitrogen and the pyridine nitrogen act as anionic donors, with iron-nitrogen bonds of 1.901(4) Å and 1.969(4) Å, respectively. The N_{amide}-C_{amide} distance is elongated to 1.432(6) Å consistent with amide formation at N(1). Likewise, a C_{amide}-C_{ipso} distance of 1.397(7) Å is observed, consistent with double bond formation. The sum of the angles around C(2) is 359.99(27)°, indicating the lack of a hydrogen at this position. The C_{imine}-N_{imine} bond length of 1.297(7) Å and the C_{imine}-C_{ipso} bond length of 1.477(7) Å observed for the unmodified half of the chelate are typical for a neutral chelate.[12]

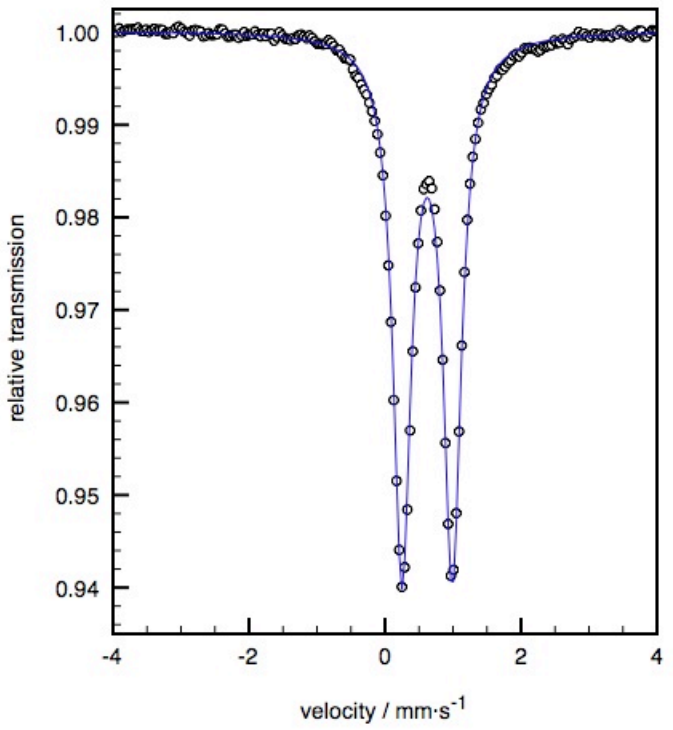

Figure 3.9 Zero-field Mössbauer spectrum of **1-N(^iPr2Ph)SiHPh** at 80 K; $\delta = 0.62$ mm·s^{-1}, $\Delta E_Q = 0.74$ mm·s^{-1}.

Mössbauer spectroscopy was used to further establish the electronic structure of the silane addition products, **1-N(^iPr2Ph)SiHPh** and **1-N(^Me3Ph)SiHPh**. The zero-

field Mössbauer spectrum of **1-N(^iPr2Ph)SiHPh** at 80 K exhibits a doublet with an isomer shift of 0.62 mm·s^{-1} and a quadrupole splitting of 0.74 mm·s^{-1} (Figure 3.9). The observed isomer shift is consistent with a high-spin iron(II) center, as expected from the effective magnetic moment of 5.2(2) μ_B at 20 °C. In addition, both the isomer shift and the quadrupole splitting for **1-N(^iPr2Ph)SiHPh** are similar to those observed for the three-coordinate, high-spin iron(II) β-diketiminate amide complex prepared by Holland and coworkers, L$^{t\text{Bu}}$FeNH^{t}Bu (L$^{t\text{Bu}}$ = HC[C(^{t}Bu)N(2,6-^{i}Pr$_2$C$_6$H$_3$)]$_2$), where δ = 0.63 mm·s^{-1} and ΔE_Q = 1.11 mm·s^{-1}.[13]

As with hydrogenation, 1,2-addition of the appropriate silane is proposed as the first step for hydrosilylation of the Fe-N$_{imide}$ bond. However, the observation of different hydrosilylation products depending on the imide substituent is consistent with two competing pathways. When R = 1-Ad or 2-Ad, initial 1,2-addition is likely followed by reduction elimination to form the silylamine (Figure 3.10). In the presence of dinitrogen, **1-(N$_2$)$_2$** is the resulting iron species, and in the absence of dinitrogen **1-(Aryl)** is observed. Reductive elimination of ammonia and aniline from amido hydride complexes, while rare, has been observed for hafnium,[14] platinum[15] and iridium.[16] The iridium pincer complex (PCP)Ir(H)(NH$_2$) (PCP = η^3-C$_6$H$_3$-2,6-(CH$_2$P^{t}Bu$_2$)$_2$) underwent reductive elimination of ammonia within ten minutes at 23 °C, while reductive elimination of aniline from the analogous complex (PCP)Ir(H)(NHPh) was significantly slower.[16] Bergman and coworkers also observed reductive elimination of alkyl amines from Cp*IrPPh$_3$(H)(NHR) (R = Ph, CH$_2$Ph) at ambient temperature.[17] Treatment of **1-N(^1Ad)** and **1-N(^2Ad)** with PhSiD$_3$ demonstrated that there is no involvement of the bis(imino)pyridine ligand during silane addition. ^{2}H NMR spectroscopy of the iron products of the reactions confirmed no deuterium incorporation into the chelate.

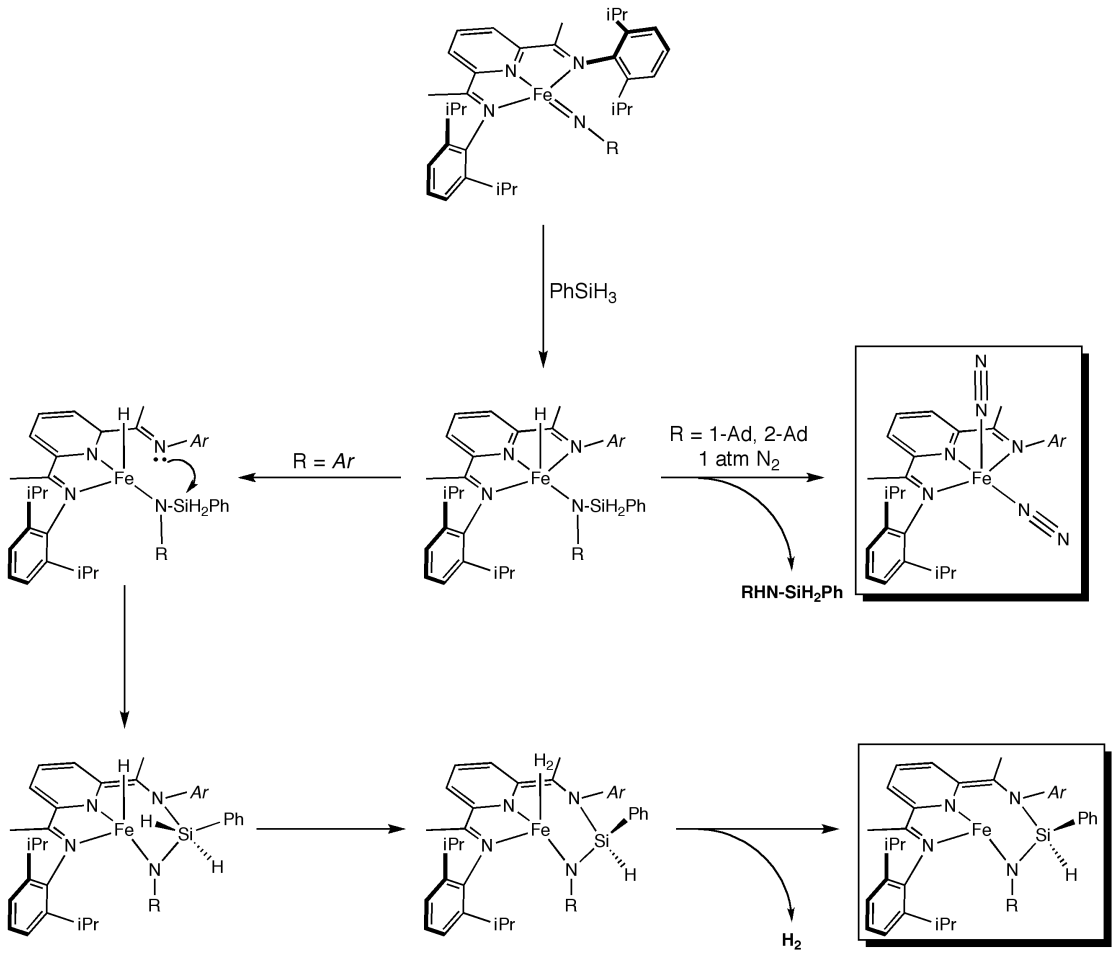

Figure 3.10 Proposed mechanisms for hydrosilylation of aryl and alkyl bis(imino)pyridine iron imides.

With **1-N(^iPr2Ph)SiHPh** and **1-N(^Me3Ph)SiHPh**, 1,2-addition of silane is also the likely first step. Dissociation of a bis(imino)pyridine chelate arm may occur to allow phenylsilane access to the sterically crowded metal center. However, instead of reduction elimination to furnish the silylamine product, nucleophilic attack at silicon may occur to form the seven-membered metallocycle. Pentacoordinate silicon complexes are well-documented,[18,19] and intramolecular attack by amines on H_2SiPhR and HMeSiPhR groups to generate the corresponding pentacoordinate silylamines has also been reported.[20,21] Tilley and coworkers observed that treatment of a tantalum

imide complex with $PhSiH_3$ furnished a ditantalum complex with pentacoordinate silylamine ligands following 1,2-addition and loss of dihydrogen, similar to **1-N(^{iPr2}Ph)SiHPh** and **1-N(^{Me3}Ph)SiHPh**.[4c] Treatment of **1-N(^{iPr2}Ph)SiHPh** and **1-N(^{Me3}Ph)SiHPh** with $PhSiD_3$ indicated no further involvement of the bis(imino)pyridine ligand, as ^{2}H NMR spectroscopy established the absence of deuterium incorporation into the chelate.

The proximity of silicon to the metal center could facilitate β-H elimination and formation of a dihydrogen ligand, perhaps through a σ Si-H interaction with iron. Previous isolation of the bis(imino)pyridine iron bis(silane) compound, (^{iPr}PDI)Fe(η^2-$SiH_3Ph)_2$, establishes that phenylsilane can interact with bis(imino)pyridine iron in a σ fashion, leading to elongation of the Si-H bond.[22] In addition, formation of a dihydrogen ligand is likely as coordination of two hydride ligands would lead to a formally Fe(IV) center. Loss of dihydrogen from the metal center would lead to the observed products, **1-N(^{iPr2}Ph)SiHPh** and **1-N(^{Me3}Ph)SiHPh**. Formation of similar silylamines with loss of dihydrogen has also been reported, where treatment of H_2SiPh_2 with $PhNH_2$ in the presence of 5 mol % *Ar*Cr(CO)$_2$(η^2-$HSiHPh_2$) (*Ar* = C_6H_6) furnished $Ph_2SiHNHPh$ and dihydrogen.[23] Dihydrogen loss was proposed to proceed by metal hydride formation from Si-H bond activation of the η^2-silane ligand, followed by loss of H_2 from the resulting chromium dihydride complex.

Based on the proposed mechanism, the lack of clean reactivity observed with Ph_2SiH_2 is likely based on steric hindrance from the additional phenyl group. It is possible that the initial 1,2-addition to the Fe-N bond is not possible, leading to other (possible radical) chemistry. This is supported by the observation that the reaction of **1-N(^{1}Ad)** and **1-N(^{2}Ad)** is much slower for Ph_2SiH_2 than $PhSiH_3$. Moreover, if 1,2-addition of Ph_2SiH_2 to **1-N(^{iPr2}Ph)SiHPh** and **1-N(^{Me3}Ph)SiHPh** occurs, it is also

possible that subsequent nucleophilic attack at silicon is blocked by the more hindered silicon center.

The different reaction pathways observed for silane addition to N-aryl-substituted and N-alkyl-substituted bis(imino)pyridine iron imides may arise from a difference in the rate of 1,2-addition. As with hydrogenation, silane addition to the N-alkyl-substituted bis(imino)pyridine iron imide complexes is generally slow while reaction with the N-aryl-substituted bis(imino)pyridine iron imides is fast. If the rate of initial 1,2-addition is very slow for **1-N(^{1}Ad)** and **1-N(^{2}Ad)** compared to the rate of reductive elimination, only formation of the silylamine product would be expected. For **1-N(^{iPr2}Ph)SiHPh** and **1-N(^{Me3}Ph)SiHPh** the rate of 1,2-addition is likely very fast, indicating that subsequent nucleophilic attack at silicon occurs before reductive elimination. The increased steric bulk of **1-N(^{iPr2}Ph)SiHPh** and **1-N(^{Me3}Ph)SiHPh** may also facilitate nucleophilic attack at silicon. Dissociation of a bis(imino)pyridine ligand arm may be necessary for silane addition across the Fe-N bond, resulting in an imine group that is already positioned for nucleophilic attack on the silicon atom. Because the imide substituents of **1-N(^{1}Ad)** and **1-N(^{2}Ad)** are less bulky, dissociation of a bis(imino)pyridine ligand arm may not occur during or preceding 1,2-addition of the silane.

3.4 Cycloaddition Chemistry of Iron Imides

Transition metal imides are well-known to undergo cycloaddition with heterocumulenes and other unsaturated organic molecules.[24] Bis(imino)pyridine iron imide complexes with small imide substituents were observed to undergo cycloaddition with organic azides to form a five-membered metallocycle, which is discussed in Chapter 4 in greater detail. Reaction of bis(imino)pyridine iron imides with olefins was also explored with the aim of NR-group transfer and aziridine

formation.[6] However, no change in the starting material was observed after treatment of a benzene-d_6 solution of **1-N(**^{1}**Ad)** or **1-N(**^{Me3}**Ph)** with one equivalent of ethylene or 1-hexene, or twenty equivalents of ethylene, at 23 °C after one week. Heating the reaction mixture to 45 °C for 24 hours also produced no change.

In contrast, addition of one equivalent of trimethylsilylacetylene to a pentane solution of **1-N(**^{1}**Ad)** furnished the cycloaddition product, (^{iPr}PDI)FeN(^{1}Ad)CHC(SiMe$_3$) (**1-N(**^{1}**Ad)CHC(SiMe$_3$)**) (Figure 3.11). The benzene-d_6 ^{1}H NMR spectrum of **1-N(**^{1}**Ad)CHC(SiMe$_3$)** at 23 °C exhibited paramagnetically broadened resonances consistent with a C_s symmetric molecule. Two isomers are possible from cycloaddition of the terminal alkyne, but only one isomer was observed by ^{1}H NMR spectroscopy. Similarly, treatment of a pentane solution of **1-N(**^{Me3}**Ph)** with trimethylsilylacetylene at 23 °C yielded the cycloaddition product, (^{iPr}PDI)FeN(^{Me3}Ph)CHC(SiMe$_3$) (**1-N(**^{Me3}**Ph)CHC(SiMe$_3$)**). As with **1-N(**^{1}**Ad)CHC(SiMe$_3$)**, only one isomer of **1-N(**^{Me3}**Ph)CHC(SiMe$_3$)** was observed by ^{1}H NMR spectroscopy. Solution measurements at 23 °C establish effective magnetic moments of 4.9(1) μ_B and 4.9(2) μ_B for **1-N(**^{1}**Ad)CHC(SiMe$_3$)** and **1-N(**^{Me3}**Ph)CHC(SiMe$_3$)**. These values indicate a high-spin iron(II) center with four unpaired electrons, as expected for a bis(imino)pyridine iron complex with two X-type ligands.[25]

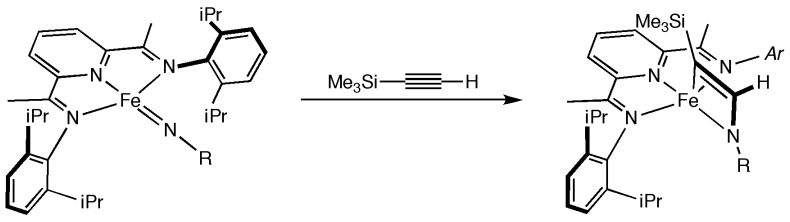

1-N(^{1}**Ad)** (R = 1-Ad)
1-N(^{Me3}**Ph)** (R = 2,4,6-Me$_3$-C$_6$H$_3$)

1-N(^{1}**Ad)CHC(SiMe$_3$)** (R = 1-Ad)
1-N(^{Me3}**Ph)CHC(SiMe$_3$)** (R = 2,4,6-Me$_3$-C$_6$H$_3$)

Figure 3.11 Cycloaddition of SiMe$_3$C≡CH to bis(imino)pyridine iron imides.

The molecular structure of **1-N(1Ad)CHC(SiMe3)** establishes C_s symmetry and idealized square pyramidal geometry (Figure 3.12). Cycloaddition of trimethylsilylacetylene places the trimethylsilyl group over the pyridine ring of the chelate, while the hydrogen points into the pocket of the isopropyl methyl groups (Figure 3.13). A Fe-N_{amide} bond length of 1.9573(14) Å is observed, consistent with a single bond (Table 3.3). The iron-carbon distance of 1.9932(17) Å is similar to those observed for other iron-alkyl bonds.[26] Lengthening of the C-C bond in the trimethylsilylacetylene fragment to 1.372(2) Å is observed, consistent with a C=C double bond. Both the amide nitrogen and the carbon bound to the iron center are planar, with the sum of angles around the atoms equal to 360.00(20)° and 359.92(20)°, respectively (Table 3.3).

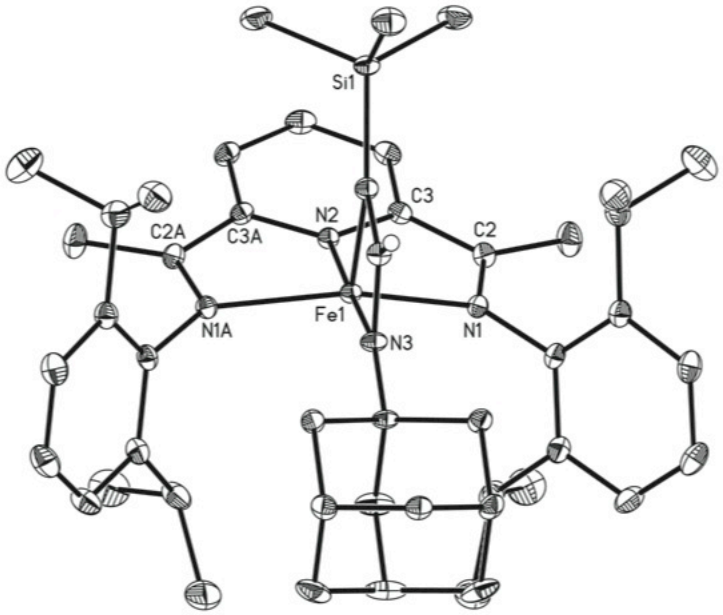

Figure 3.12 Molecular structure of **1-N(1Ad)CHC(SiMe3)** at 30 % probability ellipsoids. Hydrogen atoms omitted for clarity.

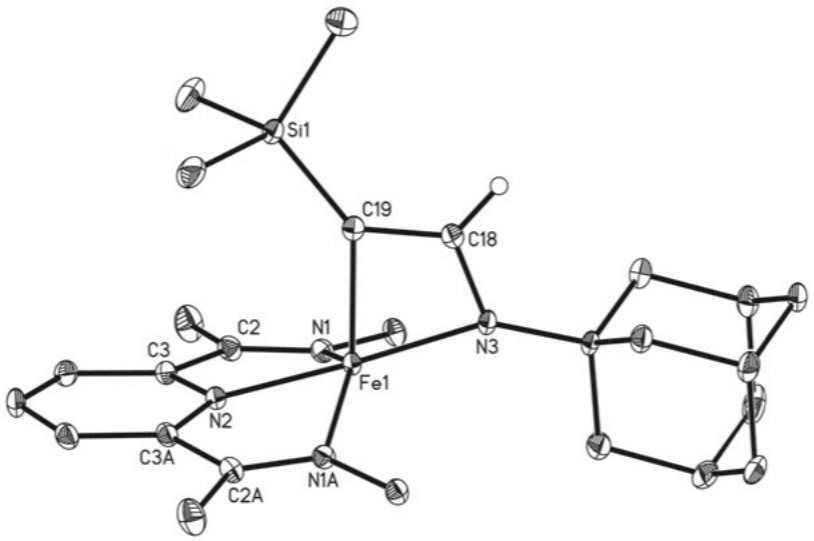

Figure 3.13 Molecular structure of **1-N(^{1}Ad)CHC(SiMe$_3$)** at 30 % probability ellipsoids. Hydrogen atoms and aryl groups omitted for clarity.

Table 3.3 Selected bond distances (Å) and angles (°) for **1-N(^{1}Ad)CHC(SiMe$_3$)**.

Fe(1)-N(1)	2.1517(11)	C(18)-C(19)	1.372(2)
Fe(1)-N(2)	1.9446(14)	C(19)-Si(1)	1.8118(18)
Fe(1)-N(3)	1.9573(14)	N(2)-Fe(1)-N(3)	177.19(6)
Fe(1)-C(19)	1.9932(17)	N(2)-Fe(1)-C(19)	105.60(6)
N(1)-C(2)	1.3095(15)	Fe(1)-C(19)-C(18)	58.45(9)
C(2)-C(3)	1.4437(18)	N(3)-C(18)-C(19)	115.41(15)
N(3)-C(18)	1.362(2)		

Consistent with the effective magnetic moment suggesting a high-spin iron(II) center, an Fe-N_{pyr} distance of 1.9446(14) Å and an Fe-N_{imine} distance of 2.1517(11) Å

are observed[27] (the Fe-N_{imine} bonds are equivalent by a symmetry plane in the molecule). Modest distortions to the bis(imino)pyridine chelate are observed compared to neutral ligand reference values, however the C_{imine}-N_{imine} and C_{ipso}-C_{imine} bond lengths are still consistent with a neutral chelate and an iron(II) center.

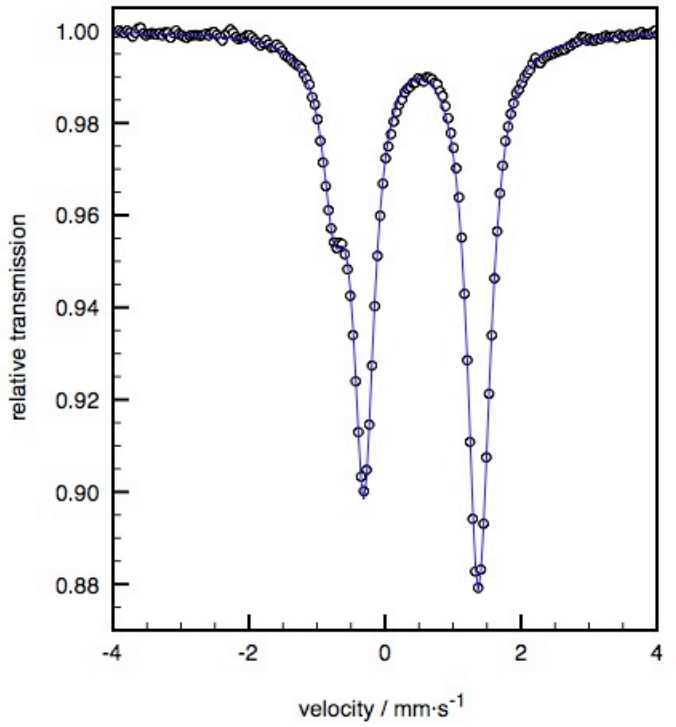

Figure 3.14 Zero-field Mössbauer spectrum of **1-N(**^{Me3}**Ph)CHC(SiMe$_3$)** at 80 K; δ = 0.52 mm·s^{-1}, ΔE_Q = 1.66 mm·s^{-1}.

Mössbauer spectroscopy was utilized to further elucidate the electronic structure of **1-N(**^{1}**Ad)CHC(SiMe$_3$)** and **1-N(**^{Me3}**Ph)CHC(SiMe$_3$)**, and also supports a high-spin iron(II) center. The zero-field Mössbauer spectrum of **1-N(**^{Me3}**Ph)CHC(SiMe$_3$)** exhibits a quadrupole doublet with an isomer shift of 0.52 mm·s^{-1} and a quadrupole splitting of 1.66 mm·s^{-1} (Figure 3.14). The observed isomer shift is consistent with a high-spin iron(II) center,[28] while the quadrupole splitting is similar to other five-coordinate bis(imino)pyridine iron(II) complexes such as

(^{iPr}PDI)$FeCl_2$ (ΔE_Q = 2.40 mm·s^{-1}).[29] A small impurity (12 %) was observed in the Mössbauer spectrum of **1-N(^Me3^Ph)CHC(SiMe3)** (δ = 0.63 mm·s^{-1}, ΔE_Q = 2.22 mm·s^{-1}), likely a result of decomposition during sample transfer.

Treatment of bis(imino)pyridine iron imides with additional alkynes did not lead to metallocycle formation. Addition of one equivalent of phenyl acetylene in benzene-d_6 at 23 °C led to polymerization of the alkyne and decomposition of the iron species. No reactivity was observed with one equivalent of internal alkynes such as diphenylacetylene, ditolylacetylene or 2-butyne in benzene-d_6 at 23 °C.

3.5 Conclusions

Bis(imino)pyridine iron imide compounds are shown to undergo both hydrogenation and silane addition to the iron-nitrogen bond. Exposure of (^{Ar}PDI)FeN(R) (^{Ar}PDI = ^{iPr}PDI, ^{iPr}*p*-^{t}BuPDI; R = 1-Ad, 2-Ad, ^{Cy}Octyl) to four atmospheres of dihydrogen at 23 °C furnished the corresponding bis(imino)pyridine iron amine complex (^{Ar}PDI)Fe(NH_2R) (^{Ar}PDI = ^{iPr}PDI, ^{iPr}*p*-^{t}BuPDI; R = 1-Ad, 2-Ad, ^{Cy}Octyl), with the exception of **1-N(^1^Ad)**. Full conversion to **1-NH$_2$^2^Ad** after 6 hours at 23 °C was observed for **1-N(^2^Ad)**, while the other alkyl iron imides reached full conversion after ~ 36 hours. Treatment of **1-N(^1^Ad)** and **1-N(^2^Ad)** with phenylsilane and diphenylsilane resulted in silane addition across the iron-nitrogen bond followed by an unusual example of reductive elimination to furnish the corresponding silylamines. In contrast, treatment of (^{iPr}PDI)FeN*Ar* (*Ar* = 2,6-^{i}Pr$_2$-C_6H_3, 2,4,6-Me_3-C_6H_2) with phenylsilane resulted in modification of the bis(imino)pyridine ligand with observed loss of dihydrogen. No further reductive elimination of the silylamine was observed, in contrast to **1-N(^1^Ad)** and **1-N(^2^Ad)**. The hydrosilylation products, (^{iPr}PDI)FeN*Ar*SiHPh (*Ar* = 2,6-^{i}Pr$_2$-C_6H_3, 2,4,6-Me_3-C_6H_2), were characterized by X-ray crystallography, magnetic susceptibility measurements and Mössbauer

spectroscopy, and are most consistent with a high-spin iron(II) metal center and an overall $S = 2$ molecule.

The hydrosilylation products, (^{iPr}PDI)FeN*Ar*SiHPh, are likely formed by 1,2-addition across the iron-nitrogen bond, followed by nucleophilic attack at silicon and β-hydrogen elimination with loss of dihydrogen. The divergent reaction pathways observed for silane addition to the N-alkyl-substituted and N-aryl-substituted bis(imino)pyridine iron imide complexes likely arise from a difference in both the rate of 1,2-addition and the steric bulk of the imide substituent. Both hydrogenation and silane addition to the N-aryl-substituted bis(imino)pyridine iron imide complexes is fast while the analogous reactions with N-alkyl-substituted bis(imino)pyridine iron imide complexes is slow. For **1-N(^{iPr2}Ph)SiHPh** and **1-N(^{Me3}Ph)SiHPh** the increased steric bulk may facilitate nucleophilic attack at silicon by requiring dissociation of a chelate arm prior to silane addition.

The [2 + 2] cycloaddition chemistry of bis(imino)pyridine iron imide complexes was also investigated. Treatment of **1-N(^{1}Ad)** and **1-N(^{Me3}Ph)** with trimethylsilylacetylene afforded the azametallacyclobutane products, **1-N(^{1}Ad)CHC(SiMe$_3$)** and **1-N(^{Me3}Ph)CHC(SiMe$_3$)**, respectively. Based on X-ray crystallography, Mössbauer spectroscopy and magnetic susceptibility measurements, the cycloaddition products, **1-N(^{1}Ad)CHC(SiMe$_3$)** and **1-N(^{Me3}Ph)CHC(SiMe$_3$)**, are best described as high-spin iron(II) with an unreduced bis(imino)pyridine chelate, to give an overall $S = 2$ molecule. No reactivity was observed with either alkenes or internal alkynes.

The comparative rates of hydrogenation and silane addition, and the competing reaction pathways highlight the intrinsic differences in reactivity between alkyl- and aryl-substituted bis(imino)pyridine iron imides, as is also observed with C-H activation chemistry.[7] Although the [2 + 2] cycloaddition chemistry of alkyl and aryl-

substituted bis(imino)pyridine iron imide complexes was identical, it illustrates the reactivity of the iron-nitrogen multiple bond and the scope of possible bond-forming reactions with bis(imino)pyridine iron imide complexes. Overall, bis(imino)pyridine iron imides exhibit a wide range of reactivity to afford new N-H, N-Si and N-C bonds.

3.6 Experimental Procedures

General Considerations. All air- and moisture-sensitive manipulations were carried out using standard vacuum line, Schlenk, and cannula techniques or in an MBraun inert atmosphere dry box containing an atmosphere of purified nitrogen. Solvents for air- and moisture-sensitive manipulations were initially dried and deoxygenated using literature procedures. Benzene-d_6 was purchased from Cambridge Isotope Laboratories and dried over 4 Å molecular sieves. 1-adamantyl amine and 1-adamantyl azide were purchased from Acros and dried on the vacuum line before use. Cyclooctyl amine was purchased from Acros and distilled from calcium hydride before use. Phenylsilane and diphenylsilane were purchased from Acros and dried over $LiAlH_4$ before use. Trimethylsilylacetylene was purchased from Acros and dried over 4 Å molecular sieves before use. 2-adamantyl azide,[30] 2-adamantyl amine[31] and cyclooctyl azide[32] were prepared according to the literature procedures. The complexes **1-$(N_2)_2$**,[22] **1-N(^{iPr2}Ph)**[2] and **1-N(^{Me3}Ph)**[2] were prepared according to literature procedures. The complexes **1-N(^{1}Ad)**, **1-N(^{2}Ad)**, **1-N(^{Cy}Oct)**, **^{tBu}1-N(^{1}Ad)** and **^{tBu}1-N(^{Cy}Oct)** were prepared according to procedures described in Chapter 2 of this work.

^{1}H NMR spectra were recorded on Varian Mercury 300, Inova 400, and 500 spectrometers operating at 299.76, 399.78, and 500.62 MHz, respectively. All ^{1}H chemical shifts are reported relative to $SiMe_4$ using the ^{1}H (residual) shift of the solvent as a secondary standard. Solution magnetic moments were determined by

Evans method[33] using a ferrocene standard and are the average value of at least two independent measurements. Gouy balance measurements were performed with a Johnson Matthey instrument that was calibrated with $HgCo(SCN)_4$. Peak width at half height is given for paramagnetically broadened resonances. Infrared spectra were collected on a Thermo Nicolet spectrometer. Elemental analyses were performed at Robertson Microlit Laboratories, Inc., in Madison, NJ.

Single crystals suitable for X-ray diffraction were coated with polyisobutylene oil in a drybox, transferred to a nylon loop and then quickly transferred to the goniometer head of a Bruker X8 APEX2 diffractometer equipped with a molybdenum X-ray tube (λ = 0.71073 Å). Preliminary data revealed the crystal system. A hemisphere routine was used for data collection and determination of lattice constants. The space group was identified and the data were processed using the Bruker SAINT+ program and corrected for absorption using SADABS. The structures were solved using direct methods (SHELXS) completed by subsequent Fourier synthesis and refined by full-matrix least-squares procedures.

^{57}Fe Mössbauer spectra were recorded on a SEE Co. Mössbauer spectrometer (MS4) at 80 K in constant acceleration mode. ^{57}Co/Rh was used as the radiation source. WMOSS software was used for the quantitative evaluation of the spectral parameters (leastsquares fitting to Lorentzian peaks). The minimum experimental line widths were 0.23 mm s^{-1}. The temperature of the samples was controlled by a Janis Research Co. CCS-850 He/N_2 cryostat within an accuracy of ±0.3 K. Isomer shifts were determined relative to α-iron at 298 K.

Representative Hydrogenation of an Iron Imide Complex. A thick-walled bomb was charged with a solution of 0.043 g (0.065 mmol) of **(^{iPr}PDI)FeN(^{Cy}Oct)** in approximately 20 mL of pentane. The bomb was degassed, and four atmospheres of

dihydrogen were added at -196 °C. The reaction mixture was warmed to ambient temperature and stirred for 36 hours, during which time there was a color change from bright purple to red. ^{1}H NMR spectroscopy confirmed conversion to a mixture of **(^{iPr}PDI)Fe($NH_2{}^{Cy}$Oct)** (91%) and **(^{iPr}PDEA)Fe($NH_2{}^{Cy}$Oct)** (9 %).

Preparation of (^{iPr}PDI)Fe($NH_2{}^1$Ad). A 20-mL scintillation vial was charged with 0.100 g (0.168 mmol) of **(^{iPr}PDI)Fe(N_2)$_2$** and approximately 10 mL of diethyl ether, resulting in a dark green solution. A solution of 0.025 g (0.168 mmol) 1-adamantyl amine in 5 mL diethyl ether was added to the vial, resulting in an immediate color change of the solution to red-brown. The solution was stirred for 15 minutes, followed by removal of the volatiles. The resulting brown solid was recrystallized from pentane at -35 °C to yield 0.079 g (68 %) of dark red-brown crystals identified as **(^{iPr}PDI)Fe($NH_2{}^1$Ad)**. ^{1}H NMR (benzene-d_6): δ = -6.96 (s, 6H, C(CH_3)), 0.27 (d, 6.7 Hz, 12H, CH(CH_3)$_2$), 0.67 (m, 6H, adamantyl CH_2), 1.19 (m, 3H, adamantyl CH_2), 1.21 (m, 3H, adamantyl CH_2), 1.25 (d, 6.7 Hz, 12H, CH(CH_3)$_2$), 1.57 (m, 3H, adamantyl C*H*), 2.69 (septet, 6.7 Hz, C*H*(CH$_3$)$_2$), 5.35 (s, 2H, NH_2), 7.31 (d, 7.6 Hz, 4H, *m-aryl*), 7.70 (t, 7.6 Hz, 2H, *p-aryl*), 8.87 (t, 7.2 Hz, 1H, *p-pyridine*), 12.84 (d, 7.2 Hz, 2H, *m-pyridine*). ^{13}C {^{1}H} NMR (benzene-d_6): δ = 23.27 (CH(*C*H$_3$)$_2$), 24.85 (CH(*C*H$_3$)$_2$), 28.42 (*C*H(CH$_3$)$_2$), 30.63 (adamantyl *C*H), 35.84 (adamantyl *C*H$_2$), 41.86 (C(*C*H$_3$)), 44.84 (adamantyl *C*H$_2$), 102.54 (*m-pyridine*), 124.78 (*m-aryl*), 125.58 (*p-aryl*), 136.35, 143.25 (*p-pyridine*), 165.55, 168.12, 193.79. IR (KBr): ν_{NH} = 3268, 3303 cm^{-1}.

Preparation of (^{iPr}*p*-^{t}BuPDI)Fe($NH_2{}^1$Ad) (^{tBu}1-$NH_2{}^1$Ad). This compound was prepared in a similar manner to **(^{iPr}PDI)Fe($NH_2{}^1$Ad)** with 0.055 g (0.085 mmol) of **(^{iPr}*p*-^{t}BuPDI)Fe(N_2)$_2$** and 0.013 g (0.086 mmol) 1-adamantyl amine. The resulting red

solid was recrystallized from pentane at -35 °C to yield 0.059 g (94 %) of a dark red powder identified as **(^{iPr}*p*-^{t}BuPDI)Fe($NH_2{}^{1}$Ad)**. ^{1}H NMR (benzene-d_6): δ = -7.60 (s, 6H, C(CH_3)), 0.27 (d, 6.5 Hz, 12H, CH(CH_3)$_2$), 0.62 (m, 6H, adamantyl CH_2), 1.17 (m, 3H, adamantyl CH_2), 1.20 (m, 3H, adamantyl CH_2), 1.26 (d, 6.5 Hz, 12H, CH(CH_3)$_2$), 1.46 (s, 9H, ^{t}Bu CH_3), 1.57 (m, 3H, adamantyl C*H*), 2.85 (septet, 6.5 Hz, C*H*(CH$_3$)$_2$), 5.00 (s, 2H, NH_2), 7.32 (d, 7.5 Hz, 4H, *m-aryl*), 7.72 (t, 7.5 Hz, 2H, *p-aryl*), 13.06 (s, 2H, *m-pyridine*). ^{13}C {^{1}H} NMR (benzene-d_6): δ = 23.18 (CH(*C*H$_3$)$_2$), 24.83 (CH(*C*H$_3$)$_2$), 28.23 (*C*H(CH$_3$)$_2$), 29.01 (^{t}Bu *C*H$_3$), 30.55 (adamantyl *C*H), 35.84 (adamantyl *C*H$_2$), 36.78 (C(*C*H$_3$)), 44.67 (adamantyl *C*H$_2$), 99.85 (*m-pyridine*), 124.68 (*m-aryl*), 125.44 (*p-aryl*), 135.74, 163.25, 165.91, 169.00, 195.47. IR (KBr): ν_{NH} = 3244, 3300 cm^{-1}; ν_{ND} = 2270, 2299 cm^{-1}.

Preparation of (^{iPr}PDI)Fe($NH_2{}^{Cy}$Octyl). This compound was prepared in a similar manner to **(^{iPr}PDI)Fe($NH_2{}^{1}$Ad)** with 0.047 g (0.079 mmol) of **(^{iPr}PDI)Fe(N_2)$_2$** and 11 μL (0.079 mmol) cyclooctyl amine. The resulting red solid was recrystallized from pentane at -35 °C to yield 0.042 g (80 %) of a dark red powder identified as **(^{iPr}PDI)Fe($NH_2{}^{Cy}$Octyl)**. Analysis for $C_{41}H_{60}N_4Fe$: Calc. C, 74.08; H, 9.10; N, 8.43. Found C, 74.26; H, 8.77; N, 8.52. ^{1}H NMR (benzene-d_6): δ = -6.21 (s, 6H, C(CH_3)), 0.04 (d, 6.8 Hz, 12H, CH(CH_3)$_2$), 0.04 (m, 2H, cyclooctyl CH_2), 0.76 (m, 2H, cyclooctyl CH_2), 0.89 (m, 2H, cyclooctyl CH_2), 1.10 (m, 2H, cyclooctyl CH_2), 1.19 (m, 6H, cyclooctyl CH_2), 1.25 (d, 6.8 Hz, 12H, CH(CH_3)$_2$), 2.17 (m, 1H, cyclooctyl C*H*), 2.71 (septet, 6.8 Hz, 4H, C*H*(CH$_3$)$_2$), 4.81 (s, 2H, NH_2), 7.28 (d, 7.2 Hz, 4H, *m-aryl*), 7.67 (t, 7.2 Hz, 2H, *p-aryl*), 8.78 (t, 7.6 Hz, 1H, *p-pyridine*), 12.27 (d, 7.6 Hz, 2H, *m-pyridine*). ^{13}C {^{1}H} NMR (benzene-d_6): δ = 23.07 (CH(*C*H$_3$)$_2$), 23.47 (cyclooctyl *C*H$_2$), 24.58 (CH(*C*H$_3$)$_2$), 25.08 (cyclooctyl *C*H$_2$), 28.04 (cyclooctyl *C*H$_2$), 28.47 (*C*H(CH$_3$)$_2$), 34.79 (cyclooctyl *C*H$_2$), 39.47 (C(*C*H$_3$)), 55.88 (cyclooctyl *C*H),

102.92 (*m-pyridine*), 124.47 (*m-aryl*), 125.30 (*p-aryl*), 136.51, 140.55 (*p-pyridine*), 164.20, 165.70, 190.34. IR (KBr): ν_{NH} = 3240, 3305 cm^{-1}; ν_{ND} = 2269, 2300 cm^{-1}.

Preparation of (^{iPr}*p*-^{t}BuPDI)Fe(NH_2^{Cy}Octyl) (^{tBu}1-NH_2^{Cy}Octyl). This compound was prepared in a similar manner to **(^{iPr}PDI)Fe(NH_2^{1}Ad)** with 0.115 g (0.177 mmol) of **(^{iPr}*p*-^{t}BuPDI)Fe(N_2)$_2$** and 25 μL (0.177 mmol) cyclooctyl amine. The resulting red solid was recrystallized from pentane at -35 °C to yield 0.104 g (82 %) of a dark red powder identified as **(^{iPr}*p*-^{t}BuPDI)Fe(NH_2^{Cy}Octyl)**. ^{1}H NMR (benzene-d_6): δ = -6.74 (s, 6H, C(C*H*$_3$)), 0.04 (d, 7.1 Hz, 12H, CH(C*H*$_3$)$_2$), 0.04 (m, 2H, cyclooctyl C*H*$_2$), 0.74 (m, 2H, cyclooctyl C*H*$_2$), 0.89 (m, 2H, cyclooctyl C*H*$_2$), 1.13 (m, 2H, cyclooctyl C*H*$_2$), 1.20 (m, 6H, cyclooctyl C*H*$_2$), 1.27 (d, 7.1 Hz, 12H, CH(C*H*$_3$)$_2$), 1.48 (s, 9H, ^{t}Bu C*H*$_3$), 2.12 (m, 1H, cyclooctyl C*H*), 2.81 (septet, 7.1 Hz, 4H, C*H*(CH$_3$)$_2$), 4.62 (s, 2H, N*H*$_2$), 7.29 (d, 7.4 Hz, 4H, *m-aryl*), 7.68 (t, 7.4 Hz, 2H, *p-aryl*), 12.47 (s, 2H, *m-pyridine*). ^{13}C {^{1}H} NMR (benzene-d_6): δ = 22.98 (CH(*C*H$_3$)$_2$), 23.45 (cyclooctyl *C*H$_2$), 24.56 (CH(*C*H$_3$)$_2$), 25.10 (cyclooctyl *C*H$_2$), 28.03 (cyclooctyl *C*H$_2$), 28.30 (*C*H(CH$_3$)$_2$), 29.36 (^{t}Bu *C*H$_3$), 34.67 (cyclooctyl *C*H$_2$), 40.76 (C(*C*H$_3$)), 55.31 (cyclooctyl *C*H), 100.26 (*m-pyridine*), 124.37 (*m-aryl*), 125.11 (*p-aryl*), 136.05, 162.27, 163.42, 166.48, 191.72. IR (KBr): ν_{NH} = 3232, 3299 cm^{-1}; ν_{ND} = 2260, 2302 cm^{-1}.

Preparation of (^{iPr}PDI)Fe(NH_2^{2}Ad). This compound was prepared in a similar manner to **(^{iPr}PDI)Fe(NH_2^{1}Ad)** with 0.065 g (0.110 mmol) of **(^{iPr}PDI)Fe(N_2)$_2$** and 0.017 g (0.110 mmol) 2-adamantyl amine. The resulting brown powder was recrystallized from pentane at -35 °C to yield 0.057 g (76 %) of a dark red-brown powder identified as **(^{iPr}PDI)Fe(NH_2^{2}Ad)**. ^{1}H NMR (benzene-d_6): δ = -6.21 (s, 6H, C(C*H*$_3$)), -0.08 (d, 6.8 Hz, 12H, CH(C*H*$_3$)$_2$), 0.57 (m, 2H, adamantyl C*H*$_2$), 1.18 (m,

2H, adamantyl CH_2), 1.23 (m, 2H, adamantyl CH_2), 1.23 (d, 6.8 Hz, 12H, CH(CH_3)$_2$), 1.39 (m, 2H, adamantyl CH_2), 1.46 (m, 2H, adamantyl CH_2), 1.51 (m, 2H, adamantyl CH_2), 1.53 (m, 1H, adamantyl C*H*), 1.61 (m, 1H, adamantyl C*H*), 2.14 (m, 1H, adamantyl C*H*), 2.80 (septet, 6.8 Hz, 4H, C*H*(CH$_3$)$_2$), 5.21 (s, 2H, NH_2), 7.25 (d, 7.8 Hz, 4H, *m-aryl*), 7.65 (t, 7.8 Hz, 2H, *p-aryl*), 8.77 (t, 7.5 Hz, 1H, *p-pyridine*), 12.22 (d, 7.5 Hz, 2H, *m-pyridine*). ^{13}C {^{1}H} NMR (benzene-d_6): δ = 22.99 (CH(*C*H$_3$)$_2$), 24.30 (CH(*C*H$_3$)$_2$), 27.47 (adamantyl *C*H), 27.83 (adamantyl *C*H), 28.63 (*C*H(CH$_3$)$_2$), 31.11 (adamantyl *C*H$_2$), 33.95 (adamantyl *C*H), 37.79 (adamantyl *C*H$_2$), 37.91 (adamantyl *C*H$_2$), 40.72 (C(*C*H$_3$)), 56.02 (adamantyl *C*H), 103.03 (*m-pyridine*), 124.54 (*m-aryl*), 136.52, 140.24 (*p-pyridine*), 163.68, 165.69, 189.94. IR (KBr): ν_{NH} = 3278, 3311 cm^{-1}; ν_{ND} = 2293, 2304 cm^{-1}.

Addition of PhSiH$_3$ to (iPrPDI)FeN(1Ad). A 20 mL scintillation vial was charged with 0.051 g (0.074 mmol) of **(iPrPDI)FeN(1Ad)** and 10 mL of pentane. PhSiH$_3$ (9.2 μL, 0.074 mmol) was added to the vial by microsyringe. The reaction mixture was stirred for 24 hours, over which time a gradual color change to green was observed. ^{1}H NMR spectroscopy established complete conversion to **(iPrPDI)Fe(N$_2$)$_2$** and PhH$_2$Si-NH(^{1}Ad). The reaction mixture was quenched with basic water, extracted into methylene chloride and filtered through a glass frit to yield iPrPDI ligand and 1-adamantyl amine.

Characterization of PhH$_2$Si-NH(1Ad). ^{1}H NMR (benzene-d_6): δ = 0.97 (d, 1H, N*H*), 1.45 (m, 6H, adamantyl CH_2), 1.63 (m, 6H, adamantyl CH_2), 1.86 (m, 3H, adamantyl C*H*), 5.19 (d, 4.0 Hz, 2H, SiH_2), 7.21 (d, 8.0 Hz, 4H, *o- or m-aryl*), 7.68 (t, 8.0 Hz, 2H, *p-aryl*), 7.72 (d, 8.0 Hz, 4H, *o- or m-aryl*). ^{13}C {^{1}H} NMR (benzene-d_6): δ = 24.87 (*adamantyl*), 30.64 (*adamantyl*), 36.81 (*adamantyl*), 47.00 (*adamantyl*), 125.81 (*aryl*),

127.12 (*aryl*), 130.39 (*aryl*), 135.31 (*aryl*). IR (KBr): ν_{NH} = 3378 cm^{-1}, ν_{SiH} = 2035 cm^{-1}. GC-MS (EI) *m/z* 151, 124, 108 (consistent with hydrolysis of Si-N bond).

Addition of Ph_2SiH_2 to (^{iPr}PDI)FeN(^{1}Ad). A 20 mL scintillation vial was charged with 0.059 g (0.086 mmol) of **(^{iPr}PDI)FeN(^{1}Ad)** in benzene-d_6. Ph_2SiH_2 (2.4 μL, 0.086 mmol) was added to the vial by microsyringe. The reaction mixture was stirred for 48 hours, over which time a gradual color change to green was observed. ^{1}H NMR spectroscopy established complete conversion to a mixture of **(^{iPr}PDI)Fe(N_2)$_2$** and **(^{iPr}PDI)Fe(Aryl)**, and Ph_2HSi-NH(^{1}Ad). The reaction mixture was quenched with basic water, extracted into methylene chloride and filtered through a glass frit to yield ^{iPr}PDI ligand and 1-adamantyl amine.

Characterization of Ph_2HSi-NH(^{1}Ad): ^{1}H NMR (benzene-d_6): δ = 0.97 (s, 1H, N*H*), 1.45 (m, 6H, adamantyl CH_2), 1.69 (m, 6H, adamantyl CH_2), 1.86 (m, 3H, adamantyl C*H*), 5.83 (s, 1H, Si*H*), 7.22 (d, 8.0 Hz, 4H, *o- or m-aryl*), 7.74 (t, 8.0 Hz, 2H, *p-aryl*), 7.75 (d, 8.0 Hz, 4H, *o- or m-aryl*). ^{13}C {^{1}H} NMR (benzene-d_6): δ = 25.43 (*adamantyl*), 30.42 (*adamantyl*), 34.99 (*adamantyl*), 48.63 (*adamantyl*), 129.33 (*aryl*), 127.84 (*aryl*), 131.72 (*aryl*), 134.26 (*aryl*). IR (KBr): ν_{NH} = 3383 cm^{-1}, ν_{SiH} = 2037 cm^{-1}. GC-MS (EI) *m/z* 200, 183, 151, 106 (consistent with hydrolysis of Si-N bond).

Addition of $PhSiH_3$ to (^{iPr}PDI)FeN(^{2}Ad). A 100 mL round bottom flask fitted with a needle valve was charged with 0.080 g (0.116 mmol) of **(^{iPr}PDI)FeN(^{2}Ad)** and 50 mL of pentane. $PhSiH_3$ (0.116 mmol) was added by gas bulb on the vacuum line at -78 °C. The reaction mixture was gradually warmed to ambient temperature, during which time a color change to green was observed. ^{1}H NMR spectroscopy established complete conversion to **(^{iPr}PDI)Fe(Aryl)** and PhH_2Si-NH(^{2}Ad). The reaction mixture

was quenched with basic water, extracted into methylene chloride and filtered through a glass frit to yield ^{iPr}PDI ligand and 2-adamantyl amine.

Characterization of PhH_2Si-NH(^{2}Ad). ^{1}H NMR (benzene-d_6): δ = 1.07 (s, 1H, N*H*), 1.18-1.44 (m, 12H, adamantyl CH_2), 2.01 (m, 2H, adamantyl CH_2), 4.14 (br s, 1H, adamantyl C*H*), 5.24 (s, 2H, Si*H*), 7.36 (d, 7.9 Hz, 2H, *o- or m-aryl*), 7.81 (t, 7.9 Hz, 1H, *p-aryl*), 7.84 (d, 7.9 Hz, 2H, *o- or m-aryl*). IR (KBr): ν_{NH} = 3386 cm^{-1}, ν_{SiH} = 2037 cm^{-1}.

Addition of Ph_2SiH_2 to (^{iPr}PDI)FeN(^{2}Ad). A J. Young tube was charged with 0.010 g (0.015 mmol) of **(^{iPr}PDI)FeN(^{1}Ad)** in benzene-d_6. Ph_2SiH_2 (2.8 μL, 0.015 mmol) was added to the vial by microsyringe. The reaction mixture was stirred for 24 hours, over which time a gradual color change to green was observed. ^{1}H NMR spectroscopy established complete conversion to **(^{iPr}PDI)Fe$(N_2)_2$** and Ph_2HSi-NH(^{2}Ad). The reaction mixture was quenched with basic water, extracted into methylene chloride and filtered through a glass frit to yield ^{iPr}PDI ligand and 2-adamantyl amine.

Characterization of Ph_2HSi-NH(^{2}Ad). ^{1}H NMR (benzene-d_6): δ = 1.10 (s, 1H, N*H*), 1.22-1.45 (m, 12H, adamantyl CH_2), 2.04 (m, 2H, adamantyl CH_2), 4.12 (br s, 1H, adamantyl C*H*), 5.91 (s, 2H, Si*H*), 7.38 (d, 7.8 Hz, 4H, *o- or m-aryl*), 7.80 (t, 7.8 Hz, 2H, *p-aryl*), 7.84 (d, 7.8 Hz, 4H, *o- or m-aryl*). IR (KBr): ν_{NH} = 3384 cm^{-1}, ν_{SiH} = 2038 cm^{-1}.

Preparation of (^{iPr}PDI)FeN(^{iPr2}Ph)SiHPh. A 100 mL round bottom flask fitted with a needle valve was charged with 0.049 g (0.069 mmol) **(^{iPr}PDI)FeN(2,6-^{i}Pr$_2$-C_6H_3)** and 50 mL of pentane. The flask was degassed on the vacuum line, and $PhSiH_3$ (0.069 mmol) was added by gas bulb at -78 °C. There was a color change from indigo to bright green concomitant with bubbling of the solution. After stirring thirty minutes,

the volatiles were removed to give a green powder. The powder was recrystallized from pentane at -35 °C to afford 0.035 g (63 %) of bright green needles identified as **(^{iPr}PDI)FeN(^{iPr2}Ph)SiHPh**. Analysis for $C_{51}H_{66}N_4SiFe$: Calc. C, 74.79; H, 8.12; N, 6.84. Found C, 74.49; H, 8.06; N, 6.48. Magnetic susceptibility (benzene-d_6, 293 K): μ_{eff} = 5.2(2) μ_B. ^{1}H NMR (benzene-d_6): δ = -80.76 (24.8, 1H), -63.56 (609.6, 3H), -39.17 (266.1, 1H), -35.17 (66.37, 1H), -29.21 (390.2, 3H), -20.40 (339.5, 1H), -19.92 (383.8, 3H), -14.56 (310.5, 3H), -12.27 (100.9, 3H), -11.80 (381.4, 1H), -11.12 (36.4, 1H), -9.06 (30.3, 1H), -8.51 (72.8, 1H), -7.90 (29.9, 3H), -4.96 (61.4, 1H), -2.46 (231.4, 1H), -2.27 (255.1, 3H), -1.85 (38.7, 1H), 2.65 (24.6, 2H), 3.19 (12.3, 1H), 4.30 (40.2, 1H), 10.52 (150.7, 3H), 12.63 (138.4, 2H), 12.82 (137.7, 3H), 13.55 (107.7, 3H), 28.73 (122.9, 3H), 42.38 (119.6, 1H), 56.01 (64.9, 3H), 59.47 (200.6, 3H), 76.90 (121.0, 1H), 90.24 (177.2, 1H), 114.80 (341.3, 1H), 196.97 (113.4, 3H), 216.40 (65.2, 3H). IR (KBr): ν_{SiH} = 2168 cm^{-1}.

Preparation of (^{iPr}PDI)FeN(^{Me3}Ph)SiHPh. This compound was prepared in a similar manner to **(^{iPr}PDI)FeN(^{iPr2}Ph)SiHPh** with 0.049 g (0.065 mmol) of **(^{iPr}PDI)FeN(2,4,6-Me$_3$-C$_6$H$_3$)** and 8.1 μL (0.065 mmol) of $PhSiH_3$. The resulting bright green solid was recrystallized from pentane at -35 °C to yield 0.030 g (60 %) of bright green needles identified as **(^{iPr}PDI)FeN(^{Me3}Ph)SiHPh**. Analysis for $C_{48}H_{60}N_4SiFe$: Calc. C, 74.20; H, 7.78; N, 7.21. Found C, 73.99; H, 7.47; N, 6.88. Magnetic susceptibility (benzene-d_6, 293 K): μ_{eff} = 4.9(1) μ_B. ^{1}H NMR (benzene-d_6): δ = -22.02 (27.3 Hz, 2H), -21.61 (47.7 Hz, 2H), -19.58 (25.2 Hz, 2H), -11.09 (88.1 Hz, 6H), -10.57 (95.2 Hz, 6H), -9.86 (27.1 Hz, 6H), -8.88 (32.0 Hz, 6H), -5.00 (23.4 Hz, 1H), -4.68 (13.3 Hz, 1H), -4.11 (88.8 Hz, 6H), -2.25 (33.1 Hz, 3H), 0.60 (35.8 Hz, 3H), 3.05 (14.6 Hz, 1H), 3.48 (25.7 Hz, 2H), 5.38 (25.7 Hz, 2H), 7.89 (19.1 Hz, 1H),

10.45 (16.2 Hz, 1H), 11.41 (16.0 Hz, 1H), 11.67 (18.5 Hz, 1H), 26.4 (48.6 Hz, 2H), 30.8 (53.3 Hz, 2H), 63.0 (40.6 Hz, 3H). IR (KBr): ν_{SiH} = 2107 cm^{-1}.

Toepler Pump Experiment for Addition of $PhSiH_3$ to (^{iPr}PDI)FeN(2,6-$^{i}Pr_2$-C_6H_3). A small glass ampoule was charged with 7.9 μL (0.063 mmol) $PhSiH_3$ and 0.5 mL diethyl ether, and flame-sealed under vacuum at -78 °C. A thick-walled bomb was charged with 0.045 g (0.063 mmol) **(^{iPr}PDI)FeN(2,6-$^{i}Pr_2$-C_6H_3)**, the glass ampoule and a stir bar. Approximately 15 mL of diethyl ether was vacuum transferred into the vessel at -78 °C. The reaction mixture was let warm to room temperature and the glass ampoule inside the vessel was broken with stirring. A rapid color change to bright green was observed, concomitant with liberation of dihydrogen. The gas mixture was collected with a Toepler pump into a volume of 43.7 mL. After 30 minutes, 23 Torr (88 %) of gas was collected. The gas mixture was cycled through a burn tube over 0.5 h; 23 Torr (88 %) of dihydrogen was burned. The ^{1}H NMR spectrum of the bright green solid remaining in the vessel confirmed formation of **(^{iPr}PDI)FeN(2,6-$^{i}Pr_2$-C_6H_3)**.

Preparation of (^{iPr}PDI)FeN(^{1}Ad)CHC($SiMe_3$). This compound was prepared in a similar manner to **(^{iPr}PDI)FeN(^{Me3}Ph)CHC($SiMe_3$)** with 0.049 g (0.071 mmol) of **(^{iPr}PDI)FeN(^{1}Ad)** and 10.2 μL (0.071 mmol) of trimethylsilylacetylene, yielding 0.039 g (70 %) of black crystals identified as **(^{iPr}PDI)FeN(^{1}Ad)CHC($SiMe_3$)**. Analysis for $C_{48}H_{68}N_4SiFe$: Calc. C, 73.44; H, 8.73; N, 7.14. Found C, 72.98; H, 8.94; N, 6.91. Magnetic susceptibility (benzene-d_6, 297 K): μ_{eff} = 4.9(1) μ_B. ^{1}H NMR (benzene-d_6): δ = -69.26 (232.5 Hz, 6H, C(CH_3)), -18.37 (72.8 Hz, 2H), -17.83 (551.9 Hz, 6H), -2.25 (287.5 Hz, 6H), -0.50 (36.7 Hz, 3H, adamantyl CH_2), 0.10 (Hz, 6H), 2.54 (82.2 Hz, 2H), 3.19 (125.4 Hz, 6H), 4.29 (305.8 Hz, 6H), 5.43 (82.2 Hz, 6H),

9.12 (285.9 Hz, 9H, Si*Me*$_3$), 12.51 (73.8 Hz, 2H), 16.47 (60.0 Hz, 2H), 49.07 (88.6 Hz, 2H), 86.48 (173.8 Hz, 2H), 191.38 (282.5 Hz, 1H, *p-pyridine*), one resonance not located.

Preparation of (^{iPr}PDI)FeN(^{Me3}Ph)CHC(SiMe$_3$). A 20 mL scintillation vial was charged with 0.028 g (0.037 mmol) of **(^{iPr}PDI)FeN(2,4,6-Me$_3$-C$_6$H$_2$)** and 5 mL of pentane. Trimethylsilylacetylene (5.9 μL, 0.037 mmol) was added to the vial by microsyringe, and there was a rapid color change of the solution to black. After stirring for 30 minutes, the solution was concentrated and cooled to -35 °C to yield 0.024 g (74 %) of black crystals of **(^{iPr}PDI)FeN(^{Me3}Ph)CHC(SiMe$_3$)**. Analysis for $C_{47}H_{64}N_4SiFe$: Calc. C, 73.41; H, 8.39; N, 7.29. Found C, 73.19; H, 8.66; N, 7.23. Magnetic susceptibility (benzene-*d*$_6$, 297 K): μ_{eff} = 4.9(2) μ_B. ^{1}H NMR (benzene-*d*$_6$): δ = -74.00 (399.2 Hz, 6H, C(C*H*$_3$)), -17.29 (82.4 Hz, 2H), -0.29 (501.4 Hz, 6H), 1.25 (48.4 Hz, 6H), 1.92 (15.4 Hz, 2H), 2.77 (297.8 Hz, 6H), 3.27 (313.2 Hz, 6H), 4.52 (124.7 Hz, 6H), 9.10 (432.1 Hz, 9H), 11.33 (123.9 Hz, 2H), 18.55 (104.6 Hz, 2H), 23.00 (31.9 Hz, 1H), 68.47 (169.4 Hz, 2H), 80.49 (969.2 Hz, 3H), 86.19 (290.5 Hz, 2H), 97.17 (157.3 Hz, 2H), 198.77 (373.6 Hz, 1H, *p-pyridine*).

REFERENCES

[1] (a) Mehn, M. P.; Peters, J. C. *J. Inorg. Biochem.* **2006**, *100*, 634-643. (b) Cowley, R. E.; Bill, E.; Neese, F.; Brennessel, W. W.; Holland, P. L. *Inorg. Chem.* **2009**, *48*, 4828-4836. (c) Cowley, R. E.; Eckert, N. A.; Elhaik, J.; Holland, P. L. *Chem. Commun.* **2009**, 1760-1762.

[2] Bart, S. C.; Lobkovsky, E.; Bill, E.; Chirik, P. J. *J. Am. Chem. Soc.* **2006**, *128*, 5302-5303.

[3] Brown, S. D.; Peters, J. C. *J. Am. Chem. Soc.* **2004**, *126*, 4538-4539.

[4] (a) Burckhardt, U.; Casty, G. L.; Tilley, T. D. *Organometallics* **2000**, *19*, 3830-3841. (b) Ignatov, S. K.; Rees, N. H.; Merkoulov, A. A.; Dubberley, S. R.; Razuvaev, A. G.; Mountford, P., Nikonov, G. I. *Chem. Eur. J.* **2008**, *14*, 296-310. (c) Fryzuk, M. D.; MacKay, B. A.; Patrick, B. O. *J. Am. Chem. Soc.* **2003**, *125*, 3234-3235.

[5] Duncan, A. P.; Bergman, R. G. *Chem. Rec.* **2002**, *2*, 431-445.

[6] Waterman, R.; Hillhouse, G. L. *J. Am. Chem. Soc.* **2003**, *125*, 13350-13351.

[7] See Chapter 2 of this work.

[8] Bart, S. C.; Lobkovsky, E.; Bill, E.; Wieghardt, K.; Chirik, P. J. *Inorg. Chem.* **2007**, *46*, 7055-7063.

[9] Bart, S. C.; Bowman, A. C.; Lobkovsky, E.; Chirik, P. J. *J. Am. Chem. Soc.* **2007**, *129*, 7212-7213.

[10] (a) Archer, A. M.; Bouwkamp, M. W.; Cortez, M.-P.; Lobkovsky, E.; Chirik, P. J. *Organometallics* **2006**, *25*, 4269-4278. (b) Trovitch, R. J.; Ph.D. Thesis, Cornell University, 2009.

[11] Structure of **1-N(^{iPr2}Ph)SiHPh** obtained by Dr. Suzanne Bart, 2006. CU X-Ray ID: scb48.

[12] Knijnenburg, Q.; Gambarotta, S.; Budzelaar, P. H. M. *Dalton Trans.* **2006**, 5442-5448.

[13] Andres, H.; Bominaar, E. L.; Smith, J. M.; Eckert, N. A.; Holland, P. L.; Münck, E. *J. Am. Chem. Soc.* **2002**, *124*, 3012-3025.

[14] Hillhouse, G. L.; Bercaw, J. E. *J. Am. Chem. Soc.* **1984**, *106*, 5472-5478.

[15] Park, S.; Roundhill, D. M.; Rheingold, A. L. *Inorg. Chem.* **1987**, *26*, 3972-3974.

[16] Kanzelberger, M.; Zhang, X.; Emge, T. J.; Goldman, A. S.; Zhao, J.; Incarvito, C.; Hartwig, J. F. *J. Am. Chem. Soc.* **2003**, *125*, 13644-13645.

[17] Glueck, D. S.; Winslow, L. J. N.; Bergman, R. G. *Organometallics* **1991**, *10*, 1462-1479.

[18] Chult, C.; Corriu, R. J. P.; Reye, C.; Young, J. C. *Chem. Rev.* **1993**, *93*, 1371-1448.

[19] Kost, D.; Kalikhman, I. *Acc. Chem. Res.* **2009**, *42*, 303-314.

[20] Boyer, J.; Brelière, C.; Carré, F.; Corriu, R. J. P.; Kpoton, A.; Poirier, M.; Royo, G.; Young, J. C. *J. Chem. Soc., Dalton Trans.* **1989**, 43-51.

[21] Brelière, C.; Carré, F.; Corriu, R. J. P.; Poirier, M.; Royo, G. *Organometallics* **1986**, *5*, 388-390.

[22] Bart, S. C.; Lobkovsky, E.; Chirik, P. J. *J. Am. Chem. Soc.* **2004**, *126*, 13794-13807.

[23] Matarasso-Tchiroukhine, E. *J. Chem. Soc., Chem. Commun.* **1990**, 681-682.

[24] Duncan, A. P.; Bergman, R. G. *Chem. Rec.* **2002**, *2*, 431-445.

[25] Fernandez, I.; Trovitch, R. J.; Lobkovsky, E.; Chirik, P. J. *Organometallics*, **2008**, *27*, 109-118.

[26] Bouwkamp. M. W.; Lobkovsky, E.; Chirik, P. J. *J. Am. Chem. Soc.* **2005**, *127*, 9660-9661.

[27] Trovitch, R. J.; Ph.D. Thesis, Cornell University, 2009.

[28] Long, G. J. Mössbauer spectroscopy as a structural probe. In *Mössbauer Spectroscopy*; Dickson, D. P. E., Berry, F. J., Eds.; Cambridge University Press: Cambridge, 1986; p 70.

[29] Bart, S. C.; Chlopek, K.; Bill, E.; Bouwkamp, M. W.; Lobkovsky, E.; Neese, F.; Wieghardt, K.; Chirik, P. J. *J. Am. Chem. Soc.* **2006**, *128*, 13901-13912.

[30] Prakash, G. K. S.; Stephenson, M. A.; Shih, J. G.; Olah, G. A. *J. Org. Chem.* **1986**, *51*, 3215-3217.

[31] Miriyala, B.; Bhattacharyya, S.; Williamson, J. S. *Tetrahedron* **2004**, *60*, 1463-1471.

[32] Alvarez, S. G.; Alvarez, M. T. *Synthesis* **1997**, 413-414.

[33] Sur, S. K. *J. Magn. Reson.* **1989**, *82*, 169-173.

CHAPTER 4

SYNTHESIS AND ELECTRONIC STRUCTURE ELUCIDATION OF BIS(IMINO)PYRIDINE IRON TETRAZOLE COMPLEXES

4.1 Abstract

A series of bis(imino)pyridine iron tetrazole complexes (^{iPr}PDI)Fe[(NR^1)NN(NR^2)] (^{iPr}PDI = 2,6-(*Ar*N=CMe)$_2$C$_5$H$_3$N; *Ar* = 2,6-^{i}Pr$_2$-C$_6$H$_3$) have been prepared either by treatment of the corresponding iron imide (^{iPr}PDI)FeN(R^1) with one equivalent of organic azide, R^{2}N$_3$, or by treatment of the bis(dinitrogen) compound (^{iPr}PDI)Fe(N$_2$)$_2$ with two equivalents of azide (where R^1 = R^2). The electronic structure of these compounds was explored using a combination of ^{1}H NMR and Mössbauer spectroscopies, X-ray crystallography and solution and solid state magnetic measurements. These investigations established that the *S* = 1 bis(imino)pyridine iron compounds with weaker-field tetrazole ligands are best described as intermediate-spin iron(II) with a dianionic tetrazole ligand and a neutral bis(imino)pyridine chelate. Compounds with stronger field tetrazole ligands are *S* = 0, arising from an intermediate-spin iron(II) center antiferromagnetically coupled to both a mono-reduced bis(imino)pyridine chelate and a mono-reduced tetrazole ligand. The field strength of the tetrazole ligand was correlated to the size of the 1,4-substituents. Where R^1 = R^2 = ^{2}Ad, CH$_2$Ph and ^{Cy}Octyl the tetrazole ligand was strong-field, and where R^1 = R^2 = ^{1}Ad, 3,5-Me$_2$-C$_6$H$_3$ and 4-Me-C$_6$H$_4$ the tetrazole ligand was weak field. Where R^1 = ^{1}Ad and R^2 = CH$_2$Ph the tetrazole ligand was also weak field.

4.2 Introduction

Interest in redox-active ligands is due to the ability to engender reactivity and mediate catalysis that would not otherwise be possible.[1,2,3] Tetrazole ligands

(NR)NN(NR), also commonly referred to in the literature as tetraazadienes or tetrazenes, have long been known but not widely studied, perhaps due to the inability to prepare the corresponding free ligand. Tetrazole ligands are likely to display non-innocent behavior because they are isoelectronic with α-diimines, which are well known to participate in redox chemistry.[4] Based on this analogy, it should be possible for the tetrazole ligand to exist as a neutral chelate, a radical anion or a dianion, as shown in Figure 4.1.

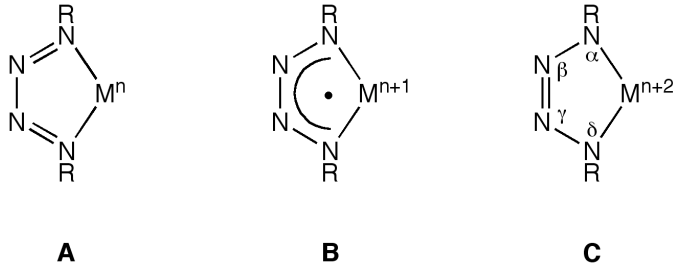

Figure 4.1 Electronic configurations of the redox-active tetrazole ligand.

The first example of a crystallographically characterized metal tetrazole complex, $(CO)_3Fe[(NMe)NN(NMe)]$, was synthesized in 1967 by Knox and Dekker.[5] The solid state structure of the compound was determined in 1968 by Doedens, supporting the previous assignment as the tricarbonyl iron tetrazole species.[6] Further investigation of the reactivity[7,8] and spectroscopic[9] properties of $(CO)_3Fe[(NMe)NN(NMe)]$ was conducted by Trogler and coworkers. Although the low resolution of the crystallographic data for $(CO)_3Fe[(NMe)NN(NMe)]$ precludes analysis of the tetrazole N-N bond lengths, examination of the metrical parameters of an isoelectronic compound, $(\eta_5\text{-}C_5H_5)Co[(NC_6F_5)NN(NC_6F_5)]$, establishes that the chelate coordinates to the metal center as a dianionic ligand C (Figure 4.1) and demonstrates the ability of the tetrazole ligand to accept two electrons.[10]

Although tetrazole complexes of other transition metals have been explored,[11] no other iron species were structurally characterized until Riordan and coworkers' recent synthesis of a tris(thioether) tetrazole complex, [PhTt^{tBu}]Fe[(NAd)NN(NAd)] (PhTt^{tBu} = phenyltris((*tert*-butylthio)-methyl)borate).[12] Holland and coworkers have also recently published a study on the characterization and electronic structure of a neutral iron β-diketiminate tetrazole complex, L^{Me}Fe[(NAd)NN(NAd)] (L^{Me} = HC[C(Me)N(2,6-^{i}Pr$_2$C$_6$H$_3$)]$_2$), and the corresponding cation.[13] Spectroscopic data indicates that the tetrazole ligands in the complexes synthesized by Holland and Riordan, (NAd)NN(NAd), are best described as radical anions. These compounds are some of the few examples, for tetrazole complexes of all metals, where the tetrazole ligand is more consistent with a radical anion than a dianion. The solid state structures of these compounds show delocalization among the bonds of the tetrazole ligand, consistent with description B (Figure 4.1).

The preparation of (CO)$_3$Fe[(NMe)NN(NMe)] suggested that (^{iPr}PDI)Fe[(NR)NN(NR)] compounds may be isolable due to the relationship between Fe(CO)$_3$ and (^{R}PDI)Fe. The possible interplay between the two redox-active chelates may give rise to iron complexes with unusual and varied electronic structures. While investigating the reactivity of iron imide compounds, it was observed that addition of one equivalent of azide to (^{iPr}PDI)FeNR, where R = alkyl, generated a new iron species subsequently identified as the tetrazole complex. Precedent for this chemistry was seen with Bergman and coworkers' studies of the cycloaddition of organic azides to zirconium imides.[14] In addition, Holland and coworkers observed that L^{Me}Fe[(NAd)NN(NAd)] can be synthesized either by addition of two equivalents of 1-adamantyl azide to [L^{Me}Fe]$_2$N$_2$ or by addition of one equivalent of 1-adamantyl azide to the iron imide complex, L^{Me}FeNAd.[13] The observation that a tetrazole complex can be generated through reaction of an iron imide with additional alkyl azide also

provides insight into the inability to synthesize iron imide complexes from azides containing small alkyl substituents. In these cases, the iron imide species initially generated appears to be more reactive towards the remaining alkyl azide than the starting material, (^{iPr}PDI)Fe(N_2)$_2$, and thus were not isolated.

4.3 Preparation of Iron Tetrazole Complexes

Addition of one equivalent of 1-adamantyl azide or benzyl azide to a stirring solution of (^{iPr}PDI)FeN(^{1}Ad) (**1-N(^{1}Ad)**) in pentane resulted in formation of a new paramagnetic compound identified as the corresponding iron tetrazole complex, (^{iPr}PDI)Fe[(N^{1}Ad)NN(NR)], where R = ^{1}Ad or CH_2Ph (Figure 4.2). A combination of solid state and solution magnetic data was used to determine the effective magnetic moment of each compound. The observed magnetic moment for (^{iPr}PDI)Fe[(N^{1}Ad)NN(N^{1}Ad)] (**1-[(N^{1}Ad)NN(N^{1}Ad)]**) at 20 °C both in solution and the solid state was 4.2(1) μ_B. For (^{iPr}PDI)Fe[(N^{1}Ad)NN(NBn)] (**1-[(N^{1}Ad)NN(NBn)]**), the observed magnetic moment at 20 °C in the solid state was 3.2(2) μ_B, consistent with two unpaired electrons.

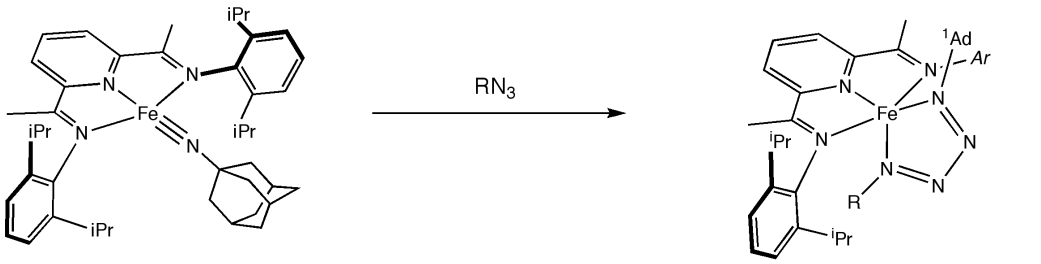

1-[(N^{1}Ad)NN(N^{1}Ad)] (R = ^{1}Ad)
1-[(N^{1}Ad)NN(NBn)] (R = CH_2Ph)

Figure 4.2 Cycloaddition of alkyl azides to (^{iPr}PDI)FeN(^{1}Ad) to generate bis(imino)pyridine iron tetrazole complexes.

The benzene-d_6 ^{1}H NMR spectra of **1-[(N^{1}Ad)NN(N^{1}Ad)]** and **1-[(N^{1}Ad)NN(NBn)]** at 20 °C establish C_s symmetric compounds in solution, consistent with square pyramidal geometry. The number of adamantyl resonances observed indicates that the apical and basal positions of the tetrazole ligand do not interconvert on the NMR timescale. Single crystal X-ray diffraction of **1-[(N^{1}Ad)NN(N^{1}Ad)]** (Figure 4.3) also establishes an essentially square pyramidal geometry, with the sum of the angles around Fe equal to 357.52(16)° and the angle between the pyridine nitrogen and the apical nitrogen of the tetrazole ligand equal to 106.00(8)°. The deviation of the sum of the angles around Fe from 360° is likely a result of the iron being lifted 0.6930(16) Å out of the idealized plane of the ligand, with the angle between the pyridine nitrogen and the basal nitrogen of the tetrazole ligand equal to 175.00(9)° (Table 4.1). In addition, the deviation of N_{pyr}-Fe-N_{apical} from 90° is due to the bite angle of the tetrazole ligand, 78.96(8)°.

The apical and basal nitrogens of the tetrazole are planar, with the sum of the angles about both nitrogens equal to 360.02(15)°. However, the Fe-N_{tet}-C angles, 138.2(2)° and 133.72(17)°, are significantly larger than the other angles about the nitrogen (Table 4.1). This is likely to place the adamantyl groups farther away from the bis(imino)pyridine chelate in order to minimize steric interactions. The apical adamantyl group on the tetrazole ligand was disordered by a 60° rotation about its three-fold axis (only one is pictured). The Fe-N_{tet} bond distances for the apical and basal positions of the tetrazole ligand are 1.981(2) Å and 1.939(2) Å respectively, consistent with Fe-N single bonds. Within the tetrazole ligand N_β-N_γ, 1.260(3) Å, is consistent with a double bond while N_α-N_β and N_γ-N_δ, 1.343(3) Å and 1.366(3) Å respectively, are between single and double bonds (Table 4.1). These N-N distances are most consistent with a tetrazole fragment in the dianionic form, C (Figure 4.1). Moreover, the bond distances for the tetrazole ligand in **1-[(N^{1}Ad)NN(N^{1}Ad)]** are

similar to the distances observed for Holland's tetrazole anion, [K(cryptand-222)][L^{Me}Fe[(NAd)NN(NAd)]], which is also described as having a dianionic tetrazole ligand.[13]

While reduction of the chelate is observed for many bis(imino)pyridine metal complexes, the solid state structure of **1-[(N^1Ad)NN(N^1Ad)]** does not show significant distortions to the ^{iPr}PDI chelate compared to neutral ligand reference values.[2] The C_{imine}-C_{ipso} bond lengths of 1.461(4) Å and 1.460(4) Å and the N_{imine}-C_{imine} bond lengths of 1.297(3) Å and 1.296(3) Å are most consistent with a neutral bis(imino)pyridine ligand. The Fe-N_{pyr} distance of 1.974(2) Å and the Fe-N_{imine} distances of 2.223(2) Å and 2.241(2) Å are notably long, generally indicating population of the d_{x2-y2} orbital. However, the iron is lifted significantly out of the ligand plane (0.6930(16) Å), which could also cause lengthening of the bonds between the iron and the bis(imino)pyridine chelate.

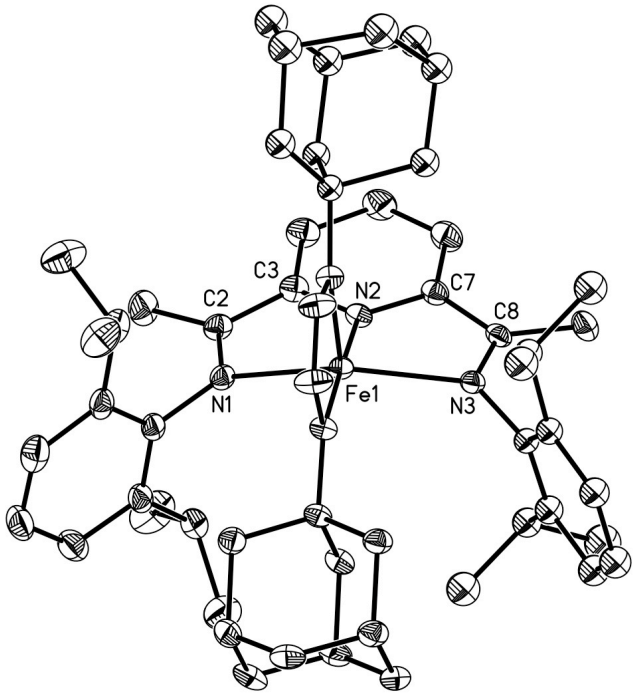

Figure 4.3 Molecular structure of **1-[(N^1Ad)NN(N^1Ad)]** at 30 % probability ellipsoids. Hydrogen atoms omitted for clarity.

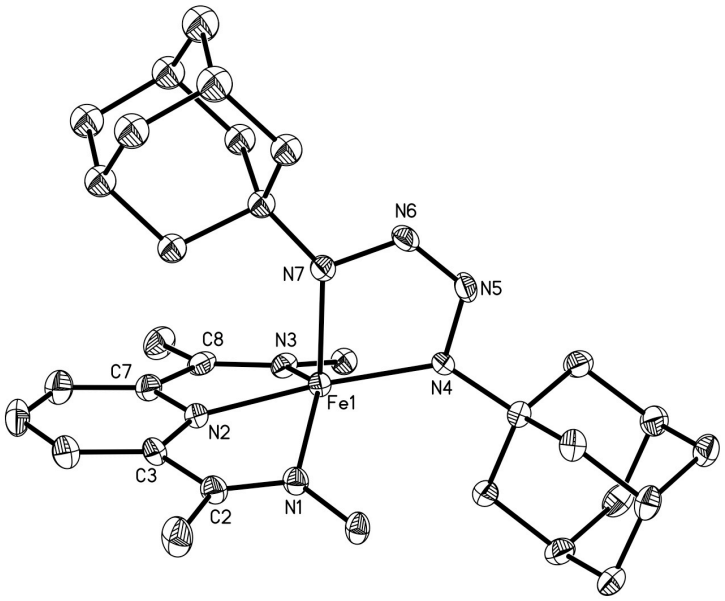

Figure 4.4 Molecular structure of **1-[(N^{1}Ad)NN(N^{1}Ad)** at 30 % probability ellipsoids. Hydrogen atoms and aryl groups omitted for clarity.

Table 4.1 Selected bond distances (Å) and angles (°) for **1-[(N^{1}Ad)NN(N^{1}Ad)]**.

Fe(1)-N(1)	2.241(2)	C(7)-C(8)	1.460(4)
Fe(1)-N(2)	1.974(2)	N(2)-Fe(1)-N(7)	106.00(8)
Fe(1)-N(3)	2.223(2)	N(4)-Fe(1)-N(2)	175.00(9)
Fe(1)-N(4)	1.939(2)	N(4)-Fe(1)-N(7)	78.96(8)
Fe(1)-N(7)	1.981(2)	Fe(1)-N(7)-C(32)	138.2(2)
N(4)-N(5)	1.343(3)	C(32)-N(7)-N(6)	109.6(3)
N(5)-N(6)	1.260(3)	Fe(1)-N(7)-N(6)	112.22(15)
N(6)-N(7)	1.366(3)	Fe(1)-N(4)-C(22)	133.72(17)
N(1)-C(2)	1.297(3)	C(22)-N(4)-N(5)	111.6(2)
N(3)-C(8)	1.296(3)	Fe(1)-N(4)-N(5)	114.68(16)
C(2)-C(3)	1.461(4)		

Inspired by the synthesis of tetrazole complexes by addition of organic azides to **1-N(¹Ad)**, (^{iPr}PDI)Fe[(N²Ad)NN(N²Ad)] (**1-[(N²Ad)NN(N²Ad)]**) and (^{iPr}PDI)Fe[(N^{Cy}Octyl)NN(N^{Cy}Octyl)] (**1-[(N^{Cy}Oct)NN(N^{Cy}Oct)]**) were prepared by addition of the appropriate alkyl azide to a pentane solution of the iron imide complex at 23 °C (Figure 4.6). As observed with **1-[(N¹Ad)NN(N¹Ad)]**, ^{1}H NMR spectroscopy establishes that **1-[(N²Ad)NN(N²Ad)]** and **1-[(N^{Cy}Oct)NN(N^{Cy}Oct)]** are C_s symmetric compounds in solution and that the apical and basal positions of the tetrazole do not interconvert on the NMR timescale.

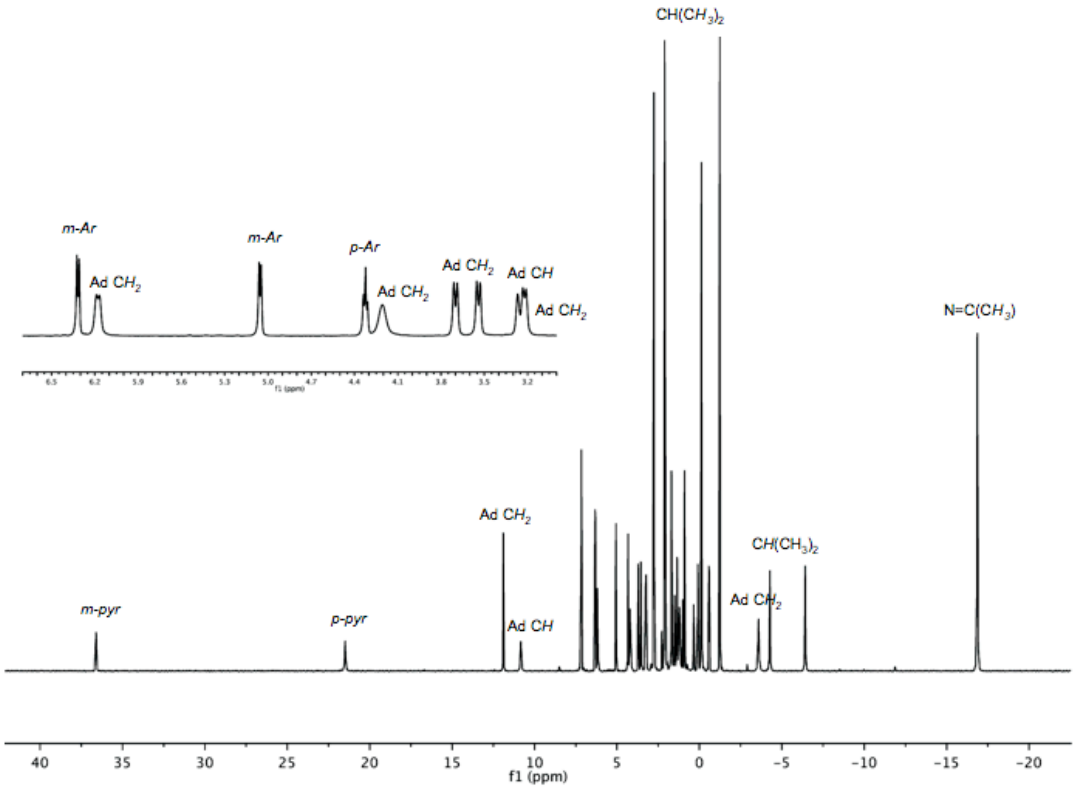

Figure 4.5 ^{1}H NMR spectrum of **1-[(N²Ad)NN(N²Ad)]** in benzene-d_6 at 20 °C.

Interestingly, while the ^{1}H NMR resonances of **1-[(N^{Cy}Oct)NN(N^{Cy}Oct)]** are well-resolved and appear within a narrow chemical shift range, **1-[(N²Ad)NN(N²Ad)]**

has resonances considerably outside the "normal" diamagnetic region. These resonances are significantly broadened and do not show the expected splitting, although other resonances in the spectrum are well resolved (Figure 4.5). However, solid state magnetic susceptibility measurements establish that **1-[(N^2Ad)NN(N^2Ad)]** and **1-[(N^{Cy}Oct)NN(N^{Cy}Oct)]** have effective magnetic moments of 0.3(1) μ_B and 0.1(1) μ_B, respectively, at 20 °C. Based on these observations, it is likely that the complexes have a singlet ground state with a small contribution from a triplet excited state, leading to temperature independent paramagnetism.[15]

While the aforementioned tetrazoles can be synthesized by addition of the appropriate azide to an iron imide, it is also possible to generate tetrazole compounds directly from the bis(dinitrogen) compound, (^{iPr}PDI)Fe(N_2)$_2$ (**1-(N_2)$_2$**) . Addition of two equivalents of RN_3 (where R = ^{1}Ad, ^{2}Ad or ^{Cy}Octyl) to **1-(N_2)$_2$** in a stirring solution of pentane resulted in rapid formation of the corresponding tetrazole complex. Upon addition of the alkyl azide an immediate color change was observed concomitant with bubbling of the solution, followed rapidly by a second color change. As expected, these observations are consistent with formation of the imide species, followed by rapid reaction of the iron imide with additional alkyl azide to generate the tetrazole product.

The observation that iron tetrazole compounds can be cleanly synthesized without direct isolation of the corresponding iron imide prompted investigation into the synthesis of tetrazole compounds where the iron imide complex has not been independently synthesized. Addition of two equivalents of benzyl azide, 3,5-dimethylphenyl azide or *p*-tolyl azide to a pentane solution of **1-(N_2)$_2$** at 23 °C resulted in rapid formation of the tetrazole compound (Figure 4.6). Notably, bis(imino)pyridine iron tetrazole compounds could not be synthesized using aryl azides with ortho-substituents. Addition of two equivalents of ortho-disubstituted aryl azides to **1-(N_2)$_2$**

resulted in formation of the iron imide species. Similarly, addition of any ortho-disubstituted aryl azide to another iron imide complex did not generate a new tetrazole product after allowing a benzene-d_6 solution of the reaction mixture to stand at 23 °C for 72 hours.

Prepared from iron imide complex:

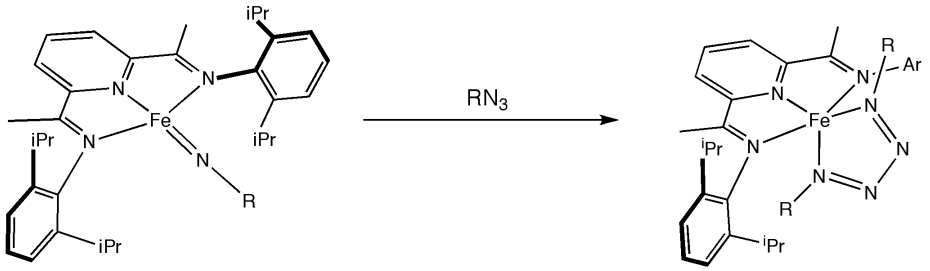

1-[(N^{2}Ad)NN(N^{2}Ad)] (R = ^{2}Ad)
1-[(N^{Cy}Oct)NN(N^{Cy}Oct)] (R = ^{Cy}Octyl)

Prepared from iron bis(dinitrogen) complex:

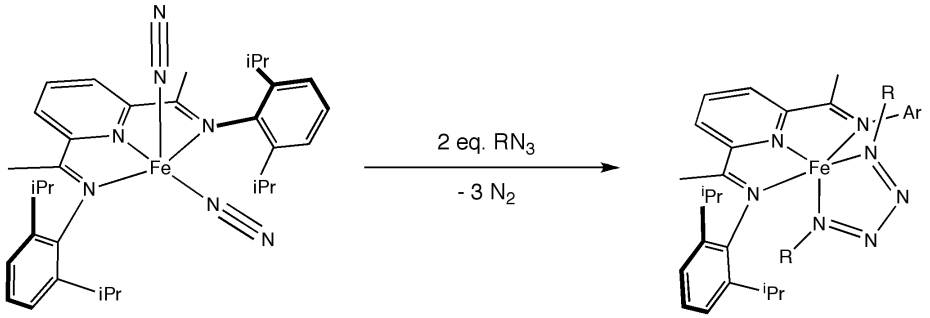

1-[(N^{2}Ad)NN(N^{2}Ad)] (R = ^{2}Ad)
1-[(N^{Cy}Oct)NN(N^{Cy}Oct)] (R = ^{Cy}Octyl)
1-[(NBn)NN(NBn)] (R = CH_2Ph)
1-[(N-3,5-Me$_2$-C$_6$H$_3$)N-N(N-3,5-Me$_2$-C$_6$H$_3$)] (R = 3,5-Me_2-C_6H_3)
1-[N-*p*Tolyl)NN(N-*p*Tolyl)] (R = 4-Me-C_6H_4)

Figure 4.6 Preparation of diamagnetic bis(imino)pyridine iron tetrazole complexes.

The benzene-d_6 ^{1}H NMR spectrum of (^{iPr}PDI)Fe[(NBn)NN(NBn)] (**1-[(NBn)NN(NBn)]**) at 20 °C exhibits the number of resonances expected for a C_s

symmetric complex, consistent with square pyramidal geometry. Like the other C_s symmetric tetrazoles, the number of tetrazole resonances indicates that the apical and basal positions do not interconvert on the NMR timescale. Although an unusually large chemical shift range is observed for **1-[(NBn)NN(NBn)]**, solid state magnetic susceptibility balance measurements establish that the compound is diamagnetic, with an effective magnetic moment of 0.3(1) μ_B at 20 °C. In contrast, (^{iPr}PDI)Fe[(N-3,5-Me_2-C_6H_3)NN(N-3,5-Me_2-C_6H_3)] (**1-[(N-3,5-Me_2-C_6H_3)NN(N-3,5-Me_2-C_6H_3)]**) and (^{iPr}PDI)Fe[(N-*p*Tolyl)NN(N-*p*Tolyl)] (**1-[(N-*p*Tolyl)NN(N-*p*Tolyl)]**) have C_{2v} symmetry by ^{1}H NMR spectroscopy, suggesting trigonal bipyramidal geometry in solution. Additionally, the benzene-d_6 ^{1}H NMR spectra for **1-[(N-3,5-Me_2-C_6H_3)NN(N-3,5-Me_2-C_6H_3)]** and **1-[(N-*p*Tolyl)NN(N-*p*Tolyl)]** at 20 °C have paramagnetically broadened resonances and chemical shift ranges greater than 250 ppm. Solid state magnetic susceptibility measurements at 20 °C establish effective magnetic moments of 3.1(2) μ_B and 3.3(2) μ_B, respectively, for (**1-[(N-3,5-Me_2-C_6H_3)NN(N-3,5-Me_2-C_6H_3)]**) and (**1-[(N-*p*Tolyl)NN(N-*p*Tolyl)]**), consistent with two unpaired electrons and an $S = 1$ ground state for both molecules.

The solid state structure of **1-[(NBn)NN(NBn)]** indicates an essentially square pyramidal geometry (Figure 4.7), with the sum of the angles around Fe equal to 360.01(15)°, and the iron lifted 0.6741(16) Å out of the idealized plane of the ligand. The angle between the pyridine nitrogen and the apical nitrogen of the tetrazole ligand is equal to 102.46(8)°, while the angle between the pyridine nitrogen and the basal nitrogen of the tetrazole ligand is equal to 176.75(8)°. The deviation of these angles from the idealized 90° and 180°, respectively, is likely due to the bite angle of the tetrazole, 77.83(8)°. The apical and basal nitrogens of the tetrazole ligand are planar, with the sum of the angles about the nitrogen equal to 358.93(27)° and 359.83(27)° respectively. As seen with **1-[(N^1Ad)NN(N^1Ad)]**, the Fe-N_{tet}-C angles are larger than

120°, at 127.46(16)° and 128.32(15)° respectively (Table 4.2). This is likely to avoid steric interaction between the benzyl groups and the bis(imino)pyridine chelate.

The distances between the metal center and the tetrazole ligand are notably shorter for **1-[(NBn)NN(NBn)]** than for **1-[(N^{1}Ad)NN(N^{1}Ad)]**, likely due to greater back-bonding from the metal center. The Fe-N_{apical} bond, 1.8241(17) Å, and the Fe-N_{basal} bond, 1.8553(19) Å, are consistent with very short Fe-N single bonds. Also in contrast to **1-[(N^{1}Ad)NN(N^{1}Ad)]**, the bonding within the tetrazole ligand for **1-[(NBn)NN(NBn)]** appears more delocalized. The N_β-N_γ distance of 1.324(2) Å is not significantly different from the N_α-N_β and N_γ-N_δ bond lengths of 1.313(2) Å and 1.343(3) Å, respectively (Table 4.2), indicating that the tetrazole ligand in **1-[(NBn)NN(NBn)]** is more consistent with the radical anion form of the tetrazole ligand, B (Figure 4.1). The ability of the bis(imino)pyridine chelate to accept electrons may allow the tetrazole to maintain an anionic configuration while preserving the iron(II) oxidation state.

Within the bis(imino)pyridine chelate of **1-[(NBn)NN(NBn)]**, distortions diagnostic of ligand reduction are observed. Elongation of the N_{imine}-C_{imine} bonds to 1.345(3) Å and 1.319(3) Å, and contraction of the C_{imine}-C_{ipso} bonds to 1.421(3) Å and 1.438(3) Å are both consistent with one-electron reduction of the chelate. Moreover, these distances indicate the ligand reduction in this compound differs significantly from **1-[(N^{1}Ad)NN(N^{1}Ad)]**. The bond from the iron center to the bis(imino)pyridine chelate also differ significantly from **1-[(N^{1}Ad)NN(N^{1}Ad)]**. The Fe-N_{pyr} distance, 1.8622(19) Å, and the Fe-N_{imine} distances, 1.9344(18) Å and 1.9981(16) Å, are shorter than would be expected with population of the d_{x2-y2} orbital, indicating a low-spin or intermediate-spin metal center for **1-[(NBn)NN(NBn)]**.[16]

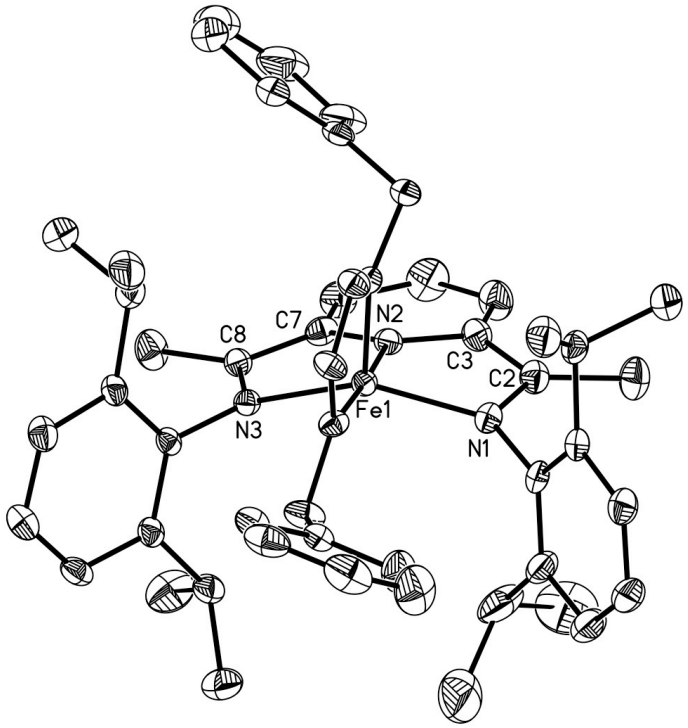

Figure 4.7 Molecular structure of **1-[(NBn)NN(NBn)]** at 30 % probability ellipsoids. Hydrogen atoms omitted for clarity.

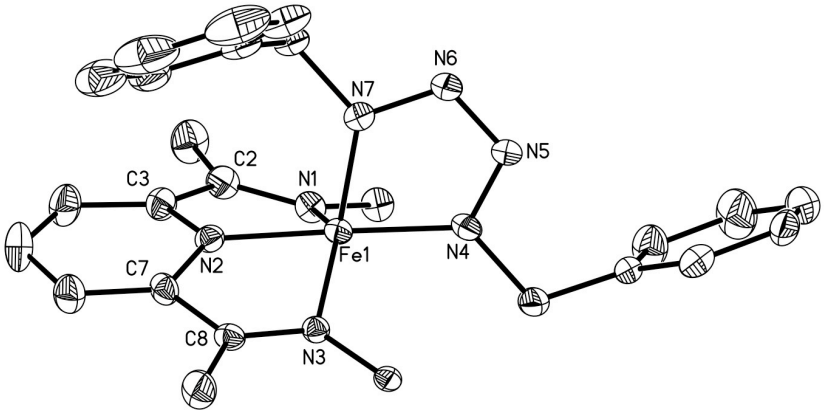

Figure 4.8 Molecular structure of **1-[(NBn)NN(NBn)** at 30 % probability ellipsoids. Hydrogen atoms and aryl groups omitted for clarity.

Table 4.2 Selected bond distances (Å) and angles (°) for **1-[(NBn)NN(NBn)]**.

Fe(1)-N(1)	1.9344(18)	C(7)-C(8)	1.438(3)
Fe(1)-N(2)	1.8622(19)	N(2)-Fe(1)-N(7)	102.46(8)
Fe(1)-N(3)	1.9981(16)	N(4)-Fe(1)-N(2)	176.75(8)
Fe(1)-N(4)	1.8553(19)	N(4)-Fe(1)-N(7)	77.83(8)
Fe(1)-N(7)	1.8241(17)	Fe(1)-N(7)-C(41)	127.46(16)
N(4)-N(5)	1.313(2)	C(41)-N(7)-N(6)	111.90(17)
N(5)-N(6)	1.324(2)	Fe(1)-N(7)-N(6)	119.57(13)
N(6)-N(7)	1.343(3)	Fe(1)-N(4)-C(34)	128.32(15)
N(1)-C(2)	1.345(3)	C(34)-N(4)-N(5)	112.67(18)
N(3)-C(8)	1.319(3)	Fe(1)-N(4)-N(5)	118.84(14)
C(2)-C(3)	1.421(3)		

Notably, a large variation is observed in the chemical shift range (in ppm) of the benzene-d_6 ^{1}H NMR spectra of the bis(imino)pyridine tetrazole compounds at 20 °C (Table 4.3), even within the series of diamagnetic tetrazole complexes. The chemical shift range is sensitive to the steric bulk of the substituents on the tetrazole ligand, which is illustrated by systematically varying the tetrazole substituents from R = ^{1}Ad to R = CH_2Ph (Figure 4.9). When a single 1-adamantyl group is replaced with a benzyl group, there is a subsequent decrease in chemical shift range in the ^{1}H NMR spectrum. When a second 1-adamantyl group is replaced, there is a further decrease in the spectral width. For all tetrazole complexes, the resonances of the in-plane chelate hydrogens move farther from the diamagnetic reference values as the steric bulk of the tetrazole substituents increases (Table 4.3).

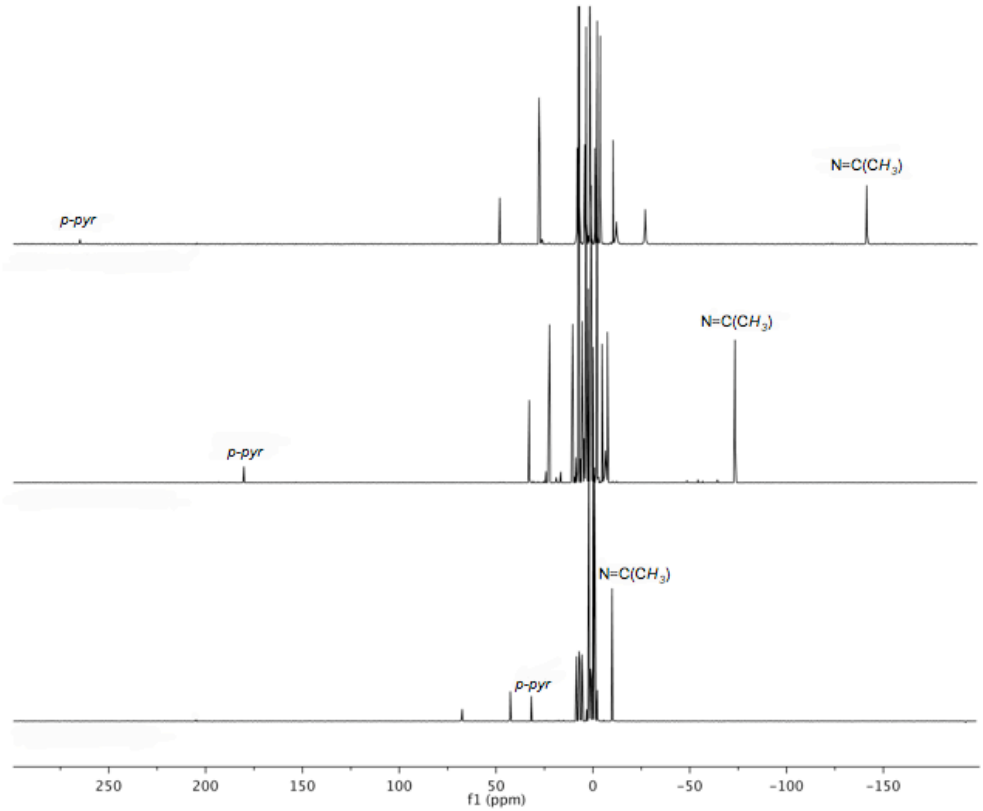

Figure 4.9 Change in ^{1}H NMR chemical shift of **1-[(NR^{1})NN(NR^{2})]** resonances as a function of tetrazole substituent, observed in benzene-d_6 at 20 °C.

Table 4.3 In-plane chelate hydrogen resonances of (^{iPr}PDI)Fe[(NR^{1})NN(NR^{2})] complexes observed by ^{1}H NMR spectroscopy in benzene-d_6 at 20 °C.

R^{1}	R^{2}	N=C(C*H*$_3$) (ppm)	*m-pyr* (ppm)	*p-pyr* (ppm)
^{1}Ad	^{1}Ad	-141.43	48.09	264.87
^{1}Ad	CH_2Ph	-72.72	32.57	178.81
3,5-Me_2-C_6H_3	3,5-Me_2-C_6H_3	-59.05	29.49	199.10
4-Me-C_6H_4	4-Me-C_6H_4	-48.88	22.84	191.31
^{2}Ad	^{2}Ad	-16.86	36.60	21.49
CH_2Ph	CH_2Ph	-9.73	8.48	31.55
^{Cy}Octyl	^{Cy}Octyl	-0.57	7.89	12.24

Overall, the bis(imino)pyridine tetrazole compounds prepared are inert and offer little reactivity. Heating the iron tetrazole compounds to 65 °C in a benzene-d_6 solution under vacuum for up to three days showed neither formation of a new compound or decomposition of the starting material. Similarly, exposure of benzene-d_6 solutions of the iron tetrazole compounds to one atmosphere of carbon monoxide produced no reaction after 48 hours at 23 °C. Although the tetrazole complexes are somewhat air-stable, addition of water results in disproportionation of the tetrazole ligand to one equivalent of azide and one equivalent of amine. When benzyl substituents were present on the tetrazole ligand, benzaldehyde was observed instead of benzyl amine.

4.4 Electronic Structure of Iron Tetrazole Complexes

From the series of bis(imino)pyridine iron tetrazole complexes prepared, representative examples were chosen for Mössbauer spectroscopy in order to further elucidate the electronic structure. The compounds **1-[(N^{1}Ad)NN(N^{1}Ad)]**, **1-[(N^{1}Ad)NN(NBn)]**, **1-[(NBn)NN(NBn)]**, **1-[(N^{Cy}Oct)NN(N^{Cy}Oct)]** and **1-[(N-3,5-Me$_2$-C$_6$H$_3$)NN(N-3,5-Me$_2$-C$_6$H$_3$)]** were selected to encompass a range of steric and magnetic properties. The Mössbauer parameters, δ and ΔE_Q, for all tetrazole complexes are summarized in Table 4.4. The iron tetrazole complexes prepared by Holland and coworkers are included for comparison. As the size of the tetrazole substituents decreases, a corresponding decrease is observed in the value of δ. The isomer shifts (δ) for the five-coordinate iron tetrazole complexes are generally larger than those observed for four-coordinate, intermediate-spin iron(II) bis(imino)pyridine complexes.[17] Increasing δ values are often correlated with increasing coordination number for iron compounds, especially between tetrahedral and octahedral

complexes.[18] The quadrupole splitting (ΔE_Q) also varies according to the geometry of the tetrazole complex.

Table 4.4 Mössbauer parameters ($mm \cdot s^{-1}$) for representative bis(imino)pyridine iron tetrazole complexes at 80 K.

Complex	δ	ΔE_Q	%
1-[(N^{1}Ad)NN(N^{1}Ad)]	0.57	3.10	96
1-[(N-3,5-Me$_2$-C$_6$H$_3$)N-N(N-3,5-Me$_2$-C$_6$H$_3$)]	0.43	1.37	100
1-[(N^{1}Ad)NN(NBn)]	0.43	1.14	74
	0.40	2.57	26
1-[(N^{Cy}Oct)NN(N^{Cy}Oct)]	0.28	2.98	100
1-[(NBn)NN(NBn)]	0.23	2.99	100
L^{Me}Fe[(NAd)NN(NAd)][13]	0.81	1.40	100
L^{Me}Fe[(NAd)NN(NAd)][13]	0.69	1.32	100

The zero-field Mössbauer spectrum of **1-[(N^{1}Ad)NN(N^{1}Ad)]** at 80 K exhibits a quadrupole doublet with an isomer shift of 0.57 $mm \cdot s^{-1}$ and a quadrupole splitting of 3.10 $mm \cdot s^{-1}$ (Table 4.4). A small amount (4 %) of impurity is present in the sample, likely a result of decomposition of the compound during sample preparation. The isomer shift of **1-[(N^{1}Ad)NN(N^{1}Ad)]** is consistent with an intermediate- or high-spin ferrous center coordinated to a moderately strong-field tetrazole ligand. By comparison, the high-spin iron(II) complex (^{iPr}PDI)$FeCl_2$ has an isomer shift of 0.89 $mm \cdot s^{-1}$ and a quadrupole splitting of 2.40 $mm \cdot s^{-1}$.[15] The similar value of ΔE_Q observed for **1-[(N^{1}Ad)NN(N^{1}Ad)]** reflects the square pyramidal geometry of the compound, and is consistent with a net electric field gradient along the z-axis.

The zero-field Mössbauer spectra of **1-[(NBn)NN(NBn)]** and **1-[(N^{Cy}Oct)NN(N^{Cy}Oct)]** at 80 K exhibit nearly identical parameters. For **1-**

[(NBn)NN(NBn)] an isomer shift of 0.23 mm·s^{-1} and a quadrupole splitting of 2.99 mm·s^{-1} are observed (Figure 4.10), while for **1-[(N^{Cy}Oct)NN(N^{Cy}Oct)]** an isomer shift of 0.28 mm·s^{-1} and a quadrupole splitting of 2.98 mm·s^{-1} are observed (Table 4.4). The isomer shifts indicate that the field strengths of the bis(benzyl) and bis(cyclooctyl)tetrazole ligands are greater than the bis(1-adamantyl)tetrazole ligand. However, the low-spin bis(imino)pyridine iron dicarbonyl complex, (^{iPr}PDI)Fe(CO)$_2$, has an isomer shift of 0.03 mm·s^{-1},[19] suggesting that **1-[(NBn)NN(NBn)]** and **1-[(N^{Cy}Oct)NN(N^{Cy}Oct)]** are still most consistent with intermediate-spin ferrous centers. The observed quadrupole splittings for **1-[(NBn)NN(NBn)]** and **1-[(N^{Cy}Oct)NN(N^{Cy}Oct)]** are similar to **1-[(N^{1}Ad)NN(N^{1}Ad)]**, consistent with square pyramidal geometry.

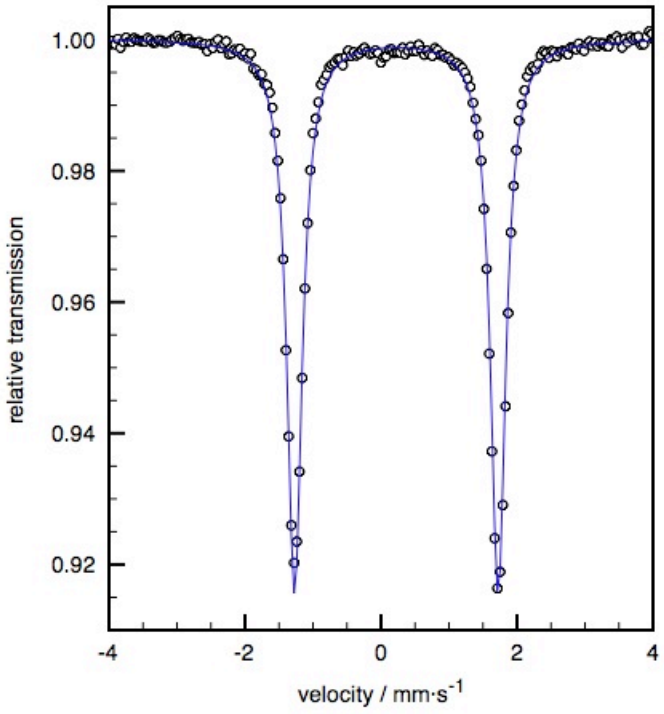

Figure 4.10 Zero-field Mössbauer spectrum of **1-[(NBn)NN(NBn)]** at 80 K; δ = 0.23 mm·s^{-1}, ΔE_Q = 2.99 mm·s^{-1}.

By comparison, the zero-field Mössbauer spectrum **1-[(N-3,5-Me$_2$-C$_6$H$_3$)NN(N-3,5-Me$_2$-C$_6$H$_3$)]** at 80 K, shown in Figure 4.11, exhibits an isomer shift of 0.43 mm·s^{-1} and a quadrupole splitting of 1.37 mm·s^{-1} (Table 4.4). The δ value is lower than the observed isomer shift for **1-[(N^{1}Ad)NN(N^{1}Ad)]**, and is consistent with intermediate-spin iron(II). The smaller ΔE_Q observed for **1-[(N-3,5-Me$_2$-C$_6$H$_3$)NN(N-3,5-Me$_2$-C$_6$H$_3$)]** is consistent with a decrease in the electric field gradient along the z-axis. This is likely caused by the change to trigonal bipyramidal geometry, as indicated by ^{1}H NMR spectroscopy.

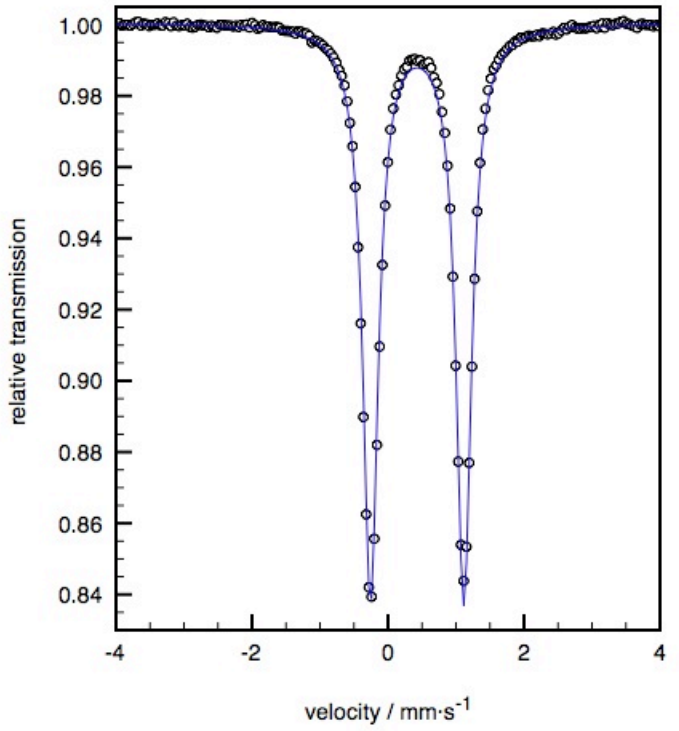

Figure 4.11 Zero-field Mössbauer spectrum of **1-[(N-3,5-Me$_2$-C$_6$H$_3$)NN(N-3,5-Me$_2$-C$_6$H$_3$)]** at 80 K; δ = 0.43 mm·s^{-1}, ΔE_Q = 1.37 mm·s^{-1}.

Similar Mössbauer parameters to **1-[(N-3,5-Me$_2$-C$_6$H$_3$)NN(N-3,5-Me$_2$-C$_6$H$_3$)]** are observed for **1-[(N^{1}Ad)NN(NBn)]** (Figure 4.12), although the presence of two iron species with virtually identical δ values, but different values of ΔE_Q, suggests the two

species are geometric isomers. This is supported by the fact that one value of ΔE_Q, 2.57 mm·s^{-1}, is similar to the square pyramidal tetrazole **1-[(N^{1}Ad)NN(N^{1}Ad)]** while the other value of ΔE_Q, 1.14 mm·s^{-1}, is similar to the trigonal bipyramidal tetrazole **1-[(N-3,5-Me$_2$-C$_6$H$_3$)NN(N-3,5-Me$_2$-C$_6$H$_3$)]**. The benzene-d_6 ^{1}H NMR spectrum of **1-[(N^{1}Ad)NN(NBn)]** at 20 °C establishes C_s symmetry in solution, but crystallization may induce some of the compound to adopt trigonal bipyramidal geometry in the solid state. The δ values, 0.40 mm·s^{-1} and 0.43 mm·s^{-1}, are similar to **1-[(N-3,5-Me$_2$-C$_6$H$_3$)NN(N-3,5-Me$_2$-C$_6$H$_3$)]**, and are both consistent with an intermediate-spin iron(II) center. Interestingly, the zero-field Mössbauer spectrum of the mixed tetrazole **1-[(N^{1}Ad)NN(NBn)]** at 80 K shows an isomer shift that is between the δ values observed for **1-[(N^{1}Ad)NN(N^{1}Ad)]** and **1-[(NBn)NN(NBn)]** (Table 4.4).

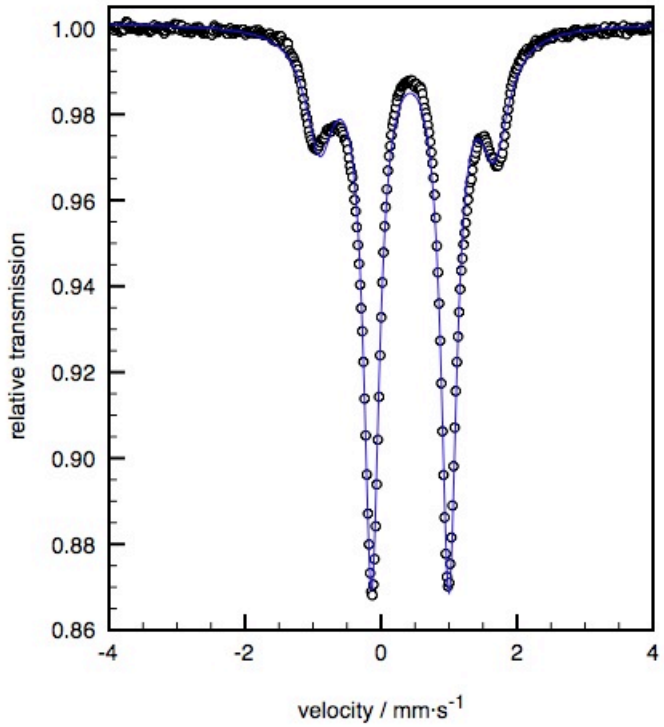

Figure 4.12 Zero-field Mössbauer spectrum of **1-[(N^{1}Ad)NN(NBn)]** at 80 K; δ = 0.43 mm·s^{-1}, ΔE_Q = 1.14 mm·s^{-1} (major isomer); δ = 0.40 mm·s^{-1}, ΔE_Q = 2.57 mm·s^{-1} (minor isomer).

With Mössbauer data in hand, a more detailed analysis of the electronic structure of the bis(imino)pyridine iron tetrazole compounds is possible. There are two distinct electronic configurations for tetrazole compounds. One comprises an intermediate-spin iron(II) center ($S_{Fe} = 1$) with a neutral bis(imino)pyridine chelate ($S_{PDI} = 0$) and a dianionic tetrazole ligand, giving an overall $S = 1$ molecule. The other is consistent with an intermediate-spin iron(II) center ($S_{Fe} = 1$) antiferromagnetically coupled to a singly reduced bis(imino)pyridine chelate ($S_{PDI} = 1/2$) and a radical anion tetrazole ligand ($S_{tet} = 1/2$), for an overall diamagnetic molecule. The spectroscopic and magnetic properties for the bis(imino)pyridine tetrazole complexes are summarized in Table 4.5.

Table 4.5 Summary of spectroscopic and magnetic properties for bis(imino)pyridine iron tetrazole complexes (^{iPr}PDI)Fe[(NR^1)NN(NR^2)].

R	^{iPr}PDI ox. state[a]	N_4R_2 ox. state[a]	Geometry	δ (mm·s^{-1})	ΔE_Q (mm·s^{-1})	μ_{eff} (μ_B)
^{1}Ad	0	- 2	sq. pyr.	0.57	3.10	4.2
^{1}Ad/CH_2Ph	0	- 2	sq. pyr.	0.40	2.57	3.2
			tbp	0.43	1.14	
3,5-Me_2-C_6H_3	0	- 2	tbp	0.43	1.37	3.1
4-Me-C_6H_4	0	- 2	tbp	-	-	3.3
^{2}Ad	- 2	0	sq. pyr.	-	-	0.3
CH_2Ph	- 2	0	sq. pyr.	0.23	2.99	0.3
^{Cy}Octyl	- 2	0	sq. pyr.	0.28	2.98	0.1

[a]Assigned based on X-ray data.

The ordering of the metal-based orbitals for the bis(imino)pyridine tetrazole complexes, presented in Figure 4.13, is based on the d-splitting diagram of (^{iPr}PDI)Fe(CO)$_2$ determined by DFT calculations.[15] For the complexes with a

dianionic tetrazole ligand, the $S = 1$ ground state arises from the two unpaired electrons on the intermediate-spin iron(II) center. This is consistent with the isomer shifts exhibited by the Mössbauer spectra, and also with the observation that the bis(imino)pyridine chelate is neutral. A net electric field gradient along the z-axis is expected for the $S = 1$ tetrazole complexes based on this molecular orbital diagram, which is supported by the relatively large magnitude of the quadrupole splittings observed for these compounds (Table 4.4). The anomalous magnetic moment observed for **1-[(N^{1}Ad)NN(N^{1}Ad)]**, 4.2(1) μ_B, can be explained by an admixture of high-spin and intermediate-spin iron centers. Because the isomer shift for **1-[(N^{1}Ad)NN(N^{1}Ad)]** is the highest observed for any tetrazole complex (Table 4.4), the bis(1-adamantyl) tetrazole ligand clearly has the weakest field strength. This reduction in field strength may lead to molecules of **1-[(N^{1}Ad)NN(N^{1}Ad)]** with both $S = 1$ and $S = 2$ ground states. This is supported by the observation of an Fe-N_{pyr} bond length, 1.974(2) Å, and Fe-N_{imine} bond lengths, 2.241(2) Å and 2.223(2) Å, that are consistent with population of the d_{x2-y2} orbital.[16]

Spectroscopic data also support an intermediate-spin iron(II) center for the $S = 0$ tetrazole complexes. The similarity in ΔE_Q values between the two classes of tetrazole complexes in particular suggests equivalent population of the metal d-orbitals (Table 4.4). However, the key difference between the $S = 1$ and the $S = 0$ tetrazole complexes is the relative reduction of the tetrazole ligand and the bis(imino)pyridine chelate. The molecular structure of **1-[(NBn)NN(NBn)]** establishes one-electron reduction of the bis(imino)pyridine chelate, as well as one-electron reduction of the tetrazole ligand. Antiferromagnetic coupling of the ligand radicals to the two unpaired electrons in the d_{xz} and d_{yz} metal-based orbitals gives rise to overall diamagnetism (Figure 4.12). However, as is often observed with antiferromagnetic coupling between ligands radicals and the metal center,[15,17] these complexes exhibit temperature

independent paramagnetism, as indicated by the large ^{1}H NMR chemical shift ranges at 20 °C.

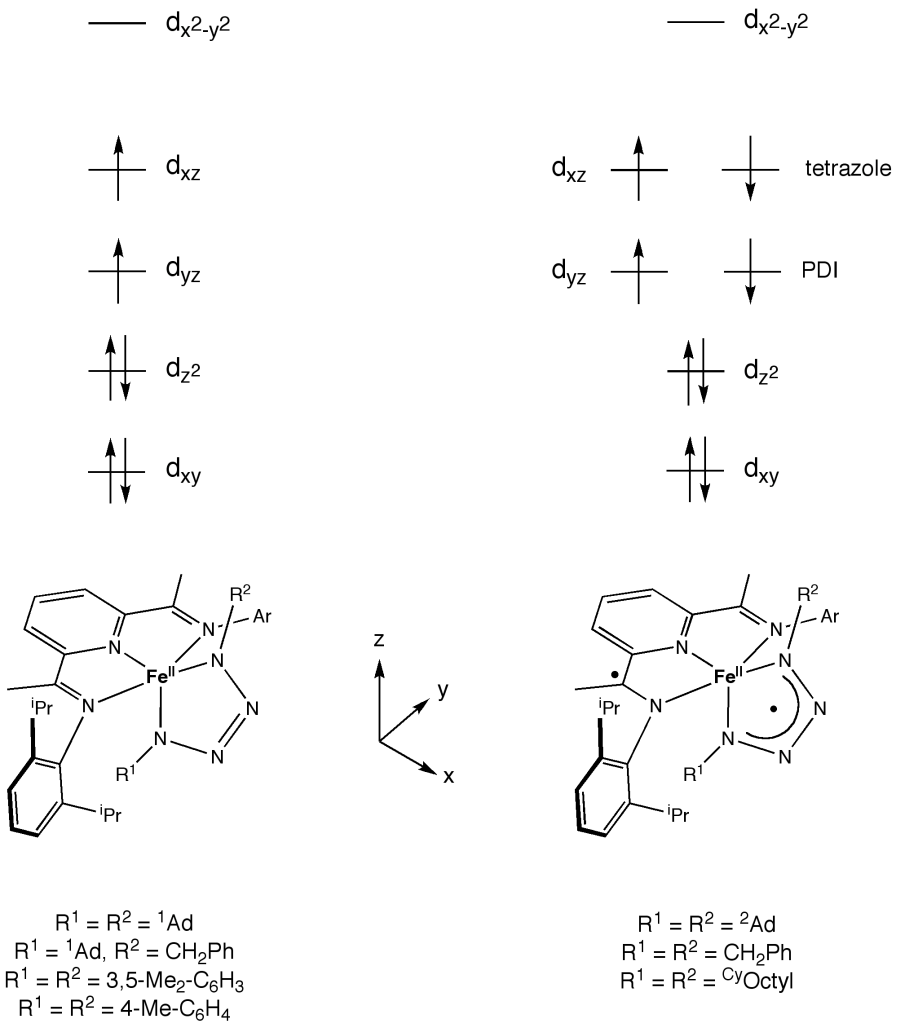

Figure 4.13 Proposed electronic structures of bis(imino)pyridine iron tetrazole complexes, including qualitative d-splitting diagram.

Whether the tetrazole ligand or the bis(imino)pyridine chelate is reduced, and the subsequent effect on electronic structure, is correlated with the field strength of the tetrazole ligand. The field strength of the tetrazole ligand is also correlated with the size of its substituents, evidenced by the observed isomer shifts and chemical shift ranges of the tetrazole complexes. An explanation for these observations is that larger

substituents keep the tetrazole ligand farther away from the metal center, preventing strong π back-bonding and leading to a weak-field tetrazole ligand. As the size of the tetrazole substituents decreases, the ligand can move closer to the metal center and π back-bonding increases. Thus, the steric bulk of the tetrazole ligand indirectly influences the electronic structure of the molecule. In addition, the redox activity of the bis(imino)pyridine chelate allows reduction of the tetrazole ligand by only one electron in the strong field cases because it can accept electron density from the metal center instead.

4.5 Conclusions

The synthesis and electronic structure of a series of bis(imino)pyridine iron tetrazole complexes were investigated. These compounds were prepared either by addition of two equivalents of organic azide to the bis(dinitrogen) compound, **1-(N_2)$_2$**, or by addition of one equivalent of azide to the corresponding iron imide compound. Two distinct electronic structures were found for the bis(imino)pyridine iron tetrazoles. One group is best described as having an intermediate-spin iron(II) center and a dianionic tetrazole ligand, with a neutral bis(imino)pyridine chelate. The other is most consistent with an intermediate-spin iron(II) center antiferromagnetically coupled to both a mono-reduced bis(imino)pyridine chelate and a mono-reduced tetrazole ligand. Increasing the steric bulk of the tetrazole ligand appeared to decrease the field strength, as observed by ^{1}H NMR and Mössbauer spectroscopies. As the field strength of the tetrazole ligand decreased, a corresponding increase in chemical shift range was observed in the ^{1}H NMR spectrum. In addition, an increase in isomer shift was seen as the field strength of the tetrazole ligand decreased. The push-pull relationship between the two redox-active chelates is evidenced by the fact that when the tetrazole ligand is doubly reduced, a neutral bis(imino)pyridine chelate is

observed, and when the tetrazole ligand is singly reduced, the bis(imino)pyridine chelate is also singly reduced.

4.6 Experimental Procedures

General Considerations. All air- and moisture-sensitive manipulations were carried out using standard vacuum line, Schlenk, and cannula techniques or in an MBraun inert atmosphere dry box containing an atmosphere of purified nitrogen. Solvents for air- and moisture-sensitive manipulations were initially dried and deoxygenated using literature procedures.[20] Benzene-d_6 and toluene-d_8 were purchased from Cambridge Isotope Laboratories and dried over 4 Å molecular sieves or titanocene, respectively. The complex **1-$(N_2)_2$** was prepared according to literature procedure.[19] 1-adamantyl azide was purchased from Aldrich and dried on the high-vacuum line before use. 2-adamantyl azide was prepared according to literature procedure[21] and dried on the high-vacuum line before use. Cyclooctyl azide,[22] benzyl azide,[22] 1-azido-3,5-dimethylbenzene[23] and 1-azido-4-methylbenzene[23] were prepared according to literature procedures and dried by passing a pentane solution of the azide through neutral alumina.

^{1}H NMR spectra were recorded on Varian Mercury 300, Inova 400, 500, and 600 spectrometers operating at 299.76, 399.78, 500.62, and 599.78 MHz, respectively. ^{13}C NMR spectra were recorded on an Inova 500 spectrometer operating at 125.893 MHz. All ^{1}H and ^{13}C NMR chemical shifts are reported relative to $SiMe_4$ using the ^{1}H (residual) and ^{13}C chemical shifts of the solvent as a secondary standard. For diamagnetic complexes, many assignments were made based on COSY and HSQC NMR experiments. Solution magnetic moments were determined by Evans method[24] using a ferrocene standard and are the average value of at least two independent measurements. Magnetic susceptibility balance measurements were performed with a

Johnson Matthey instrument that was calibrated with $HgCo(SCN)_4$. Peak widths at half heights are reported for paramagnetically broadened and shifted resonances. Infrared spectra were collected on a Thermo Nicolet spectrometer. Elemental analyses were performed at Robertson Microlit Laboratories, Inc., in Madison, NJ.

Single crystals suitable for X-ray diffraction were coated with polyisobutylene oil in a drybox, transferred to a nylon loop and then quickly transferred to the goniometer head of a Bruker X8 APEX2 diffractometer equipped with a molybdenum X-ray tube (l = 0.71073 Å). Preliminary data revealed the crystal system. A hemisphere routine was used for data collection and determination of lattice constants. The space group was identified and the data were processed using the Bruker SAINT+ program and corrected for absorption using SADABS. The structures were solved using direct methods (SHELXS) completed by subsequent Fourier synthesis and refined by full-matrix least-squares procedures.

^{57}Fe Mössbauer spectra were recorded on a SEE Co. Mössbauer spectrometer (MS4) at 80 K in constant acceleration mode. ^{57}Co/Rh was used as the radiation source. WMOSS software was used for the quantitative evaluation of the spectral parameters (leastsquares fitting to Lorentzian peaks). The minimum experimental line widths were 0.23 mm s^{-1}. The temperature of the samples was controlled by a Janis Research Co. CCS-850 He/N_2 cryostat within an accuracy of ±0.3 K. Isomer shifts were determined relative to α-iron at 298 K.

Preparation of (^{iPr}PDI)Fe[(N^1Ad)NN(N^1Ad)]. A 20-mL scintillation vial was charged with 0.093 g (0.157 mmol) of **^{iPr}PDIFe(N_2)$_2$** and ~15 mL of diethyl ether, resulting in a dark green solution. A solution of 0.056 g (0.314 mmol) 1-adamantyl azide was added to the vial. There was an immediate color change to purple concomitant with bubbling, followed by rapid formation of a brown precipitate. The

reaction was stirred for 15 minutes, and the precipitate was collected by filtration and washed with pentane. The resulting brown powder was recrystallized from toluene at -35 °C to give 0.112 g (83 %) of dark brown crystals identified as **(^{iPr}PDI)Fe[(N^1Ad)NN(N^1Ad)]**. Analysis for $C_{53}H_{73}N_7Fe$: Calc. C, 73.67; H, 8.52; N, 11.35. Found C, 73.68; H, 8.66; N, 11.02. Magnetic susceptibility (Gouy balance, 293 K): $\mu_{eff} = 4.2(1)\ \mu_B$. ^{1}H NMR (benzene-$d_6$): δ = -141.43 (64.2 Hz, 6H, C(C*H*$_3$)), -26.99 (144.7 Hz, 6H, CH(C*H*$_3$)$_2$), -12.14 (226.0 Hz, 6H, CH(C*H*$_3$)$_2$), -10.40 (18.3 Hz, 2H, C*H*(CH$_3$)$_2$ or *aryl*), -3.80 (23.0 Hz, 6H, CH(C*H*$_3$)$_2$), -2.27 (20.9 Hz, 3H, adamantyl C*H*$_2$), -2.05 (33.9 Hz, 6H, CH(C*H*$_3$)$_2$), -1.88 (28.3 Hz, 3H, adamantyl C*H*$_2$), -1.05 (28.7 Hz, 3H, adamantyl C*H*$_2$), 1.50 (21.5 Hz, 3H, adamantyl C*H*$_2$), 1.61 (16.2 Hz, 6H, adamantyl C*H*$_2$), 4.19 (49.5 Hz, 6H, adamantyl C*H*$_2$), 6.95 (17.0, 2H, C*H*(CH$_3$)$_2$ or *aryl*), 8.06 (21.2 Hz, 2H, C*H*(CH$_3$)$_2$ or *aryl*), 8.23 (245.7 Hz, 2H, C*H*(CH$_3$)$_2$ or *aryl*), 27.42 (25.2 Hz, 3H, adamantyl C*H*$_2$), 27.81 (17.2 Hz, 3H, adamantyl C*H*$_2$), 48.09 (36.1 Hz, 2H, *m-pyridine*), 264.87 (110.2 Hz, 1H, *p-pyridine*).

Alternative preparation of (^{iPr}PDI)Fe[(N^1Ad)NN(N^1Ad)]. A 20 mL scintillation vial was charged with 0.036 g (0.052 mmol) **1-N(^{1}Ad)**and 1-adamantyl azide (0.009 g, 0.052 mmol) was added to the vial, followed by rapid formation of a brown precipitate. The reaction was stirred for 10 minutes, and volatiles were removed to give a dark brown solid. Quantitative conversion to **(^{iPr}PDI)Fe[(N^1Ad)NN(N^1Ad)]** was confirmed by ^{1}H NMR spectroscopy.

Preparation of (^{iPr}PDI)Fe[(N^2Ad)NN(N^2Ad)]. This compound was prepared in a similar manner to **(^{iPr}PDI)Fe[(N^1Ad)NN(N^1Ad)]** with 0.095 g (0.160 mmol) **^{iPr}PDIFe(N_2)$_2$** and 0.057 g (0.322 mmol) 2-adamantyl azide. Recrystallization from toluene yielded 0.095 g (69 %) of dark brown crystals identified as

(^{iPr}PDI)Fe[(N^2Ad)NN(N^2Ad)]. Magnetic susceptibility (Gouy balance, 293 K): μ_{eff} = 0.3(1) μ_B. ^{1}H NMR (benzene-d_6): δ = -16.86 (s, 6H, C(C*H*$_3$)), -6.42 (br s, 2H, C*H*(CH$_3$)$_2$), -4.28 (br s, 2H, C*H*(CH$_3$)$_2$), -3.59 (br s, 1H, adamantyl C*H*), -1.24 (br s, 6H, CH(C*H*$_3$)$_2$), -0.59 (m, 2H, adamantyl C*H*$_2$), -0.13 (br s, 6H, CH(C*H*$_3$)$_2$), 0.08 (m, 2H, adamantyl C*H*$_2$), 0.34 (br s, 1H, adamantyl C*H*), 0.90 (br s, 2H, adamantyl C*H*$_2$), 1.01 (m, 1H, adamantyl C*H*), 1.34 (m, 2H, adamantyl C*H*$_2$), 1.49 (m, 1H, adamantyl C*H*), 1.69 (br s, 2H, adamantyl C*H*$_2$), 2.05 (m, 2H, adamantyl C*H*$_2$), 2.11 (s, 6H, CH(C*H*$_3$)$_2$), 2.75 (s, 6H, CH(C*H*$_3$)$_2$), 3.22 (m, 2H, adamantyl C*H*$_2$), 3.27 (m, 1H, adamantyl C*H*), 3.54 (m, 2H, adamantyl C*H*$_2$), 3.70 (m, 2H, adamantyl C*H*$_2$), 4.21 (m, 2H, adamantyl C*H*$_2$), 4.32 (t, 7.5 Hz, 2H, *p-aryl*), 5.05 (d, 7.5 Hz, 2H, *m-aryl*), 6.18 (m, 2H, adamantyl C*H*$_2$), 6.32 (d, 7.5 Hz, 2H, *m-aryl*), 10.83 (br s, 1H, adamantyl C*H*), 11.89 (br s, 2H, adamantyl C*H*$_2$), 21.49 (br s, 1H, *p-pyridine*), 36.60 (br s, 2H, *m-pyridine*). ^{13}C {^{1}H} NMR (benzene-d_6): δ = 12.16, 18.24, 24.71 (adamantyl *C*H$_2$), 26.61 (CH(*C*H$_3$)$_2$), 27.37 (adamantyl *C*H), 29.40 (adamantyl *C*H$_2$), 32.18 (adamantyl *C*H), 32.47 (adamantyl *C*H), 32.58 (CH(*C*H$_3$)$_2$), 32.75 (CH(*C*H$_3$)$_2$), 35.33 (CH(*C*H$_3$)$_2$), 37.77 (adamantyl *C*H), 38.99 (adamantyl *C*H$_2$), 41.92 (adamantyl *C*H$_2$), 47.39 (adamantyl *C*H$_2$), 51.99 (adamantyl *C*H$_2$), 104.70, 110.77 (*m-aryl*), 115.83 (*m-aryl*), 118.33, 121.21, 123.9, 135.22 (*p-aryl*), 136.31, three resonances not located.

Alternative preparation of (^{iPr}PDI)Fe[(N^2Ad)NN(N^2Ad)]. A 20 mL scintillation vial was charged with 0.014 g (0.020 mmol) **(^{iPr}PDI)FeN(^{2}Ad)** and 2-adamantyl azide (0.004 g, 0.0.020 mmol). The solids were dissolved in benzene-d_6, followed by a rapid color change to dark brown, and added to a J. Young tube. Quantitative conversion to **(^{iPr}PDI)Fe[(N^2Ad)NN(N^2Ad)]** was confirmed by ^{1}H NMR spectroscopy.

Preparation of (^{iPr}PDI)Fe[(N^{Cy}Oct)NN(N^{Cy}Oct)]. This compound was prepared in a similar manner to **(^{iPr}PDI)Fe[(N^{1}Ad)NN(N^{1}Ad)]** with 0.103 g (0.174 mmol) **^{iPr}PDIFe(N_2)$_2$** and 0.053 g (0.346 mmol) cyclooctyl azide. Recrystallization from pentane yielded 0.086 g (61 %) of dark brown crystals identified as **(^{iPr}PDI)Fe[(N^{Cy}Oct)NN(N^{Cy}Oct)]**. Magnetic susceptibility (Gouy balance, 293 K): μ_{eff} = 0.1(1) μ_B. ^{1}H NMR (benzene-*d*$_6$): δ = -0.57 (s, 6H, C(C*H*$_3$)), 0.18 (m, 2H, cyclooctyl C*H*$_2$), 0.53 (m, 2H, cyclooctyl C*H*$_2$), 0.70 (d, 6.2 Hz, 6H, CH(C*H*$_3$)$_2$), 0.85 (septet, 6.2 Hz, 2H, C*H*(CH$_3$)$_2$), 1.02 (d, 6.4 Hz, 6H, CH(C*H*$_3$)$_2$), 1.03 (m, 2H, cyclooctyl C*H*$_2$), 1.06 (m, 2H, cyclooctyl C*H*$_2$), 1.16 (d, 6.4 Hz, 6H, CH(C*H*$_3$)$_2$), 1.20 (m, 2H, cyclooctyl C*H*$_2$), 1.24 (d, 6.2 Hz, 6H, CH(C*H*$_3$)$_2$), 1.25 (m, 2H, cyclooctyl C*H*$_2$), 1.27 (m, 2H, cyclooctyl C*H*$_2$), 1.30 (m, 2H, cyclooctyl C*H*$_2$), 1.34 (m, 2H, cyclooctyl C*H*$_2$), 1.42 (m, 2H, cyclooctyl C*H*$_2$), 1.45 (m, 2H, cyclooctyl C*H*$_2$), 1.51 (m, 2H, cyclooctyl C*H*$_2$), 1.76 (m, 2H, cyclooctyl C*H*$_2$), 1.89 (m, 2H, cyclooctyl C*H*$_2$), 2.86 (septet, 6.4 Hz, 2H, C*H*(CH$_3$)$_2$), 6.09 (m, 1H, cyclooctyl C*H*), 6.66 (t, 7.4 Hz, 2H, *p-aryl*), 6.69 (m, 1H, cyclooctyl C*H*), 6.82 (d, 7.4 Hz, 2H, *m-aryl*), 6.96 (d, 7.4 Hz, 2H, *m-aryl*), 7.89 (d, 7.7 Hz, 2H, *m-pyridine*), 12.24 (t, 7.7 Hz, 1H, *p-pyridine*). ^{13}C {^{1}H} NMR (benzene-*d*$_6$): δ = 24.76 (cyclooctyl *C*H$_2$), 25.07 (CH(*C*H$_3$)$_2$), 25.40 (*C*H(CH$_3$)$_2$), 26.55 (cyclooctyl *C*H$_2$), 26.73 (CH(*C*H$_3$)$_2$), 27.38 (CH(*C*H$_3$)$_2$), 27.52 (cyclooctyl *C*H$_2$), 27.81 (CH(*C*H$_3$)$_2$), 28.60 (cyclooctyl *C*H$_2$), 28.77 (cyclooctyl *C*H$_2$), 29.72 (cyclooctyl *C*H$_2$), 31.44 (C(*C*H$_3$)), 32.47 (*C*H(CH$_3$)$_2$), 56.86 (cyclooctyl *C*H), 67.07 (cyclooctyl *C*H$_2$), 71.01 (cyclooctyl *C*H$_2$), 86.80 (cyclooctyl *C*H), 99.32 (*p-pyridine*), 121.98 (*m-aryl*), 123.21 (*m-aryl*), 128.27 (*p-aryl*), 136.41, 137.87, 139.78 (*m-pyridine*), three resonances not located.

Alternative preparation of (^{iPr}PDI)Fe[(N^{Cy}Oct)NN(N^{Cy}Oct)]. A J. Young tube was charged with 0.016 g (0.024 mmol) **(^{iPr}PDI)FeN(^{Cy}Oct)** in benzene-*d*$_6$. Cyclooctyl

azide (0.004 g, 0.024 mmol) was added by microsyringe, and there was a rapid color change to dark brown. Quantitative conversion to **(^{iPr}PDI)Fe[(N^{Cy}Oct)NN(N^{Cy}Oct)]** was confirmed by ^{1}H NMR spectroscopy.

Preparation of (^{iPr}PDI)Fe[(N^1Ad)NN(NBn)]. A 20 mL scintillation vial was charged with 0.047 g (0.068 mmol) **1-N(^{1}Ad)** and ~ 10 mL of toluene. Benzyl azide (0.009 g, 0.068 mmol) was added by microsyringe, and there was a rapid color change to dark brown. The solution was concentrated and cooled to -35 °C to precipitate 0.049 g (90 %) of dark brown crystals identified as **(^{iPr}PDI)Fe[(N^1Ad)NN(NBn)]**. Analysis for $C_{50}H_{65}N_7Fe$: Calc. C, 73.24; H, 7.99; N, 11.96. Found C, 73.45; H, 8.15; N, 12.34. Magnetic susceptibility (Gouy balance, 293 K): μ_{eff} = 3.2(2) μ_B. ^{1}H NMR (benzene-d_6): δ = -72.72 (46.0 Hz, 6H, C(CH_3)), -7.34 (22.5 Hz, 2H, CH(CH_3)$_2$), -6.46 (189.2 Hz, 6H, CH(CH_3)$_2$), -4.47 (12.6 Hz, 1H, *p-benzyl*), -2.25 (21.1 Hz, 6H, CH(CH_3)$_2$), -1.85 (35.8 Hz, 6H, CH(CH_3)$_2$), -0.17 (31.9 Hz, 3H, *adamantyl*), 0.03 (16.5 Hz, 2H), 0.59 (21.3 Hz, 2H), 2.36 (25.2 Hz, 3H, *adamantyl*), 3.46 (22.0 Hz, 6H, CH(CH_3)$_2$), 3.81 (22.4 Hz, 2H), 4.42 (58.2 Hz, 2H), 5.51 (44.2 Hz, 6H, *adamantyl*), 7.25 (23.7 Hz, 2H), 10.34 (23.3 Hz, 2H), 10.42 (25.5 Hz, 2H), 22.12 (27.4 Hz, 3H, *adamantyl*), 32.57 (32.6 Hz, 2H, *m-pyridine*), 178.81 (56.5 Hz, 1H, *p-pyridine*).

Preparation of (^{iPr}PDI)Fe[(NBn)NN(NBn)]. This compound was prepared in a similar manner to **(^{iPr}PDI)Fe[(N^1Ad)NN(N^1Ad)]** with 0.070 g (0.118 mmol) **^{iPr}PDIFe(N_2)$_2$** and 0.031 g (0.233 mmol) benzyl azide. Recrystallization from toluene yielded 0.057 g (62 %) of iridescent green crystals identified as **(^{iPr}PDI)Fe[(NBn)NN(NBn)]**. Magnetic susceptibility (Gouy balance, 293 K): μ_{eff} = 0.3(1) μ_B. ^{1}H NMR (benzene-d_6): δ = -9.73 (s, 6H, C(CH_3)), -2.24 (br s, 2H, CH(CH_3)$_2$), -0.77 (br s, 6H, CH(CH_3)$_2$), -0.05 (br s, 6H, CH(CH_3)$_2$), 1.27 (br s, 2H,

C*H*(CH_3)$_2$), 2.01 (br s, 6H, CH(C*H*$_3$)$_2$), 2.06 (br s, 6H, CH(C*H*$_3$)$_2$), 5.35 (t, 7.6 Hz, 2H, *p-aryl*), 5.58 (d, 7.6 Hz, 2H, *m-aryl*), 5.67 (d, 7.2 Hz, 2H, *o-benzyl*), 6.14 (d, 6.8 Hz, 2H, *o-benzyl*), 6.21 (t, 7.2 Hz, 1H, *p-benzyl*), 6.68 (d, 7.6 Hz, 2H, *m-aryl*), 6.84 (m, 2H, *m-benzyl*), 7.29 (t, 6.8 Hz, 1H, *p-benzyl*), 7.37 (m, 2H, *m-benzyl*), 8.48 (d, 7.3 Hz, 2H, *m-pyridine*), 31.55 (br s, 1H, *p-pyridine*), 42.27 (br s, 2H, benzyl C*H*$_2$), 66.85 (br s, 2H, benzyl C*H*$_2$). ^{13}C {^{1}H} NMR (benzene-*d*$_6$): δ = 18.02 (*C*H(CH_3)$_2$), 25.34 (CH(*C*H$_3$)$_2$), 34.30 (CH(*C*H$_3$)$_2$), 35.77 (CH(*C*H$_3$)$_2$), 36.58 (CH(*C*H$_3$)$_2$), 51.56 (*C*H(CH_3)$_2$), 72.03 (C(*C*H$_3$)), 108.64, 112.26, 116.33 (*m-aryl*), 120.63 (*m-aryl*), 121.03 (*o-benzyl*), 126.45, 126.62 (*o-benzyl*), 127.19 (*p-benzyl*), 129.74 (*m-benzyl*), 130.21 (*p-benzyl*), 130.84 (*m-benzyl*), 132.99 (*p-aryl*), 204.26, 211.09, four resonances not located.

Preparation of (^{iPr}PDI)Fe[(N-3,5-Me$_2$-C$_6$H$_3$)NN(N-3,5-Me$_2$-C$_6$H$_3$)]. This compound was prepared in a similar manner to **(^{iPr}PDI)Fe[(N^1Ad)NN(N^1Ad)]** with 0.101 g (0.170 mmol) **^{iPr}PDIFe(N$_2$)$_2$** and 0.050 g (0.340 mmol) 3,5-dimethylphenyl azide. Recrystallization from toluene yielded 0.124 g (91 %) of dark green-brown crystals identified as **(^{iPr}PDI)Fe[(N-3,5-Me$_2$-C$_6$H$_3$)NN(N-3,5-Me$_2$-C$_6$H$_3$)]**. Analysis for $C_{49}H_{61}N_7Fe$: Calc. C, 73.21; H, 7.65; N, 12.20. Found C, 73.01; H, 7.35; N, 11.79. Magnetic susceptibility (Gouy balance, 293 K): μ_{eff} = 3.1(2) μ_B. ^{1}H NMR (benzene-*d*$_6$): δ = -84.83 (379.4 Hz, 4H, *o-phenyl*), -80.71 (108.5 Hz, 2H, *p-phenyl* or *p-aryl*), -59.05 (95.7 Hz, 6H, C(C*H*$_3$)), -24.81 (32.2 Hz, 12H, CH(C*H*$_3$)$_2$ or phenyl C*H*$_3$), -8.57 (28.8 Hz, 2H, *p-phenyl* or *p-aryl*), 1.25 (88.6 Hz, 12H, CH(C*H*$_3$)$_2$ or phenyl C*H*$_3$), 2.17 (54.7 Hz, 12H, CH(C*H*$_3$)$_2$ or phenyl C*H*$_3$), 9.74 (890.5 Hz, 4H), 10.72 (35.9 Hz, 4H), 29.49 (76.1 Hz, 2H, *m-pyridine*), 199.10 (128.6 Hz, 1H, *p-pyridine*).

Preparation of (^{iPr}PDI)Fe[(N-*p*Tolyl)NN(N-*p*Tolyl)]. This compound was prepared in a similar manner to **(^{iPr}PDI)Fe[(N^1Ad)NN(N^1Ad)]** with 0.060 g (0.101 mmol) **^{iPr}PDIFe(N_2)$_2$** and 0.027 g (0.203 mmol) *p*-tolyl azide. Recrystallization from toluene yielded 0.124 g (91 %) of dark green-brown crystals identified as **(^{iPr}PDI)Fe[(N-*p*Tolyl)NN(N-*p*Tolyl)]**. Analysis for $C_{47}H_{57}N_7Fe$: Calc. C, 72.76; H, 7.40; N, 12.64. Found C, 73.09; H, 7.71; N, 12.69. Magnetic susceptibility (Gouy balance, 293 K): μ_{eff} = 3.3(2) μ_B. ^{1}H NMR (benzene-d_6): δ = -87.67 (405.6 Hz, 4H), -48.88 (80.4 Hz, 6H, C(CH_3)), -34.92 (38.6 Hz, 2H, *p-aryl*), -7.96 (21.0 Hz, 4H), 1.62 (34.9 Hz, 12H, CH(CH_3)$_2$), 2.15 (41.0 Hz, 12H, CH(CH_3)$_2$), 10.28 (25.8 Hz, 4H), 22.84 (60.0 Hz, 2H, *m-pyridine*), 50.04 (33.6 Hz, 4H), 95.64 (40.3 Hz, 6H, tolyl CH_3), 191.31 (127.9 Hz, 1H, *p-pyridine*).

REFERENCES

[1] Butin, K. P.; Beloglazkina, E. K.; Zyk, N. V. *Russ. Chem. Rev.* **2005**, *74*, 531-553.

[2] Knijnenburg, Q.; Gambarotta, S.; Budzelaar, P. H. M. *Dalton Trans.* **2006**, 5442-5448.

[3] (a) Blackmore, K. J.; Ziller, J. W.; Heyduk, A. F. *Inorg. Chem.* **2005**, *44*, 5559-5561. (b) Blackmore, K. J.; Lal, N.; Ziller, J. W.; Heyduk, A. F. *J. Am. Chem. Soc.* **2008**, *130*, 2728-2729.

[4] (a) Bart, S. C.; Hawrelak, E. J.; Schmisseur, A. K.; Lobkovsky, E.; Chirik, P. J. *Organometallics* **2004**, *23*, 237-246. (b) Bart, S. C.; Hawrelak, E. J.; Lobkovsky, E.; Chirik, P.J. *Organometallics* **2005**, *24*, 5518-5527. (c) Khusniyarov, M. M.; Harms, K.; Burghaus, O.; Sundermeyer, J. *Eur. J. Inorg. Chem.* **2006**, *15*, 2985-2996. (d) Muresan, N.; Chlopek, K.; Weyhermüller, T.; Neese, F.; Wieghardt, K. *Inorg. Chem.* **2007**, *46*, 5327.

[5] Dekker, M.; Knox, G. R. *Chem. Commun.* **1967**, 1243-1244.

[6] Doedens, R. J. *Chem. Commun.* **1968**, 1271-1272.

[7] Johnson, C. E.; Trogler, W. C. *J. Am. Chem. Soc.* **1981**, *103*, 6352-6358.

[8] Chang, C.; Johnson, C. E.; Richmond, T. G.; Chen, Y.; Trogler, W. C.; Basolo, F. *Inorg. Chem.* **1981**, *20*, 3167-3172.

[9] Trogler, W. C.; Johnson, C. E.; Ellis, D. E. *Inorg. Chem.* **1981**, *20*, 980-986.

[10] Gross, M. E.; Trogler, W. C.; Ibers, J. A. *J. Am. Chem. Soc.* **1981**, *103*, 192-193.

[11] (a) Gross, M. E.; Trogler, W. C. *J. Organomet. Chem.* **1981**, *209*, 407-414. (b) Gross, M. E.; Trogler, W. C.; Ibers, J. A. *Organometallics* **1982**, *1*, 732-739. (c) Gross, M. E.; Johnson, C. E.; Maroney, M. J.; Trogler, W. C. *Inorg. Chem.* **1984**, *23*, 2968-2973. (d) Maroney, M. J.; Trogler, W. C. *J. Am. Chem. Soc.* **1984**, *106*, 4144-4151.

[12] Mock, M. T.; Popescu, C. V.; Yap, G. P. A.; Dougherty, W. G.; Riordan, C. G. *Inorg. Chem.* **2008**, *47*, 1889-1891.

[13] Cowley, R. E.; Bill, E.; Neese, F.; Brennessel, W. W.; Holland, P. L. *Inorg. Chem.* **2009**, *48*, 4828-4836.

[14] Meyer, K. E.; Walsh, P. J.; Bergman, R. G. *J. Am. Chem. Soc.* **1995**, *117*, 974-985.

[15] Bart, S. C.; Chłopek, K.; Bill, E.; Bouwkamp, M. W.; Lobkovsky, E.; Neese, F.; Wieghardt, K.; Chirik, P. J. *J. Am. Chem. Soc.* **2006**, *128*, 13901-13912.

[16] Trovitch, R. J.; Ph.D. Thesis, Cornell University, 2009.

[17] Bart, S. C.; Lobkovsky, E.; Bill, E.; Wieghardt, K.; Chirik, P. J. *Inorg. Chem.* **2007**, *46*, 7055-7063.

[18] Greenwood, N. N.; Gibb, T. C. *Mössbauer Spectroscopy*; Chapman and Hall: London, 1971.

[19] Bart, S. C.; Lobkovsky, E.; Chirik, P. J. *J. Am. Chem. Soc.* **2004**, *126*, 13794-13807.

[20] Pangborn, A. B.; Giardello, M. A.; Grubbs, R. H.; Rosen, R. K.; Timmers, F. J. *Organometallics* **1996**, *15*, 1518-1520.

[21] Prakash, G. K. S.; Stephenson, M. A.; Shih, J. G.; Olah, G. A. *J. Org. Chem.* **1986**, *51*, 3215-3217.

[22] Alvarez, S. G.; Alvarez, M. T. *Synthesis* **1997**, 413-414.

[23] Liu, Q.; Tor, Y. *Org. Lett.* **2003**, *5*, 2571-2572.

[24] Sur, S. K. *J. Magn. Reson.* **1989**, *82*, 169-173.

CHAPTER 5

SYNTHESIS OF AN IRON AMMONIA COMPOUND FROM N-N BOND CLEAVAGE IN HYDRAZINE AND FROM AN N-H GROUP TRANSFER REAGENT*

5.1 Abstract

Preparation of the bis(imino)pyridine iron ammonia compound (^{iPr}PDI)Fe(NH_3) (^{iPr}PDI = 2,6-(2,6-$^{i}Pr_2$-C_6H_3N=CMe)$_2C_5H_3N$) by hydrazine disproportionation and by N-H group transfer was explored. Treatment of (^{iPr}PDI)Fe(N_2)$_2$ with hydrazine resulted in formation of (^{iPr}PDI)Fe(NH_3) along with N_2 and H_2, as determined by Toepler pump experiments. Treatment of (^{iPr}PDI)Fe(N_2)$_2$ with the N-H group transfer reagent Hdbabh (dbabh = 2,3:5,6-dibenzo-7-azabicyclo[2.2.1]hepta-2,5-diene) resulted in formation of (^{iPr}PDI)Fe(NH_3) and the iron amide complex (^{iPr}PDI)Fe(dbabh) in an approximately 1:2 ratio. This reaction likely proceeds through initial N-H group transfer to generate the parent iron imide (^{iPr}PDI)FeNH, followed by H-atom abstraction and capture of the [dbabh] radical by (^{iPr}PDI)Fe(N_2)$_2$. The electronic structures of (^{iPr}PDI)Fe(NH_3) and (^{iPr}PDI)Fe(dbabh) were investigated using a combination of X-ray crystallography, Mössbauer spectroscopy and SQUID magnetometry. (^{iPr}PDI)Fe(NH_3) is best described as an intermediate-spin iron(II) center (S_{Fe} = 1) antiferromagnetically coupled to a doubly reduced chelate (S_{PDI} = 1), while (^{iPr}PDI)Fe(dbabh) is most consistent with a high-spin iron(II) center antiferromagnetically coupled to a singly reduced chelate. The reactivity of N-H group transfer reagents was further explored by addition of

* Parts of this chapter have been reproduced with permission from (a) Bart, S. C.; Bowman, A. C.; Lobkovsky, E.; Chirik, P. J. *J. Am. Chem. Soc.* **2007**, *129*, 7212-7213. Copyright 2007 American Chemical Society. (b) Bowman, A. C.; Bart, S. C.; Heinemann, F. W.; Meyer, K.; Chirik, P. J. *Inorg. Chem.* **2009**, *48*, 5587-5589. Copyright 2009 American Chemical Society.

NC(dbabh) to (^{iPr}PDI)Fe(N_2)$_2$, furnishing the iron cyanamide complex (^{iPr}PDI)Fe(NC(dbabh)) and the putative terminal cyanoimide compound (^{iPr}PDI)Fe(NCN).

5.2 Introduction

Much effort has been focused on elucidating the mechanism of dinitrogen reduction to ammonia by nitrogenase.[1] In regards to this, iron complexes containing multiply bonded nitrogen ligands continue to be of interest. However, there are still only a few examples of iron species containing parent amide[2,3] and parent imide[4]. In addition, iron compounds containing neutral, hydrogenated ligands such as hydrazine and diazene are quite rare. The interaction of hydrazine with discrete metal centers is of interest due to the potential formation of hydrazine as an intermediate in the reduction of dinitrogen to ammonia by the MoFe cofactor of nitrogenase.[5] Hydrazine itself can also be a substrate for nitrogenase, being reduced to give two equivalents of ammonia, albeit not as readily as dinitrogen.[6] While some iron hydrazine complexes have been isolated,[7] disproportionation to NH_3, N_2 and H_2 or to diazene[7d] and H_2 is more commonly observed. Numerous metal salts,[8] cubane clusters[9] and even carbon nanofiber-supported iridium[10] have also been shown to effect hydrazine decomposition, yielding varying ratios of the aforementioned products depending on the specific reaction conditions.

Iron imide complexes are of interest not only due to possible intermediacy in nitrogen fixation schemes,[11] but also because they may participate in NR group transfer chemistry. The aziridination of olefins, often using Cu(I) and Cu(II) catalysts, has been demonstrated to be effective for a variety of substrates.[12] Metal imides have also been implicated in aryl and vinyl C-H amination reactions. In this case, addition of a rhodium catalyst to an azide-bearing substrate results in intramolecular C-H

amination to form an indole, likely through a rhodium imide intermediate.[13] Inspired by this observation, addition of olefins to isolated bis(imino)pyridine iron imides, (^{iPr}PDI)FeNR (^{iPr}PDI = 2,6-(2,6-^{i}Pr$_2$-C$_6$H$_3$N=CMe)$_2$C$_5$H$_3$N), was carried out, but no reaction was observed. Because the steric bulk of the imide substituent may inhibit reactivity, synthesis of the parent iron imide is an attractive target. In addition, the ability to generate parent aziridines would be synthetically useful.

5.3 Hydrazine Cleavage by a Bis(imino)pyridine Iron Center

Investigation of the reactivity of (^{iPr}PDI)Fe(N$_2$)$_2$ (**1-(N$_2$)$_2$**) with hydrazine was prompted by the observation that hydrogenation of the iron diazoalkane compound (^{iPr}PDI)Fe(N$_2$CHSiMe$_3$) (**1-N$_2$CHSiMe$_3$**) results in formation of tetramethylsilane and the iron ammonia compound, (^{iPr}PDI)Fe(NH$_3$) (**1-NH$_3$**).[14] One possible mechanism for this transformation involves hydrogenation of the diazoalkane ligand to hydrazine and tetramethylsilane, followed by disproportionation of the hydrazine to ammonia and N$_2$. To explore this possibility, the addition of hydrazine to **1-(N$_2$)$_2$** was studied at 23 °C. Treatment of a pentane solution of **1-(N$_2$)$_2$** with two equivalents of anhydrous hydrazine resulted in an immediate color change from dark green to red-brown, concomitant with bubbling of the solution. ^{1}H NMR spectroscopy established quantitative formation of a new diamagnetic iron species identified as **1-NH$_3$** (Figure 5.1a). As expected with hydrazine disproportionation, the formation of both of dinitrogen (~ 3.5 equivalents) and dihydrogen (~ 2.5 equivalents) was observed by analyzing the gas evolved from the reaction mixture by Toepler pump. Moreover, addition of 0.25 and 0.50 equivalents of hydrazine to **1-(N$_2$)$_2$** yielded 35 % and 75 % conversion to **1-NH$_3$**, respectively, showing that 1.4 equivalents of ammonia are formed for each equivalent of hydrazine.

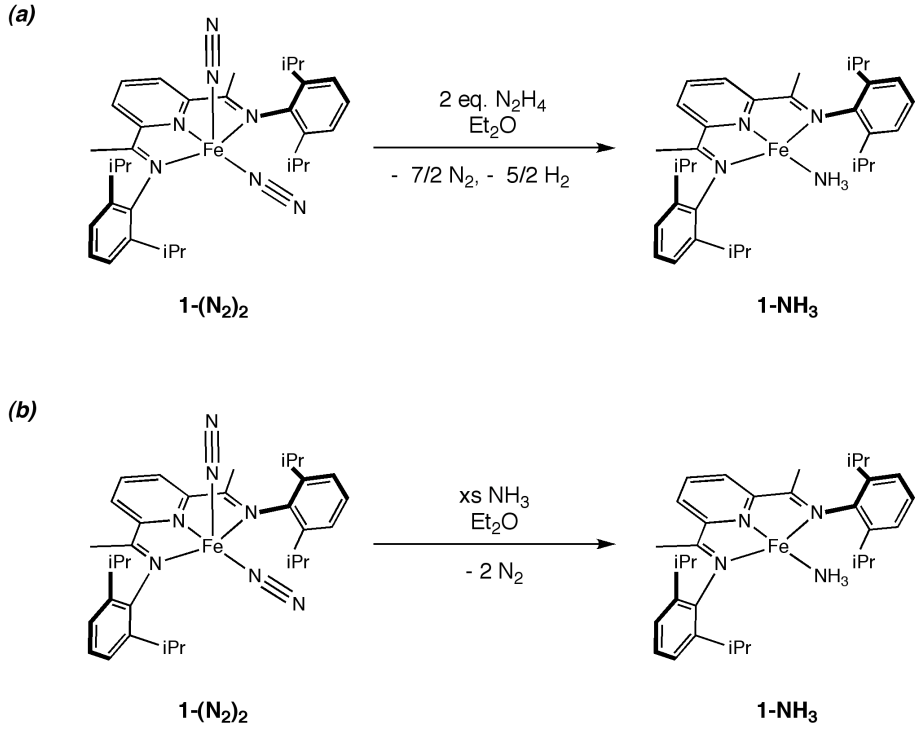

Figure 5.1 (a) Formation of **1-NH$_3$** from hydrazine disproportionation. (b) Formation of **1-NH$_3$** by addition of ammonia.

1-NH$_3$ was independently prepared by gas bulb addition of anhydrous ammonia to a stirring pentane solution of **1-(N$_2$)$_2$** at 23 °C (Figure 5.1b). The benzene-d_6 ^{1}H NMR spectrum of **1-NH$_3$** exhibits resonances shifted by temperature independent paramagnetism, commonly observed where neutral donor ligands are coordinated to bis(imino)pyridine iron complexes.[15] The previously published solid state structure of **1-NH$_3$**[14] (Figure 5.2) establishes idealized square planar geometry, with the sum of the angles around iron equal to 360.01(16)° and an N_{pyr}-Fe-N_{amm} angle of 179.26° (Table 5.1). Examination of the metrical parameters of the bis(imino)pyridine chelate establishes C_{imine}-N_{imine} distances of 1.358(3) Å and 1.371(3) Å, and C_{imine}-C_{ipso} distances of 1.420(3) Å and 1.436(3) Å. Compared to neutral ligand reference values,[16] The C_{imine}-N_{imine} bonds are elongated and the C_{imine}-C_{ipso} bonds are contracted, indicating two-electron reduction of the chelate.[16] The Fe-

N_{imine} and Fe-N_{pyr} bonds lengths for **1-NH_3** (Table 5.1) are similar to the distances observed for intermediate-spin neutral ligand complexes of bis(imino)pyridine iron,[17] suggesting that **1-NH_3** is best described as intermediate-spin iron(II) with an empty $d_{x^2-y^2}$ orbital.

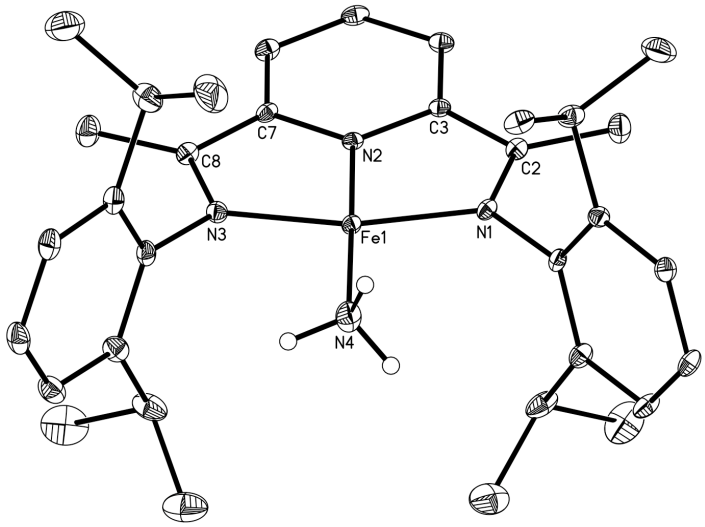

Figure 5.2 Molecular structure of **1-NH_3** at 30 % probability ellipsoids. Hydrogen atoms, except on the ammonia ligand, are omitted for clarity.

Table 5.1 Selected bond distances (Å) and angles (°) for **1-NH_3**.

Fe(1)-N(4)	2.008(2)	N(3)-C(8)	1.371(3)
Fe(1)-N(1)	1.9018(18)	C(2)-C(3)	1.420(3)
Fe(1)-N(2)	1.8296(18)	C(7)-C(8)	1.436(3)
Fe(1)-N(3)	1.8915(19)	N(2)-Fe(1)-N(4)	179.27(8)
N(1)-C(2)	1.358(3)		

The zero-field Mössbauer spectrum of **1-NH_3** at 80 K exhibits a quadrupole doublet with an isomer shift of 0.33 mm·s^{-1} and a quadrupole splitting of 2.22 mm·s^{-1}

(Figure 5.3). The observed isomer shift is typical for intermediate-spin neutral ligand complexes of bis(imino)pyridine iron.[17] The quadrupole splitting, while slightly larger in magnitude than other complexes of this type, is consistent with a square planar intermediate-spin iron(II) center. In comparison, the zero-field Mössbauer spectrum of (^{iPr}PDI)Fe($NH_2{}^t$Bu) at 80 K establishes an isomer shift of 0.39 mm·s^{-1} and a quadrupole splitting of 1.78 mm·s^{-1}.

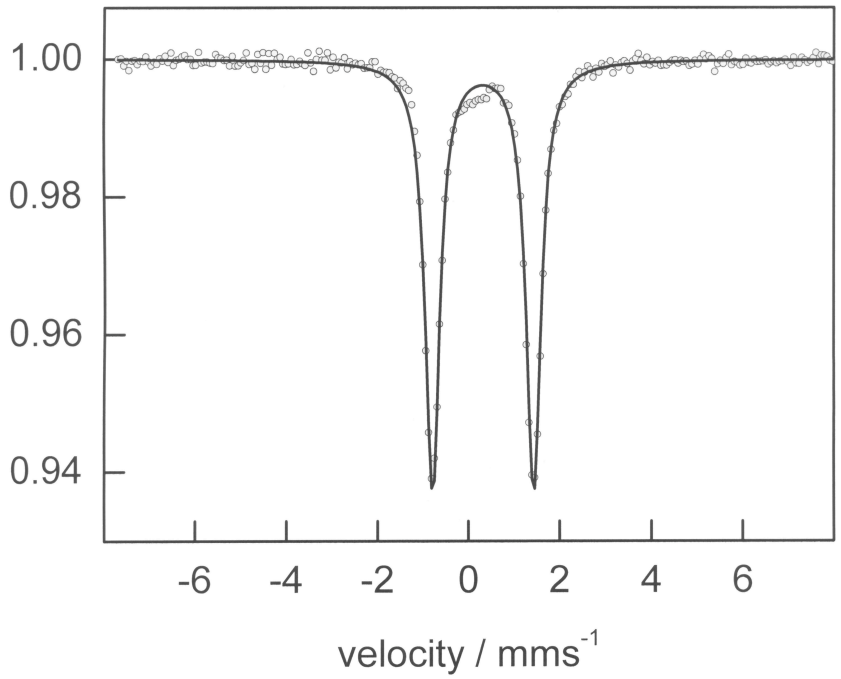

Figure 5.3 Zero-field Mössbauer spectrum of **1-NH$_3$** at 80 K; δ = 0.33 mm·s^{-1}, ΔE_Q = 2.22 mm·s^{-1}.

The Mössbauer parameters for **1-NH$_3$**, in combination with the observed diamagnetism of the compound, are wholly representative of an intermediate-spin iron(II) center antiferromagnetically coupled to a triplet diradical bis(imino)pyridine chelate. Overall, isolation and characterization of **1-NH$_3$** along with observation of H_2 and N_2 evolution demonstrate that **1-(N$_2$)$_2$** is competent for the disproportionation of hydrazine to NH_3, N_2 and H_2.

5.4 Reactivity of Bis(imino)pyridine Iron with an N-H Group Transfer Reagent

Based on previous work indicating that the bis(imino)pyridine chelate is capable of supporting an iron imide,[18] preparation of the parent iron imide complex, (^{iPr}PDI)FeNH, was targeted. Hdbabh (dbabh = 2,3:5,6-dibenzo-7-azabicyclo[2.2.1]hepta-2,5-diene) was initially chosen as an N-H group transfer reagent based on possible loss of anthracene as a driving force for the reaction. The corresponding lithium amide, Li[dbabh], has been successfully utilized as a synthon for metal nitride complexes.[19,20] Cummins and Mindiola observed that treatment of $Cr(I)_2(NRAr_F)_2$ (R = $C(CD_3)_2CH_3$, Ar_F = 2,5-C_6H_3FMe) with Li[dbabh](OEt_2) at -90 °C furnished the desire chromium nitride, $Cr(I)(N)(NRA_F)_2$, with loss of anthracene upon warming to room temperature.[19] Additional work by Cummins and coworkers, as well as by Peters and Lu, demonstrates that Li[dbabh] can also be used to generate metal amide complexes, although loss of anthracene to furnish the corresponding nitride is not always observed.[21]

Addition of one equivalent of Hdbabh to a diethyl ether solution of **1-$(N_2)_2$** at 23 °C led to formation of two new iron products and 1/3 of an equivalent of anthracene (Figure 5.4). The iron products were identified as **1-NH_3** and the paramagnetic bis(imino)pyridine iron amide, (^{iPr}PDI)Fe(dbabh) (**1-dbabh**). Additional anthracene loss from **1-dbabh** was not observed following the initial reaction. Allowing the reaction mixture to stand in solution at 23 °C for up to one week produced no change, and heating the mixture to 45 °C for 24 hours resulted in decomposition of the iron species with no additional anthracene loss. Changing the order of addition also did not result in any observable change to the ratio of the products.

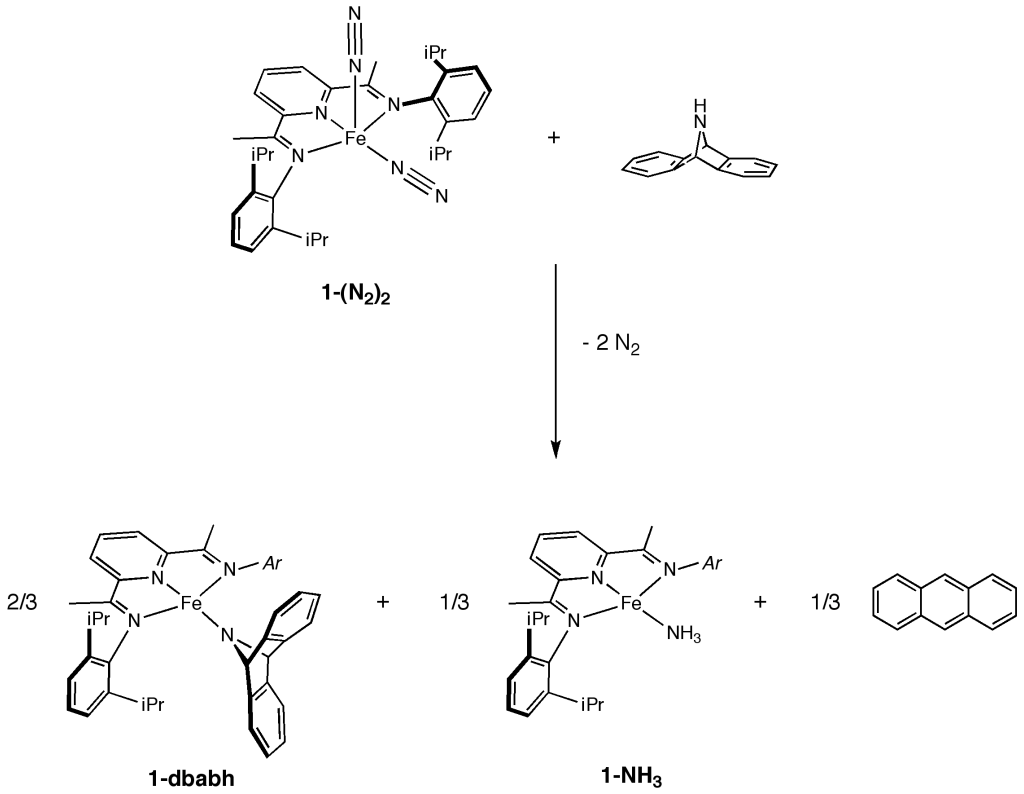

Figure 5.4 N-H bond cleavage of Hdbabh by **1-$(N_2)_2$** to generate **1-NH_3**, **1-dbabh** and anthracene.

Characterization of **1-dbabh** by X-ray diffraction[22] establishes idealized square planar geometry, consistent with the C_{2v} symmetry observed by ^{1}H NMR spectroscopy (Figure 5.5). The sum of the angles around iron is equal to 362.17(13)°, with the iron lifted 0.3880(17) Å out of the idealized plane of the bis(imino)pyridine chelate. In addition, the N_{pyr}-Fe-N_{amide} angle is 169.92(7)° (Table 5.2). The slight deviation of these angles from 360° and 180°, respectively, is likely to avoid steric interaction between the dbabh substituent and the aryl groups of the chelate. The Fe-N_{amide} bond length, 1.9075(16) Å, is consistent with a Fe-N single bond, and is significantly shorter than the bond observed between the iron center and the ammonia ligand in **1-NH_3** (d_{Fe-N} = 2.008(2) Å). In addition, the sum of the angles around N(4) is 359.99(13)°, demonstrating both the planarity of the dbabh nitrogen and the absence

of a hydrogen atom at that position. These observations indicate that a proton was lost from the Hdbabh ligand during formation **1-dbabh**.

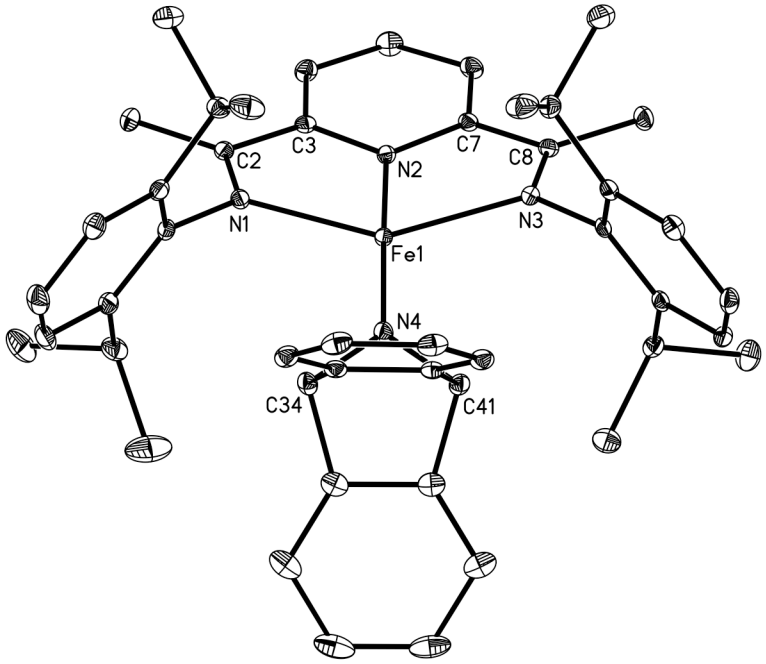

Figure 5.5 Molecular structure of **1-dbabh** at 30 % probability ellipsoids. Hydrogen atoms omitted for clarity.

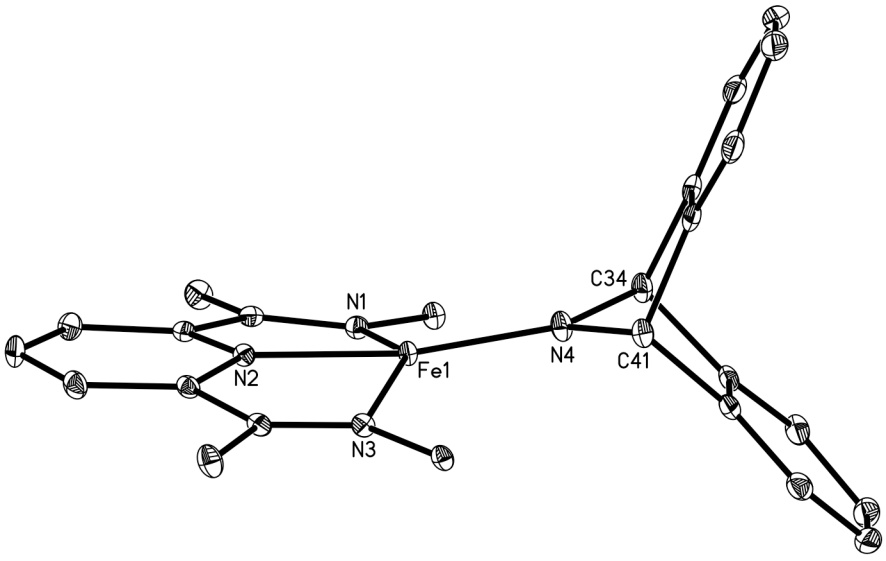

Figure 5.6 Molecular structure of **1-dbabh** at 30 % probability ellipsoids. Hydrogen atoms and aryl groups omitted for clarity.

Table 5.2 Selected bond distances (Å) and angles (°) for **1-dbabh**.

Fe(1)-N(4)	1.9075(16)	C(2)-C(3)	1.441(3)
Fe(1)-N(1)	2.1780(16)	C(7)-C(8)	1.457(3)
Fe(1)-N(2)	2.0049(16)	N(4)-Fe(1)-N(2)	169.92(7)
Fe(1)-N(3)	2.2214(16)	Fe(1)-N(4)-C(34)	132.52(13)
N(1)-C(2)	1.318(3)	Fe(1)-N(4)-N(41)	132.43(12)
N(3)-C(8)	1.301(2)	C(41)-Fe(1)-C(34)	95.04(14)

Distortions to the bis(imino)pyridine chelate are observed for **1-dbabh**, although they are not as prominent as those observed for **1-NH$_3$**. The slight elongation of the C_{imine}-N_{imine} bonds to 1.318(3) Å and 1.301(2) Å, and contraction of the C_{imine}-C_{ipso} bonds to 1.441(3) Å and 1.457(3) Å are suggestive of one-electron reduction of the chelate (Table 5.2).[16] Lengthening of the bonds between the iron center and the chelate is also observed, consistent with population of the d_{x2-y2} orbital. The Fe-N_{imine} bond lengths, 2.1780(16) Å and 2.2214(16) Å, and the Fe-N_{pyr} bond length of 2.0049(16) Å are typical of a high-spin iron center.[23]

In order to further probe the electronic structure of **1-dbabh**, variable temperature solid state SQUID measurements were collected between 5 and 300 K.[24] These data, shown in Figure 5.7, indicate that the effective magnetic moment of **1-dbabh** undergoes a steady decline from 3.90 μ_B to 2.90 μ_B with decreasing temperature. This is consistent with three unpaired electrons and an overall $S = 3/2$ ground state for the molecule, and is similar to the variable temperature magnetic data observed for other high-spin bis(imino)pyridine iron compounds with X-type ligands.[25]

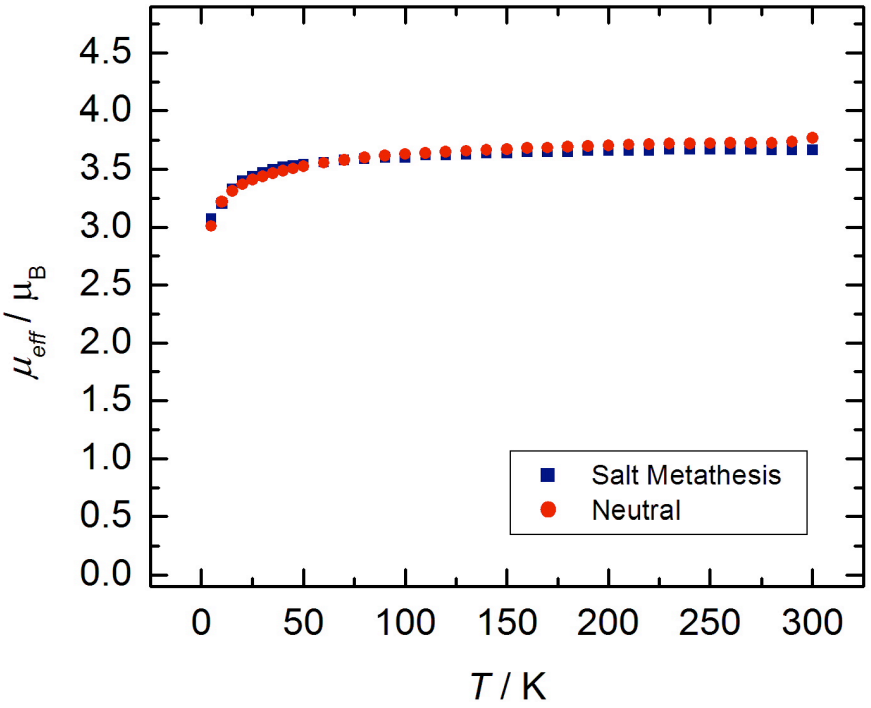

Figure 5.7 Variable temperature SQUID magnetization data (at 1 T) for samples of **1-dbabh**. Data for samples made using the neutral Hdbabh (red circles) and by salt metathesis with Li[dbabh] (blue squares) are shown and are corrected for underlying diamagnetism.

In addition, the zero-field Mössbauer spectrum of the reaction of Hdbabh with **1-$(N_2)_2$** was obtained at 80 K (Figure 5.8). As well as providing insight into the electronic structure of **1-dbabh**, this spectrum was used to measure the relative amounts of **1-NH_3** and **1-dbabh** in the reaction mixture. Analysis of the Mössbauer spectrum establishes that **1-dbabh** is the major product, accounting for ~ 80 % of the mixture. The other 20 % is comprised of **1-NH_3**, which was identified by comparison to the spectrum of an independently prepared sample. This ratio deviates slightly from the expected stoichiometry of 2:1, likely due to recrystallization of the reaction mixture prior to obtaining the Mössbauer spectrum. The Mössbauer parameters for **1-dbabh**, $\delta = 0.75$ mm·s^{-1} and $\Delta E_Q = 1.22$ mm·s^{-1}, are consistent with high-spin iron(II) and are similar to the parameters observed for analogous compounds with mono-X

ligands.[23] These parameters, in combination with the solid state magnetic and crystallographic data, indicate that **1-dbabh** is best described by a high-spin iron(II) center antiferromagnetically coupled to a mono-reduced bis(imino)pyridine chelate to give an overall $S = 3/2$ molecule.

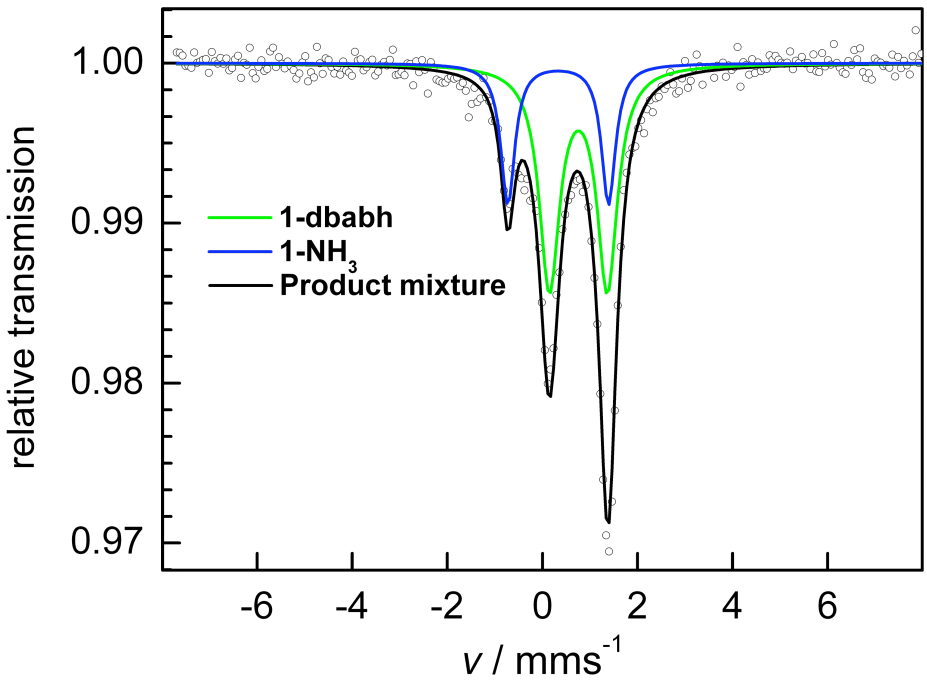

Figure 5.8 Zero-field Mössbauer spectrum of the product mixture from addition of Hdbabh to **1-$(N_2)_2$** at 80 K.

After investigation of the electronic structure of **1-dbabh**, further experiments were carried out to explore the mechanism of **1-NH_3** formation. Isotopic labeling of the N-H group transfer reagent was used to investigate the source of the protons in the ammonia ligand. Ddbabh, the ^{2}H isotopologue of Hdbabh, was prepared and added to **1-$(N_2)_2$**. Analysis of the product mixture by ^{1}H and ^{2}H NMR spectroscopy established formation of **1-ND_3** as the sole iron ammonia species, indicating that Ddbabh (or Hdbabh) is the only source of hydrogen in formation of the ammonia ligand. This observation was confirmed by solid state IR (KBr) spectroscopy. Involvement of the

bis(imino)pyridine chelate was investigated through addition of Hdbabh to the isotopically labeled bis(dinitrogen) compound, **1**-$(N_2)_2$**, where ** denotes deuteration of the imine methyl groups. The only observed iron products were **1**-dbabh** and **1**-NH_3**, ruling out participation of the imine methyl groups in formation of the iron ammonia compound.

The observations from isotopic labeling studies indicate that a possible mechanism is initial N-H group transfer from Hdbabh to form the parent iron imide species, (^{iPr}PDI)FeNH, along with anthracene. This intermediate, likely very reactive, could then abstract H-atoms from available Hdbabh molecules to form **1-NH_3** as well as [dbabh] radicals, which are trapped by remaining **1-$(N_2)_2$** to yield the other observed product, **1-dbabh**. This mechanism should ideally lead to formation of **1-NH_3**, **1-dbabh** and anthracene in a ratio of 1:2:1 (Figure 5.9). The Mössbauer spectrum of the reaction mixture (Figure 5.8) establishes formation of **1-dbabh** and **1-NH_3** in a 4:1 ratio, although deviation from the ideal 2:1 ratio is likely due to recrystallization of the reaction mixture. Moreover, hydrolysis of the reaction mixture yielded Hdbabh and anthracene in a 2:1 ratio. Because independent hydrolysis of **1-dbabh** cleanly furnished Hdbabh and ^{iPr}PDI, comparing the relative amounts of Hdbabh and anthracene can be used to measure the relative amounts of **1-dbabh** and **1-NH_3** in the reaction mixture.

Attempts were made to capture the putative (^{iPr}PDI)FeNH intermediate with additional reagents. Iron imides have been shown to undergo hydrogenation of the Fe-N bond[18,26,27] and participate in intra- and intermolecular C-H activation.[28] In addition, bis(imino)pyridine iron imides are generally reactive towards unsaturated molecules, such as azides and alkynes, as well as primary and secondary silanes.[26] Treatment of **1-$(N_2)_2$** with Hdbabh under an atmosphere of either H_2 or D_2 did not change the ratio of products. With D_2, no deuterium incorporation into any of the products was

observed. Performing the reaction in the presence of possible H-atom donors, such as 1,4-cyclohexadiene, 9,10-dihydroanthracene and fluorene also had no effect on the product ratio. Likewise, performing the reaction in the presence of styrene or phenyl silane did not lead to formation of a new iron species. When addition of Hdbabh to **1-$(N_2)_2$** was conducted in diethyl ether at -78 °C for 12 hours, a new paramagnetic species was observed as a minor product and the amount of anthracene generated increased from one third of an equivalent to nearly half an equivalent (46 %). Hydrolysis of the product mixture gave a small amount of modified bis(imino)pyridine chelate in addition to a majority of unmodified chelate, possibly indicating C-H activation of the bis(imino)pyridine ligand by a transient iron imide species.

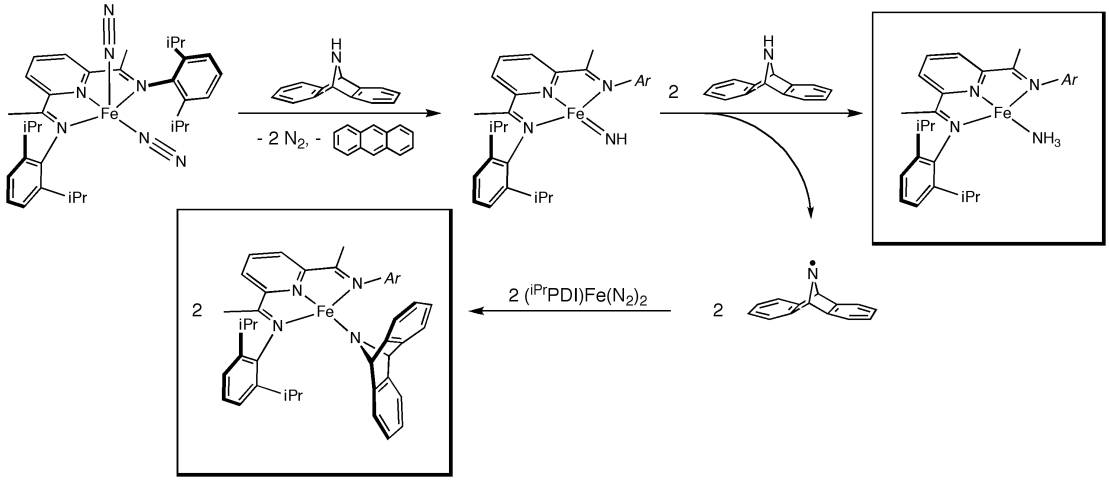

Figure 5.9 Proposed mechanism for N-H bond cleavage by **1-$(N_2)_2$**.

The formation of **1-dbabh** from cleavage of Hdbabh is remarkable because previous attempts to synthesize a bis(imino)pyridine iron amide have been unsuccessful. Addition of one equivalent of either $Li(NMe_2)$ or $KN(SiMe_3)_2$ to (^{iPr}PDI)FeCl (**1-Cl**) resulted in formation of an intractable mixture of iron products instead of the desired salt metathesis yield (^{iPr}PDI)$FeNMe_2$ or (^{iPr}PDI)$FeN(SiMe_3)_2$,

respectively. Moreover, treatment of (^{iPr}PDI)$FeCl_2$ (**1-Cl$_2$**) with two equivalents of $LiNMe_2$ led to deprotonation of the bis(imino)pyridine backbone methyl groups to form (^{iPr}PDEA)$Fe(NHMe_2)$ (^{iPr}PDEA = 2,6-(2,6-$^{i}Pr_2$-$C_6H_3NC{=}CH_2)_2C_5H_3N$).[29] Similarly, addition of two equivalents of $KN(SiMe_3)_2$ to a tetrahydrofuran slurry of **1-Cl$_2$** resulted in formation of (^{iPr}PDEA)$Fe(THF)_2$ (**2-(THF)$_2$**).[29] Conversely, salt metathesis proved to be a viable route for the preparation of **1-dbabh**. Addition of one equivalent of Li(dbabh) to a diethyl ether solution of **1-Cl** resulted in clean formation of **1-dbabh** (Figure 5.10). However, treatment of **1-Cl$_2$** with two equivalents of Li(dbabh) did not yield the desired iron amide. Instead, a range of unidentified iron species was observed in the product mixture. The inability of Li(dbabh) to reduce **1-Cl$_2$** was identified as the impediment to iron amide formation, as addition of one equivalent of Li(dbabh) to **1-Cl$_2$** did not result in formation of **1-Cl**.

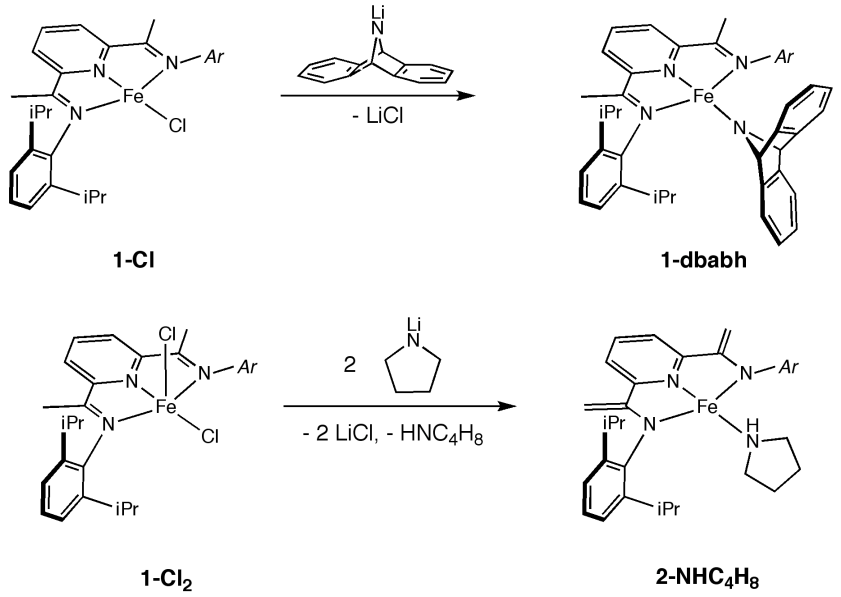

Figure 5.10 Preparation of **1-dbabh** by salt metathesis and chelate deprotonation of **1-Cl$_2$** by a lithium amide.

Encouraged by the successful preparation of **1-dbabh** by salt metathesis, the reactivity of other cyclic amines was explored. However, treatment of **1-Cl** with one equivalent of lithium pyrrolidide, $Li(NC_4H_8)$, produced a complex mixture of iron species. As with most other lithium amides, addition of two equivalents of $Li(NC_4H_8)$ to a tetrahydrofuran solution of **1-Cl$_2$** at 23 °C resulted in chelate deprotonation and formation of (^{iPr}PDEA)Fe(NHC_4H_8) (**2-NHC$_4$H$_8$**), shown in Figure 5.10. **2-NHC$_4$H$_8$** was independently prepared by addition of pyrrolidine to a diethyl ether solution of **2-(THF)$_2$** at 23 °C. The benzene-d_6 ^{1}H NMR spectrum at 23 °C displays the two characteristic methylene backbone resonances at δ = -49.13 and -39.22 ppm, and the IR spectrum (KBr) indicates formation of C=C and N-H bonds with stretches at 1587 and 3219 cm^{-1} respectively.

5.5 Further Investigation of N-R Group Transfer Reagents

Inspired by the observation of N-H group transfer from Hdbabh, additional reagents that are either commercially available or more readily synthesized were explored as possible N-H donors. Cyclic amines and aziridines were targeted due to the presence of ring strain as a possible driving force for N-H loss. Treatment of a pentane solution of **1-(N$_2$)$_2$** with one equivalent of pyrrolidine at 23 °C resulted in immediate formation of the diamagnetic iron pyrrolidine compound, (^{iPr}PDI)Fe(NHC_4H_8) (**1-(NHC$_4$H$_8$)**), with loss of dinitrogen (Figure 5.11). The benzene-d_6 ^{1}H NMR spectrum of **1-(NHC$_4$H$_8$)** displays resonances shifted by temperature independent paramagnetism. Allowing **1-(NHC$_4$H$_8$)** to stand in solution at 23 °C produced no change. Because the pyrrolidine ligand may not have sufficient ring strain to induce N-H group loss, aziridine chemistry was then explored.

Treatment of a pentane solution of **1-(N$_2$)$_2$** with cyclohexene imine (7-azabicyclo[4.1.0]heptane) at 23 °C resulted in quantitative formation of the

diamagnetic iron aziridine compound, (^{iPr}PDI)Fe((NHC$_6$H$_{10}$) (**1-(NHC$_6$H$_{10}$)**) (Figure 5.11). As observed with other amine coordination compounds,[17] the benzene-d_6 ^{1}H NMR spectrum of **1-(NHC$_6$H$_{10}$)** displays resonances shifted by temperature independent paramagnetism.[15] Although allowing a benzene-d_6 solution of **1-(NHC$_6$H$_{10}$)** to stand at 23 °C for several days produced no change, heating the solution at 65 °C for 24 hours led to the formation of a mixture of iron species. Examination of the volatile reaction products showed formation of ammonia and cyclohexene in an ~ 3:4 ratio. This suggests that upon heating, **1-(NHC$_6$H$_{10}$)** undergoes loss of cyclohexene to furnish the parent iron imide, which is likely thermally unstable. Thus, aziridines seem to display similar N-H group transfer chemistry to Hdbabh upon heating, although the iron products that are generated decompose under the reaction conditions.

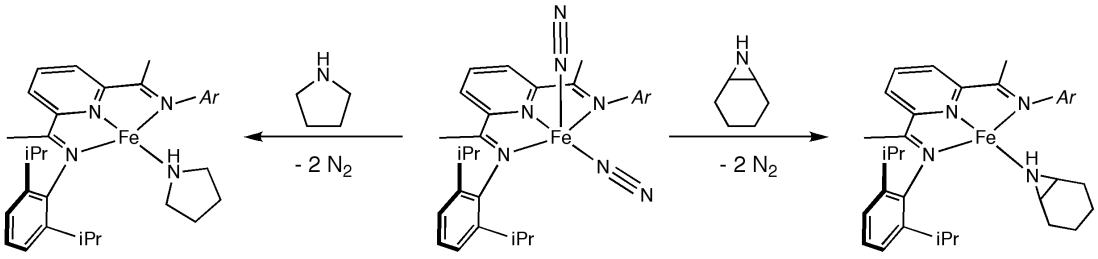

Figure 5.11 Addition of cyclic amines to **1-(N$_2$)$_2$** to probe N-H group transfer.

The observed group transfer from Hdbabh also prompted investigation into use of [dbabh] and anthracene elimination as a scaffold for other group transfer reactions. Cummins and coworkers have shown that NC(dbabh) can participate in NCN group transfer to complexes of molybdenum, vanadium and uranium.[30] In most cases formation of a bridging NCN dimer is observed, however when bulky ligands are employed the terminal cyanoimide compound can be isolated.[31] Another attractive application for such group transfer is the synthesis of iron imides with small alkyl

groups. Previous attempts to prepare iron imide complexes from alkyl azides with small alkyl groups, such as benzyl, resulted in formation of the tetrazole species instead.[32] Thus, $PhCH_2$(dbabh) was explored in an effort to prepare the benzyl imide compound, (^{iPr}PDI)FeN(CH_2Ph). However, treatment of a benzene-d_6 solution of **1-$(N_2)_2$** with one equivalent of $PhCH_2$(dbabh) produced no change, even after allowing the solution to stand for one week at 23 °C. Heating the solution at 45 °C for 24 hours did not lead to formation of any new iron species. The lack of reactivity is likely due to steric hindrance about the $PhCH_2$(dbabh) nitrogen, preventing interaction with the iron center.

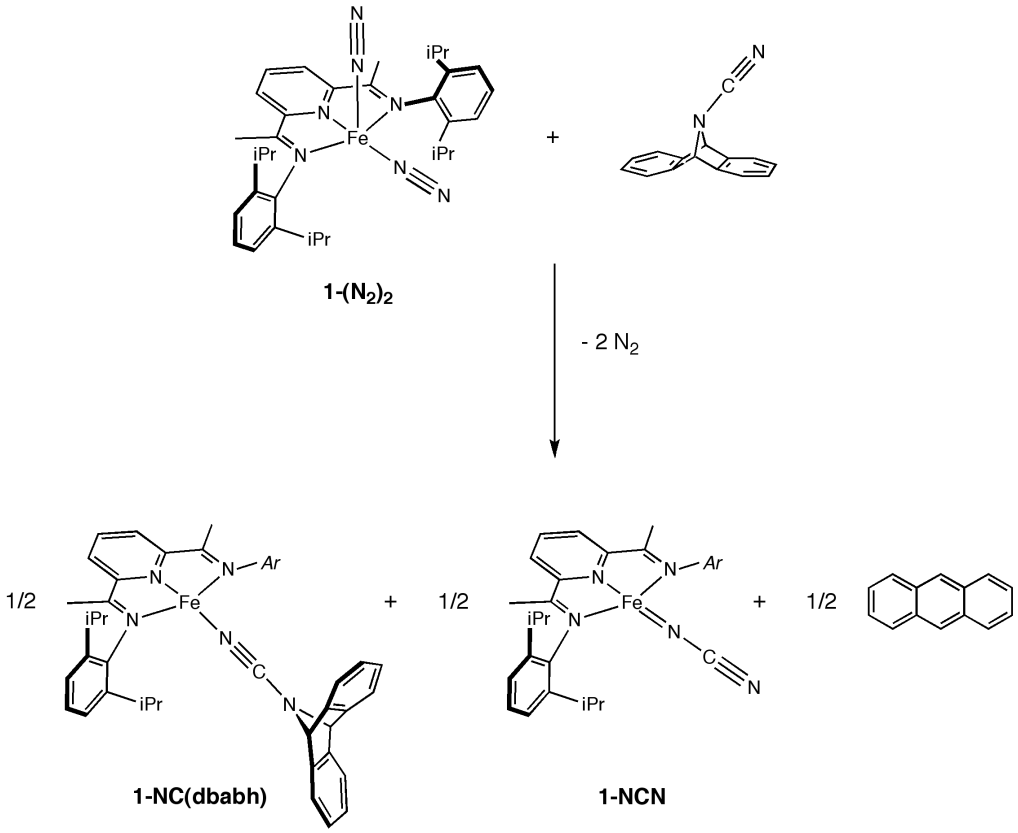

Figure 5.12 NCN group transfer to **1-$(N_2)_2$** to give a terminal iron cyanoimide.

Based on the lack of reactivity of $PhCH_2$(dbabh), the less bulky NC(dbabh) was explored. Treatment of a pentane solution of **1-$(N_2)_2$** with NC(dbabh) at 23 °C

resulted in formation of the diamagnetic iron cyanamide compound, (^{iPr}PDI)Fe(NC(dbabh)) (**1-NC(dbabh)**), another paramagnetic iron species and anthracene (Figure 5.12). The paramagnetic species is tentatively assigned as the terminal cyanoimide, (^{iPr}PDI)Fe(NCN) **(1-NCN**). In addition, the amount of anthracene generated was approximately equal to the amount of **1-NC(dbabh)** formed, indicating the two iron products are formed in an ~ 1:1 ratio. Allowing a benzene-d_6 solution of the product mixture to stand at 23 °C for 48 hours produced no appreciable change in the product ratio, suggesting that **1-NC(dbabh)** is not an intermediate in the formation of **1-NCN**.

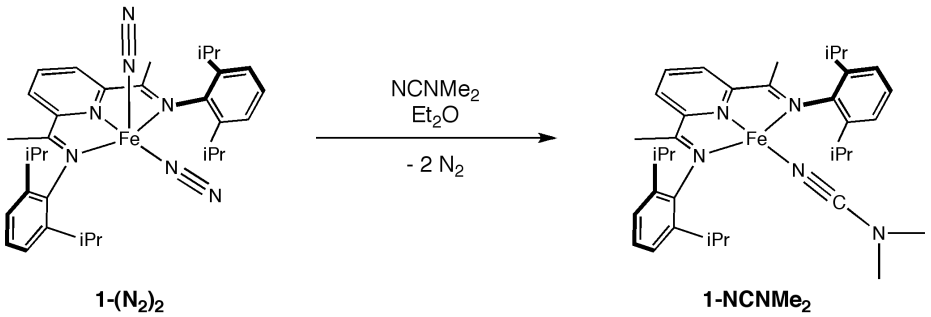

Figure 5.13 Preparation of **1-NCNMe$_2$**.

Although attempts to separate the two products were unsuccessful, **1-NC(dbabh)** was characterized by analogy to the dimethyl cyanamide complex, (^{iPr}PDI)Fe(NCNMe$_2$) (**1-NCNMe$_2$**), which was prepared by treating **1-(N$_2$)$_2$** with dimethyl cyanamide (Figure 5.13). Both iron cyanamide compounds, **1-NC(dbabh)** and **1-NCNMe$_2$**, exhibit spectroscopic data typical of intermediate-spin neutral ligand bis(imino)pyridine compounds.[17] The benzene-d_6 ^{1}H NMR spectra exhibit resonances shifted by temperature independent paramagnetism. Another notable feature is the NCN stretch in the IR spectrum (toluene), which appears as a sharp, albeit weak, peak at slightly lower energy than the free cyanamide. This is consistent with an iron

cyanamide coordination compound where the NCN bond is relatively unperturbed by the metal center.

While positive identification of the paramagnetic species generated in the reaction was not feasible without a solid state structure, a reasonable assignment can be made based on spectroscopy and the stoichiometry of the reaction. The formation of anthracene suggests there is transfer of the NCN group from NC(dbabh) to the metal center to give either the terminal or bridging cyanoimide compound. The IR spectrum (toluene) exhibits an intense stretch at 2175 cm^{-1}, consistent with either a terminal or bridging cyanoimide species.[30,31] In order to probe whether the product is a monomer or a dimer, half of an equivalent of NC(dbabh) was added to a solution of **1-$(N_2)_2$** in diethyl ether at 23 °C. Analysis of the product mixture by ^{1}H NMR spectroscopy showed formation of **1-NC(dbabh)**, the paramagnetic iron species and anthracene as before, along with unreacted **1-$(N_2)_2$**. The amount of remaining **1-$(N_2)_2$** was approximately equal to the amount of **1-NC(dbabh)** and anthracene combined, indicating that half an equivalent of **1-$(N_2)_2$** remained. This suggests that only one metal center is needed for formation of each product, leading to assignment of the paramagnetic product as the terminal cyanoimide, **1-NCN**.

5.6 Conclusions

The bis(dinitrogen) compound, **1-$(N_2)_2$**, is competent for hydrazine disproportionation into NH_3, N_2 and H_2. Capture of NH_3 by the iron center resulted in formation of the iron ammonia compound, **1-NH_3**. Similar to other neutral amine compounds, **1-NH_3** exhibits temperature independent paramagnetism and is best described as intermediate-spin iron(II) antiferromagnetically coupled to a triplet diradical bis(imino)pyridine chelate. **1-$(N_2)_2$** was also shown to be competent for N-H bond cleavage of Hdbabh, resulting in formation of both **1-NH_3** and **1-dbabh**. These

products are purportedly generated by initial formation of the parent iron imide followed by hydrogen abstraction to furnish **1-NH$_3$**. Subsequent [dbabh] radical capture by **1-(N$_2$)$_2$** occurs to form **1-dbabh**. Isotopic labeling studies and investigation of the iron aziridine compound, **1-NHC$_6$H$_{10}$**, support this mechanism. Analogous to **1-Cl**, **1-dbabh** is best described a as high-spin iron(II) center antiferromagnetically coupled to a singly reduced bis(imino)pyridine chelate to give an overall $S = 3/2$ molecule. Additional attempts to synthesize an iron amide species were unsuccessful. Further exploration of the [dbabh] scaffold resulted in formation of the putative terminal cyanoimide complex, **1-NCN**.

5.7 Experimental Procedures

General Considerations. All air- and moisture-sensitive manipulations were carried out using standard vacuum line, Schlenk, and cannula techniques or in an MBraun inert atmosphere dry box containing an atmosphere of purified nitrogen. Solvents for air- and moisture-sensitive manipulations were initially dried and deoxygenated using literature procedures.[33] Hydrogen and deuterium gas were passed through a column containing manganese oxide supported on vermiculite and 4 Å molecular sieves before admission to the high vacuum line. Benzene-d_6 was purchased from Cambridge Isotope Laboratories and dried over 4 Å molecular sieves. Anhydrous ammonia was purchased from Air Gas, dried over 4 Å molecular sieves and passed through a liquid nitrogen trap before use. Hydrazine was purchased from Acros and dried over 4 Å molecular sieves before use. Pyrrolidine was purchased from Aldrich and dried over calcium hydride before use. The complexes **1-Cl$_2$**,[34] **1-(N$_2$)$_2$**,[35] **1-Cl**,[25] Li[dbabh],[19] NC(dbabh),[30] Hdbabh[36] and cyclohexene imine[37] were prepared according to literature procedures. D(dbabh) was prepared by addition of Li[dbabh] to D_2O. The resulting precipitate was collected by filtration and washed with ice water to obtain the desired

reagent as an off-white solid. Li[NC_4H_8] was prepared by deprotonation of the respective amine with ^{n}BuLi (1.6 M in hexanes) in a solution of diethyl ether. The resulting precipitate was collected by filtration and washed with pentane to obtain the desired reagent as a white solid. The deuterated bis(imino)pyridine ligand, 2,6-(2,6-$^{i}Pr_2$-C_6H_3N=CMe)$_2C_5H_3N$-*d*$_6$ (^{iPr}PDI-*d*$_6$) was prepared according to the literature method.[38] The labeled dinitrogen complex, **1**-$(N_2)_2$**, was prepared following the procedure for **1-$(N_2)_2$** using ^{iPr}PDI-*d*$_6$.[35]

^{1}H NMR spectra were recorded on Varian Mercury 300, Inova 400, and 500 spectrometers operating at 299.76, 399.78, and 500.62 MHz, respectively. All ^{1}H chemical shifts are reported relative to $SiMe_4$ using the ^{1}H (residual) shift of the solvent as a secondary standard. Solution magnetic moments were determined by Evans method[39] using a ferrocene standard and are the average value of at least two independent measurements. Gouy balance measurements were performed with a Johnson Matthey instrument that was calibrated with $HgCo(SCN)_4$. Peak width at half height is given for paramagnetically broadened resonances. Infrared spectra were collected on a Thermo Nicolet spectrometer. Elemental analyses were performed at Robertson Microlit Laboratories, Inc., in Madison, NJ.

Single crystals suitable for X-ray diffraction were coated with polyisobutylene oil in a drybox, transferred to a nylon loop and then quickly transferred to the goniometer head of a Bruker X8 APEX2 diffractometer equipped with a molybdenum X-ray tube (λ = 0.71073 Å). Preliminary data revealed the crystal system. A hemisphere routine was used for data collection and determination of lattice constants. The space group was identified and the data were processed using the Bruker SAINT+ program and corrected for absorption using SADABS. The structures were solved using direct methods (SHELXS) completed by subsequent Fourier synthesis and refined by full-matrix least-squares procedures.

SQUID magnetization data of powdered samples were recorded with a SQUID magnetometer (Quantum Design) at 10 kOe between 5 and 300 K for all samples. Values of the magnetic susceptibility were corrected for the underlying diamagnetic increment by using tabulated Pascal constants and the effect of the blank sample holders (gelatin capsule/straw). Samples used for magnetization measurement were recrystallized multiple times and checked for chemical composition by ^{1}H NMR spectroscopy. The program julX written by E. Bill was used for (elements of) the simulation and analysis of magnetic susceptibiltiy data.[40]

^{57}Fe Mössbauer spectra were recorded on a WissEl Mössbauer spectrometer (MRG-500) at 77 K in constant acceleration mode. ^{57}Co/Rh was used as the radiation source. WinNormos for Igor Pro software was used for the quantitative evaluation of the spectral parameters (leastsquares fitting to Lorentzian peaks). The minimum experimental line widths were 0.23 mm s^{-1}. The temperature of the samples was controlled by an MBBC-HE0106 MÖSSBAUER He/N_2 cryostat within an accuracy of ±0.3 K. Isomer shifts were determined relative to α-iron at 298 K.

Preparation of (^{iPr}PDI)Fe(NH_3) (1-NH_3). A 100-mL round-bottom flask fitted with a needle valve was charged with 0.148 g (0.250 mmol) **1-(N_2)$_2$** and approximately 30 mL of pentane. The flask was submerged in liquid nitrogen and degassed, then a slight excess of anhydrous ammonia (2 equivalents) was added by gas bulb. The flask was warmed to room temperature, accompanied by a rapid color changed to red-brown. The reaction mixture was stirred one hour, then volatiles were removed to yield a dark brown solid. Recrystallization from diethyl ether at -35 °C yielded 0.107 g (75 %) of a red-brown powder identified as **1-NH_3**. Analysis for $C_{33}H_{46}N_4Fe$: Calc. C, 71.50; H, 8.40; N, 10.10. Found C, 71.19; H, 8.65; N, 9.92. ^{1}H NMR (benzene-d_6): δ = -5.83 (s, 6H, C(CH_3)), -0.52 (d, 6.6 Hz, 12H, CH(CH_3)$_2$), 1.22 (d, 6.6 Hz, 12H, CH(CH_3)$_2$),

2.65 (septet, 6.6 Hz, 4H, C*H*(CH_3)$_2$), 3.14 (s, 3H, N*H*$_3$), 7.23 (d, 7.8 Hz, 4H, *m-aryl*), 7.64 (t, 7.8 Hz, 2H, *p-aryl*), 8.70 (t, 8.4 Hz, 1H, *p-pyridine*), 11.84 (d, 8.4 Hz, 2H, *m-pyridine*). ^{13}C {^{1}H} NMR (benzene-d_6): δ = 23.48 (CH(*C*H_3)$_2$), 23.96 (CH(*C*H_3)$_2$), 28.25 (*C*H(CH_3)$_2$), 38.90 (C(*C*H_3), 103.22 (*m-pyridine*), 124.07 (*m-aryl*), 124.97 (*p-aryl*), 136.43 (*p-pyridine*), 138.73, 163.25, 164.15, 187.95. IR (KBr): ν_{NH} = 3340 cm^{-1}.

Preparation of (^{iPr}PDI)Fe(dbabh) (1-dbabh). A 20 mL scintillation vial was charged with 0.094 g (0.164 mmol) of bright green **1-Cl** and approximately 15 mL of diethyl ether. The solution was cooled to -35 ºC and 0.045 g (0.164 mmol) of white Li[dbabh] was added with a spatula. The reaction mixture was stirred for 12 hours, over which time there was a gradual color change to red-brown. The solution was filtered through Celite, and volatiles were removed to give a dark red-brown solid. Recrystallization from diethyl ether/pentane at -35 °C yielded 0.087 g (73 %) of dark red-brown crystals identified as **1-dbabh**. Analysis for $C_{47}H_{53}N_4Fe$: Calc. C, 77.34; H, 7.32; N, 7.68. Found C, 76.86; H, 7.29; N, 7.58. ^{1}H NMR (benzene-d_6): δ = -233.76 (190.8 Hz, 6H, C(C*H*$_3$)), -130.17 (454.3 Hz, 4H, C*H*(CH_3)$_2$), -53.85 (181.1 Hz, 12H, CH(C*H*$_3$)$_2$), -24.69 (52.8 Hz, 12H, CH(C*H*$_3$)$_2$), -17.09 (41.6 Hz, 2H, *p-aryl*), -10.28 (47.5 Hz, 4H, *m-aryl*), 24.74 (40.6 Hz, 2H, *m-pyridine* or *dbabh*), 38.43 (72.2 Hz, 2H, *dbabh*), 84.75 (102.6 Hz, 2H, *m-pyridine* or *dbabh*), 164.88 (500.3 Hz, 1H, *p-pyridine*).

Addition of H(dbabh) to ^{iPr}PDIFe(N_2)$_2$. A 20 mL scintillation vial was charged with 0.050 g (0.084 mmol) of dark green **1-(N_2)$_2$** and approximately 10 mL of diethyl ether. To the stirring solution was added 0.016 g (0.084 mmol) of 2,3:5,6-dibenzo-7-azabicyclo[2.2.1]hepta-2,5-diene (Hdbabh). An immediate color change to dark reddish-brown was observed. The solution was stirred for 30 minutes and the volatiles

were removed to yield a dark reddish-brown powder, which was shown by ^{1}H NMR and Mössbauer spectroscopy to be a mixture of **1-dbabh** and **1-NH$_3$**.

Addition of D(dbabh) to 1-(N$_2$)$_2$. A J. Young NMR tube was charged with 0.016 g (0.027 mmol) of **1-(N$_2$)$_2$** and approximately 0.5 mL of benzene-*d$_6$*. To the tube was added 0.005 g (0.027 mmol) of deutero-2,3:5,6-dibenzo-7-aza bicyclo[2.2.1]hepta-2,5-diene (Ddbabh), resulting in an immediate color change to dark reddish-brown. ^{1}H NMR spectroscopy established absence of the NH_3 peak of **1-ND$_3$** while the corresponding ND_3 peak was observed by ^{2}H NMR spectroscopy.

Preparation of (^{iPr}PDI)Fe(NHC$_4$H$_8$) (1-NHC$_4$H$_8$). A 20 mL scintillation vial was charged with 0.047 g (0.079 mmol) of **1-(N$_2$)$_2$** and approximately 10 mL of pentane. To the dark green solution was added 7.3 μL (0.079 mmol) of pyrrolidine resulting in a color change from dark green to red-brown. The reaction mixture was stirred for 30 minutes after which time the solution was concentrated and cooled to –35 ºC to yield 0.031 g (64 %) of a red-brown powder identified as **1-(NHC$_4$H$_8$)**. Analysis for $C_{37}H_{52}N_4Fe$: Calc. C, 73.00; H, 8.61; N, 9.20. Found C, 72.80; H, 8.61; N, 9.33. ^{1}H NMR (benzene-*d$_6$*): δ = -6.72 (s, 6H, C(C*H$_3$*)), 0.06 (d, 12H, CH(C*H$_3$*)$_2$), 1.06 (m, 2H, *pyrr*), 1.16 (m, 2H, *pyrr*), 1.25 (d, 12H, CH(C*H$_3$*)$_2$), 1.30 (m, 2H, *pyrr*), 1.36 (m, 2H, *pyrr*), 2.25 (quintet, C*H*(CH$_3$)$_2$), 7.23 (d, 4H, *m-aryl*), 7.66 (t, 2H, *p-aryl*), 8.77 (s, 2H, N*H*), 8.82 (t, 1H, *p-pyridine*), 12.79 (d, 2H, *m-pyridine*). ^{13}C {^{1}H} NMR (benzene-*d$_6$*): δ = 23.18 (CH(*C*H$_3$)$_2$), 24.52 (CH(*C*H$_3$)$_2$), 28.68 ((*C*H(CH$_3$)$_2$), 41.29 (C(*C*H$_3$)), 47.90 (NH*C*H$_2$), 102.67 (*m-pyridine*), 124.28 (*m-aryl*), 125.27 (*p-aryl*), 135.62, 144.14, 166.14, 193.53, two resonances not located. IR (KBr): ν_{NH} = 3219 cm^{-1}.

Preparation of ^{iPr}PDIFe(NHC$_6$H$_{10}$) (1-NHC$_6$H$_{10}$). A 20 mL scintillation vial was charged with 0.050 g (0.084 mmol) of **1-(N$_2$)$_2$** and approximately 10 mL of diethyl ether. With stirring, cyclohexene imine (0.008 g, 0.084 mmol) was added to the vial by microsyringe inducing an immediate color change to red-brown. The reaction mixture was stirred for 30 minutes, then the solution was concentrated and chilled to -35 °C to yield 0.047 g (88 %) of a dark red-brown powder identified as **1-NHC$_6$H$_{10}$**. Analysis for $C_{39}H_{54}N_4Fe$: Calc. C, 73.80; H, 8.57; N, 8.83. Found C, 74.19; H, 8.60; N, 8.93. ^{1}H NMR (benzene-*d$_6$*): δ = -6.41 (s, 6H, C(C*H$_3$*)), -0.25 (d, 6.2 Hz, 12H, CH(C*H$_3$*)$_2$), 0.81 (m, 4H, *aziridine*), 1.16 (d, 6.2 Hz, 12H, CH(C*H$_3$*)$_2$), 1.38 (m, 4H, *aziridine*), 1.63 (m, 2H, *aziridine*), 2.74 (quintet, 6.2 Hz, 4H, C*H*(CH$_3$)$_2$), 4.71 (s, 1H, N*H*), 7.24 (d, 7.3 Hz, 4H, *m-aryl*), 7.64 (t, 7.3 Hz, 2H, *p-aryl*), 8.77 (t, 7.2 Hz, 1H, *p-pyridine*), 12.52 (d, 7.2 Hz, 2H, *m-pyridine*). ^{13}C {^{1}H} NMR (benzene-*d$_6$*): δ = 19.57 (*aziridine*), 22.89 (CH(*C*H$_3$)$_2$ or *aziridine*), 23.24 (CH(*C*H$_3$)$_2$ or *aziridine*), 24.02 (CH(*C*H$_3$)$_2$), 28.93 ((*C*H(CH$_3$)$_2$), 34.79 (NH*C*H), 39.51 (C(*C*H$_3$)), 102.18 (*m-pyridine*), 124.29 (*m-aryl*), 125.14 (*p-aryl*), 135.91 (*p-pyridine*), 142.22, 165.41, 166.18, 191.18. IR (KBr): ν_{NH} = 3257 cm^{-1}.

Preparation of (^{iPr}PDI)Fe(NCNMe$_2$) (1-NCNMe$_2$). A 20 mL scintillation vial was charged with 0.060 g (0.101 mmol) of **1-(N$_2$)$_2$** and approximately 10 mL of pentane. Upon addition of 8.5 μL (0.111 mmol) of dimethyl cyanamide via microsyringe, there was an immediate color change to red. The reaction mixture was stirred for 30 minutes, then the solution was concentrated and chilled to -35 °C to yield 0.053 g (87 %) of a dark red powder identified as **1-NCNMe$_2$**. Analysis for $C_{36}H_{49}N_5Fe$: Calc. C, 71.16; H, 8.13; N, 11.52. Found C, 70.77; H, 8.16; N, 11.12. ^{1}H NMR (benzene-*d$_6$*): δ = -4.66 (s, 6H, C(C*H$_3$*)), -0.18 (d, 6.5 Hz, 12H, CH(C*H$_3$*)$_2$), 1.34 (d, 6.5 Hz, 12H, CH(C*H$_3$*)$_2$), 1.87 (s, 6H, N(C*H$_3$*)$_2$), 3.07 (septet, 6.5 Hz, 4H, C*H*(CH$_3$)$_2$), 7.32 (d, 7.4

Hz, 4H, *m-aryl*), 7.57 (t, 7.4 Hz, 2H, *p-aryl*), 8.97 (t, 7.5 Hz, 1H, *p-pyridine*), 11.21 (d, 7.5 Hz, 2H, *m-pyridine*). ^{13}C {^{1}H} NMR (benzene-d_6): δ = 23.83 (CH(*C*H_3)$_2$), 24.11 (CH(*C*H_3)$_2$), 29.01 (*C*H(CH$_3$)$_2$), 36.65 (C(*C*H$_3$)), 103.65 (*m-pyridine*), 123.43 (*m-aryl*), 124.16 (*p-aryl*), 136.67, 138.52 (*p-pyridine*), 164.45, 165.67, 180.52, one resonance not located. IR (tol): ν_{NCN} = 2209 cm^{-1}.

Addition of NC(dbabh) to (^{iPr}PDI)Fe(N$_2$)$_2$. A 20 mL scintillation vial was charged with ~15 mL of diethyl ether and 0.081 g (0.136 mmol) **1-(N$_2$)$_2$**. NC(dbabh) (0.030 g, 0.136 mmol) was added by spatula, and there was a rapid color change to dark red-brown. The reaction was stirred 30 minutes, then the solution was concentrated and cooled to -35 °C to yield a dark red-brown powder identified as a mixture of **(^{iPr}PDI)Fe(NC(dbabh))** and **(^{iPr}PDI)Fe(NCN)**.

Characterization of 1-NC(dbabh). ^{1}H NMR (benzene-d_6): δ = -5.24 (s, 6H, C(C*H*$_3$)), -0.55 (d, 6.6 Hz, 12H, CH(C*H*$_3$)$_2$), 1.24 (d, 6.6 Hz, 12H, CH(C*H*$_3$)$_2$), 2.81 (septet, 6.6 Hz, 4H, C*H*(CH$_3$)$_2$), 5.39 (s, 1H, *dbabh*), 5.77 (s, 1H, *dbabh*), 6.30 (br s, 2H, *dbabh*), 6.70 (m, 4H, *dbabh*), 6.89 (m, 2H, *dbabh*), 7.25 (d, 7.6 Hz, 4H, *m-aryl*), 7.75 (t, 7.6 Hz, 2H, *p-aryl*), 8.67 (t, 7.5 Hz, 1H, *p-pyridine*), 12.11 (d, 7.5 Hz, 2H, *m-pyridine*). IR (tol): ν_{NCN} = 2280 cm^{-1}.

Characterization of 1-NCN. ^{1}H NMR (benzene-d_6): δ = -101.88 (243.8 Hz, 6H, C(C*H*$_3$)), -45.35 (574.6 Hz, 4H, C*H*(CH$_3$)$_2$), -13.72 (233.4 Hz, 12H, CH(C*H*$_3$)$_2$), -8.93 (140.0 Hz, 12H, CH(C*H*$_3$)$_2$), -7.20 (81.7 Hz, 2H, *p-aryl*), -1.06 (133.0 Hz, 4H, *m-aryl*), 46.26 (135.8 Hz, 2H, *m-pyridine*), 207.44 (283.9 Hz, 1H, *p-pyridine*). IR (tol): ν_{NCN} = 2175, 1275 cm^{-1}.

Preparation of (^{iPr}PDEA)Fe(NHC$_4$H$_8$) (2-NHC$_4$H$_8$). A 20 mL scintillation vial was charged with 0.084 g (0.142 mmol) of **1-Cl$_2$** and approximately 15 mL of

tetrahydrofuran. To the vial, 0.022 g (0.286 mmol) of Li[NC_4H_8] was added slowly by spatula. There was an immediate color change from green to brown. The reaction mixture was stirred for 30 minutes after which time the volatiles were removed to yield a green-brown solid. The solid was extracted into diethyl ether, filtered through Celite and recrystallized at -35 °C to yield 0.036 g (43 %) of a dark green powder identified as **(^{iPr}PDEA)Fe(NHC$_4$H$_8$)**. Analysis for $C_{37}H_{50}N_4Fe$: Calc. C, 73.25; H 8.31,; N, 9.24. Found C, 72.76; H, 7.92; N, 8.91. Magnetic susceptibilty (benzene-*d_6*, 293 K): μ_{eff} = 4.1(1) μ_B. ^{1}H NMR (benzene-*d_6*): δ = - 49.13 (71.5 Hz, 2H, C=C*H_2*), -39.22 (80.7 Hz, 2H, C=C*H_2*), -22.78 (111.2 Hz, 12H, CH(C*H_3*)$_2$), -19.13 (42.3 Hz, 1H, *p-pyridine*), -6.43 (35.8 Hz, 2H), 0.14 (9.0 Hz, 2H), 1.39 (16.4 Hz, 4H), 2.26 (5.7 Hz, 2H), 3.54 (16.3 Hz, 4H), 16.04 (46.8 Hz, 12H, CH(C*H_3*)$_2$), 45.07 (41.7 Hz, 4H), 108.5 (49.1 Hz, 2H), N*H* not located. IR (KBr): ν_{NH} = 3219 cm^{-1}, ν_{CC} = 1587 cm^{-1}**.**

Toepler Pump Experiment for Addition of N_2H_4 to (^{iPr}PDI)Fe(N_2)$_2$. A small glass ampoule was charged with 3.7 μL (0.132 mmol) N_2H_4 and 0.5 mL toluene, and flame-sealed under vacuum at -78 °C. A thick-walled glass vessel was charged with 0.039 g (0.066 mmol) **1-(N_2)$_2$**, the glass ampoule and a stir bar. Approximately 15 mL of diethyl ether was vacuum transferred into the vessel at -78 °C. The reaction mixture was let warm to room temperature and the glass ampoule inside the vessel was broken with stirring. There was an immediate color change to dark brown concomitant with liberation of a mixture of dihydrogen and dinitrogen. The gas mixture was collected with a Toepler pump into a volume of 43.7 mL. After 1.5 h, 52 Torr (1.9 eq.) of gas was collected. The gas mixture was cycled through a burn tube over 0.5 h; 14 Torr (0.5 eq.) of dihydrogen was burned, and 38 Torr (1.4 eq.) of dinitrogen was recollected over 1 h. The ^{1}H NMR spectrum of the dark brown solid remaining in the vessel confirmed formation of **1-NH$_3$**.

REFERENCES

[1] (a) Hoffmann, B. M.; Dean, D. R.; Seefeldt, L. C. *Acc. Chem. Res.* **2009**, *42*, 609. (b) Peters, J. C.; Mehn, M. P. In *Activation of Small Molecules*; Tolman, W. B., Ed.; Wiley: New York, 2006; pp 81-120.

[2] Fox, D. J.; Bergman, R. G. *J. Am. Chem. Soc.* **2003**, *125*, 8984-8985.

[3] Fox, D. J.; Bergman, R. G. *Organometallics* **2004**, *23*, 1656-1670.

[4] Brown, S. D.; Mehn, M. P.; Peters, J. C. *J. Am. Chem. Soc.* **2005**, *127*, 13146-13147.

[5] (a) Thorneley, R. N. F.; Eady, R. R.; Lowe, D. J. *Nature* **1978**, *272*, 557-558. (b) Dilworth, M. J.; Eady, R. R. *Biochem* **1991**, *277*, 465-468.

[6] (a) Barney, B. M.; Laryukhin, M.; Igarashi, R. Y.; Lee, H.; Dos Santos, P. C.; Yang, T.; Hoffman, B. M.; Dean, D. R.; Seefeldt, L. C. *Biochem.* **2005**, *44*, 8030-8037. (b) Barney, B. M.; Yang, T.; Igarashi, R. Y.; Dos Santos, P. C.; Laryukhin, M.; Lee, H.; Hoffman, B. M.; Dean, D. R.; Seefeldt, L. C. *J. Am. Chem. Soc.* **2005**, *127*, 14960-14961.

[7] (a) Goedken, V. L.; Peng, S.; Molin-Norris, J.; Park, Y. *J. Am. Chem. Soc.* **1976**, *98*, 8391-8400. (b) Sellmann, D.; Shaban, S. Y.; Heinemann, F. W. *Eur. J. Inorg. Chem.* **2004**, 4591-4601. (c) Crossland, J. L.; Zakharov, L. N.; Tyler, D. R. *Inorg. Chem.* **2007**, *46*, 10476-10478. (d) Field, L. D.; Li, H. L.; Dalgarno, S. J.; Turner, P. *Chem. Commun.* **2008**, 1680-1682. (e) Saouma, C. T.; Müller, P.; Peters, J. C. *J. Am. Chem. Soc.* **2009**, *131*, 10358-10359.

[8] Schmidt, E. *Hydrazine and its Derivatives: Preparation, Properties and Applications*; Wiley-Interscience: New York, 1984; pp 681-696.

[9] (a) Hozumi, Y.; Imasaka, Y.; Tanaka, K.; Tanaka, T. *Chem. Lett.* **1983**, 897-900. (b) Coucouvanis, D.; Demadis, K. D.; Malinak, S. M.; Mosier, P. E.; Tyson, M. A.; Laughlin, L. J. *J. Mol. Cat. A* **1996**, *107*, 123-135.

[10] Vieira, R.; Pham-Huu, C.; Keller, N.; Ledoux, M. J. *Chem. Commun.* **2002**, 954-955.

[11] Hendrich, M. P.; Gunderson, W.; Behan, R. K.; Green, M. T.; Mehn, M. P.; Betley, T. A.; Lu, C. C.; Peters, J. C. *PNAS* **2006**, *46*, 17107-17112.

[12] Minakata, S. *Acc. Chem. Res.* **2009**, *42*, 1172-1182.

[13] (a) Stokes, B. J.; Dong, H.; Leslie, B. E.; Pumphrey, A. L.; Driver, T. G. *J. Am.*

Chem. Soc. **2007**, *129*, 7500-7501. (b) Shen, M.; Leslie, B. E.; Driver, T. G. *Angew. Chem., Int. Ed.* **2008**, *47*, 5056-5059.

[14] Bart, S. C.; Bowman, A. C.; Lobkovsky, E.; Chirik, P. J. *J. Am. Chem. Soc.* **2007**, *129*, 7212-7213.

[15] Bart, S. C.; Chlopek, K.; Bill, E.; Bouwkamp, M. W.; Lobkovsky, E.; Neese, F.; Wieghardt, K.; Chirik, P. J. *J. Am. Chem. Soc.* **2006**, *128*, 13901-13912.

[16] Knijnenburg, Q.; Gambarotta, S.; Budzelaar, P. H. M. *Dalton Trans.* **2006**, 5442-5448.

[17] Bart, S. C.; Lobkovsky, E.; Bill, E.; Wieghardt, K.; Chirik, P. J. *Inorg. Chem.* **2007**, *46*, 7055-7063.

[18] Bart, S. C.; Lobkovsky, E.; Bill, E.; Chirik, P. J. *J. Am. Chem. Soc.* **2006**, *128*, 5302-5303.

[19] Mindiola, D. J.; Cummins, C. C. *Angew. Chem., Int. Ed.* **1998**, *37*, 945-947.

[20] Betley, T. A.; Peters, J. C. *J. Am. Chem. Soc.* **2004**, *126*, 6252-6254.

[21] (a) Meyer, K.; Mindiola, D. J.; Baker, T. A.; Davis, W. M.; Cummins, C. C. *Angew. Chem. Int. Ed.* **2000**, *39,* 3063-3066. (b) MacBeth, C. E.; Thomas, J. C.; Betley, T. A.; Peters, J. C. *Inorg. Chem.* **2004**, *43*, 4645-4662. (c) Lu, C. C.; Peters, J. C. *Inorg. Chem.* **2006**, *45*, 8597-8607. (d) Adhikari, D.; Basuli, F.; Fan, H.; Huffman, J. C.; Pink, M.; Mindiola, D. J. *Inorg. Chem.* **2008**, *47*, 4439-4441.

[22] Crystals obtained by Dr. Suzanne Bart.

[23] Trovitch, R. J.; Ph.D. Thesis, Cornell University, 2009.

[24] Data collected with the assistance of Dr. Suzanne Bart.

[25] Bouwkamp, M. W.; Bart, S. C.; Hawrelak, E. J.; Trovitch, R. J.; Lobkovsky, E.; Chirik, P. J. *Chem. Commun.* **2005**, 3406-3408.

[26] See Chapter 3 of this work.

[27] Brown, S. D.; Peters, J. C. *J. Am. Chem. Soc.* **2004**, *126*, 4538-4539.

[28] (a) Eckert, N. A.; Vaddadi, S.; Stoian, S.; Lachicotte, R. J.; Cundari, T. R.; Holland, P. L. *Angew. Chem. Int. Ed.* **2006**, *45*, 6868-6871. (b) King, E. R.; Betley, T. A. *Inorg. Chem.* **2009**, *48*, 2361-2363. (c) See Chapter 2 of this work.

[29] Bouwkamp, M. W.; Lobkovsky, E.; Chirik, P. J. *Inorg. Chem.* **2006**, *45*, 2-4.

[30] Mindiola, D. J.; Tsai, Y.; Hara, R.; Chen, Q.; Meyer, K.; Cummins, C. C. *Chem. Commun.* **2001**, *1*, 125-126.

[31] Soo, H. S.; Figueroa, J. S.; Cummins, C. C. *J. Am. Chem. Soc.* **2004**, *126*, 11370-11376.

[32] See Chapter 4 of this work.

[33] Pangborn, A. B.; Giardello, M. A.; Grubbs, R. H.; Rosen, R. K.; Timmers, F. J. *Organometallics* **1996**, *15*, 1518-1520.

[34] Small, B. L.; Brookhart, M.; Bennett, A. M. A. *J. Am. Chem. Soc.* **1998**, *120*, 4049-4050.

[35] Bart, S. C.; Lobkovsky, E.; Chirik, P. J. *J. Am. Chem. Soc.* **2004**, *126*, 13794-13807.

[36] Carpino, L. A.; Padykula, R. E.; Barr, D. E.; Hall, F. H.; Krause, J. G.; Dufresne, R. F.; Thoman, C. J. *J. Org. Chem.* **1988**, *53*, 2565-2572.

[37] Fang, Y.; Jacobsen, E. N. *J. Am. Chem. Soc.* **2008**, *130*, 5660-5661.

[38] Clentsmith, G. K. B.; Gibson, V. C.; Hitchcock, P. B.; Kimberley, B. S.; Rees, C. W. *Chem. Commun.* **2002**, *14*, 1498-1499.

[39] Sur, S. K. *J. Magn. Reson.* **1989**, *82*, 169-173.

[40] http://ewww.mpi-muelheim.mpg.de/bac/logins/bill/julX_en.php.

APPENDIX A

COMPUTATIONAL DATA

Table A.1 Computed and experimental bond distances for bis(imino)pyridine cobalt dinitrogen complexes.

	$[1\text{-}N_2]^+$		$[1\text{-}N_2]$		$[1\text{-}N_2]^-$
	Calc. (Å)	**Exp. (Å)**[a]	**Calc. (Å)**	**Exp. (Å)**	**Calc. (Å)**
$Co\text{-}N_{pyr}$	1.844	1.812(3)	1.839	1.8084(14)	1.830
$Co\text{-}N_{imine}$	1.965	1.915(4)	1.932	1.8773(14)	1.920
$Co\text{-}N_{imine}$	1.964	1.908(3)	1.932	1.8719(15)	1.920
$Co\text{-}N_2$	1.853	1.841(3)	1.810	1.7884(16)	1.782
$N_{imine}\text{-}C_{imine}$	1.302 1.302	1.303(5) 1.303(5)	1.337 1.337	1.341(2) 1.331(2)	1.368 1.368
$C_{imine}\text{-}C_{ipso}$	1.479 1.479	1.458(5) 1.464(4)	1.443 1.443	1.418(2) 1.429(2)	1.417 1.418
$C_{ipso}\text{-}N_{pyr}$	1.347 1.347	1.354(4) 1.356(5)	1.368 1.367	1.379(2) 1.367(2)	1.389 1.389
N-N	1.102	1.112(5)	1.110	1.104(2)	1.122

[a]Gibson, V. C.; Humphries, M. J.; Tellmann, K. P.; Wass, D. F.; White, A. J. P.; Williams, D. J. *Chem. Commun.* **2001**, 2252-2253.

Table 2. Metal contributions (%) to frontier orbitals of $[1\text{-}N_2]^+$, $[1\text{-}N_2]$, and $[1\text{-}N_2]^-$.

	$[1\text{-}N_2]^+$	$[1\text{-}N_2]$	$[1\text{-}N_2]^-$
$d_{x2\text{-}y2}$	73	73	70
PDI a_2	6	12	12
PDI b_2	11	11	10
d_{z2}	92	88	89
d_{yz}	82	80	75
d_{xz}	79	73	72
d_{xy}	75	77	72

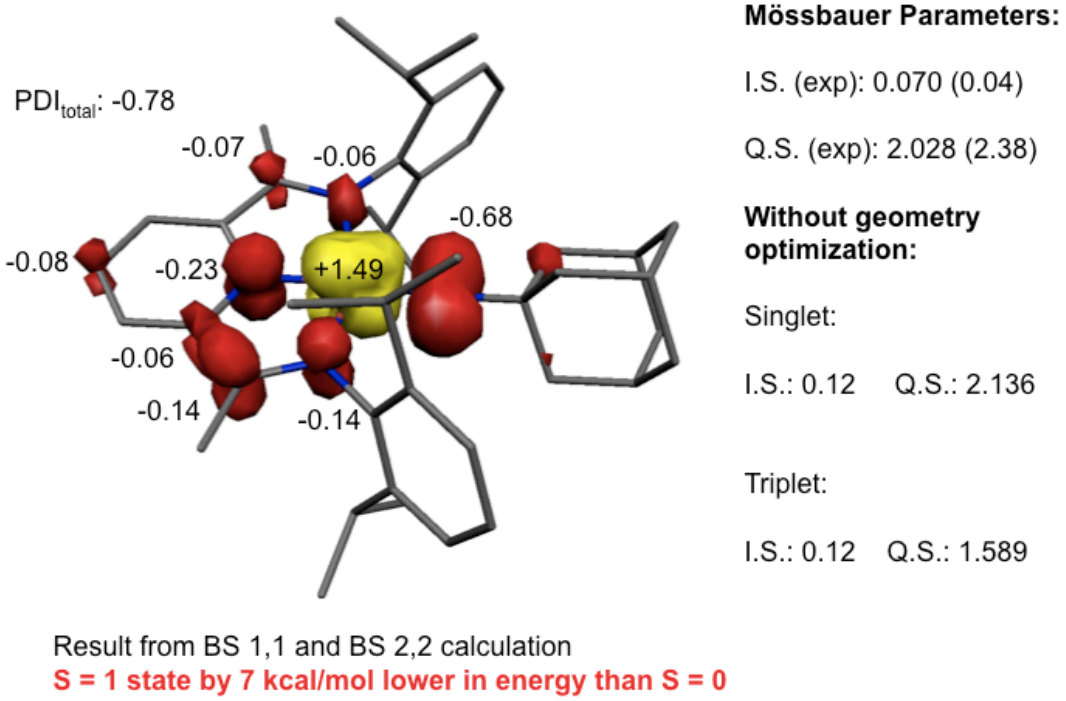

Figure A.1 Spin density plot and calculated Mössbauer parameters for **1-N(^{1}Ad)**

Table A.2 Summary of broken symmetry and Mössbauer calculations for **1-N(^{1}Ad)**.

Calculations			**Total Energy / Eh**[a)]	**I.S. / mms^{-1}**	**Q.S. / mms^{-1}**	**Fe=N / Å**
S = 1	Converge on the same solution	UKS 3	-3153.685222	0.262	1.026	1.726
		BS 3,1				
		BS 4,2				
		BS 5,3				
		BS 1,3				
	Fe=N bond fixed	UKS 3 const.	-3153.681452	0.189	0.967	1.648 f
S = 0	Converge on the same solution	BS 1,1	-3153.667817	0.070	-2.028	1.656
		BS 2,2				
Experimental				0.04	-2.36	1.648

Table A.3 Computed and experimental bond distances for **1-N(^{iPr2}Ph)**.

	Experimental (Å)	**Calculated (Å)**
$Fe\text{-}N_{imide}$	1.710	1.705
$Fe\text{-}N_{imine}$	1.987 2.034	1.978 1.997
$Fe\text{-}N_{pyr}$	1.840	1.824
$N_{imine}\text{-}C_{imine}$	1.331 1.320	1.349 1.347
$C_{imine}\text{-}C_{ipso}$	1.431 1.437	1.435 1.436
$C_{ipso}\text{-}N_{pyr}$	1.373 1.377	1.392 1.392

Table A.4 Computed and experimental bond distances for **1-N(^{1}Ad)**.

	Experimental (Å)	**Calculated (Å)**
$Fe\text{-}N_{imide}$	1.648	1.565
$Fe\text{-}N_{imine}$	1.932 1.932	1.956 1.956
$Fe\text{-}N_{pyr}$	1.895	1.893
$N_{imine}\text{-}C_{imine}$	1.340 1.340	1.353 1.354
$C_{imine}\text{-}C_{ipso}$	1.418 1.418	1.425 1.425
$C_{ipso}\text{-}N_{pyr}$	1.377 1.377	1.390 1.390

APPENDIX B

IRON AND COBALT K-EDGE XAS DATA

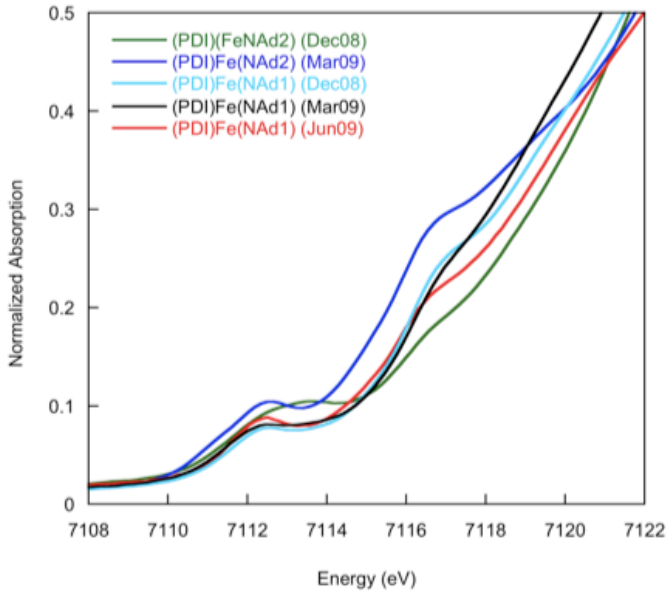

	1-Ad	**2-Ad**
Dec '08	7112.1 eV	7113.1 eV
Mar '09	7111.9 eV	7112.1 eV

Figure C.1 Bis(imino)pyridine iron imide XAS data.

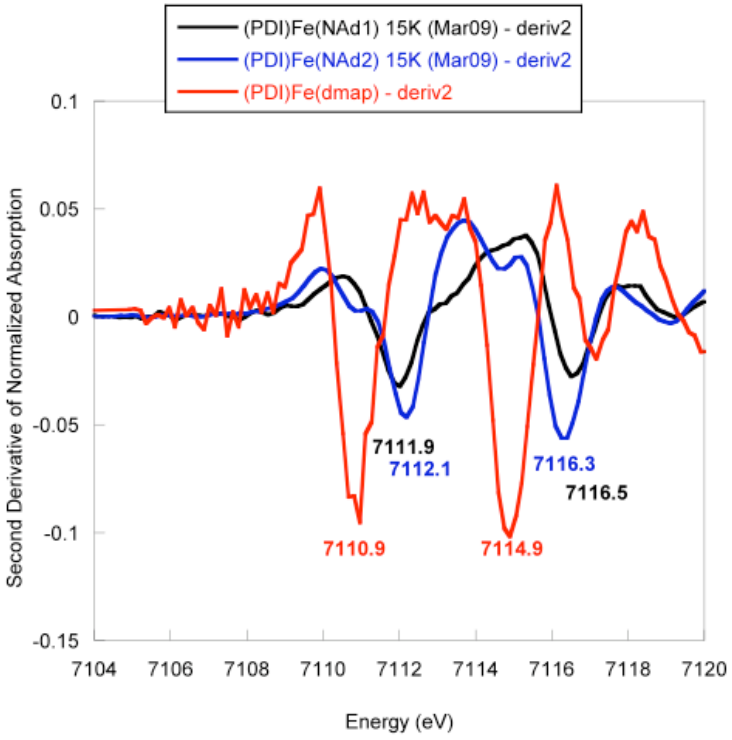

Figure C.2 Second-derivative of pre-edge area.

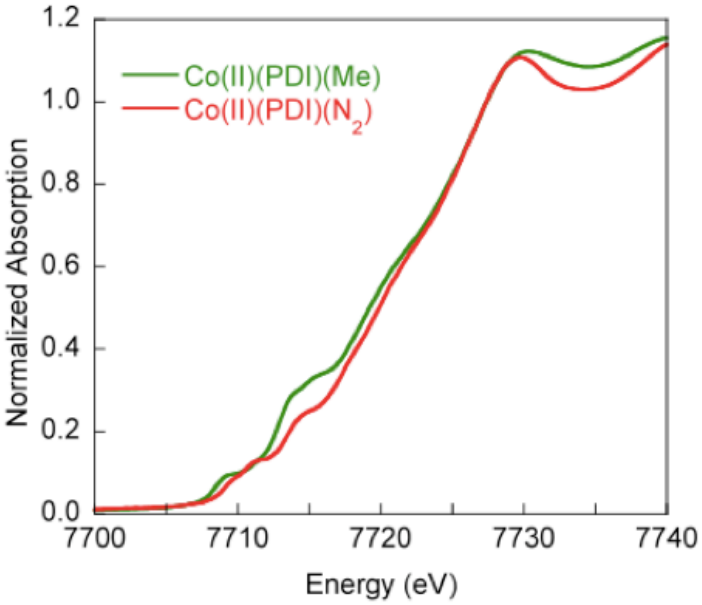

Figure C.3 Bis(imino)pyridine cobalt XAS data.

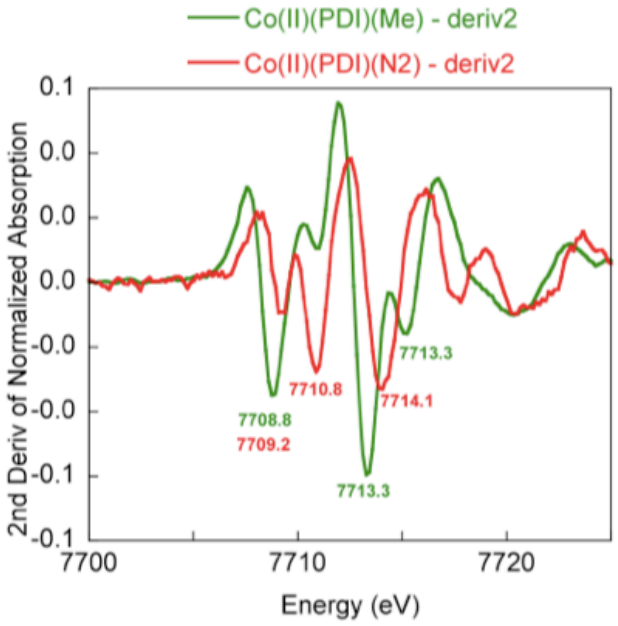

Figure C.4 Second derivative of XAS data.

APPENDIX C

CRYSTAL STRUCTURE DATA

Table C.1 Compilation of X-ray data for compounds discussed in this manuscript.

Compound	CU X-Ray ID	Location
1-N_2	acb13	Appendix C
(^{Cy}APDI)$_2$Co	acb16	Appendix C
5-Cl	acb17	Appendix C
5-Me	acb22	Appendix C
1-N(^{1}Ad)	acb3	Appendix C
1-N(^{Cy}Oct)	acb19	Appendix C
1-N(^{2}Ad)	acb26	Appendix C
2-NH_2^{1}Ad	acb5	Appendix C
1-N(^{1}Ad)CHC(SiMe_3)	acb7	Appendix C
1-[(N^{1}Ad)NN(N^{1}Ad)]	acb6	Appendix C
1-[(NBn)NN(NBn)]	acb4	Appendix C

Table C.2 Crystal data and structure refinement for **1-N_2**.

Identification code	acb13	
Empirical formula	C33 H43 Co N5	
Formula weight	568.65	
Temperature	173(2) K	
Wavelength	0.71073 Å	
Crystal system	Orthorhombic	
Space group	P2(1)2(1)2(1)	
Unit cell dimensions	a = 8.4360(12) Å	α= 90°.
	b = 17.851(3) Å	β= 90°.
	c = 20.117(3) Å	γ = 90°.
Volume	3029.5(8) Å^3	

Z	4
Density (calculated)	1.247 Mg/m^3
Absorption coefficient	0.596 mm^{-1}
F(000)	1212
Crystal size	0.45 x 0.25 x 0.20 mm^3
Theta range for data collection	2.28 to 28.53°.
Index ranges	-10<=h<=11, -23<=k<=23, -23<=l<=27
Reflections collected	21677
Independent reflections	7486 [R(int) = 0.0439]
Completeness to theta = 28.53°	99.1 %
Absorption correction	Semi-empirical from equivalents
Max. and min. transmission	0.8901 and 0.7753
Refinement method	Full-matrix least-squares on F^2
Data / restraints / parameters	7486 / 0 / 363
Goodness-of-fit on F^2	1.027
Final R indices [I>2sigma(I)]	R1 = 0.0416, wR2 = 0.0742
R indices (all data)	R1 = 0.0606, wR2 = 0.0806
Absolute structure parameter	0.688(9)
Largest diff. peak and hole	0.351 and -0.329 $e.Å^{-3}$

Table C.3 Atomic coordinates (x 10^4) and equivalent isotropic displacement parameters ($Å^2$x 10^3) for **1-N_2**. U(eq) is defined as one third of the trace of the orthogonalized U^{ij} tensor.

	x	y	z	U(eq)
Co(1)	1261(1)	4012(1)	8737(1)	20(1)
N(1)	614(2)	3241(1)	8167(1)	21(1)
N(2)	129(2)	3466(1)	9327(1)	18(1)
N(3)	1594(2)	4609(1)	9492(1)	19(1)
N(4)	2383(2)	4553(1)	8156(1)	31(1)
N(5)	3080(2)	4884(1)	7795(1)	54(1)
C(1)	-849(2)	2030(1)	8053(1)	32(1)
C(2)	-283(2)	2697(1)	8432(1)	22(1)

C(3)	-592(2)	2814(1)	9117(1)	20(1)
C(4)	-1459(2)	2397(1)	9574(1)	27(1)
C(5)	-1551(2)	2629(1)	10225(1)	28(1)
C(6)	-807(2)	3283(1)	10430(1)	24(1)
C(7)	43(2)	3701(1)	9973(1)	20(1)
C(8)	912(2)	4382(1)	10054(1)	20(1)
C(9)	1033(3)	4781(1)	10708(1)	31(1)
C(10)	1080(2)	3196(1)	7479(1)	22(1)
C(11)	153(2)	3556(1)	6999(1)	26(1)
C(12)	743(2)	3586(1)	6356(1)	31(1)
C(13)	2185(2)	3276(1)	6194(1)	32(1)
C(14)	3055(2)	2906(1)	6673(1)	31(1)
C(15)	2519(2)	2847(1)	7321(1)	24(1)
C(16)	-1431(2)	3907(1)	7166(1)	34(1)
C(17)	-2686(3)	3735(1)	6644(1)	49(1)
C(18)	-1292(3)	4749(1)	7257(1)	64(1)
C(19)	3493(2)	2428(1)	7836(1)	29(1)
C(20)	4068(3)	1666(1)	7583(1)	57(1)
C(21)	4881(3)	2889(1)	8071(1)	52(1)
C(22)	2542(2)	5280(1)	9484(1)	22(1)
C(23)	4189(2)	5210(1)	9527(1)	29(1)
C(24)	5090(2)	5859(1)	9474(1)	39(1)
C(25)	4403(3)	6541(1)	9388(1)	39(1)
C(26)	2781(3)	6606(1)	9343(1)	34(1)
C(27)	1810(2)	5970(1)	9396(1)	25(1)
C(28)	4998(2)	4462(1)	9634(1)	40(1)
C(29)	5539(3)	4388(1)	10357(1)	54(1)
C(30)	6385(3)	4339(1)	9164(1)	54(1)
C(31)	26(2)	6055(1)	9336(1)	31(1)
C(32)	-635(3)	6621(1)	9831(1)	39(1)
C(33)	-441(3)	6272(1)	8634(1)	54(1)

Table C.4 Bond lengths [Å] and angles [°] for **1-N_2**.

Co(1)-N(4)	1.7884(16)	C(8)-N(3)-Co(1)	116.65(11)
Co(1)-N(2)	1.8084(14)	C(22)-N(3)-Co(1)	123.17(11)
Co(1)-N(1)	1.8719(15)	N(5)-N(4)-Co(1)	179.55(19)
Co(1)-N(3)	1.8773(14)	N(1)-C(2)-C(3)	112.59(16)
N(1)-C(2)	1.341(2)	N(1)-C(2)-C(1)	123.66(16)
N(1)-C(10)	1.442(2)	C(3)-C(2)-C(1)	123.72(16)
N(2)-C(7)	1.367(2)	N(2)-C(3)-C(4)	118.80(16)
N(2)-C(3)	1.379(2)	N(2)-C(3)-C(2)	109.86(15)
N(3)-C(8)	1.331(2)	C(4)-C(3)-C(2)	131.35(17)
N(3)-C(22)	1.439(2)	C(5)-C(4)-C(3)	119.84(16)
N(4)-N(5)	1.104(2)	C(4)-C(5)-C(6)	120.67(17)
C(1)-C(2)	1.494(2)	C(7)-C(6)-C(5)	119.40(17)
C(2)-C(3)	1.418(2)	N(2)-C(7)-C(6)	119.53(16)
C(3)-C(4)	1.390(2)	N(2)-C(7)-C(8)	110.01(15)
C(4)-C(5)	1.376(2)	C(6)-C(7)-C(8)	130.45(17)
C(5)-C(6)	1.387(2)	N(3)-C(8)-C(7)	112.62(15)
C(6)-C(7)	1.384(2)	N(3)-C(8)-C(9)	124.77(15)
C(7)-C(8)	1.429(2)	C(7)-C(8)-C(9)	122.62(16)
C(8)-C(9)	1.500(2)	C(11)-C(10)-C(15)	122.17(16)
C(10)-C(11)	1.399(3)	C(11)-C(10)-N(1)	119.05(16)
C(10)-C(15)	1.401(3)	C(15)-C(10)-N(1)	118.56(16)
C(11)-C(12)	1.386(3)	C(12)-C(11)-C(10)	117.44(18)
C(11)-C(16)	1.513(3)	C(12)-C(11)-C(16)	120.55(17)
C(12)-C(13)	1.375(3)	C(10)-C(11)-C(16)	122.00(17)
C(13)-C(14)	1.379(3)	C(13)-C(12)-C(11)	121.54(19)
C(14)-C(15)	1.385(3)	C(12)-C(13)-C(14)	119.89(19)
C(15)-C(19)	1.519(3)	C(13)-C(14)-C(15)	121.30(19)
C(16)-C(18)	1.520(3)	C(14)-C(15)-C(10)	117.55(17)
C(16)-C(17)	1.522(3)	C(14)-C(15)-C(19)	120.16(17)
C(19)-C(21)	1.508(3)	C(10)-C(15)-C(19)	122.28(16)
C(19)-C(20)	1.531(3)	C(11)-C(16)-C(18)	111.62(18)
C(22)-C(27)	1.390(2)	C(11)-C(16)-C(17)	112.19(16)
C(22)-C(23)	1.397(3)	C(18)-C(16)-C(17)	109.62(18)
C(23)-C(24)	1.390(3)	C(21)-C(19)-C(15)	111.36(16)
C(23)-C(28)	1.515(3)	C(21)-C(19)-C(20)	110.10(18)
C(24)-C(25)	1.359(3)	C(15)-C(19)-C(20)	112.50(16)
C(25)-C(26)	1.376(3)	C(27)-C(22)-C(23)	121.91(17)
C(26)-C(27)	1.404(3)	C(27)-C(22)-N(3)	119.42(17)
C(27)-C(31)	1.517(3)	C(23)-C(22)-N(3)	118.56(15)
C(28)-C(30)	1.520(3)	C(24)-C(23)-C(22)	117.70(17)
C(28)-C(29)	1.529(3)	C(24)-C(23)-C(28)	119.97(18)
C(31)-C(33)	1.516(3)	C(22)-C(23)-C(28)	122.33(17)
C(31)-C(32)	1.525(3)	C(25)-C(24)-C(23)	121.6(2)
N(4)-Co(1)-N(2)	179.80(8)	C(24)-C(25)-C(26)	120.5(2)
N(4)-Co(1)-N(1)	98.73(7)	C(25)-C(26)-C(27)	120.50(19)
N(2)-Co(1)-N(1)	81.47(6)	C(22)-C(27)-C(26)	117.83(18)
N(4)-Co(1)-N(3)	98.18(7)	C(22)-C(27)-C(31)	122.65(17)

N(2)-Co(1)-N(3)	81.63(6)	C(26)-C(27)-C(31)	119.49(18)
N(1)-Co(1)-N(3)	163.07(6)	C(23)-C(28)-C(30)	112.67(18)
C(2)-N(1)-C(10)	119.72(15)	C(23)-C(28)-C(29)	110.20(18)
C(2)-N(1)-Co(1)	116.93(12)	C(30)-C(28)-C(29)	110.43(19)
C(10)-N(1)-Co(1)	123.30(11)	C(33)-C(31)-C(27)	110.97(18)
C(7)-N(2)-C(3)	121.74(14)	C(33)-C(31)-C(32)	110.12(17)
C(7)-N(2)-Co(1)	119.09(11)	C(27)-C(31)-C(32)	112.09(16)
C(3)-N(2)-Co(1)	119.15(11)	C(8)-N(3)-Co(1)	116.65(11)
C(8)-N(3)-C(22)	120.18(14)	C(22)-N(3)-Co(1)	123.17(11)

Table C.5 Crystal data and structure refinement for **(^{Cy}APDI)$_2$Co**.

Identification code	acb16	
Empirical formula	C42 H62 Co N6	
Formula weight	709.91	
Temperature	173(2) K	
Wavelength	0.71073 Å	
Crystal system	Monoclinic	
Space group	P2(1)/n	
Unit cell dimensions	a = 16.257(3) Å	α= 90°.
	b = 13.358(2) Å	β= 95.926(9)°.
	c = 18.117(3) Å	γ = 90°.
Volume	3913.5(11) Å^3	
Z	4	
Density (calculated)	1.205 Mg/m^3	
Absorption coefficient	0.475 mm^{-1}	
F(000)	1532	
Crystal size	0.45 x 0.20 x 0.15 mm^3	
Theta range for data collection	1.78 to 24.71°.	
Index ranges	-14<=h<=19, -15<=k<=15, -21<=l<=20	
Reflections collected	34060	
Independent reflections	6655 [R(int) = 0.0552]	
Completeness to theta = 24.71°	99.7 %	
Absorption correction	Semi-empirical from equivalents	
Max. and min. transmission	0.9321 and 0.8146	
Refinement method	Full-matrix least-squares on F^2	

Data / restraints / parameters	6655 / 0 / 446
Goodness-of-fit on F^2	1.062
Final R indices [I>2sigma(I)]	R1 = 0.0514, wR2 = 0.1259
R indices (all data)	R1 = 0.0760, wR2 = 0.1388
Largest diff. peak and hole	0.593 and -0.505 e.Å^{-3}

Table C.6 Atomic coordinates (x 10^4) and equivalent isotropic displacement parameters (Å^{2}x 10^3) for **(^{Cy}APDI)$_2$Co**. U(eq) is defined as one third of the trace of the orthogonalized U^{ij} tensor.

	x	y	z	U(eq)
Co(1)	2389(1)	2651(1)	308(1)	34(1)
N(1)	3224(1)	2753(2)	-630(1)	45(1)
N(2)	3408(1)	3267(1)	761(1)	40(1)
N(3)	2135(1)	2878(1)	1477(1)	35(1)
N(4)	2608(1)	1006(1)	482(1)	43(1)
N(5)	1389(1)	2015(1)	-193(1)	31(1)
N(6)	1607(1)	3940(1)	-123(1)	33(1)
C(1)	4616(2)	3307(3)	-908(2)	109(2)
C(2)	3928(2)	3149(2)	-414(2)	57(1)
C(3)	4063(2)	3453(2)	363(2)	55(1)
C(4)	4797(2)	3860(3)	693(2)	77(1)
C(5)	4880(2)	4058(3)	1446(2)	75(1)
C(6)	4230(2)	3862(2)	1853(2)	57(1)
C(7)	3492(2)	3481(2)	1510(1)	41(1)
C(8)	2763(2)	3260(2)	1882(1)	38(1)
C(9)	2800(2)	3504(2)	2698(1)	60(1)
C(10)	3060(2)	2386(2)	-1399(1)	48(1)
C(11)	3010(2)	1260(2)	-1396(1)	61(1)
C(12)	2797(2)	835(3)	-2177(2)	71(1)
C(13)	2006(2)	1275(3)	-2523(2)	75(1)
C(14)	2061(2)	2394(3)	-2556(2)	89(1)
C(15)	2283(2)	2843(3)	-1780(2)	74(1)

C(16)	1368(2)	2651(2)	1812(1)	37(1)
C(17)	1184(2)	1538(2)	1806(2)	84(1)
C(18)	360(2)	1323(2)	2136(2)	109(1)
C(19)	-330(2)	1887(2)	1782(2)	82(1)
C(20)	-160(2)	2970(2)	1760(2)	56(1)
C(21)	637(2)	3188(2)	1420(2)	56(1)
C(22)	2026(2)	-671(2)	141(2)	60(1)
C(23)	2015(2)	460(2)	163(1)	38(1)
C(24)	1313(2)	988(2)	-214(1)	34(1)
C(25)	616(2)	544(2)	-584(1)	45(1)
C(26)	-8(2)	1119(2)	-934(1)	49(1)
C(27)	74(2)	2149(2)	-924(1)	43(1)
C(28)	767(1)	2591(2)	-557(1)	34(1)
C(29)	927(2)	3659(2)	-511(1)	36(1)
C(30)	317(2)	4358(2)	-932(1)	53(1)
C(31)	3331(2)	520(2)	884(1)	56(1)
C(32)	4116(2)	832(4)	572(2)	128(2)
C(33)	4900(2)	368(4)	1000(2)	126(2)
C(34)	4937(2)	593(3)	1804(2)	75(1)
C(35)	4171(2)	296(3)	2104(2)	68(1)
C(36)	3416(2)	780(2)	1682(1)	52(1)
C(37)	1801(2)	5011(2)	-39(1)	37(1)
C(38)	2486(2)	5308(2)	-507(2)	57(1)
C(39)	2718(2)	6408(2)	-395(2)	65(1)
C(40)	2954(2)	6643(2)	410(2)	59(1)
C(41)	2271(2)	6362(2)	878(2)	52(1)
C(42)	2042(2)	5262(2)	770(1)	42(1)

Table C.7 Bond lengths [Å] and angles [°] for **(^{Cy}APDI)$_2$Co**.

Co(1)-N(2)	1.9520(19)	C(3)-N(2)-Co(1)	121.85(16)
Co(1)-N(5)	1.9704(18)	C(7)-N(2)-Co(1)	119.57(17)
Co(1)-N(3)	2.2197(19)	C(8)-N(3)-C(16)	119.9(2)
Co(1)-N(6)	2.2320(18)	C(8)-N(3)-Co(1)	112.26(17)
Co(1)-N(4)	2.2442(19)	C(16)-N(3)-Co(1)	127.86(14)
Co(1)-N(1)	2.286(2)	C(23)-N(4)-C(31)	119.6(2)
N(1)-C(2)	1.285(3)	C(23)-N(4)-Co(1)	112.81(15)
N(1)-C(10)	1.475(3)	C(31)-N(4)-Co(1)	127.57(16)
N(2)-C(3)	1.369(3)	C(24)-N(5)-C(28)	118.75(19)
N(2)-C(7)	1.381(3)	C(24)-N(5)-Co(1)	120.73(15)
N(3)-C(8)	1.299(3)	C(28)-N(5)-Co(1)	120.46(14)
N(3)-C(16)	1.473(3)	C(29)-N(6)-C(37)	119.83(18)
N(4)-C(23)	1.297(3)	C(29)-N(6)-Co(1)	112.80(14)
N(4)-C(31)	1.468(3)	C(37)-N(6)-Co(1)	127.31(14)
N(5)-C(24)	1.377(3)	N(1)-C(2)-C(3)	116.7(3)
N(5)-C(28)	1.384(3)	N(1)-C(2)-C(1)	124.3(3)
N(6)-C(29)	1.303(3)	C(3)-C(2)-C(1)	118.9(3)
N(6)-C(37)	1.470(3)	N(2)-C(3)-C(4)	121.6(3)
C(1)-C(2)	1.518(4)	N(2)-C(3)-C(2)	114.2(2)
C(2)-C(3)	1.458(4)	C(4)-C(3)-C(2)	124.1(3)
C(3)-C(4)	1.389(4)	C(5)-C(4)-C(3)	119.5(3)
C(4)-C(5)	1.382(4)	C(6)-C(5)-C(4)	119.4(3)
C(5)-C(6)	1.375(4)	C(5)-C(6)-C(7)	120.4(3)
C(6)-C(7)	1.390(4)	N(2)-C(7)-C(6)	120.6(3)
C(7)-C(8)	1.451(4)	N(2)-C(7)-C(8)	114.3(2)
C(8)-C(9)	1.510(3)	C(6)-C(7)-C(8)	125.1(2)
C(10)-C(15)	1.505(4)	N(3)-C(8)-C(7)	116.8(2)
C(10)-C(11)	1.506(4)	N(3)-C(8)-C(9)	125.9(2)
C(11)-C(12)	1.531(4)	C(7)-C(8)-C(9)	117.3(2)
C(12)-C(13)	1.492(4)	N(1)-C(10)-C(15)	111.0(2)
C(13)-C(14)	1.499(5)	N(1)-C(10)-C(11)	109.5(2)
C(14)-C(15)	1.537(4)	C(15)-C(10)-C(11)	111.3(2)
C(16)-C(21)	1.502(3)	C(10)-C(11)-C(12)	112.0(2)
C(16)-C(17)	1.517(4)	C(13)-C(12)-C(11)	110.2(3)
C(17)-C(18)	1.549(5)	C(12)-C(13)-C(14)	110.9(3)
C(18)-C(19)	1.445(5)	C(13)-C(14)-C(15)	111.2(3)
C(19)-C(20)	1.473(4)	C(10)-C(15)-C(14)	111.6(3)
C(20)-C(21)	1.519(4)	N(3)-C(16)-C(21)	111.71(19)
C(22)-C(23)	1.512(3)	N(3)-C(16)-C(17)	111.9(2)
C(23)-C(24)	1.451(3)	C(21)-C(16)-C(17)	108.6(2)
C(24)-C(25)	1.388(3)	C(16)-C(17)-C(18)	110.9(2)
C(25)-C(26)	1.374(4)	C(19)-C(18)-C(17)	113.2(3)
C(26)-C(27)	1.382(4)	C(18)-C(19)-C(20)	112.6(3)
C(27)-C(28)	1.380(3)	C(19)-C(20)-C(21)	111.7(3)
C(28)-C(29)	1.450(3)	C(16)-C(21)-C(20)	112.6(2)
C(29)-C(30)	1.510(3)	N(4)-C(23)-C(24)	116.7(2)
C(31)-C(36)	1.479(4)	N(4)-C(23)-C(22)	124.2(2)

C(31)-C(32)	1.506(5)	C(24)-C(23)-C(22)	119.0(2)
C(32)-C(33)	1.551(4)	N(5)-C(24)-C(25)	120.4(2)
C(33)-C(34)	1.483(5)	N(5)-C(24)-C(23)	113.97(19)
C(34)-C(35)	1.464(4)	C(25)-C(24)-C(23)	125.6(2)
C(35)-C(36)	1.522(4)	C(26)-C(25)-C(24)	120.7(2)
C(37)-C(42)	1.514(3)	C(25)-C(26)-C(27)	119.0(2)
C(37)-C(38)	1.519(4)	C(28)-C(27)-C(26)	120.4(2)
C(38)-C(39)	1.526(4)	C(27)-C(28)-N(5)	120.8(2)
C(39)-C(40)	1.503(4)	C(27)-C(28)-C(29)	125.5(2)
C(40)-C(41)	1.511(4)	N(5)-C(28)-C(29)	113.71(19)
C(41)-C(42)	1.524(3)	N(6)-C(29)-C(28)	116.83(19)
N(2)-Co(1)-N(5)	177.13(8)	N(6)-C(29)-C(30)	124.8(2)
N(2)-Co(1)-N(3)	77.03(8)	C(28)-C(29)-C(30)	118.4(2)
N(5)-Co(1)-N(3)	105.78(8)	N(4)-C(31)-C(36)	111.7(2)
N(2)-Co(1)-N(6)	104.49(7)	N(4)-C(31)-C(32)	111.0(2)
N(5)-Co(1)-N(6)	76.05(7)	C(36)-C(31)-C(32)	107.8(3)
N(3)-Co(1)-N(6)	94.19(7)	C(31)-C(32)-C(33)	112.7(3)
N(2)-Co(1)-N(4)	103.77(8)	C(34)-C(33)-C(32)	111.0(3)
N(5)-Co(1)-N(4)	75.71(7)	C(35)-C(34)-C(33)	111.1(3)
N(3)-Co(1)-N(4)	92.42(7)	C(34)-C(35)-C(36)	111.8(3)
N(6)-Co(1)-N(4)	151.74(7)	C(31)-C(36)-C(35)	112.3(2)
N(2)-Co(1)-N(1)	75.18(8)	N(6)-C(37)-C(42)	110.25(18)
N(5)-Co(1)-N(1)	102.00(8)	N(6)-C(37)-C(38)	111.0(2)
N(3)-Co(1)-N(1)	152.21(7)	C(42)-C(37)-C(38)	110.5(2)
N(6)-Co(1)-N(1)	93.12(7)	C(37)-C(38)-C(39)	111.2(2)
N(4)-Co(1)-N(1)	93.70(8)	C(40)-C(39)-C(38)	111.5(2)
C(2)-N(1)-C(10)	119.6(2)	C(39)-C(40)-C(41)	111.3(2)
C(2)-N(1)-Co(1)	112.05(18)	C(40)-C(41)-C(42)	110.6(2)
C(10)-N(1)-Co(1)	128.31(16)	C(37)-C(42)-C(41)	111.9(2)
C(3)-N(2)-C(7)	118.5(2)		

Table C.8 Crystal data and structure refinement for **5-Cl**.

Identification code	acb17	
Empirical formula	C15 H23 Cl Co N3	
Formula weight	339.74	
Temperature	173(2) K	
Wavelength	0.71073 Å	
Crystal system	Orthorhombic	
Space group	P2(1)2(1)2(1)	
Unit cell dimensions	a = 7.7384(3) Å	α= 90°.
	b = 11.3479(5) Å	β= 90°.

	c = 18.1263(9) Å γ = 90°.
Volume	1591.75(12) $Å^3$
Z	4
Density (calculated)	1.418 Mg/m^3
Absorption coefficient	1.240 mm^{-1}
F(000)	712
Crystal size	0.40 x 0.30 x 0.03 mm^3
Theta range for data collection	2.12 to 30.02°.
Index ranges	-9<=h<=10, -15<=k<=15, -25<=l<=20
Reflections collected	11259
Independent reflections	4615 [R(int) = 0.0460]
Completeness to theta = 30.02°	99.6 %
Absorption correction	Semi-empirical from equivalents
Max. and min. transmission	0.9697 and 0.6369
Refinement method	Full-matrix least-squares on F^2
Data / restraints / parameters	4615 / 0 / 207
Goodness-of-fit on F^2	0.945
Final R indices [I>2sigma(I)]	R1 = 0.0422, wR2 = 0.0630
R indices (all data)	R1 = 0.0623, wR2 = 0.0686
Absolute structure parameter	0.012(15)
Largest diff. peak and hole	0.318 and -0.379 $e.Å^{-3}$

Table C.9 Atomic coordinates (x 10^4) and equivalent isotropic displacement parameters ($Å^2$x 10^3) for **5-Cl**. U(eq) is defined as one third of the trace of the orthogonalized U^{ij} tensor.

	x	y	z	U(eq)
Co(1)	3126(1)	242(1)	879(1)	19(1)
Cl(1)	1483(1)	1204(1)	1681(1)	29(1)
N(1)	5261(2)	1112(1)	984(1)	22(1)
N(2)	3936(2)	40(1)	-36(1)	19(1)
N(3)	1500(2)	-922(1)	549(1)	20(1)
C(1)	7756(3)	1948(2)	272(1)	38(1)

C(2)	6127(3)	1256(2)	362(1)	24(1)
C(3)	5356(2)	670(2)	-258(1)	23(1)
C(4)	5822(3)	671(2)	-992(1)	31(1)
C(5)	4844(3)	62(2)	-1504(1)	32(1)
C(6)	3373(3)	-535(2)	-1276(1)	29(1)
C(7)	2923(2)	-537(2)	-540(1)	22(1)
C(8)	1519(3)	-1114(2)	-166(1)	23(1)
C(9)	252(3)	-1881(2)	-575(1)	35(1)
C(10)	6011(3)	1581(2)	1674(1)	28(1)
C(11)	5675(3)	739(2)	2299(1)	31(1)
C(12)	5301(3)	2816(2)	1822(2)	43(1)
C(13)	323(3)	-1627(2)	1017(1)	27(1)
C(14)	-1378(3)	-1008(2)	1149(1)	40(1)
C(15)	1248(3)	-1920(2)	1735(1)	31(1)

Table C.10 Bond lengths [Å] and angles [°] for **5-Cl**.

Co(1)-N(2)	1.7870(16)	C(2)-N(1)-Co(1)	114.38(14)
Co(1)-N(3)	1.9203(16)	C(10)-N(1)-Co(1)	127.04(14)
Co(1)-N(1)	1.9334(15)	C(7)-N(2)-C(3)	120.80(17)
Co(1)-Cl(1)	2.2188(6)	C(7)-N(2)-Co(1)	118.66(13)
N(1)-C(2)	1.321(3)	C(3)-N(2)-Co(1)	119.05(13)
N(1)-C(10)	1.478(3)	C(8)-N(3)-C(13)	118.84(16)
N(2)-C(7)	1.371(2)	C(8)-N(3)-Co(1)	114.47(13)
N(2)-C(3)	1.371(2)	C(13)-N(3)-Co(1)	126.64(14)
N(3)-C(8)	1.314(3)	N(1)-C(2)-C(3)	113.51(18)
N(3)-C(13)	1.480(3)	N(1)-C(2)-C(1)	125.9(2)
C(1)-C(2)	1.494(3)	C(3)-C(2)-C(1)	120.60(19)
C(2)-C(3)	1.435(3)	N(2)-C(3)-C(4)	119.53(19)
C(3)-C(4)	1.379(3)	N(2)-C(3)-C(2)	110.21(18)
C(4)-C(5)	1.382(3)	C(4)-C(3)-C(2)	130.26(19)
C(5)-C(6)	1.387(3)	C(3)-C(4)-C(5)	120.3(2)
C(6)-C(7)	1.379(3)	C(4)-C(5)-C(6)	119.6(2)
C(7)-C(8)	1.438(3)	C(7)-C(6)-C(5)	119.7(2)
C(8)-C(9)	1.506(3)	N(2)-C(7)-C(6)	119.96(18)
C(10)-C(11)	1.505(3)	N(2)-C(7)-C(8)	109.61(18)
C(10)-C(12)	1.530(3)	C(6)-C(7)-C(8)	130.37(19)
C(13)-C(14)	1.512(3)	N(3)-C(8)-C(7)	113.40(17)
C(13)-C(15)	1.522(3)	N(3)-C(8)-C(9)	125.03(18)
N(2)-Co(1)-N(3)	81.49(7)	C(7)-C(8)-C(9)	121.56(19)

N(2)-Co(1)-N(1)	81.80(7)	N(1)-C(10)-C(11)	109.92(17)
N(3)-Co(1)-N(1)	160.32(7)	N(1)-C(10)-C(12)	109.77(17)
N(2)-Co(1)-Cl(1)	150.73(5)	C(11)-C(10)-C(12)	112.8(2)
N(3)-Co(1)-Cl(1)	99.61(5)	N(3)-C(13)-C(14)	112.07(17)
N(1)-Co(1)-Cl(1)	100.05(5)	N(3)-C(13)-C(15)	108.59(16)
C(2)-N(1)-C(10)	118.56(17)	C(14)-C(13)-C(15)	112.04(19)

Table C.11 Crystal data and structure refinement for **5-Me**.

Identification code	acb22	
Empirical formula	C16 H26 Co N3	
Formula weight	319.33	
Temperature	173(2) K	
Wavelength	0.71073 Å	
Crystal system	Monoclinic	
Space group	P2(1)/c	
Unit cell dimensions	a = 11.2905(5) Å	α= 90°.
	b = 7.9626(3) Å	β= 100.1670(10)°.
	c = 18.4333(8) Å	γ = 90°.
Volume	1631.16(12) $Å^3$	
Z	4	
Density (calculated)	1.300 Mg/m^3	
Absorption coefficient	1.047 mm^{-1}	
F(000)	680	
Crystal size	0.22 x 0.20 x 0.15 mm^3	
Theta range for data collection	1.83 to 27.48°.	
Index ranges	-14<=h<=14, -7<=k<=10, -23<=l<=23	
Reflections collected	12346	
Independent reflections	3730 [R(int) = 0.0464]	
Completeness to theta = 27.48°	99.8 %	
Absorption correction	Semi-empirical from equivalents	
Max. and min. transmission	0.8588 and 0.8024	
Refinement method	Full-matrix least-squares on F^2	
Data / restraints / parameters	3730 / 0 / 208	

Goodness-of-fit on F^2	1.084
Final R indices [I>2sigma(I)]	R1 = 0.0407, wR2 = 0.0879
R indices (all data)	R1 = 0.0649, wR2 = 0.0973
Largest diff. peak and hole	0.512 and -0.369 e.$Å^{-3}$

Table C.12 Atomic coordinates (x 10^4) and equivalent isotropic displacement parameters ($Å^2$x 10^3) for **5-Me**. U(eq) is defined as one third of the trace of the orthogonalized U^{ij} tensor.

	x	y	z	U(eq)
Co(1)	7417(1)	6406(1)	1700(1)	21(1)
N(1)	8258(1)	4322(2)	1646(1)	22(1)
N(2)	7470(1)	5715(2)	2639(1)	21(1)
N(3)	6376(1)	8061(2)	1999(1)	24(1)
C(1)	9262(2)	1912(3)	2410(1)	35(1)
C(2)	8583(2)	3542(2)	2286(1)	25(1)
C(3)	8203(2)	4389(2)	2896(1)	23(1)
C(4)	8492(2)	4074(3)	3644(1)	29(1)
C(5)	8083(2)	5155(3)	4141(1)	31(1)
C(6)	7388(2)	6545(3)	3878(1)	28(1)
C(7)	7087(2)	6827(2)	3126(1)	23(1)
C(8)	6401(2)	8145(2)	2720(1)	24(1)
C(9)	5773(2)	9448(3)	3104(1)	38(1)
C(10)	8523(2)	3499(3)	973(1)	28(1)
C(11)	7601(2)	3996(3)	306(1)	37(1)
C(12)	9810(2)	3867(3)	871(1)	41(1)
C(13)	5513(2)	9159(3)	1511(1)	27(1)
C(14)	6082(2)	10823(3)	1353(1)	39(1)
C(15)	5006(2)	8236(3)	811(1)	34(1)
C(16)	8146(2)	7797(3)	1015(1)	30(1)

Table C.13 Bond lengths [Å] and angles [°] for **5-Me**.

Co(1)-N(2)	1.8072(16)	C(2)-N(1)-Co(1)	114.87(13)
Co(1)-N(3)	1.9103(16)	C(10)-N(1)-Co(1)	126.85(12)
Co(1)-N(1)	1.9228(16)	C(3)-N(2)-C(7)	120.46(16)
Co(1)-C(16)	1.967(2)	C(3)-N(2)-Co(1)	118.68(13)
N(1)-C(2)	1.326(2)	C(7)-N(2)-Co(1)	117.75(13)
N(1)-C(10)	1.479(2)	C(8)-N(3)-C(13)	118.16(16)
N(2)-C(3)	1.373(2)	C(8)-N(3)-Co(1)	114.75(13)
N(2)-C(7)	1.383(2)	C(13)-N(3)-Co(1)	126.98(13)
N(3)-C(8)	1.326(2)	N(1)-C(2)-C(3)	113.62(17)
N(3)-C(13)	1.488(3)	N(1)-C(2)-C(1)	126.37(18)
C(1)-C(2)	1.504(3)	C(3)-C(2)-C(1)	119.99(18)
C(2)-C(3)	1.440(3)	N(2)-C(3)-C(4)	120.31(18)
C(3)-C(4)	1.383(3)	N(2)-C(3)-C(2)	109.63(16)
C(4)-C(5)	1.394(3)	C(4)-C(3)-C(2)	130.04(18)
C(5)-C(6)	1.393(3)	C(3)-C(4)-C(5)	119.76(19)
C(6)-C(7)	1.385(3)	C(6)-C(5)-C(4)	119.54(19)
C(7)-C(8)	1.434(3)	C(7)-C(6)-C(5)	120.03(19)
C(8)-C(9)	1.503(3)	N(2)-C(7)-C(6)	119.74(18)
C(10)-C(11)	1.517(3)	N(2)-C(7)-C(8)	109.34(17)
C(10)-C(12)	1.527(3)	C(6)-C(7)-C(8)	130.92(19)
C(13)-C(15)	1.508(3)	N(3)-C(8)-C(7)	113.60(17)
C(13)-C(14)	1.523(3)	N(3)-C(8)-C(9)	125.40(18)
N(2)-Co(1)-N(3)	81.46(7)	C(7)-C(8)-C(9)	121.00(18)
N(2)-Co(1)-N(1)	81.58(7)	N(1)-C(10)-C(11)	110.72(17)
N(3)-Co(1)-N(1)	160.83(7)	N(1)-C(10)-C(12)	110.87(17)
N(2)-Co(1)-C(16)	147.11(8)	C(11)-C(10)-C(12)	112.42(18)
N(3)-Co(1)-C(16)	98.34(8)	N(3)-C(13)-C(15)	109.89(17)
N(1)-Co(1)-C(16)	100.75(8)	N(3)-C(13)-C(14)	111.95(16)
C(2)-N(1)-C(10)	118.22(16)	C(15)-C(13)-C(14)	111.66(18)

Table C.14 Crystal data and structure refinement for **1-N(^{1}Ad)**.

Identification code	acb3	
Empirical formula	C43 H58 Fe N4	
Formula weight	686.78	
Temperature	173(2) K	
Wavelength	0.71073 Å	
Crystal system	Monoclinic	
Space group	P2(1)/m	
Unit cell dimensions	a = 8.8669(5) Å	α= 90°.
	b = 19.9508(10) Å	β= 92.519(3)°.

	c = 10.3408(5) Å γ = 90°.
Volume	1827.54(16) $Å^3$
Z	2
Density (calculated)	1.248 Mg/m^3
Absorption coefficient	0.449 mm^{-1}
F(000)	740
Crystal size	0.80 x 0.35 x 0.05 mm^3
Theta range for data collection	1.97 to 28.31°.
Index ranges	-11<=h<=11, -25<=k<=26, -13<=l<=13
Reflections collected	19001
Independent reflections	4674 [R(int) = 0.0491]
Completeness to theta = 28.31°	100.0 %
Absorption correction	Semi-empirical from equivalents
Max. and min. transmission	0.9779 and 0.7155
Refinement method	Full-matrix least-squares on F^2
Data / restraints / parameters	4674 / 0 / 349
Goodness-of-fit on F^2	1.026
Final R indices [I>2sigma(I)]	R1 = 0.0417, wR2 = 0.0904
R indices (all data)	R1 = 0.0632, wR2 = 0.0987
Largest diff. peak and hole	0.528 and -0.322 $e.Å^{-3}$

Table C.15 Atomic coordinates (x 10^4) and equivalent isotropic displacement parameters ($Å^2$x 10^3) for **1-N(1Ad)**. U(eq) is defined as one third of the trace of the orthogonalized U^{ij} tensor.

	x	y	z	U(eq)
Fe(1)	6980(1)	2500	1559(1)	15(1)
N(1)	6910(1)	1565(1)	1075(1)	16(1)
N(2)	8022(2)	2500	-2(1)	15(1)
N(3)	6428(2)	2500	3061(2)	19(1)
C(1)	7800(2)	654(1)	-383(1)	28(1)
C(2)	7673(2)	1363(1)	55(1)	19(1)
C(3)	8293(2)	1906(1)	-628(1)	17(1)

C(4)	9008(2)	1899(1)	-1804(1)	21(1)
C(5)	9390(2)	2500	-2375(2)	22(1)
C(6)	6153(2)	1061(1)	1815(1)	18(1)
C(7)	4580(2)	1014(1)	1663(1)	20(1)
C(8)	3857(2)	549(1)	2425(1)	23(1)
C(9)	4657(2)	130(1)	3270(1)	26(1)
C(10)	6202(2)	172(1)	3376(1)	25(1)
C(11)	6994(2)	639(1)	2661(1)	20(1)
C(12)	3685(2)	1439(1)	682(1)	24(1)
C(13)	2003(2)	1486(1)	921(2)	36(1)
C(14)	3879(2)	1180(1)	-692(2)	34(1)
C(15)	8699(2)	678(1)	2831(1)	26(1)
C(16)	9430(2)	-12(1)	2904(2)	40(1)
C(17)	9184(2)	1101(1)	4006(2)	40(1)
C(18)	5441(2)	2500	4130(2)	18(1)
C(19)	5754(2)	3126(1)	4983(1)	22(1)
C(20)	3781(2)	2500	3666(2)	24(1)
C(21)	2743(2)	2500	4813(2)	26(1)
C(22)	3062(2)	3126(1)	5632(1)	27(1)
C(23)	4706(2)	3124(1)	6128(1)	23(1)
C(24)	5010(3)	2500	6952(2)	24(1)

Symmetry transformations used to generate equivalent atoms:
#1 x,-y+1/2,z

Table C.16 Bond lengths [Å] and angles [°] for **1-N(^{1}Ad)**.

Fe(1)-N(3)	1.6481(15)	C(3)-N(2)-Fe(1)	120.16(8)
Fe(1)-N(2)	1.8950(15)	C(3)#1-N(2)-Fe(1)	120.16(8)
Fe(1)-N(1)	1.9325(11)	C(18)-N(3)-Fe(1)	159.87(15)
Fe(1)-N(1)#1	1.9325(11)	N(1)-C(2)-C(3)	112.48(12)
N(1)-C(2)	1.3395(16)	N(1)-C(2)-C(1)	124.89(12)
N(1)-C(6)	1.4474(17)	C(3)-C(2)-C(1)	122.54(12)
N(2)-C(3)	1.3773(15)	N(2)-C(3)-C(4)	120.89(12)
N(2)-C(3)#1	1.3773(15)	N(2)-C(3)-C(2)	110.12(11)
N(3)-C(18)	1.440(2)	C(4)-C(3)-C(2)	128.89(12)
C(1)-C(2)	1.490(2)	C(5)-C(4)-C(3)	119.48(13)
C(2)-C(3)	1.4178(19)	C(4)#1-C(5)-C(4)	119.89(17)
C(3)-C(4)	1.3954(18)	C(7)-C(6)-C(11)	122.02(12)
C(4)-C(5)	1.3852(17)	C(7)-C(6)-N(1)	118.01(12)
C(5)-C(4)#1	1.3852(17)	C(11)-C(6)-N(1)	119.97(12)
C(6)-C(7)	1.400(2)	C(8)-C(7)-C(6)	117.50(13)
C(6)-C(11)	1.4043(19)	C(8)-C(7)-C(12)	120.69(13)
C(7)-C(8)	1.3922(19)	C(6)-C(7)-C(12)	121.79(12)
C(7)-C(12)	1.519(2)	C(9)-C(8)-C(7)	121.64(14)
C(8)-C(9)	1.383(2)	C(10)-C(9)-C(8)	119.74(13)
C(9)-C(10)	1.373(2)	C(9)-C(10)-C(11)	121.47(14)
C(10)-C(11)	1.397(2)	C(10)-C(11)-C(6)	117.58(14)
C(11)-C(15)	1.516(2)	C(10)-C(11)-C(15)	119.66(13)
C(12)-C(13)	1.525(2)	C(6)-C(11)-C(15)	122.75(12)
C(12)-C(14)	1.529(2)	C(7)-C(12)-C(13)	114.34(13)
C(15)-C(16)	1.523(2)	C(7)-C(12)-C(14)	110.79(13)
C(15)-C(17)	1.525(2)	C(13)-C(12)-C(14)	108.76(13)
C(18)-C(20)	1.528(3)	C(11)-C(15)-C(16)	112.30(13)
C(18)-C(19)	1.5466(18)	C(11)-C(15)-C(17)	111.45(12)
C(18)-C(19)#1	1.5466(18)	C(16)-C(15)-C(17)	110.87(14)
C(19)-C(23)	1.5369(19)	N(3)-C(18)-C(20)	111.62(15)
C(20)-C(21)	1.533(3)	N(3)-C(18)-C(19)	109.76(11)
C(21)-C(22)	1.529(2)	C(20)-C(18)-C(19)	108.99(11)
C(21)-C(22)#1	1.529(2)	N(3)-C(18)-C(19)#1	109.76(11)
C(22)-C(23)	1.523(2)	C(20)-C(18)-C(19)#1	108.99(11)
C(23)-C(24)	1.5270(18)	C(19)-C(18)-C(19)#1	107.63(15)
C(24)-C(23)#1	1.5270(18)	C(23)-C(19)-C(18)	109.79(12)
N(3)-Fe(1)-N(2)	168.10(8)	C(21)-C(20)-C(18)	111.10(16)
N(3)-Fe(1)-N(1)	103.71(3)	C(22)-C(21)-C(22)#1	109.62(17)
N(2)-Fe(1)-N(1)	77.89(3)	C(22)-C(21)-C(20)	109.00(12)
N(3)-Fe(1)-N(1)#1	103.71(3)	C(22)#1-C(21)-C(20)	109.00(12)
N(2)-Fe(1)-N(1)#	177.89(3)	C(23)-C(22)-C(21)	109.62(13)
N(1)-Fe(1)-N(1)#1	149.86(6)	C(24)-C(23)-C(22)	109.43(13)
C(2)-N(1)-C(6)	118.00(11)	C(24)-C(23)-C(19)	109.45(13)
C(2)-N(1)-Fe(1)	118.91(9)	C(22)-C(23)-C(19)	110.06(12)
C(6)-N(1)-Fe(1)	122.96(8)	C(23)#1-C(24)-C(23)	109.37(16)
C(3)-N(2)-C(3)#1	118.82(15)		

Table C.17 Crystal data and structure refinement for **1-N(^{Cy}Oct)**.

Identification code	acb19	
Empirical formula	C41 H58 Fe N4	
Formula weight	662.76	
Temperature	293(2) K	
Wavelength	0.97820 Å	
Crystal system	Monoclinic	
Space group	P2(1)/c	
Unit cell dimensions	a = 23.764(5) Å	α= 90°.
	b = 14.825(3) Å	β= 107.52(3)°.
	c = 21.812(4) Å	γ = 90°.
Volume	7328(3) Å^3	
Z	8	
Density (calculated)	1.201 Mg/m^3	
Absorption coefficient	0.445 mm^{-1}	
F(000)	2864	
Crystal size	0.35 x 0.30 x 0.15 mm^3	
Theta range for data collection	1.24 to 32.28°.	
Index ranges	-22<=h<=22, -14<=k<=0, 0<=l<=21	
Reflections collected	7129	
Independent reflections	7129 [R(int) = 0.0000]	
Completeness to theta = 32.28°	71.3 %	
Absorption correction	None	
Max. and min. transmission	0.9363 and 0.8598	
Refinement method	Full-matrix least-squares on F^2	
Data / restraints / parameters	7129 / 128 / 824	
Goodness-of-fit on F^2	1.118	
Final R indices [I>2sigma(I)]	R1 = 0.0763, wR2 = 0.2243	
R indices (all data)	R1 = 0.0780, wR2 = 0.2304	
Largest diff. peak and hole	1.047 and -0.529 e.Å^{-3}	

Table C.18 Atomic coordinates (x 10^4) and equivalent isotropic displacement parameters ($Å^2$x 10^3) for **1-N(^{Cy}Oct)**. U(eq) is defined as one third of the trace of the orthogonalized U^{ij} tensor.

	x	y	z	U(eq)
Fe(1)	-1279(1)	4208(1)	-2885(1)	24(1)
N(1)	-1812(1)	3312(2)	-3345(1)	25(1)
N(2)	-1325(1)	3439(2)	-2222(1)	24(1)
N(3)	-692(1)	4718(2)	-2170(1)	25(1)
N(4)	-1259(2)	4954(2)	-3438(1)	33(1)
C(1)	-2403(2)	1916(3)	-3323(2)	41(1)
C(2)	-1973(2)	2638(3)	-3021(2)	28(1)
C(3)	-1666(2)	2670(2)	-2361(2)	26(1)
C(4)	-1669(2)	2048(3)	-1877(2)	31(1)
C(5)	-1312(2)	2200(3)	-1257(2)	33(1)
C(6)	-961(2)	2962(3)	-1119(2)	31(1)
C(7)	-958(2)	3572(2)	-1603(2)	26(1)
C(8)	-615(2)	4351(3)	-1581(2)	26(1)
C(9)	-216(2)	4727(3)	-970(2)	35(1)
C(10)	-2084(2)	3331(3)	-4030(2)	28(1)
C(11)	-2583(2)	3884(3)	-4291(2)	31(1)
C(12)	-2813(2)	3904(3)	-4950(2)	40(1)
C(13)	-2579(2)	3402(3)	-5349(2)	38(1)
C(14)	-2104(2)	2854(3)	-5084(2)	35(1)
C(15)	-1845(2)	2808(3)	-4425(2)	30(1)
C(16)	-2861(2)	4422(3)	-3873(2)	39(1)
C(17)	-2807(2)	5439(3)	-3967(2)	53(1)
C(18)	-3504(2)	4149(4)	-3991(3)	56(2)
C(19)	-1291(2)	2243(3)	-4153(2)	29(1)
C(20)	-766(2)	2698(3)	-4278(2)	48(1)
C(21)	-1362(2)	1282(3)	-4427(3)	55(2)
C(22)	-387(2)	5551(2)	-2215(2)	25(1)
C(23)	-613(2)	6368(3)	-2061(2)	27(1)
C(24)	-328(2)	7164(3)	-2138(2)	30(1)

C(25)	153(2)	7167(3)	-2370(2)	28(1)
C(26)	371(2)	6351(3)	-2512(2)	28(1)
C(27)	112(2)	5533(2)	-2433(2)	23(1)
C(28)	-1159(2)	6418(3)	-1831(2)	33(1)
C(29)	-1060(2)	7005(3)	-1236(2)	53(1)
C(30)	-1690(2)	6736(4)	-2365(2)	53(1)
C(31)	384(2)	4642(3)	-2563(2)	29(1)
C(32)	766(2)	4238(3)	-1936(2)	51(1)
C(33)	728(2)	4733(3)	-3040(2)	46(1)
C(34)	-1049(2)	5478(3)	-3880(2)	37(1)
C(35)	-1146(2)	6497(3)	-3781(2)	40(1)
C(36)	-1078(2)	7140(3)	-4266(2)	55(2)
C(37)	-500(2)	7238(3)	-4383(2)	56(2)
C(38)	-258(2)	6449(3)	-4649(2)	52(1)
C(39)	-694(2)	5917(3)	-5190(2)	47(1)
C(40)	-945(2)	5072(3)	-4990(2)	48(1)
C(41)	-1350(2)	5149(3)	-4564(2)	40(1)
Fe(1A)	-4156(1)	6097(1)	-1237(1)	29(1)
N(1A)	-3594(1)	5259(2)	-726(1)	29(1)
N(2A)	-4647(1)	5242(2)	-1013(1)	28(1)
N(3A)	-4908(1)	6689(2)	-1514(2)	32(1)
N(4A)	-3762(2)	6807(2)	-1528(2)	40(1)
C(1A)	-3400(2)	3791(3)	-125(2)	40(1)
C(2A)	-3786(2)	4514(3)	-497(2)	28(1)
C(3A)	-4406(2)	4499(3)	-644(2)	28(1)
C(4A)	-4770(2)	3894(3)	-448(2)	33(1)
C(5A)	-5368(2)	4048(3)	-614(2)	34(1)
C(6A)	-5610(2)	4804(3)	-956(2)	35(1)
C(7A)	-5246(2)	5412(3)	-1147(2)	30(1)
C(8A)	-5388(2)	6255(3)	-1457(2)	33(1)
C(9A)	-5999(2)	6618(3)	-1670(2)	44(1)
C(10A)	-2963(2)	5358(3)	-593(2)	33(1)
C(11A)	-2699(2)	5047(3)	-1056(2)	41(1)
C(12A)	-2096(2)	5167(3)	-921(2)	54(1)
C(13A)	-1768(2)	5580(3)	-366(3)	58(2)

C(14A)	-2035(2)	5863(3)	76(2)	46(1)
C(15A)	-2639(2)	5767(3)	-27(2)	37(1)
C(16A)	-3049(2)	4598(3)	-1672(2)	51(1)
C(17A)	-3015(3)	5136(4)	-2253(3)	86(2)
C(18A)	-2847(3)	3626(4)	-1721(3)	80(2)
C(19A)	-2925(2)	6091(3)	472(2)	40(1)
C(20A)	-3017(3)	7097(4)	456(3)	89(2)
C(21A)	-2604(3)	5768(5)	1146(3)	91(2)
C(22A)	-4998(2)	7571(3)	-1821(2)	36(1)
C(23A)	-5214(2)	7629(3)	-2487(2)	40(1)
C(24A)	-5302(2)	8494(3)	-2763(2)	46(1)
C(25A)	-5174(2)	9256(3)	-2391(2)	56(2)
C(26A)	-4941(2)	9176(3)	-1733(2)	54(2)
C(27A)	-4848(2)	8341(3)	-1433(2)	43(1)
C(28A)	-5331(2)	6818(3)	-2932(2)	42(1)
C(29A)	-5947(3)	6853(4)	-3421(3)	78(2)
C(30A)	-4861(3)	6711(4)	-3271(3)	68(2)
C(31A)	-4585(2)	8267(3)	-708(2)	49(1)
C(32A)	-5060(2)	8223(4)	-382(3)	69(2)
C(33A)	-4169(3)	9035(5)	-411(3)	86(2)
C(34A)	-3483(2)	7628(4)	-1602(2)	61(2)
C(35A)	-3534(5)	7781(6)	-2310(3)	173(4)
C(36A)	-3437(5)	8539(5)	-2607(4)	139(4)
C(37A)	-3271(5)	9450(4)	-2354(3)	118(3)
C(38A)	-3125(4)	9679(5)	-1703(4)	115(3)
C(39A)	-2525(4)	9262(5)	-1282(5)	168(5)
C(40A)	-2511(3)	8433(4)	-988(3)	87(2)
C(41A)	-2846(2)	7611(3)	-1203(3)	60(2)

Table C.19 Bond lengths [Å] for **1-N(^{Cy}Oct)**.

Fe(1)-N(4)	1.648(3)	Fe(1A)-N(4A)	1.658(3)
Fe(1)-N(2)	1.870(3)	Fe(1A)-N(2A)	1.884(3)
Fe(1)-N(1)	1.901(3)	Fe(1A)-N(1A)	1.917(3)

Fe(1)-N(3)	1.908(3)	Fe(1A)-N(3A)	1.917(3)
N(1)-C(2)	1.345(5)	N(1A)-C(2A)	1.347(5)
N(1)-C(10)	1.438(5)	N(1A)-C(10A)	1.446(5)
N(2)-C(3)	1.378(5)	N(2A)-C(3A)	1.382(5)
N(2)-C(7)	1.383(4)	N(2A)-C(7A)	1.388(5)
N(3)-C(8)	1.355(5)	N(3A)-C(8A)	1.347(5)
N(3)-C(22)	1.451(5)	N(3A)-C(22A)	1.455(5)
N(4)-C(34)	1.440(5)	N(4A)-C(34A)	1.419(6)
C(1)-C(2)	1.489(5)	C(1A)-C(2A)	1.484(6)
C(2)-C(3)	1.405(5)	C(2A)-C(3A)	1.409(5)
C(3)-C(4)	1.404(5)	C(3A)-C(4A)	1.402(6)
C(4)-C(5)	1.381(5)	C(4A)-C(5A)	1.375(6)
C(5)-C(6)	1.383(6)	C(5A)-C(6A)	1.374(6)
C(6)-C(7)	1.392(5)	C(6A)-C(7A)	1.396(6)
C(7)-C(8)	1.406(5)	C(7A)-C(8A)	1.413(6)
C(8)-C(9)	1.491(5)	C(8A)-C(9A)	1.486(6)
C(10)-C(15)	1.400(6)	C(10A)-C(15A)	1.383(6)
C(10)-C(11)	1.413(5)	C(10A)-C(11A)	1.418(6)
C(11)-C(12)	1.377(6)	C(11A)-C(12A)	1.384(6)
C(11)-C(16)	1.504(6)	C(11A)-C(16A)	1.506(6)
C(12)-C(13)	1.383(6)	C(12A)-C(13A)	1.371(7)
C(13)-C(14)	1.369(6)	C(13A)-C(14A)	1.371(7)
C(14)-C(15)	1.385(5)	C(14A)-C(15A)	1.390(6)
C(15)-C(19)	1.522(5)	C(15A)-C(19A)	1.523(6)
C(16)-C(18)	1.527(6)	C(16A)-C(17A)	1.520(7)
C(16)-C(17)	1.531(6)	C(16A)-C(18A)	1.534(7)
C(19)-C(20)	1.515(6)	C(19A)-C(20A)	1.507(7)
C(19)-C(21)	1.534(6)	C(19A)-C(21A)	1.515(7)
C(22)-C(23)	1.405(5)	C(22A)-C(23A)	1.390(6)
C(22)-C(27)	1.405(5)	C(22A)-C(27A)	1.402(6)
C(23)-C(24)	1.396(5)	C(23A)-C(24A)	1.406(6)
C(23)-C(28)	1.528(6)	C(23A)-C(28A)	1.516(6)
C(24)-C(25)	1.380(6)	C(24A)-C(25A)	1.371(6)
C(25)-C(26)	1.387(6)	C(25A)-C(26A)	1.380(7)
C(26)-C(27)	1.394(5)	C(26A)-C(27A)	1.387(6)
C(27)-C(31)	1.534(5)	C(27A)-C(31A)	1.520(6)
C(28)-C(29)	1.520(6)	C(28A)-C(29A)	1.531(6)
C(28)-C(30)	1.513(6)	C(28A)-C(30A)	1.522(7)
C(31)-C(32)	1.518(6)	C(31A)-C(32A)	1.507(7)
C(31)-C(33)	1.511(6)	C(31A)-C(33A)	1.519(7)
C(34)-C(41)	1.529(6)	C(34A)-C(41A)	1.502(6)
C(34)-C(35)	1.552(6)	C(34A)-C(35A)	1.529(8)
C(35)-C(36)	1.470(6)	C(35A)-C(36A)	1.350(9)
C(36)-C(37)	1.476(7)	C(36A)-C(37A)	1.468(9)
C(37)-C(38)	1.497(7)	C(37A)-C(38A)	1.398(9)
C(38)-C(39)	1.533(6)	C(38A)-C(39A)	1.571(10)
C(39)-C(40)	1.506(6)	C(39A)-C(40A)	1.381(9)
C(40)-C(41)	1.529(6)	C(40A)-C(41A)	1.455(7)

Table C.20 Angles [°] for **1-N(^{Cy}Oct)**.

N(4)-Fe(1)-N(2)	175.14(16)	N(4A)-Fe(1A)-N(2A)	172.78(15)
N(4)-Fe(1)-N(1)	104.15(14)	N(4A)-Fe(1A)-N(1A)	104.97(16)
N(2)-Fe(1)-N(1)	78.35(13)	N(2A)-Fe(1A)-N(1A)	77.92(14)
N(4)-Fe(1)-N(3)	99.03(14)	N(4A)-Fe(1A)-N(3A)	99.77(16)
N(2)-Fe(1)-N(3)	78.89(13)	N(2A)-Fe(1A)-N(3A)	78.40(14)
N(1)-Fe(1)-N(3)	156.34(13)	N(1A)-Fe(1A)-N(3A)	154.17(15)
C(2)-N(1)-C(10)	116.8(3)	C(2A)-N(1A)-C(10A)	117.1(3)
C(2)-N(1)-Fe(1)	119.4(2)	C(2A)-N(1A)-Fe(1A)	119.4(3)
C(10)-N(1)-Fe(1)	123.7(2)	C(10A)-N(1A)-Fe(1A)	123.4(3)
C(3)-N(2)-C(7)	119.3(3)	C(3A)-N(2A)-C(7A)	119.1(3)
C(3)-N(2)-Fe(1)	120.0(2)	C(3A)-N(2A)-Fe(1A)	120.4(3)
C(7)-N(2)-Fe(1)	120.1(2)	C(7A)-N(2A)-Fe(1A)	119.9(3)
C(8)-N(3)-C(22)	118.5(3)	C(8A)-N(3A)-C(22A)	117.4(3)
C(8)-N(3)-Fe(1)	118.3(2)	C(8A)-N(3A)-Fe(1A)	119.2(3)
C(22)-N(3)-Fe(1)	122.6(2)	C(22A)-N(3A)-Fe(1A)	123.3(3)
C(34)-N(4)-Fe(1)	160.9(3)	C(34A)-N(4A)-Fe(1A)	157.7(4)
N(1)-C(2)-C(3)	111.8(3)	N(1A)-C(2A)-C(3A)	112.1(3)
N(1)-C(2)-C(1)	124.5(3)	N(1A)-C(2A)-C(1A)	124.9(4)
C(3)-C(2)-C(1)	123.7(3)	C(3A)-C(2A)-C(1A)	123.0(4)
N(2)-C(3)-C(2)	110.1(3)	N(2A)-C(3A)-C(4A)	120.1(3)
N(2)-C(3)-C(4)	120.9(3)	N(2A)-C(3A)-C(2A)	110.0(3)
C(2)-C(3)-C(4)	129.0(3)	C(4A)-C(3A)-C(2A)	129.8(4)
C(5)-C(4)-C(3)	119.3(4)	C(5A)-C(4A)-C(3A)	119.9(4)
C(6)-C(5)-C(4)	119.9(4)	C(6A)-C(5A)-C(4A)	120.6(4)
C(5)-C(6)-C(7)	120.4(3)	C(5A)-C(6A)-C(7A)	119.5(4)
N(2)-C(7)-C(6)	120.1(3)	N(2A)-C(7A)-C(6A)	120.6(3)
N(2)-C(7)-C(8)	109.9(3)	N(2A)-C(7A)-C(8A)	110.1(3)
C(6)-C(7)-C(8)	130.0(3)	C(6A)-C(7A)-C(8A)	129.3(4)
N(3)-C(8)-C(7)	112.6(3)	N(3A)-C(8A)-C(7A)	112.3(3)
N(3)-C(8)-C(9)	124.4(3)	N(3A)-C(8A)-C(9A)	125.0(4)
C(7)-C(8)-C(9)	122.9(3)	C(7A)-C(8A)-C(9A)	122.7(4)
C(15)-C(10)-C(11)	121.3(3)	C(15A)-C(10A)-C(11A)	122.1(4)
C(15)-C(10)-N(1)	119.3(3)	C(15A)-C(10A)-N(1A)	119.3(4)
C(11)-C(10)-N(1)	119.3(3)	C(11A)-C(10A)-N(1A)	118.6(3)
C(12)-C(11)-C(10)	117.0(4)	C(12A)-C(11A)-C(10A)	117.4(4)
C(12)-C(11)-C(16)	120.9(4)	C(12A)-C(11A)-C(16A)	120.3(4)
C(10)-C(11)-C(16)	122.1(3)	C(10A)-C(11A)-C(16A)	122.3(4)
C(11)-C(12)-C(13)	122.6(4)	C(13A)-C(12A)-C(11A)	121.4(5)
C(14)-C(13)-C(12)	119.3(4)	C(12A)-C(13A)-C(14A)	119.8(5)
C(13)-C(14)-C(15)	121.3(4)	C(13A)-C(14A)-C(15A)	121.9(4)
C(14)-C(15)-C(10)	118.4(4)	C(10A)-C(15A)-C(14A)	117.4(4)
C(14)-C(15)-C(19)	119.6(4)	C(10A)-C(15A)-C(19A)	121.8(4)
C(10)-C(15)-C(19)	121.9(3)	C(14A)-C(15A)-C(19A)	120.9(4)
C(11)-C(16)-C(18)	110.9(4)	C(11A)-C(16A)-C(17A)	111.0(4)

C(11)-C(16)-C(17)	111.9(4)	C(11A)-C(16A)-C(18A)	112.1(4)
C(18)-C(16)-C(17)	110.9(4)	C(17A)-C(16A)-C(18A)	109.8(5)
C(20)-C(19)-C(15)	110.3(3)	C(20A)-C(19A)-C(15A)	112.9(4)
C(20)-C(19)-C(21)	110.1(4)	C(20A)-C(19A)-C(21A)	111.2(5)
C(15)-C(19)-C(21)	112.3(3)	C(15A)-C(19A)-C(21A)	112.9(4)
C(23)-C(22)-C(27)	121.3(3)	C(23A)-C(22A)-C(27A)	121.8(4)
C(23)-C(22)-N(3)	118.9(3)	C(23A)-C(22A)-N(3A)	119.6(3)
C(27)-C(22)-N(3)	119.8(3)	C(27A)-C(22A)-N(3A)	118.6(3)
C(22)-C(23)-C(24)	117.7(4)	C(22A)-C(23A)-C(24A)	117.7(4)
C(22)-C(23)-C(28)	122.9(3)	C(22A)-C(23A)-C(28A)	123.9(4)
C(24)-C(23)-C(28)	119.4(3)	C(24A)-C(23A)-C(28A)	118.2(4)
C(25)-C(24)-C(23)	122.1(4)	C(25A)-C(24A)-C(23A)	121.4(4)
C(24)-C(25)-C(26)	119.0(4)	C(24A)-C(25A)-C(26A)	119.5(4)
C(27)-C(26)-C(25)	121.5(4)	C(25A)-C(26A)-C(27A)	121.7(4)
C(26)-C(27)-C(22)	118.3(4)	C(26A)-C(27A)-C(22A)	117.9(4)
C(26)-C(27)-C(31)	120.0(4)	C(26A)-C(27A)-C(31A)	120.9(4)
C(22)-C(27)-C(31)	121.7(3)	C(22A)-C(27A)-C(31A)	121.3(4)
C(29)-C(28)-C(30)	110.9(4)	C(23A)-C(28A)-C(29A)	111.8(4)
C(29)-C(28)-C(23)	112.3(3)	C(23A)-C(28A)-C(30A)	111.9(4)
C(30)-C(28)-C(23)	110.9(3)	C(29A)-C(28A)-C(30A)	110.6(4)
C(32)-C(31)-C(33)	110.8(4)	C(32A)-C(31A)-C(33A)	108.3(5)
C(32)-C(31)-C(27)	110.2(3)	C(32A)-C(31A)-C(27A)	111.3(4)
C(33)-C(31)-C(27)	113.3(3)	C(33A)-C(31A)-C(27A)	113.6(4)
N(4)-C(34)-C(41)	109.1(3)	N(4A)-C(34A)-C(41A)	110.0(4)
N(4)-C(34)-C(35)	109.6(3)	N(4A)-C(34A)-C(35A)	110.1(5)
C(41)-C(34)-C(35)	113.7(3)	C(41A)-C(34A)-C(35A)	110.3(6)
C(36)-C(35)-C(34)	118.5(4)	C(36A)-C(35A)-C(34A)	129.4(7)
C(37)-C(36)-C(35)	119.8(4)	C(35A)-C(36A)-C(37A)	130.6(7)
C(36)-C(37)-C(38)	118.5(4)	C(38A)-C(37A)-C(36A)	124.1(7)
C(37)-C(38)-C(39)	116.8(4)	C(37A)-C(38A)-C(39A)	113.8(8)
C(40)-C(39)-C(38)	116.1(4)	C(40A)-C(39A)-C(38A)	120.9(7)
C(39)-C(40)-C(41)	119.3(4)	C(39A)-C(40A)-C(41A)	131.4(6)
C(34)-C(41)-C(40)	114.9(4)	C(40A)-C(41A)-C(34A)	122.1(5)

Table C.21 Crystal data and structure refinement for **1-N(^{2}Ad)**.

Identification code	acb26
Empirical formula	C43 H58 Fe N4
Formula weight	686.78
Temperature	223(2) K
Wavelength	0.71073 Å
Crystal system	Monoclinic
Space group	C2/c

Unit cell dimensions	a = 29.160(4) Å	α= 90°.
	b = 14.6320(19) Å	β= 94.477(5)°.
	c = 20.850(3) Å	γ = 90°.
Volume	8869(2) $Å^3$	
Z	8	
Density (calculated)	1.029 Mg/m^3	
Absorption coefficient	0.370 mm^{-1}	
F(000)	2960	
Crystal size	0.10 x 0.10 x 0.10 mm^3	
Theta range for data collection	1.56 to 22.72°.	
Index ranges	-31<=h<=31, -15<=k<=13, -21<=l<=22	
Reflections collected	26619	
Independent reflections	5970 [R(int) = 0.0655]	
Completeness to theta = 22.72°	99.9 %	
Absorption correction	Semi-empirical from equivalents	
Max. and min. transmission	0.9640 and 0.9640	
Refinement method	Full-matrix least-squares on F^2	
Data / restraints / parameters	5970 / 0 / 442	
Goodness-of-fit on F^2	1.079	
Final R indices [I>2sigma(I)]	R1 = 0.0572, wR2 = 0.1434	
R indices (all data)	R1 = 0.0892, wR2 = 0.1564	
Largest diff. peak and hole	0.393 and -0.347 $e.Å^{-3}$	

Table C.22 Atomic coordinates (x 10^4) and equivalent isotropic displacement parameters ($Å^2$x 10^3) for **1-N(²Ad)**. U(eq) is defined as one third of the trace of the orthogonalized U^{ij} tensor.

	x	y	z	U(eq)
Fe(1)	3087(1)	8802(1)	8749(1)	40(1)
N(1)	2455(1)	9239(2)	8506(1)	39(1)
N(2)	2721(1)	7816(2)	9009(1)	33(1)
N(3)	3557(1)	7917(2)	9063(1)	43(1)
N(4)	3399(1)	9715(2)	8569(2)	71(1)

C(1)	1609(1)	8936(2)	8460(2)	51(1)
C(2)	2103(1)	8692(2)	8618(1)	36(1)
C(3)	2248(1)	7847(2)	8918(1)	33(1)
C(4)	1985(1)	7144(2)	9117(1)	41(1)
C(5)	2194(1)	6387(2)	9427(1)	42(1)
C(6)	2669(1)	6349(2)	9518(1)	40(1)
C(7)	2930(1)	7061(2)	9296(1)	38(1)
C(8)	3415(1)	7136(2)	9317(1)	43(1)
C(9)	3730(1)	6402(2)	9599(2)	62(1)
C(10)	2353(1)	10128(2)	8216(1)	42(1)
C(11)	2294(1)	10871(2)	8627(2)	53(1)
C(12)	2245(1)	11726(2)	8335(2)	63(1)
C(13)	2252(1)	11842(2)	7684(2)	59(1)
C(14)	2289(1)	11096(2)	7298(2)	55(1)
C(15)	2338(1)	10219(2)	7551(2)	46(1)
C(16)	2280(1)	10764(3)	9348(2)	72(1)
C(17)	2701(2)	11170(3)	9717(2)	93(2)
C(18)	1836(2)	11164(3)	9575(2)	110(2)
C(19)	2359(1)	9391(2)	7114(2)	58(1)
C(20)	2809(1)	9361(3)	6789(2)	78(1)
C(21)	1943(1)	9366(3)	6616(2)	88(1)
C(22)	4044(1)	8069(2)	9027(2)	49(1)
C(23)	4308(1)	8415(2)	9561(2)	55(1)
C(24)	4768(1)	8602(3)	9488(2)	76(1)
C(25)	4958(1)	8443(4)	8918(2)	99(2)
C(26)	4698(1)	8078(4)	8406(2)	106(2)
C(27)	4232(1)	7878(3)	8447(2)	73(1)
C(28)	4108(1)	8597(3)	10196(2)	61(1)
C(29)	4362(1)	8050(3)	10740(2)	92(2)
C(30)	4099(2)	9601(3)	10361(2)	102(2)
C(31)	3947(1)	7448(3)	7873(2)	88(1)
C(32)	3996(2)	6429(4)	7867(3)	150(2)
C(33)	4041(2)	7828(4)	7221(2)	116(2)
C(34)	3780(2)	10230(4)	8480(3)	161(2)
C(35)	3849(2)	11125(3)	8873(2)	102(2)

C(36)	4335(2)	11364(5)	8839(3)	177(3)
C(37)	4453(2)	11673(5)	8138(3)	154(3)
C(38)	4101(2)	12296(4)	7883(3)	171(3)
C(39)	3622(2)	11968(3)	7839(3)	112(2)
C(40)	3583(2)	11075(4)	7532(3)	131(2)
C(41)	3921(2)	10384(4)	7785(3)	127(2)
C(42)	4391(2)	10706(5)	7803(4)	174(3)
C(43)	3547(2)	11830(4)	8563(3)	167(3)

Table C.23 Bond lengths [Å] and angles [°] for **1-N(^{2}Ad)**.

Fe(1)-N(4)	1.675(3)	C(3)-C(4)-C(5)	120.0(3)
Fe(1)-N(2)	1.898(2)	C(6)-C(5)-C(4)	119.4(3)
Fe(1)-N(3)	1.960(2)	C(5)-C(6)-C(7)	119.5(3)
Fe(1)-N(1)	1.978(2)	N(2)-C(7)-C(6)	120.7(3)
N(1)-C(2)	1.337(4)	N(2)-C(7)-C(8)	111.0(3)
N(1)-C(10)	1.456(4)	C(6)-C(7)-C(8)	128.3(3)
N(2)-C(3)	1.378(3)	N(3)-C(8)-C(7)	113.1(3)
N(2)-C(7)	1.376(3)	N(3)-C(8)-C(9)	124.5(3)
N(3)-C(8)	1.339(4)	C(7)-C(8)-C(9)	122.3(3)
N(3)-C(22)	1.444(4)	C(15)-C(10)-C(11)	122.6(3)
N(4)-C(34)	1.367(6)	C(15)-C(10)-N(1)	119.3(3)
C(1)-C(2)	1.496(4)	C(11)-C(10)-N(1)	118.0(3)
C(2)-C(3)	1.434(4)	C(12)-C(11)-C(10)	116.3(3)
C(3)-C(4)	1.368(4)	C(12)-C(11)-C(16)	121.1(3)
C(4)-C(5)	1.399(4)	C(10)-C(11)-C(16)	122.7(3)
C(5)-C(6)	1.384(4)	C(13)-C(12)-C(11)	122.3(3)
C(6)-C(7)	1.392(4)	C(14)-C(13)-C(12)	119.6(3)
C(7)-C(8)	1.414(4)	C(13)-C(14)-C(15)	121.7(3)
C(8)-C(9)	1.503(4)	C(10)-C(15)-C(14)	117.4(3)
C(10)-C(15)	1.390(4)	C(10)-C(15)-C(19)	121.5(3)
C(10)-C(11)	1.403(4)	C(14)-C(15)-C(19)	121.1(3)
C(11)-C(12)	1.394(5)	C(11)-C(16)-C(17)	112.3(3)
C(11)-C(16)	1.515(5)	C(11)-C(16)-C(18)	110.9(3)
C(12)-C(13)	1.370(5)	C(17)-C(16)-C(18)	111.3(3)
C(13)-C(14)	1.365(4)	C(20)-C(19)-C(15)	111.4(3)
C(14)-C(15)	1.390(4)	C(20)-C(19)-C(21)	111.1(3)
C(15)-C(19)	1.521(4)	C(15)-C(19)-C(21)	111.0(3)
C(16)-C(17)	1.517(5)	C(23)-C(22)-C(27)	122.2(3)
C(16)-C(18)	1.530(6)	C(23)-C(22)-N(3)	119.7(3)
C(19)-C(20)	1.523(5)	C(27)-C(22)-N(3)	118.0(3)

C(19)-C(21)	1.535(5)	C(24)-C(23)-C(22)	117.4(3)
C(22)-C(23)	1.399(4)	C(24)-C(23)-C(28)	120.2(3)
C(22)-C(27)	1.393(5)	C(22)-C(23)-C(28)	122.3(3)
C(23)-C(24)	1.390(5)	C(25)-C(24)-C(23)	121.4(4)
C(23)-C(28)	1.512(5)	C(26)-C(25)-C(24)	120.5(4)
C(24)-C(25)	1.368(5)	C(25)-C(26)-C(27)	121.0(4)
C(25)-C(26)	1.368(6)	C(22)-C(27)-C(26)	117.4(3)
C(26)-C(27)	1.401(5)	C(22)-C(27)-C(31)	122.1(3)
C(27)-C(31)	1.537(5)	C(26)-C(27)-C(31)	120.5(3)
C(28)-C(30)	1.510(5)	C(30)-C(28)-C(23)	112.7(3)
C(28)-C(29)	1.532(5)	C(30)-C(28)-C(29)	110.8(3)
C(31)-C(32)	1.499(7)	C(23)-C(28)-C(29)	111.0(3)
C(31)-C(33)	1.514(6)	C(32)-C(31)-C(33)	109.4(4)
C(34)-C(41)	1.554(7)	C(32)-C(31)-C(27)	111.5(4)
C(34)-C(35)	1.550(7)	C(33)-C(31)-C(27)	115.1(4)
C(35)-C(36)	1.468(7)	N(4)-C(34)-C(41)	119.0(5)
C(35)-C(43)	1.472(7)	N(4)-C(34)-C(35)	117.9(5)
C(36)-C(37)	1.593(8)	C(41)-C(34)-C(35)	109.8(4)
C(37)-C(38)	1.444(8)	C(36)-C(35)-C(43)	111.0(5)
C(37)-C(42)	1.582(9)	C(36)-C(35)-C(34)	105.2(5)
C(38)-C(39)	1.472(7)	C(43)-C(35)-C(34)	108.1(5)
C(39)-C(40)	1.455(7)	C(35)-C(36)-C(37)	113.0(4)
C(39)-C(43)	1.556(7)	C(38)-C(37)-C(42)	110.4(5)
C(40)-C(41)	1.480(7)	C(38)-C(37)-C(36)	108.5(5)
C(41)-C(42)	1.446(7)	C(42)-C(37)-C(36)	97.3(6)
N(4)-Fe(1)-N(2)	175.64(13)	C(37)-C(38)-C(39)	117.5(5)
N(4)-Fe(1)-N(3)	102.93(12)	C(40)-C(39)-C(38)	111.2(5)
N(2)-Fe(1)-N(3)	78.23(10)	C(40)-C(39)-C(43)	107.3(4)
N(4)-Fe(1)-N(1)	101.30(12)	C(38)-C(39)-C(43)	100.7(5)
N(2)-Fe(1)-N(1)	77.66(10)	C(39)-C(40)-C(41)	115.5(5)
N(3)-Fe(1)-N(1)	155.75(10)	C(42)-C(41)-C(40)	112.9(5)
C(2)-N(1)-C(10)	118.2(2)	C(42)-C(41)-C(34)	110.1(5)
C(2)-N(1)-Fe(1)	118.33(19)	C(40)-C(41)-C(34)	102.3(5)
C(10)-N(1)-Fe(1)	123.46(18)	C(41)-C(42)-C(37)	112.2(5)
C(3)-N(2)-C(7)	119.4(2)	C(35)-C(43)-C(39)	113.1(5)
C(3)-N(2)-Fe(1)	120.93(18)	C(32A)-C(31A)-C(27A)	111.3(4)
C(7)-N(2)-Fe(1)	119.68(18)	C(33A)-C(31A)-C(27A)	113.6(4)
C(8)-N(3)-C(22)	119.2(2)	N(4A)-C(34A)-C(41A)	110.0(4)
C(8)-N(3)-Fe(1)	117.79(19)	N(4A)-C(34A)-C(35A)	110.1(5)
C(22)-N(3)-Fe(1)	123.0(2)	C(41A)-C(34A)-C(35A)	110.3(6)
C(34)-N(4)-Fe(1)	158.7(4)	C(36A)-C(35A)-C(34A)	129.4(7)
N(1)-C(2)-C(3)	112.8(2)	C(35A)-C(36A)-C(37A)	130.6(7)
N(1)-C(2)-C(1)	124.0(3)	C(38A)-C(37A)-C(36A)	124.1(7)
C(3)-C(2)-C(1)	123.3(3)	C(37A)-C(38A)-C(39A)	113.8(8)
C(4)-C(3)-N(2)	120.9(3)	C(40A)-C(39A)-C(38A)	120.9(7)
C(4)-C(3)-C(2)	128.7(3)	C(39A)-C(40A)-C(41A)	131.4(6)
N(2)-C(3)-C(2)	110.3(2)	C(40A)-C(41A)-C(34A)	122.1(5)

Table C.24 Crystal data and structure refinement for **2-NH_2-^{1}Ad**.

Identification code	acb5	
Empirical formula	C43 H60 Fe N4	
Formula weight	688.80	
Temperature	173(2) K	
Wavelength	0.71073 Å	
Crystal system	Monoclinic	
Space group	P2(1)/n	
Unit cell dimensions	a = 13.4290(9) Å	α= 90°.
	b = 18.0517(11) Å	β= 103.695(3)°.
	c = 16.2227(10) Å	γ = 90°.
Volume	3820.8(4) $Å^3$	
Z	4	
Density (calculated)	1.197 Mg/m^3	
Absorption coefficient	0.429 mm^{-1}	
F(000)	1488	
Crystal size	0.40 x 0.30 x 0.25 mm^3	
Theta range for data collection	1.77 to 26.37°.	
Index ranges	-16<=h<=16, -21<=k<=22, -20<=l<=19	
Reflections collected	42713	
Independent reflections	7812 [R(int) = 0.0760]	
Completeness to theta = 26.37°	100.0 %	
Absorption correction	Semi-empirical from equivalents	
Max. and min. transmission	0.9003 and 0.8470	
Refinement method	Full-matrix least-squares on F^2	
Data / restraints / parameters	7812 / 0 / 585	
Goodness-of-fit on F^2	1.068	
Final R indices [I>2sigma(I)]	R1 = 0.0508, wR2 = 0.1221	
R indices (all data)	R1 = 0.0776, wR2 = 0.1361	
Largest diff. peak and hole	0.496 and -0.615 $e.Å^{-3}$	

Table C.25 Atomic coordinates (x 10^4) and equivalent isotropic displacement parameters ($Å^2$x 10^3) for **2-NH_2-^{1}Ad**. U(eq) is defined as one third of the trace of the orthogonalized U^{ij} tensor.

	x	y	z	U(eq)
Fe(1)	5793(1)	8312(1)	8647(1)	22(1)
N(1)	5063(1)	7837(1)	9460(1)	24(1)
N(2)	6051(1)	9050(1)	9659(1)	22(1)
N(3)	6555(1)	9152(1)	8251(1)	23(1)
N(4)	6063(2)	7433(1)	7823(1)	37(1)
C(1)	4633(2)	7946(1)	10834(1)	38(1)
C(2)	5086(2)	8180(1)	10223(1)	26(1)
C(3)	5664(1)	8890(1)	10323(1)	24(1)
C(4)	5817(2)	9375(1)	11004(1)	30(1)
C(5)	6363(2)	10019(1)	10966(1)	34(1)
C(6)	6738(2)	10175(1)	10268(1)	31(1)
C(7)	6569(1)	9674(1)	9602(1)	23(1)
C(8)	6861(2)	9749(1)	8780(1)	26(1)
C(9)	7346(2)	10364(1)	8607(2)	37(1)
C(10)	4522(2)	7149(1)	9303(1)	24(1)
C(11)	5069(2)	6481(1)	9423(1)	28(1)
C(12)	4546(2)	5822(1)	9189(2)	35(1)
C(13)	3499(2)	5817(1)	8853(2)	38(1)
C(14)	2958(2)	6474(1)	8757(2)	34(1)
C(15)	3449(2)	7146(1)	8985(1)	28(1)
C(16)	6215(2)	6460(1)	9836(2)	34(1)
C(17)	6797(2)	5871(1)	9470(2)	46(1)
C(18)	6368(2)	6352(1)	10792(2)	49(1)
C(19)	2824(2)	7852(1)	8896(1)	33(1)
C(20)	2027(2)	7825(2)	9430(2)	54(1)
C(21)	2294(2)	8033(2)	7980(2)	57(1)
C(22)	6739(1)	9195(1)	7420(1)	22(1)
C(23)	6036(2)	9573(1)	6772(1)	30(1)
C(24)	6162(2)	9524(1)	5953(1)	39(1)

C(25)	6958(2)	9139(1)	5759(1)	38(1)
C(26)	7670(2)	8815(1)	6397(1)	34(1)
C(27)	7593(2)	8840(1)	7238(1)	26(1)
C(28)	5177(2)	10040(1)	6962(2)	40(1)
C(29)	5262(2)	10846(1)	6704(2)	58(1)
C(30)	4124(2)	9742(2)	6552(2)	56(1)
C(31)	8448(2)	8534(1)	7945(2)	37(1)
C(32)	9340(2)	9070(2)	8134(2)	71(1)
C(33)	8826(2)	7776(2)	7765(2)	57(1)
C(34)	5320(2)	7162(1)	7033(1)	28(1)
C(35)	5906(4)	6879(3)	6406(3)	43(2)
C(36)	4581(4)	6609(3)	7214(3)	42(1)
C(37)	4686(4)	7856(3)	6601(4)	38(1)
C(38)	5145(5)	6608(4)	5582(4)	43(2)
C(39)	4565(5)	7277(4)	5178(4)	53(2)
C(40)	3900(5)	7602(4)	5750(5)	50(2)
C(41)	3220(5)	7035(4)	5952(4)	51(2)
C(42)	3830(5)	6341(4)	6388(4)	46(2)
C(43)	4432(5)	6054(4)	5782(4)	47(2)
C(35')	5671(4)	7346(4)	6263(3)	59(2)
C(36')	5249(4)	6307(2)	7092(3)	47(1)
C(37')	4304(3)	7470(3)	7025(3)	51(1)
C(38')	4790(5)	6212(5)	5523(5)	88(3)
C(39')	4886(4)	7049(4)	5474(3)	59(2)
C(40')	3886(5)	7417(4)	5441(4)	56(2)
C(41')	3506(4)	7199(4)	6243(3)	57(2)
C(42')	3437(5)	6393(5)	6276(5)	69(2)
C(43')	4441(5)	6027(3)	6317(4)	69(2)

Table C.26 Bond lengths [Å] for **2-NH_2-^{1}Ad**.

Fe(1)-N(1)	2.0117(17)	C(23)-C(28)	1.519(3)
Fe(1)-N(3)	2.0177(16)	C(24)-C(25)	1.373(3)

Fe(1)-N(2)	2.0776(16)	C(25)-C(26)	1.364(3)
Fe(1)-N(4)	2.1606(19)	C(26)-C(27)	1.393(3)
N(1)-C(2)	1.378(3)	C(27)-C(31)	1.522(3)
N(1)-C(10)	1.431(2)	C(28)-C(30)	1.512(3)
N(2)-C(3)	1.333(3)	C(28)-C(29)	1.525(4)
N(2)-C(7)	1.339(2)	C(31)-C(33)	1.511(3)
N(3)-C(8)	1.378(2)	C(31)-C(32)	1.514(4)
N(3)-C(22)	1.430(2)	C(34)-C(37')	1.470(5)
N(4)-C(34)	1.507(3)	C(34)-C(35')	1.474(5)
C(1)-C(2)	1.347(3)	C(34)-C(36)	1.485(6)
C(2)-C(3)	1.487(3)	C(34)-C(35)	1.515(6)
C(3)-C(4)	1.386(3)	C(34)-C(36')	1.551(5)
C(4)-C(5)	1.383(3)	C(34)-C(37)	1.581(5)
C(5)-C(6)	1.373(3)	C(35)-C(38)	1.557(8)
C(6)-C(7)	1.386(3)	C(36)-C(42)	1.551(8)
C(7)-C(8)	1.482(3)	C(37)-C(40)	1.593(8)
C(8)-C(9)	1.350(3)	C(38)-C(43)	1.472(10)
C(10)-C(11)	1.402(3)	C(38)-C(39)	1.502(9)
C(10)-C(15)	1.411(3)	C(39)-C(40)	1.547(10)
C(11)-C(12)	1.389(3)	C(40)-C(41)	1.459(10)
C(11)-C(16)	1.527(3)	C(41)-C(42)	1.571(10)
C(12)-C(13)	1.383(3)	C(42)-C(43)	1.505(10)
C(13)-C(14)	1.379(3)	C(35')-C(39')	1.549(8)
C(14)-C(15)	1.389(3)	C(36')-C(43')	1.539(7)
C(15)-C(19)	1.514(3)	C(37')-C(41')	1.533(7)
C(16)-C(17)	1.521(3)	C(38')-C(43')	1.508(10)
C(16)-C(18)	1.528(3)	C(38')-C(39')	1.520(11)
C(19)-C(21)	1.523(3)	C(39')-C(40')	1.488(9)
C(19)-C(20)	1.530(3)	C(40')-C(41')	1.556(9)
C(22)-C(27)	1.404(3)	C(41')-C(42')	1.460(11)
C(22)-C(23)	1.411(3)	C(42')-C(43')	1.489(9)
C(23)-C(24)	1.382(3)		

Table C.27 Angles [°] for **2-NH_2-^{1}Ad**.

N(1)-Fe(1)-N(3)	153.08(7)	C(26)-C(27)-C(31)	120.59(19)
N(1)-Fe(1)-N(2)	76.79(6)	C(22)-C(27)-C(31)	120.93(19)
N(3)-Fe(1)-N(2)	76.56(6)	C(30)-C(28)-C(23)	112.9(2)
N(1)-Fe(1)-N(4)	105.78(8)	C(30)-C(28)-C(29)	109.9(2)
N(3)-Fe(1)-N(4)	100.54(8)	C(23)-C(28)-C(29)	111.3(2)
N(2)-Fe(1)-N(4)	159.80(7)	C(33)-C(31)-C(32)	109.4(2)
C(2)-N(1)-C(10)	116.92(16)	C(33)-C(31)-C(27)	114.2(2)
C(2)-N(1)-Fe(1)	119.12(13)	C(32)-C(31)-C(27)	109.9(2)
C(10)-N(1)-Fe(1)	123.95(13)	C(37')-C(34)-C(35')	112.9(3)
C(3)-N(2)-C(7)	123.11(17)	C(37')-C(34)-C(36)	66.0(3)
C(3)-N(2)-Fe(1)	118.38(13)	C(35')-C(34)-C(36)	132.9(3)

C(7)-N(2)-Fe(1)	118.47(13)	C(37')-C(34)-N(4)	108.2(2)
C(8)-N(3)-C(22)	116.92(16)	C(35')-C(34)-N(4)	111.6(3)
C(8)-N(3)-Fe(1)	119.24(13)	C(36)-C(34)-N(4)	112.9(3)
C(22)-N(3)-Fe(1)	123.70(12)	C(37')-C(34)-C(35)	138.6(3)
C(34)-N(4)-Fe(1)	126.17(14)	C(35')-C(34)-C(35)	35.4(3)
C(1)-C(2)-N(1)	127.00(19)	C(36)-C(34)-C(35)	112.5(3)
C(1)-C(2)-C(3)	120.37(19)	N(4)-C(34)-C(35)	109.6(2)
N(1)-C(2)-C(3)	112.60(17)	C(37')-C(34)-C(36')	107.8(3)
N(2)-C(3)-C(4)	119.67(19)	C(35')-C(34)-C(36')	108.2(4)
N(2)-C(3)-C(2)	113.10(17)	C(36)-C(34)-C(36')	42.7(3)
C(4)-C(3)-C(2)	127.22(19)	N(4)-C(34)-C(36')	107.9(2)
C(5)-C(4)-C(3)	118.4(2)	C(35)-C(34)-C(36')	75.8(3)
C(6)-C(5)-C(4)	120.7(2)	C(37')-C(34)-C(37)	45.3(3)
C(5)-C(6)-C(7)	119.0(2)	C(35')-C(34)-C(37)	72.1(3)
N(2)-C(7)-C(6)	119.11(19)	C(36)-C(34)-C(37)	107.8(3)
N(2)-C(7)-C(8)	113.06(17)	N(4)-C(34)-C(37)	107.4(2)
C(6)-C(7)-C(8)	127.78(19)	C(35)-C(34)-C(37)	106.2(3)
C(9)-C(8)-N(3)	126.9(2)	C(36')-C(34)-C(37)	141.4(3)
C(9)-C(8)-C(7)	120.38(19)	C(34)-C(35)-C(38)	110.0(4)
N(3)-C(8)-C(7)	112.65(17)	C(34)-C(36)-C(42)	111.6(4)
C(11)-C(10)-C(15)	120.27(18)	C(34)-C(37)-C(40)	109.5(4)
C(11)-C(10)-N(1)	119.63(17)	C(43)-C(38)-C(39)	110.2(5)
C(15)-C(10)-N(1)	120.00(18)	C(43)-C(38)-C(35)	110.7(5)
C(12)-C(11)-C(10)	119.01(19)	C(39)-C(38)-C(35)	106.8(5)
C(12)-C(11)-C(16)	119.35(19)	C(38)-C(39)-C(40)	110.8(6)
C(10)-C(11)-C(16)	121.59(18)	C(41)-C(40)-C(39)	110.5(6)
C(13)-C(12)-C(11)	120.9(2)	C(41)-C(40)-C(37)	109.2(6)
C(14)-C(13)-C(12)	119.9(2)	C(39)-C(40)-C(37)	105.7(5)
C(13)-C(14)-C(15)	121.1(2)	C(40)-C(41)-C(42)	111.9(6)
C(14)-C(15)-C(10)	118.69(19)	C(43)-C(42)-C(41)	106.5(5)
C(14)-C(15)-C(19)	119.55(18)	C(43)-C(42)-C(36)	109.4(6)
C(10)-C(15)-C(19)	121.76(18)	C(41)-C(42)-C(36)	107.6(5)
C(17)-C(16)-C(18)	110.43(19)	C(38)-C(43)-C(42)	112.8(5)
C(17)-C(16)-C(11)	113.80(19)	C(34)-C(35')-C(39')	109.3(4)
C(18)-C(16)-C(11)	109.2(2)	C(43')-C(36')-C(34)	108.5(4)
C(15)-C(19)-C(21)	113.2(2)	C(34)-C(37')-C(41')	110.7(4)
C(15)-C(19)-C(20)	111.38(19)	C(43')-C(38')-C(39')	108.1(5)
C(21)-C(19)-C(20)	109.4(2)	C(40')-C(39')-C(38')	111.0(5)
C(27)-C(22)-C(23)	119.92(18)	C(40')-C(39')-C(35')	107.9(5)
C(27)-C(22)-N(3)	120.46(17)	C(38')-C(39')-C(35')	110.5(5)
C(23)-C(22)-N(3)	119.58(17)	C(39')-C(40')-C(41')	109.2(5)
C(24)-C(23)-C(22)	118.3(2)	C(42')-C(41')-C(37')	109.0(5)
C(24)-C(23)-C(28)	120.16(19)	C(42')-C(41')-C(40')	108.5(5)
C(22)-C(23)-C(28)	121.56(19)	C(37')-C(41')-C(40')	107.9(5)
C(25)-C(24)-C(23)	122.1(2)	C(41')-C(42')-C(43')	112.3(5)
C(26)-C(25)-C(24)	119.2(2)	C(42')-C(43')-C(38')	108.9(6)
C(25)-C(26)-C(27)	121.9(2)	C(42')-C(43')-C(36')	110.3(6)
C(26)-C(27)-C(22)	118.37(18)	C(38')-C(43')-C(36')	108.9(5)

Table C.28 Crystal data and structure refinement for **1-N(^{1}Ad)CHC(SiMe$_3$)**.

Identification code	acb7	
Empirical formula	C54 H74 Fe N4 Si	
Formula weight	863.11	
Temperature	173(2) K	
Wavelength	0.71073 Å	
Crystal system	Orthorhombic	
Space group	Pnma	
Unit cell dimensions	a = 17.9318(14) Å	α= 90°.
	b = 14.0871(11) Å	β= 90°.
	c = 19.1581(15) Å	γ = 90°.
Volume	4839.5(7) Å^3	
Z	4	
Density (calculated)	1.185 Mg/m^3	
Absorption coefficient	0.376 mm^{-1}	
F(000)	1864	
Crystal size	0.60 x 0.50 x 0.40 mm^3	
Theta range for data collection	1.79 to 28.28°.	
Index ranges	-23<=h<=20, -12<=k<=18, -25<=l<=24	
Reflections collected	35528	
Independent reflections	6241 [R(int) = 0.0522]	
Completeness to theta = 28.28°	99.9 %	
Absorption correction	Semi-empirical from equivalents	
Max. and min. transmission	0.8642 and 0.8060	
Refinement method	Full-matrix least-squares on F^2	
Data / restraints / parameters	6241 / 0 / 458	
Goodness-of-fit on F^2	1.059	
Final R indices [I>2sigma(I)]	R1 = 0.0408, wR2 = 0.0926	
R indices (all data)	R1 = 0.0630, wR2 = 0.1014	
Largest diff. peak and hole	0.301 and -0.343 e.Å^{-3}	

Table C.29 Atomic coordinates (x 10^4) and equivalent isotropic displacement parameters (Å^{2}x 10^3) for **1-N(^{1}Ad)CHC(SiMe$_3$)**. U(eq) is defined as one third of the trace of the orthogonalized U^{ij} tensor.

	x	y	z	U(eq)
Fe(1)	2244(1)	2500	6830(1)	15(1)
Si(1)	922(1)	2500	8241(1)	20(1)
N(1)	2644(1)	1060(1)	6849(1)	18(1)
N(2)	3026(1)	2500	7533(1)	16(1)
N(3)	1420(1)	2500	6160(1)	19(1)
C(1)	3284(1)	-123(1)	7603(1)	32(1)
C(2)	3047(1)	852(1)	7398(1)	20(1)
C(3)	3262(1)	1661(1)	7814(1)	18(1)
C(4)	3666(1)	1649(1)	8431(1)	22(1)
C(5)	3851(1)	2500	8749(1)	25(1)
C(6)	2414(1)	337(1)	6367(1)	19(1)
C(7)	1788(1)	-227(1)	6504(1)	23(1)
C(8)	1565(1)	-870(1)	5995(1)	29(1)
C(9)	1937(1)	-945(1)	5370(1)	34(1)
C(10)	2550(1)	-383(1)	5243(1)	32(1)
C(11)	2806(1)	264(1)	5735(1)	24(1)
C(12)	1349(1)	-164(1)	7179(1)	28(1)
C(13)	530(1)	56(1)	7052(1)	37(1)
C(14)	1415(1)	-1082(1)	7602(1)	48(1)
C(15)	3515(1)	824(1)	5605(1)	32(1)
C(16)	3653(1)	1069(1)	4843(1)	45(1)
C(17)	4183(1)	286(2)	5889(1)	48(1)
C(18)	949(1)	2500	6717(1)	19(1)
C(19)	1287(1)	2500	7360(1)	19(1)
C(20)	1262(1)	1447(1)	8740(1)	34(1)
C(21)	-123(1)	2500	8253(1)	34(1)
C(22)	1159(1)	2500	5442(1)	19(1)
C(23)	698(1)	1612(1)	5277(1)	22(1)
C(24)	472(1)	1612(1)	4504(1)	24(1)

C(25)	1173(1)	1615(1)	4053(1)	36(1)
C(26)	1633(1)	2500	4211(1)	38(1)
C(27)	1849(1)	2500	4982(1)	33(1)
C(28)	15(1)	2500	4345(1)	22(1)
C(1S)	617(1)	2500	10739(1)	44(1)
C(2S)	206(1)	2500	11345(1)	50(1)
C(3S)	561(1)	2500	11978(1)	46(1)
C(4S)	1325(1)	2500	12014(1)	38(1)
C(5S)	1736(1)	2500	11408(1)	41(1)
C(6S)	1384(1)	2500	10774(1)	42(1)

Symmetry transformations used to generate equivalent atoms:
#1 x,-y+1/2,z

Table C.30 Bond lengths [Å] and angles [°] for **1-N(^{1}Ad)CHC(SiMe$_3$)**.

Fe(1)-N(2)	1.9446(14)	C(20)-Si(1)-C(20)#1	105.19(10)
Fe(1)-N(3)	1.9573(14)	C(19)-Si(1)-C(21)	111.91(9)
Fe(1)-C(19)	1.9932(17)	C(20)-Si(1)-C(21)	108.71(6)
Fe(1)-N(1)	2.1517(11)	C(20)#1-Si(1)-C(21)	108.71(6)
Fe(1)-N(1)#1	2.1517(11)	C(2)-N(1)-C(6)	121.03(11)
Fe(1)-C(18)	2.3322(17)	C(2)-N(1)-Fe(1)	114.12(8)
Si(1)-C(19)	1.8113(18)	C(6)-N(1)-Fe(1)	124.26(8)
Si(1)-C(20)	1.8672(16)	C(3)-N(2)-C(3)#1	119.89(14)
Si(1)-C(20)#1	1.8673(16)	C(3)-N(2)-Fe(1)	119.72(7)
Si(1)-C(21)	1.873(2)	C(3)#1-N(2)-Fe(1)	119.73(7)
N(1)-C(2)	1.3095(15)	C(18)-N(3)-C(22)	122.81(14)
N(1)-C(6)	1.4343(16)	C(18)-N(3)-Fe(1)	87.35(10)
N(2)-C(3)	1.3662(14)	C(22)-N(3)-Fe(1)	149.84(11)
N(2)-C(3)#1	1.3663(14)	N(1)-C(2)-C(3)	114.45(11)
N(3)-C(18)	1.362(2)	N(1)-C(2)-C(1)	125.19(12)
N(3)-C(22)	1.453(2)	C(3)-C(2)-C(1)	120.36(11)
C(1)-C(2)	1.4898(19)	N(2)-C(3)-C(4)	120.51(12)
C(2)-C(3)	1.4437(18)	N(2)-C(3)-C(2)	112.52(10)
C(3)-C(4)	1.3857(17)	C(4)-C(3)-C(2)	126.97(12)
C(4)-C(5)	1.3851(16)	C(5)-C(4)-C(3)	119.35(13)
C(5)-C(4)#1	1.3850(16)	C(4)#1-C(5)-C(4)	119.87(17)
C(6)-C(7)	1.4013(18)	C(7)-C(6)-C(11)	121.37(12)
C(6)-C(11)	1.4045(17)	C(7)-C(6)-N(1)	120.89(11)
C(7)-C(8)	1.3893(19)	C(11)-C(6)-N(1)	117.58(11)
C(7)-C(12)	1.5166(19)	C(8)-C(7)-C(6)	117.97(12)

C(8)-C(9)	1.374(2)	C(8)-C(7)-C(12)	119.20(12)
C(9)-C(10)	1.377(2)	C(6)-C(7)-C(12)	122.83(11)
C(10)-C(11)	1.3897(19)	C(9)-C(8)-C(7)	121.52(13)
C(11)-C(15)	1.5158(19)	C(8)-C(9)-C(10)	119.80(13)
C(12)-C(13)	1.519(2)	C(9)-C(10)-C(11)	121.42(13)
C(12)-C(14)	1.531(2)	C(10)-C(11)-C(6)	117.90(12)
C(15)-C(17)	1.518(2)	C(10)-C(11)-C(15)	120.47(12)
C(15)-C(16)	1.522(2)	C(6)-C(11)-C(15)	121.52(12)
C(18)-C(19)	1.372(2)	C(7)-C(12)-C(13)	112.16(12)
C(22)-C(27)	1.521(3)	C(7)-C(12)-C(14)	111.17(13)
C(22)-C(23)	1.5318(16)	C(13)-C(12)-C(14)	109.40(13)
C(22)-C(23)#1	1.5318(16)	C(11)-C(15)-C(17)	110.11(13)
C(23)-C(24)	1.5356(17)	C(11)-C(15)-C(16)	114.33(13)
C(24)-C(25)	1.525(2)	C(17)-C(15)-C(16)	109.15(13)
C(24)-C(28)	1.5258(17)	N(3)-C(18)-C(19)	115.41(15)
C(25)-C(26)	1.525(2)	N(3)-C(18)-Fe(1)	56.97(8)
C(26)-C(25)#1	1.525(2)	C(19)-C(18)-Fe(1)	58.45(9)
C(26)-C(27)	1.527(3)	C(18)-C(19)-Si(1)	132.58(14)
C(28)-C(24)#1	1.5258(17)	C(18)-C(19)-Fe(1)	85.65(11)
C(1S)-C(2S)	1.376(3)	Si(1)-C(19)-Fe(1)	141.77(10)
C(1S)-C(6S)	1.377(3)	N(3)-C(22)-C(27)	106.65(14)
C(2S)-C(3S)	1.369(3)	N(3)-C(22)-C(23)	111.71(9)
C(3S)-C(4S)	1.372(3)	C(27)-C(22)-C(23)	108.60(9)
C(4S)-C(5S)	1.375(3)	N(3)-C(22)-C(23)#1	111.70(9)
C(5S)-C(6S)	1.369(3)	C(27)-C(22)-C(23)#1	108.61(9)
N(2)-Fe(1)-N(3)	177.19(6)	C(23)-C(22)-C(23)#1	109.44(14)
N(2)-Fe(1)-C(19)	105.60(6)	C(22)-C(23)-C(24)	110.01(11)
N(3)-Fe(1)-C(19)	71.58(6)	C(25)-C(24)-C(28)	109.09(12)
N(2)-Fe(1)-N(1)	75.41(3)	C(25)-C(24)-C(23)	109.15(11)
N(3)-Fe(1)-N(1)	105.21(3)	C(28)-C(24)-C(23)	109.55(12)
C(19)-Fe(1)-N(1)	106.19(3)	C(24)-C(25)-C(26)	109.66(13)
N(2)-Fe(1)-N(1)#1	75.41(3)	C(25)#1-C(26)-C(25)	109.64(17)
N(3)-Fe(1)-N(1)#1	105.21(3)	C(25)#1-C(26)-C(27)	109.19(10)
C(19)-Fe(1)-N(1)#1	106.19(3)	C(25)-C(26)-C(27)	109.19(10)
N(1)-Fe(1)-N(1)#1	140.99(5)	C(22)-C(27)-C(26)	110.76(15)
N(2)-Fe(1)-C(18)	141.50(6)	C(24)-C(28)-C(24)#1	110.10(15)
N(3)-Fe(1)-C(18)	35.68(6)	C(2S)-C(1S)-C(6S)	119.6(2)
C(19)-Fe(1)-C(18)	35.90(6)	C(3S)-C(2S)-C(1S)	119.9(2)
N(1)-Fe(1)-C(18)	109.48(3)	C(2S)-C(3S)-C(4S)	120.6(2)
N(1)#1-Fe(1)-C(18)	109.48(3)	C(5S)-C(4S)-C(3S)	119.5(2)
C(19)-Si(1)-C(20)	111.03(6)	C(6S)-C(5S)-C(4S)	120.1(2)
C(19)-Si(1)-C(20)#1	111.03(6)	C(5S)-C(6S)-C(1S)	120.3(2)

Table C.31 Crystal data and structure refinement for **1-[(N^{1}Ad)NN(N^{1}Ad)]**.

Identification code	acb6

Empirical formula	C53 H75 Fe N7	
Formula weight	866.05	
Temperature	203(2) K	
Wavelength	0.71073 Å	
Crystal system	Orthorhombic	
Space group	Pbcn	
Unit cell dimensions	a = 29.4026(17) Å	α= 90°.
	b = 18.0173(10) Å	β= 90°.
	c = 23.0034(12) Å	γ = 90°.
Volume	12186.2(12) $Å^3$	
Z	8	
Density (calculated)	0.944 Mg/m^3	
Absorption coefficient	0.281 mm^{-1}	
F(000)	3744	
Crystal size	0.60 x 0.50 x 0.40 mm^3	
Theta range for data collection	1.59 to 24.11°.	
Index ranges	-33<=h<=21, -20<=k<=17, -15<=l<=26	
Reflections collected	32384	
Independent reflections	9702 [R(int) = 0.0597]	
Completeness to theta = 24.11°	99.9 %	
Absorption correction	Semi-empirical from equivalents	
Max. and min. transmission	0.8958 and 0.8494	
Refinement method	Full-matrix least-squares on F^2	
Data / restraints / parameters	9702 / 0 / 483	
Goodness-of-fit on F^2	1.024	
Final R indices [I>2sigma(I)]	R1 = 0.0589, wR2 = 0.1553	
R indices (all data)	R1 = 0.0968, wR2 = 0.1732	
Largest diff. peak and hole	0.658 and -0.551 $e.Å^{-3}$	

Table C.32 Atomic coordinates (x 10^4) and equivalent isotropic displacement parameters ($Å^2$x 10^3) for **1-[(N^1Ad)NN(N^1Ad)]**. U(eq) is defined as one third of the trace of the orthogonalized U^{ij} tensor.

	x	y	z	U(eq)

Fe(1)	1788(1)	5856(1)	1258(1)	25(1)
N(1)	2054(1)	6730(1)	1863(1)	29(1)
N(2)	1687(1)	6811(1)	858(1)	28(1)
N(3)	1194(1)	5683(1)	678(1)	28(1)
N(4)	1847(1)	4944(1)	1699(1)	26(1)
N(5)	2193(1)	4506(1)	1534(1)	40(1)
N(6)	2435(1)	4730(1)	1117(1)	39(1)
N(7)	2325(1)	5401(1)	879(1)	30(1)
C(1)	2368(1)	8005(2)	1848(1)	52(1)
C(2)	2123(1)	7357(2)	1601(1)	34(1)
C(3)	1929(1)	7423(1)	1018(1)	32(1)
C(4)	1967(1)	8032(2)	660(1)	44(1)
C(5)	1743(1)	8034(2)	132(1)	46(1)
C(6)	1467(1)	7440(2)	-16(1)	44(1)
C(7)	1440(1)	6835(2)	356(1)	32(1)
C(8)	1143(1)	6191(2)	284(1)	31(1)
C(9)	804(1)	6180(2)	-198(1)	42(1)
C(10)	2172(1)	6662(1)	2467(1)	32(1)
C(11)	1864(1)	6937(2)	2879(1)	37(1)
C(12)	1987(1)	6864(2)	3464(1)	48(1)
C(13)	2392(1)	6551(2)	3631(1)	55(1)
C(14)	2680(1)	6279(2)	3217(1)	51(1)
C(15)	2581(1)	6321(2)	2625(1)	38(1)
C(16)	1425(1)	7324(2)	2720(1)	43(1)
C(17)	1448(1)	8160(2)	2833(2)	76(1)
C(18)	1011(1)	7015(2)	3046(2)	57(1)
C(19)	2911(1)	6026(2)	2179(1)	47(1)
C(20)	3121(1)	5279(2)	2344(2)	64(1)
C(21)	3288(1)	6593(2)	2057(2)	74(1)
C(22)	1593(1)	4620(2)	2186(1)	30(1)
C(23)	1420(1)	3839(2)	2053(1)	36(1)
C(24)	1875(1)	4592(2)	2748(1)	36(1)
C(25)	1183(1)	5117(2)	2285(1)	33(1)
C(26)	894(1)	4829(2)	2790(1)	40(1)

C(27)	724(1)	4051(2)	2650(1)	43(1)
C(28)	1136(1)	3540(2)	2560(1)	39(1)
C(29)	1422(1)	3516(2)	3109(1)	43(1)
C(30)	1586(1)	4299(2)	3253(1)	40(1)
C(31)	1180(1)	4810(2)	3337(1)	44(1)
C(32)	2649(2)	5582(3)	413(2)	31(1)
C(33)	3116(2)	5323(3)	452(2)	41(1)
C(34)	2631(2)	6431(2)	278(2)	34(1)
C(35)	2427(2)	5225(3)	-176(2)	38(1)
C(36)	2709(2)	5436(3)	-724(2)	44(1)
C(37)	3176(2)	5162(3)	-621(3)	55(2)
C(38)	3432(2)	5558(3)	-73(2)	53(2)
C(39)	3396(2)	6371(3)	-173(2)	50(1)
C(40)	2916(2)	6641(3)	-272(2)	41(1)
C(41)	2707(2)	6265(3)	-793(2)	46(1)
C(32')	2585(3)	5561(5)	325(3)	16(2)
C(33')	3049(3)	5981(5)	598(4)	46(2)
C(34')	2374(3)	6027(4)	-62(3)	40(2)
C(35')	2787(3)	4848(5)	61(4)	44(2)
C(36')	2846(4)	5516(6)	-860(5)	62(3)
C(37')	3131(4)	5061(7)	-457(5)	67(4)
C(38')	3441(4)	5396(6)	-233(5)	53(3)
C(39')	3377(4)	6211(6)	79(4)	57(3)
C(40')	3094(3)	6636(6)	-313(4)	49(3)
C(41')	2700(3)	6237(6)	-586(4)	46(3)
C(42)	862(1)	5098(2)	733(1)	29(1)
C(43)	434(1)	5271(2)	962(1)	37(1)
C(44)	135(1)	4682(2)	1074(1)	44(1)
C(45)	255(1)	3962(2)	957(1)	47(1)
C(46)	673(1)	3804(2)	716(1)	41(1)
C(47)	985(1)	4364(2)	603(1)	33(1)
C(48)	280(1)	6060(2)	1099(1)	40(1)
C(49)	-180(1)	6225(2)	814(2)	63(1)
C(50)	252(1)	6202(2)	1751(1)	52(1)
C(51)	1442(1)	4194(2)	320(1)	36(1)

C(52)	1409(1)	4305(2)	-329(1)	51(1)
C(53)	1626(1)	3417(2)	448(1)	53(1)

Table C.33 Bond lengths [Å] for **1-[(N^1Ad)NN(N^1Ad)]**.

Fe(1)-N(4)	1.939(2)	C(26)-C(31)	1.515(4)
Fe(1)-N(2)	1.974(2)	C(26)-C(27)	1.522(4)
Fe(1)-N(7)	1.981(2)	C(27)-C(28)	1.535(4)
Fe(1)-N(3)	2.223(2)	C(28)-C(29)	1.517(4)
Fe(1)-N(1)	2.241(2)	C(29)-C(30)	1.527(4)
N(1)-C(2)	1.297(3)	C(30)-C(31)	1.520(4)
N(1)-C(10)	1.437(3)	C(32)-C(33)	1.452(7)
N(2)-C(3)	1.364(3)	C(32)-C(34)	1.562(7)
N(2)-C(7)	1.365(3)	C(32)-C(35)	1.636(7)
N(3)-C(8)	1.296(3)	C(33)-C(38)	1.582(7)
N(3)-C(42)	1.442(3)	C(34)-C(40)	1.563(6)
N(4)-N(5)	1.343(3)	C(35)-C(36)	1.557(7)
N(4)-C(22)	1.467(3)	C(36)-C(37)	1.478(8)
N(5)-N(6)	1.260(3)	C(36)-C(41)	1.501(7)
N(6)-N(7)	1.366(3)	C(37)-C(38)	1.633(8)
N(7)-C(32)	1.471(5)	C(38)-C(39)	1.486(8)
N(7)-C(32')	1.515(8)	C(39)-C(40)	1.512(7)
C(1)-C(2)	1.484(4)	C(40)-C(41)	1.509(7)
C(2)-C(3)	1.461(4)	C(32')-C(34')	1.372(11)
C(3)-C(4)	1.375(4)	C(32')-C(35')	1.540(11)
C(4)-C(5)	1.381(4)	C(32')-C(33')	1.682(12)
C(5)-C(6)	1.387(4)	C(33')-C(39')	1.589(13)
C(6)-C(7)	1.389(4)	C(34')-C(41')	1.586(12)
C(7)-C(8)	1.460(4)	C(35')-C(37')	1.610(15)
C(8)-C(9)	1.491(4)	C(36')-C(37')	1.495(16)
C(10)-C(15)	1.398(4)	C(36')-C(41')	1.506(14)
C(10)-C(11)	1.402(4)	C(37')-C(38')	1.209(15)
C(11)-C(12)	1.398(4)	C(38')-C(39')	1.645(14)
C(11)-C(16)	1.511(4)	C(39')-C(40')	1.447(14)
C(12)-C(13)	1.373(4)	C(40')-C(41')	1.503(14)
C(13)-C(14)	1.364(4)	C(42)-C(43)	1.399(4)
C(14)-C(15)	1.396(4)	C(42)-C(47)	1.402(4)
C(15)-C(19)	1.510(4)	C(43)-C(44)	1.400(4)
C(16)-C(17)	1.532(5)	C(43)-C(48)	1.525(4)
C(16)-C(18)	1.536(4)	C(44)-C(45)	1.370(4)
C(19)-C(20)	1.526(4)	C(45)-C(46)	1.379(4)
C(19)-C(21)	1.531(5)	C(46)-C(47)	1.388(4)
C(22)-C(25)	1.519(4)	C(47)-C(51)	1.524(4)
C(22)-C(23)	1.528(4)	C(48)-C(50)	1.524(4)

C(22)-C(24)	1.536(4)	C(48)-C(49)	1.531(4)
C(23)-C(28)	1.534(4)	C(51)-C(52)	1.510(4)
C(24)-C(30)	1.532(4)	C(51)-C(53)	1.529(4)
C(25)-C(26)	1.531(4)		

Table C.34 Angles [°] for **1-[(N^1Ad)NN(N^1Ad)]**.

N(4)-Fe(1)-N(2)	175.00(9)	C(31)-C(26)-C(27)	109.7(2)
N(4)-Fe(1)-N(7)	78.96(8)	C(31)-C(26)-C(25)	109.2(2)
N(2)-Fe(1)-N(7)	106.00(8)	C(27)-C(26)-C(25)	109.5(2)
N(4)-Fe(1)-N(3)	105.33(8)	C(26)-C(27)-C(28)	108.8(2)
N(2)-Fe(1)-N(3)	73.95(8)	C(29)-C(28)-C(23)	109.9(2)
N(7)-Fe(1)-N(3)	107.73(8)	C(29)-C(28)-C(27)	110.1(2)
N(4)-Fe(1)-N(1)	103.93(8)	C(23)-C(28)-C(27)	108.7(2)
N(2)-Fe(1)-N(1)	74.31(8)	C(28)-C(29)-C(30)	109.2(2)
N(7)-Fe(1)-N(1)	106.64(8)	C(31)-C(30)-C(29)	109.8(3)
N(3)-Fe(1)-N(1)	138.21(8)	C(31)-C(30)-C(24)	108.9(2)
C(2)-N(1)-C(10)	119.0(2)	C(29)-C(30)-C(24)	109.2(2)
C(2)-N(1)-Fe(1)	112.23(17)	C(26)-C(31)-C(30)	110.2(2)
C(10)-N(1)-Fe(1)	128.64(16)	N(7)-C(32)-C(33)	119.6(4)
C(3)-N(2)-C(7)	118.7(2)	N(7)-C(32)-C(34)	109.9(4)
C(3)-N(2)-Fe(1)	120.02(17)	C(33)-C(32)-C(34)	111.1(4)
C(7)-N(2)-Fe(1)	120.17(17)	N(7)-C(32)-C(35)	105.0(4)
C(8)-N(3)-C(42)	120.1(2)	C(33)-C(32)-C(35)	107.6(4)
C(8)-N(3)-Fe(1)	114.17(18)	C(34)-C(32)-C(35)	101.9(4)
C(42)-N(3)-Fe(1)	125.63(15)	C(32)-C(33)-C(38)	115.0(4)
N(5)-N(4)-C(22)	111.6(2)	C(32)-C(34)-C(40)	112.4(4)
N(5)-N(4)-Fe(1)	114.68(16)	C(36)-C(35)-C(32)	111.2(4)
C(22)-N(4)-Fe(1)	133.72(17)	C(37)-C(36)-C(41)	110.7(5)
N(6)-N(5)-N(4)	117.1(2)	C(37)-C(36)-C(35)	106.5(4)
N(5)-N(6)-N(7)	117.1(2)	C(41)-C(36)-C(35)	109.0(4)
N(6)-N(7)-C(32)	109.6(3)	C(36)-C(37)-C(38)	114.0(5)
N(6)-N(7)-C(32')	112.8(4)	C(39)-C(38)-C(33)	109.9(5)
C(32)-N(7)-C(32')	10.6(4)	C(39)-C(38)-C(37)	106.1(4)
N(6)-N(7)-Fe(1)	112.22(15)	C(33)-C(38)-C(37)	101.6(4)
C(32)-N(7)-Fe(1)	138.2(2)	C(38)-C(39)-C(40)	114.0(5)
C(32')-N(7)-Fe(1)	133.9(3)	C(41)-C(40)-C(39)	110.8(4)
N(1)-C(2)-C(3)	115.9(2)	C(41)-C(40)-C(34)	108.3(4)
N(1)-C(2)-C(1)	125.7(3)	C(39)-C(40)-C(34)	107.5(4)
C(3)-C(2)-C(1)	118.5(2)	C(36)-C(41)-C(40)	111.3(4)
N(2)-C(3)-C(4)	121.7(3)	C(34')-C(32')-N(7)	115.7(7)
N(2)-C(3)-C(2)	112.7(2)	C(34')-C(32')-C(35')	115.4(7)
C(4)-C(3)-C(2)	125.6(3)	N(7)-C(32')-C(35')	111.5(6)
C(3)-C(4)-C(5)	119.4(3)	C(34')-C(32')-C(33')	109.6(7)
C(4)-C(5)-C(6)	119.5(3)	N(7)-C(32')-C(33')	100.4(5)
C(5)-C(6)-C(7)	119.2(3)	C(35')-C(32')-C(33')	102.2(6)

N(2)-C(7)-C(6)	121.1(3)	C(39')-C(33')-C(32')	109.2(7)
N(2)-C(7)-C(8)	112.9(2)	C(32')-C(34')-C(41')	111.4(7)
C(6)-C(7)-C(8)	126.0(2)	C(32')-C(35')-C(37')	109.5(7)
N(3)-C(8)-C(7)	114.5(2)	C(37')-C(36')-C(41')	111.9(9)
N(3)-C(8)-C(9)	125.9(3)	C(38')-C(37')-C(36')	114.5(11)
C(7)-C(8)-C(9)	119.6(2)	C(38')-C(37')-C(35')	106.1(11)
C(15)-C(10)-C(11)	122.3(2)	C(36')-C(37')-C(35')	103.8(9)
C(15)-C(10)-N(1)	119.8(2)	C(37')-C(38')-C(39')	123.1(11)
C(11)-C(10)-N(1)	117.9(2)	C(40')-C(39')-C(33')	104.9(8)
C(12)-C(11)-C(10)	116.8(3)	C(40')-C(39')-C(38')	105.4(8)
C(12)-C(11)-C(16)	119.8(3)	C(33')-C(39')-C(38')	99.4(8)
C(10)-C(11)-C(16)	123.3(2)	C(39')-C(40')-C(41')	116.9(9)
C(13)-C(12)-C(11)	122.1(3)	C(36')-C(41')-C(40')	111.6(9)
C(14)-C(13)-C(12)	119.3(3)	C(36')-C(41')-C(34')	106.5(8)
C(13)-C(14)-C(15)	122.2(3)	C(40')-C(41')-C(34')	105.2(8)
C(14)-C(15)-C(10)	117.2(3)	C(43)-C(42)-C(47)	121.5(2)
C(14)-C(15)-C(19)	120.6(3)	C(43)-C(42)-N(3)	118.6(2)
C(10)-C(15)-C(19)	122.2(2)	C(47)-C(42)-N(3)	119.7(2)
C(11)-C(16)-C(17)	112.0(3)	C(42)-C(43)-C(44)	117.6(3)
C(11)-C(16)-C(18)	113.1(3)	C(42)-C(43)-C(48)	123.5(2)
C(17)-C(16)-C(18)	108.0(3)	C(44)-C(43)-C(48)	118.8(3)
C(15)-C(19)-C(20)	113.6(3)	C(45)-C(44)-C(43)	121.4(3)
C(15)-C(19)-C(21)	110.8(3)	C(44)-C(45)-C(46)	120.2(3)
C(20)-C(19)-C(21)	110.0(3)	C(45)-C(46)-C(47)	120.9(3)
N(4)-C(22)-C(25)	106.5(2)	C(46)-C(47)-C(42)	118.3(3)
N(4)-C(22)-C(23)	112.5(2)	C(46)-C(47)-C(51)	121.1(3)
C(25)-C(22)-C(23)	108.0(2)	C(42)-C(47)-C(51)	120.5(2)
N(4)-C(22)-C(24)	112.4(2)	C(50)-C(48)-C(43)	112.1(2)
C(25)-C(22)-C(24)	108.8(2)	C(50)-C(48)-C(49)	110.0(3)
C(23)-C(22)-C(24)	108.5(2)	C(43)-C(48)-C(49)	110.7(3)
C(22)-C(23)-C(28)	110.6(2)	C(52)-C(51)-C(47)	109.9(2)
C(30)-C(24)-C(22)	110.4(2)	C(52)-C(51)-C(53)	109.5(2)
C(22)-C(25)-C(26)	110.8(2)	C(47)-C(51)-C(53)	114.4(2)

Table C.35 Crystal data and structure refinement for **1-[(NBn)NN(NBn)]**.

Identification code	acb4
Empirical formula	C47 H57 Fe N7
Formula weight	775.85
Temperature	173(2) K
Wavelength	0.71073 Å
Crystal system	Monoclinic
Space group	P2(1)/c

Unit cell dimensions	a = 11.0303(3) Å	α= 90°.
	b = 25.4378(7) Å	β= 114.9230(10)°.
	c = 18.1928(6) Å	γ = 90°.
Volume	4629.3(2) $Å^3$	
Z	4	
Density (calculated)	1.113 Mg/m^3	
Absorption coefficient	0.363 mm^{-1}	
F(000)	1656	
Crystal size	0.40 x 0.20 x 0.05 mm^3	
Theta range for data collection	1.60 to 24.71°.	
Index ranges	-12<=h<=10, -29<=k<=29, -20<=l<=21	
Reflections collected	36103	
Independent reflections	7881 [R(int) = 0.0510]	
Completeness to theta = 24.71°	100.0 %	
Absorption correction	Semi-empirical from equivalents	
Max. and min. transmission	0.9821 and 0.8683	
Refinement method	Full-matrix least-squares on F^2	
Data / restraints / parameters	7881 / 0 / 531	
Goodness-of-fit on F^2	1.128	
Final R indices [I>2sigma(I)]	R1 = 0.0504, wR2 = 0.1317	
R indices (all data)	R1 = 0.0746, wR2 = 0.1407	
Largest diff. peak and hole	0.656 and -0.389 $e.Å^{-3}$	

Table C.36 Atomic coordinates (x 10^4) and equivalent isotropic displacement parameters ($Å^2$x 10^3) for **1-[(NBn)NN(NBn)]**. U(eq) is defined as one third of the trace of the orthogonalized U^{ij} tensor.

	x	y	z	U(eq)
Fe(1)	2147(1)	1721(1)	2504(1)	26(1)
N(1)	2961(2)	1036(1)	2827(1)	33(1)
N(2)	3291(2)	1707(1)	1990(1)	30(1)
N(3)	1103(2)	2120(1)	1486(1)	27(1)

N(4)	955(2)	1765(1)	2978(1)	30(1)
N(5)	1288(2)	2044(1)	3643(1)	36(1)
N(6)	2507(2)	2243(1)	3903(1)	36(1)
N(7)	3050(2)	2137(1)	3383(1)	29(1)
C(1)	5054(3)	505(1)	3110(2)	54(1)
C(2)	4103(2)	954(1)	2745(1)	39(1)
C(3)	4292(2)	1331(1)	2226(1)	38(1)
C(4)	5193(3)	1330(1)	1874(2)	51(1)
C(5)	5027(3)	1672(1)	1256(2)	61(1)
C(6)	3892(2)	2000(1)	943(2)	47(1)
C(7)	3042(2)	2002(1)	1318(1)	34(1)
C(8)	1778(2)	2267(1)	1070(1)	31(1)
C(9)	1322(2)	2664(1)	400(2)	51(1)
C(10)	2520(2)	630(1)	3219(1)	34(1)
C(11)	1663(3)	247(1)	2722(2)	48(1)
C(12)	1222(3)	-147(1)	3084(2)	58(1)
C(13)	1606(3)	-158(1)	3904(2)	52(1)
C(14)	2440(2)	222(1)	4382(2)	45(1)
C(15)	2919(2)	629(1)	4056(1)	34(1)
C(16)	1230(4)	235(1)	1810(2)	78(1)
C(17)	-204(4)	61(2)	1348(2)	113(2)
C(18)	2105(4)	-116(2)	1574(2)	114(2)
C(19)	3854(2)	1033(1)	4622(1)	39(1)
C(20)	3285(3)	1267(1)	5180(2)	57(1)
C(21)	5237(3)	802(1)	5127(2)	54(1)
C(22)	-217(2)	2336(1)	1265(1)	27(1)
C(23)	-390(2)	2805(1)	1615(1)	33(1)
C(24)	-1692(2)	2973(1)	1397(1)	42(1)
C(25)	-2778(2)	2708(1)	843(1)	43(1)
C(26)	-2589(2)	2250(1)	503(1)	38(1)
C(27)	-1305(2)	2051(1)	708(1)	31(1)
C(28)	758(3)	3129(1)	2206(2)	47(1)
C(29)	951(3)	3625(1)	1779(2)	65(1)
C(30)	554(3)	3288(1)	2957(2)	61(1)
C(31)	-1144(2)	1545(1)	324(1)	41(1)

C(32)	-1144(3)	1646(1)	-501(2)	70(1)
C(33)	-2208(3)	1138(1)	244(2)	62(1)
C(34)	-427(2)	1556(1)	2672(1)	43(1)
C(35)	-938(2)	1465(1)	3298(1)	32(1)
C(36)	-1644(2)	1849(1)	3490(2)	45(1)
C(37)	-2076(2)	1769(1)	4102(2)	55(1)
C(38)	-1805(3)	1302(1)	4502(2)	65(1)
C(39)	-1116(3)	913(2)	4325(2)	75(1)
C(40)	-695(3)	1002(1)	3718(2)	56(1)
C(41)	4457(2)	2301(1)	3704(1)	37(1)
C(42)	4676(2)	2795(1)	3322(2)	43(1)
C(43)	5246(3)	2774(1)	2774(2)	63(1)
C(44)	5483(3)	3226(2)	2427(2)	84(1)
C(45)	5116(4)	3696(2)	2626(2)	97(2)
C(46)	4560(3)	3741(1)	3174(3)	89(1)
C(47)	4336(3)	3272(1)	3528(2)	59(1)

Table C.37 Bond lengths [Å] for **1-[(NBn)NN(NBn)]**.

Fe(1)-N(7)	1.8241(17)	C(15)-C(19)	1.511(3)
Fe(1)-N(4)	1.8553(19)	C(16)-C(18)	1.504(5)
Fe(1)-N(2)	1.8622(19)	C(16)-C(17)	1.510(5)
Fe(1)-N(1)	1.9344(18)	C(19)-C(20)	1.522(4)
Fe(1)-N(3)	1.9981(16)	C(19)-C(21)	1.529(3)
N(1)-C(2)	1.345(3)	C(22)-C(27)	1.403(3)
N(1)-C(10)	1.450(3)	C(22)-C(23)	1.402(3)
N(2)-C(7)	1.361(3)	C(23)-C(24)	1.388(3)
N(2)-C(3)	1.385(3)	C(23)-C(28)	1.514(3)
N(3)-C(8)	1.319(3)	C(24)-C(25)	1.375(3)
N(3)-C(22)	1.446(3)	C(25)-C(26)	1.376(4)
N(4)-N(5)	1.313(2)	C(26)-C(27)	1.397(3)
N(4)-C(34)	1.483(3)	C(27)-C(31)	1.512(3)
N(5)-N(6)	1.324(2)	C(28)-C(30)	1.529(4)
N(6)-N(7)	1.343(3)	C(28)-C(29)	1.544(4)
N(7)-C(41)	1.470(3)	C(31)-C(32)	1.524(4)
C(1)-C(2)	1.503(3)	C(31)-C(33)	1.525(4)
C(2)-C(3)	1.421(3)	C(34)-C(35)	1.487(3)
C(3)-C(4)	1.390(4)	C(35)-C(40)	1.368(4)
C(4)-C(5)	1.372(4)	C(35)-C(36)	1.383(4)

C(5)-C(6)	1.408(4)	C(36)-C(37)	1.398(4)
C(6)-C(7)	1.373(3)	C(37)-C(38)	1.359(4)
C(7)-C(8)	1.438(3)	C(38)-C(39)	1.365(5)
C(8)-C(9)	1.498(3)	C(39)-C(40)	1.385(4)
C(10)-C(11)	1.392(3)	C(41)-C(42)	1.503(3)
C(10)-C(15)	1.395(3)	C(42)-C(47)	1.370(4)
C(11)-C(12)	1.396(4)	C(42)-C(43)	1.386(4)
C(11)-C(16)	1.521(4)	C(43)-C(44)	1.388(4)
C(12)-C(13)	1.369(4)	C(44)-C(45)	1.361(6)
C(13)-C(14)	1.364(4)	C(45)-C(46)	1.378(6)
C(14)-C(15)	1.403(3)	C(46)-C(47)	1.424(5)

Table C.38 Angles [°] for **1-[(NBn)NN(NBn)]**.

N(7)-Fe(1)-N(4)	77.83(8)	C(13)-C(14)-C(15)	121.7(2)
N(7)-Fe(1)-N(2)	102.46(8)	C(10)-C(15)-C(14)	117.5(2)
N(4)-Fe(1)-N(2)	176.75(8)	C(10)-C(15)-C(19)	123.6(2)
N(7)-Fe(1)-N(1)	104.11(7)	C(14)-C(15)-C(19)	118.9(2)
N(4)-Fe(1)-N(1)	104.09(8)	C(18)-C(16)-C(17)	108.3(3)
N(2)-Fe(1)-N(1)	79.02(8)	C(18)-C(16)-C(11)	112.2(3)
N(7)-Fe(1)-N(3)	114.00(7)	C(17)-C(16)-C(11)	112.8(3)
N(4)-Fe(1)-N(3)	98.95(7)	C(15)-C(19)-C(20)	111.5(2)
N(2)-Fe(1)-N(3)	77.95(7)	C(15)-C(19)-C(21)	111.7(2)
N(1)-Fe(1)-N(3)	138.75(8)	C(20)-C(19)-C(21)	109.7(2)
C(2)-N(1)-C(10)	117.95(18)	C(27)-C(22)-C(23)	121.88(19)
C(2)-N(1)-Fe(1)	116.22(15)	C(27)-C(22)-N(3)	117.32(19)
C(10)-N(1)-Fe(1)	125.53(15)	C(23)-C(22)-N(3)	120.77(18)
C(7)-N(2)-C(3)	119.6(2)	C(24)-C(23)-C(22)	117.1(2)
C(7)-N(2)-Fe(1)	121.18(15)	C(24)-C(23)-C(28)	119.4(2)
C(3)-N(2)-Fe(1)	118.52(15)	C(22)-C(23)-C(28)	123.5(2)
C(8)-N(3)-C(22)	118.62(17)	C(25)-C(24)-C(23)	122.3(2)
C(8)-N(3)-Fe(1)	115.55(13)	C(26)-C(25)-C(24)	119.7(2)
C(22)-N(3)-Fe(1)	124.74(14)	C(25)-C(26)-C(27)	121.0(2)
N(5)-N(4)-C(34)	112.67(18)	C(26)-C(27)-C(22)	118.0(2)
N(5)-N(4)-Fe(1)	118.84(14)	C(26)-C(27)-C(31)	119.2(2)
C(34)-N(4)-Fe(1)	128.32(15)	C(22)-C(27)-C(31)	122.88(19)
N(4)-N(5)-N(6)	112.59(18)	C(23)-C(28)-C(30)	112.6(2)
N(5)-N(6)-N(7)	111.00(17)	C(23)-C(28)-C(29)	109.7(2)
N(6)-N(7)-C(41)	111.90(17)	C(30)-C(28)-C(29)	109.7(2)
N(6)-N(7)-Fe(1)	119.57(13)	C(27)-C(31)-C(32)	111.1(2)
C(41)-N(7)-Fe(1)	127.46(16)	C(27)-C(31)-C(33)	112.8(2)
N(1)-C(2)-C(3)	112.1(2)	C(32)-C(31)-C(33)	109.9(2)
N(1)-C(2)-C(1)	125.5(2)	N(4)-C(34)-C(35)	115.40(18)
C(3)-C(2)-C(1)	122.3(2)	C(40)-C(35)-C(36)	117.8(2)
N(2)-C(3)-C(4)	119.2(2)	C(40)-C(35)-C(34)	120.9(2)
N(2)-C(3)-C(2)	110.5(2)	C(36)-C(35)-C(34)	121.3(2)

C(4)-C(3)-C(2)	129.7(2)	C(35)-C(36)-C(37)	120.9(3)
C(5)-C(4)-C(3)	120.2(2)	C(38)-C(37)-C(36)	118.9(3)
C(4)-C(5)-C(6)	119.7(3)	C(37)-C(38)-C(39)	121.6(3)
C(7)-C(6)-C(5)	118.6(2)	C(38)-C(39)-C(40)	118.5(3)
N(2)-C(7)-C(6)	121.4(2)	C(35)-C(40)-C(39)	122.2(3)
N(2)-C(7)-C(8)	110.0(2)	N(7)-C(41)-C(42)	113.76(18)
C(6)-C(7)-C(8)	128.4(2)	C(47)-C(42)-C(43)	119.4(3)
N(3)-C(8)-C(7)	113.24(19)	C(47)-C(42)-C(41)	120.0(3)
N(3)-C(8)-C(9)	125.5(2)	C(43)-C(42)-C(41)	120.7(3)
C(7)-C(8)-C(9)	121.3(2)	C(42)-C(43)-C(44)	121.7(3)
C(11)-C(10)-C(15)	121.6(2)	C(45)-C(44)-C(43)	118.3(4)
C(11)-C(10)-N(1)	117.1(2)	C(44)-C(45)-C(46)	122.5(4)
C(15)-C(10)-N(1)	121.4(2)	C(45)-C(46)-C(47)	118.3(4)
C(10)-C(11)-C(12)	118.2(2)	C(42)-C(47)-C(46)	119.9(3)
C(10)-C(11)-C(16)	122.5(2)	C(37')-C(38')-C(39')	123.1(11)
C(12)-C(11)-C(16)	119.3(2)	C(40')-C(39')-C(33')	104.9(8)
C(13)-C(12)-C(11)	121.3(3)	C(40')-C(39')-C(38')	105.4(8)
C(14)-C(13)-C(12)	119.8(3)	C(33')-C(39')-C(38')	99.4(8)
C(10)-C(11)-C(16)	123.3(2)	C(39')-C(40')-C(41')	116.9(9)
C(13)-C(12)-C(11)	122.1(3)	C(36')-C(41')-C(40')	111.6(9)
C(14)-C(13)-C(12)	119.3(3)	C(36')-C(41')-C(34')	106.5(8)

APPENDIX D

KINETIC DATA

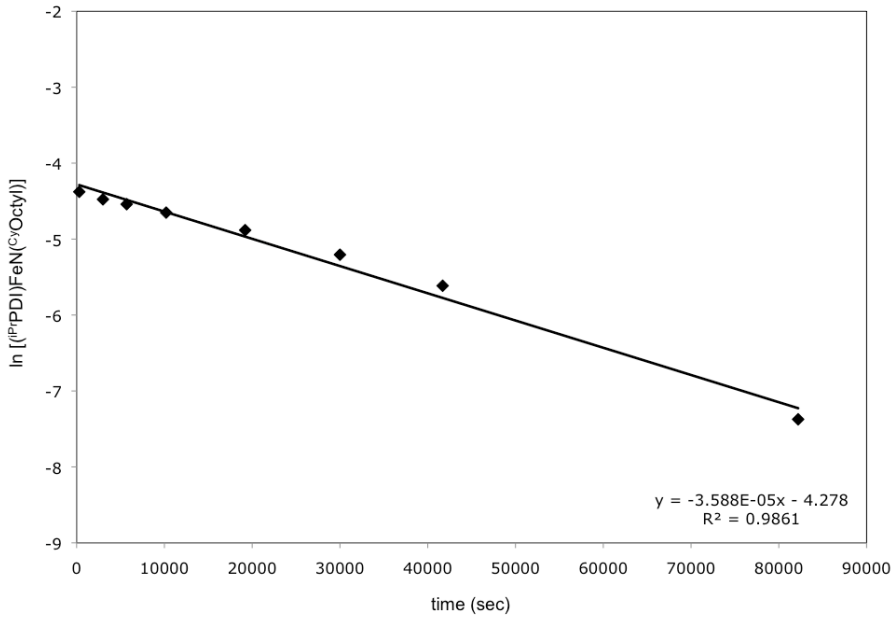

Figure D.1 Kinetic plot for C-H activation of **1-N(^{Cy}Oct)** (0.013 M) at 25 °C.

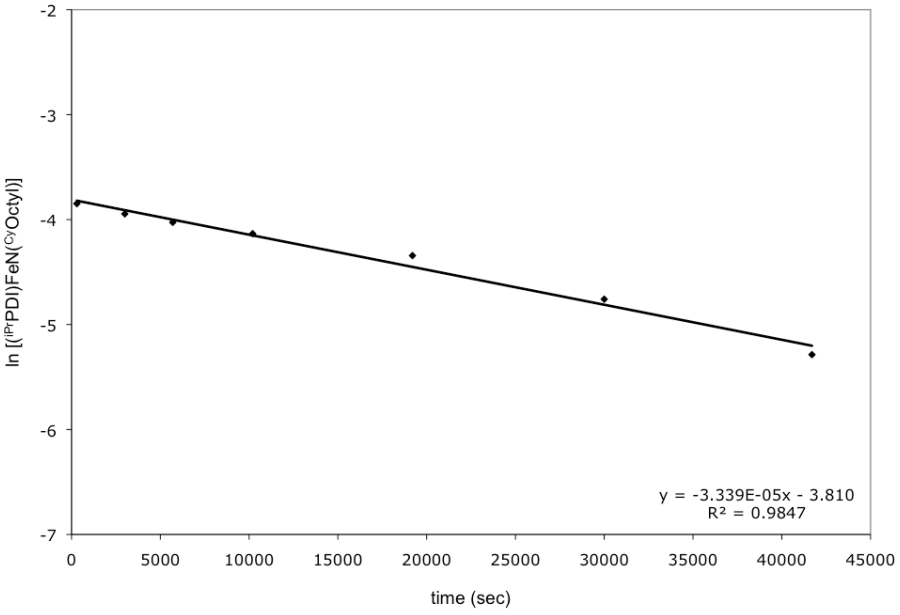

Figure D.2 Kinetic plot for C-H activation of **1-N(^{Cy}Oct)** (0.021 M) at 25 °C.

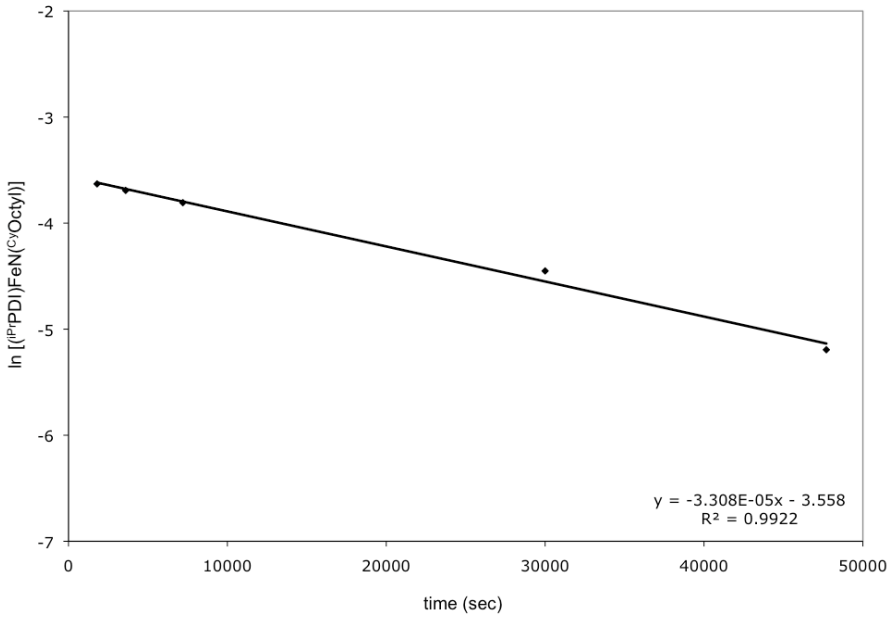

Figure D.3 Kinetic plot for C-H activation of **1-N(^{Cy}Oct)** (0.026 M) at 25 °C.

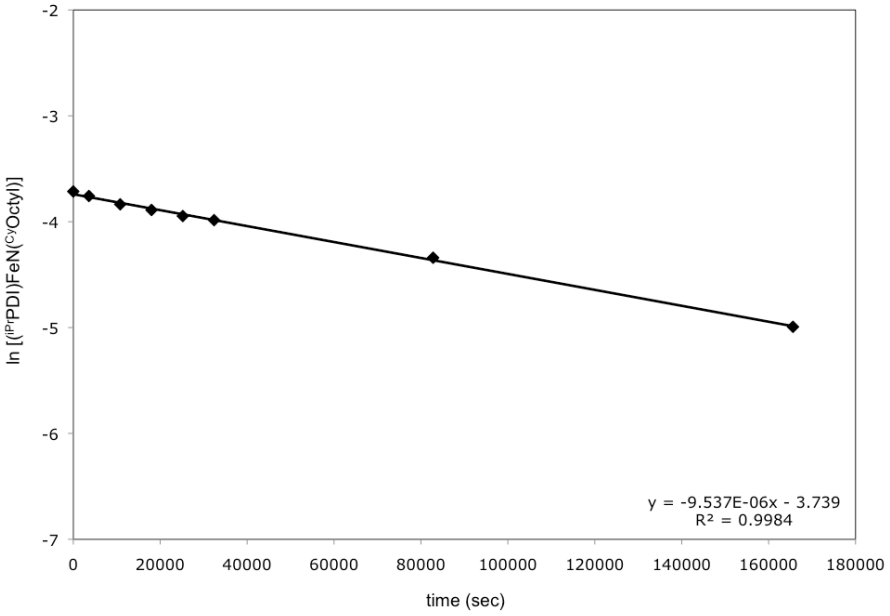

Figure D.4 Kinetic plot for C-H activation of **1-N(^{Cy}Oct)** (0.021 M) at 15 °C.

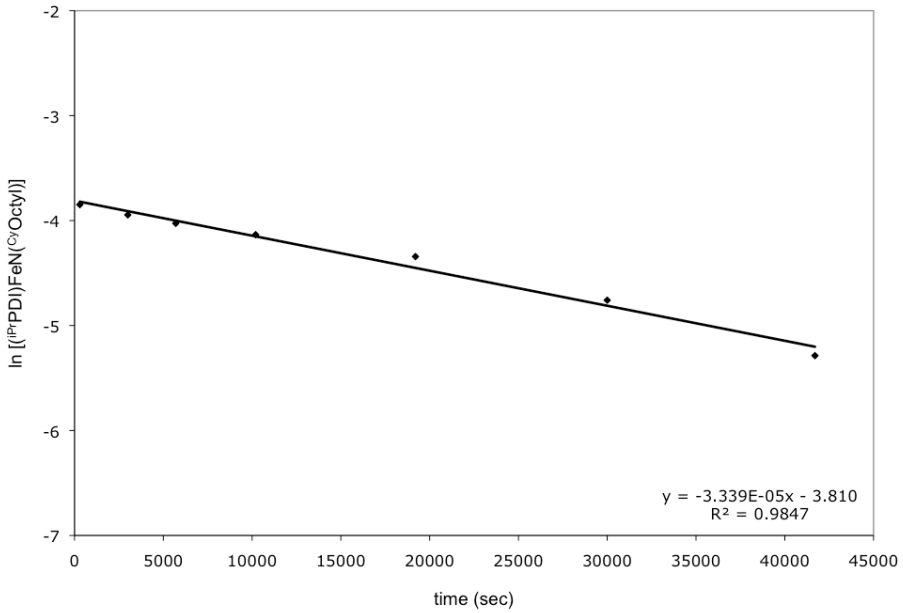

Figure D.5 Kinetic plot for C-H activation of **1-N(^{Cy}Oct)** (0.021 M) at 25 °C.

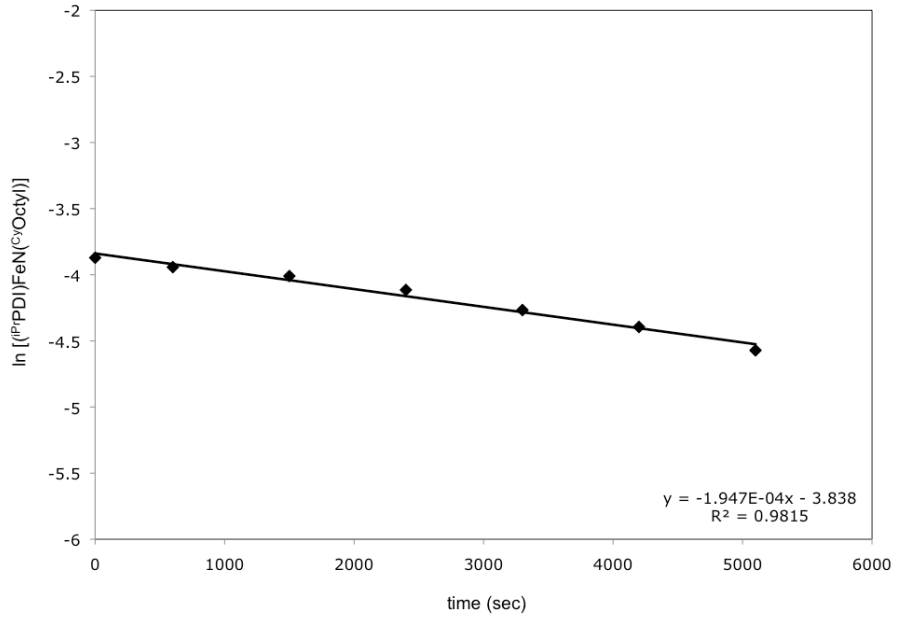

Figure D.6 Kinetic plot for C-H activation of **1-N(^{Cy}Oct)** (0.021 M) at 55 °C.

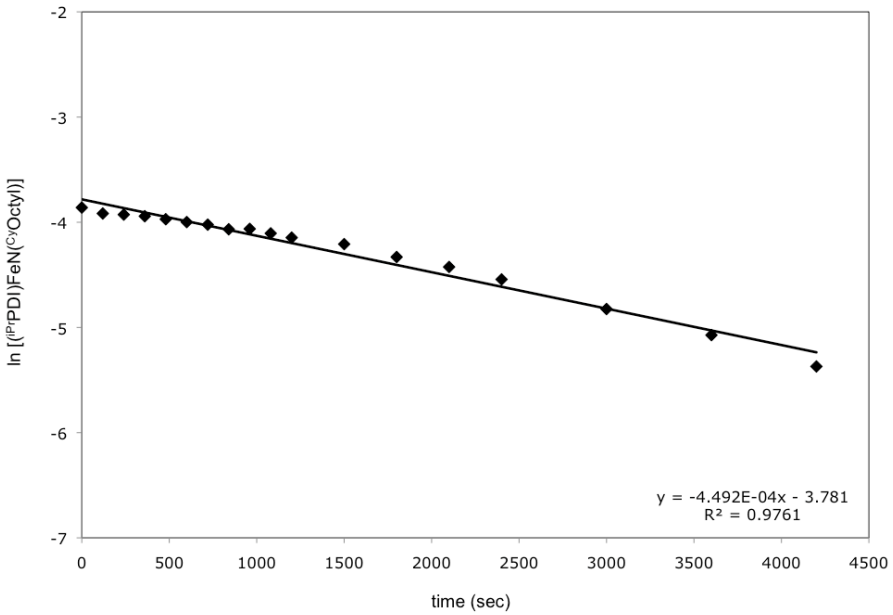

Figure D.7 Kinetic plot for C-H activation of **1-N(^{Cy}Oct)** (0.021 M) at 65 °C.

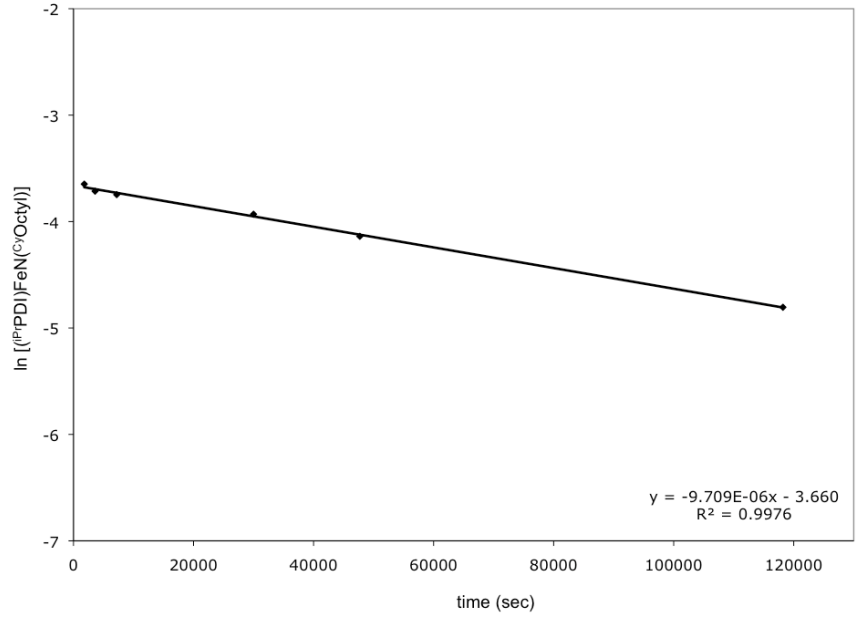

Figure D.8 Kinetic plot for C-D activation of ****1-N(^{Cy}Oct)** (0.026 M) at 25 °C.